Investigating novel methods of enhancing *in vitro* models of drug induced liver injury

Thesis submitted in accordance with the requirements of the University of Liverpool for the degree of Doctor in Philosophy

By

James Andrew Heslop

October 2015

Declaration

This thesis is the result of my own work. The material contained within this thesis has not been presented, nor is currently being presented, wholly, or in part, for any other degree or qualification.

James Andrew Heslop

This research was undertaken at the Department of Molecular and Clinical Pharmacology and the MRC centre for Drug Safety Science of the University of Liverpool

Table of contents

Section **Page no.**

Abstract

Drug induced liver injury (DILI) is a major cause of patient morbidity and mortality inferring considerable burdens onto healthcare and pharmaceutical sectors. As a consequence, substantial resources are directed towards triaging potentially dangerous new compounds at all stages of drug development. However, despite these efforts, hepatotoxic compounds remain the greatest cause of post-marketing drug withdrawal. One of the major factors preventing efficacious screening of new compounds is the lack of a truly representative *in vitro* model of hepatotoxicity. This thesis describes our efforts to utilise innovative and emerging techniques to further understand and develop *in vitro* models of hepatotoxicity.

One such technique is the generation of hepatocyte-like cells from induced pluripotent stem cells (iPSCs). iPSC-derived hepatocyte-like cells offer a reproducible, physiologically-relevant, genotypically normal and population-representative model of hepatotoxicity; however, current differentiation protocols are not capable of producing hepatocyte-like cells beyond a relatively immature phenotype, limiting their use for toxicological studies. As part of the cellular reprogramming process the epigenome of the somatic cell undergoes dramatic changes; however, the studies have shown that this 'resetting' of the epigenome to a pluripotent state is an imperfect process, resulting in an altered differentiation propensity skewed towards the lineage of origin. We evaluated if using human hepatocytes as the starting cell type and utilising the inherent 'epigenetic memory' associated with iPSCs could enhance the maturity of hepatocyte-like cells. Despite a trend towards improvement in phenotype, no significant differences were found between isogenic hepatocyte-derived and fibroblast-derived iPSCs.

The further development of hepatocyte-like cells is limited by the inability of current culture systems to adequately support the hepatic phenotype. Once placed into culture, primary human hepatocytes, the gold standard model of hepatotoxicity, quickly lose the metabolic qualities required for modelling drug induced liver injury. Thus, without a culture system which supports the hepatic phenotype, the differentiation of hepatocyte-like cells will remain sub-optimal. Using iTRAQ proteomics we attempted to identify the driving factors responsible for the process of hepatocyte dedifferentiation. Our results identified numerous novel factors, including HSF2, SMARCB1, ZEB1 and FOXO1 which may drive the selective loss of metabolic phenotype.

The proteomic assessment of hepatocyte dedifferentiation also highlighted the loss of Nrf2-related proteins during culture. Further investigation of Nrf2 in hepatocytes revealed a potentially negative relationship between Nrf2 induction and the key metabolic enzyme, CYP3A4. Furthermore, Nrf2 gene and protein expression was shown to increase during hepatocyte-like cell differentiation. Taken together, these results suggest that Nrf2 may negatively regulate the hepatic phenotype, potentially preventing the establishment of a mature phenotype during hepatocyte-like cell differentiation. A mechanistic evaluation of Nrf2 during differentiation and dedifferentiation is therefore required to gain a fuller insight into the role it plays in the maintenance and acquisition of the hepatic phenotype.

In summary, this thesis presents our contribution to the further understanding, development and enhancement of *in vitro* hepatotoxicity models, using innovative techniques to assess the impact of epigenetic memory on HLC differentiation, identifying novel influencing factors driving the loss of phenotype in hepatocyte culture systems and evaluating the influence of Nrf2 on the hepatic phenotype during differentiation and dedifferentiation.

Acknowledgements

I would like to thank my supervisors at the University of Liverpool, Dr. Chris Goldring, Dr. Neil Kitteringham and Prof. Kevin Park for their invaluable guidance and support during my PhD studies. I would also like to thank my industrial supervisor at AstraZeneca, Dr. John Mills, for maintaining the regular teleconferences between the CDSS and AZ and for the encouragement and constructive suggestions received during these meetings. In addition, I would like to express my gratitude to the AZ stem cell team in Molndal: Anna-Karin Sjögren, Gabriella Brolén and Bjorn Löwenadler, for the help received in setting up our reprogramming and stem cell culture protocols.

Throughout my PhD studies in the CDSS, I have been lucky to work alongside and learn from many talented scientists and I would like to thank all the students, technicians and post-docs who helped me during my 4 years in the lab. More specifically, thank you to Richard Kia – our work establishing the stem cell lines will remain one of my proudest achievements, but it would not have been possible without your tireless work ethic, commitment and insightful ideas during the countless discussions, weekends and late nights. Quite how you managed it with a young family and clinical work, I will never know! Thank you also to Chris Pridgeon, who picked up the late night and weekend work baton from Richard and despite there being 'a long way to go and a short time to get there', we made it.

I am also grateful for all those involved in 'Team Liver' from the pioneering Cliff Rowe and Rowena Sison-Young setting up the isolation techniques (along with the help in many other aspects of this PhD) to the more recent recruits. Without those who set up the collaboration, consent the donors, collect and isolate the specimen, none of the work presented in this thesis would have been possible.

Outside of science, thank you to my friends and family for their support and countless visits over the last 4 years. Finally, thank you to Helen. Between us, we have spent more time on trains between Liverpool and London than I care to remember, but I will be forever grateful for your unwavering support and understanding during this PhD.

List of publications

Heslop J.A, Rowe C, Walsh J, Sison-Young R.L, Jenkins R, Kamalian L, Kia R, Malik H.Z, Fenwick S.W, Mills J.S, Chadwick A.E, Kitteringham N.R, Goldring C.E and Park B.K. Mechanistic evaluation of primary human hepatocyte culture using global proteomic analysis reveals a selective dedifferentiation profile. *Submitted to Archives of Toxicology.*

Heslop J.A, Kia R, Pridgeon C, Sison-Young R.L, Hanley N.A, Mills J.S, Malik H.Z, Fenwick SW, Kitteringham N.R, Park B.K, Goldring C.E. Isogenic comparison of hepatocyte-like cells differentiated from human induced pluripotent stem cells derived from primary human hepatocytes and dermal fibroblasts. *Manuscript in preparation.*

Heslop J.A, Cummins P, Nugues C, Zhang F, Walsh J, Copple I, Jenkins R, Kia R, Mills J.S, Malik H.Z, Fenwick S.W, Kitteringham N.R, Park B.K, Goldring C.E. The role of Nrf2 in the differentiation and dedifferentiation of human hepatocytes. *Manuscript in preparation.*

Kia R, Kelly L, Sison-Young R.L, Zhang F, Pridgeon C.S, **Heslop J.A,** Metcalfe P, Kitteringham N.R, Baxter M, Harrison S, Hanley N.A, Burke Z.D, Storm M.P, Welham M.J, Tosh D, Küppers-Munther B, Edsbagge J, Starkey Lewis P.J, Bonner F, Harpur E, Sidaway J, Bowes J, Fenwick S.W, Malik H.Z, Goldring C.E, Park B.K. MicroRNA-122: A Novel Hepatocyte-Enriched in vitro Marker of Drug-Induced Cellular Toxicity. *Toxicological Sciences. 2015*

Kia R, Pridgeon C, **Heslop J.A**, Rowe C, Dudek K, Bushell M, Hanley N.A, Malik H.Z, Fenwick S.W, Kitteringham N.R, Park B.K, Goldring C.E. The global microRNA profiles of human primary hepatocytes in extended *in vitro* culture. *Manuscript in preparation.*

Heslop J.A, Hammond T.G, Santeramo I, Tort Piella A, Hopp I, Zhou J, Baty R, Graziano E.I, Proto Marco B, Caron A, Sköld P, Andrews P.W, Baxter M.A, Hay D.C, Hamdam J, Sharpe M.E, Patel S, Jones D.R, Reinhardt J, Danen E.H, Ben-David U, Stacey G, Björquist P, Piner J, Mills J, Rowe C, Pellegrini G, Sethu S, Antoine D.J, Cross M.J, Murray P, Williams D.P, Kitteringham N.R, Goldring C.E, Park B.K. Workshop review: understanding and assessing the risks of stem cell-based therapies. *Stem Cells Translational Medicine. 2015*

Kia R, Sison R.L, **Heslop J.A**, Kitteringham N.R, Hanley N.A, Mills J.S, Park B.K, Goldring C.E. Stem cell-derived hepatocytes as a predictive model for drug-induced liver injury: are we there yet? *British Journal of Clinical Pharmacol. 2013*

Sison-Young R.L, Kia R, **Heslop J.A**, Kelly L, Rowe C, Cross M.J, Kitteringham N.R, Hanley N, Park B.K, Goldring C.E. Human pluripotent stem cells for modeling toxicity. *Advances in Pharmacology, 2012*

Goldring C.E, Norris A, Kitteringham N.R, Aleo M.D, Antoine D.J, **Heslop J.A**, Howell B.A, Ingelman-Sundberg M, Kia R, Kamalian L, Koerber S, Martinou J.C, Mercer A, Moggs J, Naisbitt D.J, Powell C, Sidaway J, Sison-Young R.L, Snoeys J, Water B.V.B, Watkins P.B, Weaver R.J, Wolf A, Zhang F, and Park B.K. Mechanism-Based Markers of Drug-Induced Liver Injury to Improve the Physiological Relevance and Predictivity of In Vitro Models. *Applied in vitro Toxicology, 2015.*

Abbreviations

α-SMA: Alpha smooth muscle actin

A1AT: Alpha-1-antitrypsin

ADR: Adverse drug reaction

AhR: Aryl hydrocarbon receptor

AFP: Alpha fetoprotein

ALB: Albumin

AMPK: 5' AMP-activated protein kinase

AP-1: Activator protein 1

AR: Androgen receptor

ATF: Activating transcription factor

ATP: Adenosine triphosphate

BMP: Bone morphogenetic protein

BSEP: Bile salt export pump

CAR: Constitutive androstane receptor

CD: Cluster of differentiation

C/EBP: CCAAT/enhancer binding protein

CFTR: Cystic fibrosis transmembrane conductance regulator

CK18: Cytokeratin 18

COUP-TF: Chicken ovalbumin upstream promoter-transcription factor

CREB: cAMP responsive element-binding protein

CREM: cAMP Responsive Element Modulator

CRISPR: Clustered regularly interspaced short palindromic repeats

CXCR4: Chemokine (C-X-C motif) receptor 4

CYP: Cytochrome P450

D.E: Definitive endoderm

DEPs: Differentially expressed proteins

Dex: Dexamethasone

DILI: Drug-induced liver injury

DMSO: Dimethyl sulfoxide

DNMT: DNA methyltransferase

DSB: Double stranded break

EB: Embryoid bodies

ECAR: Extracellular acidification rate

EGF: Epidermal growth factor

ENDTP5: Ectonucleoside Triphosphate Diphosphohydrolase 5

EGR: Early growth response proteinESC: Embryonic stem cells

Elk-1: ETS domain-containing protein

ER: Estrogen receptor

ERK: Extracellular signal-regulated kinase

F2: Coagulation factor II (thrombin)

FAK: Focal adhesion kinase

FECH: Ferrochelatase

FGF: Fibroblast growth factor

FOX: Forkhead box protein

Fra-1: Activator Protein 1 transcription factor Fos-related antigen 1

FXR: Farnesoid X receptor

GATA: GATA Binding Protein

GCK: Glucokinase

GFI1: Growth factor independent 1 transcription repressor

GR: Glucocorticoid receptor

GNA12: Guanine nucleotide binding protein (G protein) alpha 12

HDAC: Histone deacetylase

HDF: Human dermal fibroblasts

HDR: Homology directed repair

H.E: Hepatic endoderm

HEPES: 4-(2-hydroxyethyl)-1-piperazineethanesulfonic acid

HIF-1: Hypoxia-inducible factor

HGF: Hepatocyte growth factor

HLC: Hepatocyte-like cell

HNF: Hepatic nuclear factor

HO-1: Heme oxygenase

HSF: Heat shock factor protein

HUVECs: Human Umbilical Vein Endothelial Cells

ICER-II: Inducible cAMP early repressor

IF: Immunofluorescence

IFN: Interferon

IGF-1R: Insulin growth factor receptor 1

Ipf1: Insulin promoter factor 1

Ins1: Insulin 1

InsR: Insulin receptor

iPSC: Induced pluripotent stem cells

IL: Interleukin

iTRAQ: Isobaric tags for relative and absolute quantitation

ITS: Insulin Transferrin Selenium

Keap1: Kelch-Like ECH-Associated Protein 1

Klf: Kruppel-like factor

LETFs: Liver-enriched transcription factors

LPS: Lipopolysaccharide

LSEC: Liver sinusoidal endothelial cell

LXR: Liver X receptor

MAFB: V-maf musculoaponeurotic fibrosarcoma oncogene homolog B

MAPKs: Mitogen-activated protein kinases

MDR: Multiple drug resistance protein

MEFs: Mouse embryonic fibroblasts

miRNA: MicroRNA

MITF: Microphthalmia-associated transcription factor

MKL2: MKL/Myocardin-Like 2

MOI: Multiplicity of infection

mRNA: Messenger ribonucleic acid

MRP: Multidrug resistance-related protein

NF-1: Neurofibromatosis type 1
NF-AT: Nuclear factor of activated T-cells
NFκB: Nuclear factor kappa-light-chain-enhancer of activated B cells
NFκBIA: NFκB inhibitor
NHEJ: Non-homologous end joining
NR1B1: Retinoic acid receptor alpha
Nrf2: Nuclear factor (erythroid-derived 2)-like 2
NRIP1: Nuclear receptor-interacting protein 1
NQO1: NAD(P)H dehydrogenase [quinone] 1

OAT: Organic anion transporting polypeptide;
OATP: Organic anion transporter
OCR: Oxygen consumption rate
OCT: Organic cation transporter
Oct4: Octamer-binding transcription factor 4
OMA1: Metalloendopeptidase OMA1.
OSKM: Oct4, Sox2, Klf4 and c-Myc
OSM: Oncostatin M
Otx2: Orthodenticle homeobox 2

PCK1: Phosphoenolpyruvate carboxykinase 1
PEDF: Pigment epithelium-derived factor
PHH: Primary human hepatocytes
Pit-1: Growth hormone factor 1
POU2F1: POU Class 2 homeobox 1
PPAR: Peroxisome proliferator-activated receptor
PRL: Prolactin
PXR: Pregnane X receptor

qRT-PCR: Quantitative reverse transcription polymerase chain reaction

ROR: RAR-related orphan receptor

ROS: Reactive oxygen species

RXR: Retinoid X receptor

SCAP: Sterol regulatory element-binding protein cleavage-activating protein

SeV: Sendai virus

SF-1: Steroidogenic factor 1

Smad3: Mothers against decapentaplegic homolog

SMARC: SWI/SNF Related, Matrix Associated, Actin Dependent Regulator of Chromatin

SMC1: Structural maintenance of chromosomes

Sox: Sex determining region Y-box

SREBP: Sterol regulatory element-binding proteins

SRF: Serum response factor

SSEA-4: Stage specific embryonic antigen-4

STAT: Signal transducer and activator of transcription

T3R: Thyroid hormone receptor

TBK1: TANK-binding kinase 1

TBX: T-box transcription factor

TFAM: Mitochondrial transcription factor A

TGF-β: Transforming growth factor- β

TNF: Tumour necrosis factor

Tra-1-60: Tumour-related antigen 1-60

Tuj1: Neuron-specific class III beta-tubulin

USF: Upstream transcription factor

VEGF: Vascular endothelial growth factor

VDR: Vitamin D receptor

Wnt: Wingless-type MMTV integration site family

ZEB1: Zinc Finger E-Box Binding Homeobox 1

Chapter 1

Introduction

1.1 Introduction

Drug induced liver injury is a major cause of drug attrition and patient mortality, conferring significant burden to all who are involved with the development and administration of drugs, including pharmaceutical companies, regulators, clinicians and patients (Russo et al., 2004; Sgro et al., 2002). Despite these concerns being well-acknowledged, attempts to reduce the incidence of DILI have thus far been unsuccessful. One of the major causes of these failings is the lack of a translational *in vitro* model with relevant physiological, pharmacological and toxicological phenotypes; consequently, these models lack the capacity to reliably screen and predict incidences of DILI in high throughput assays at the early stages of drug development (Godoy et al., 2013). Furthermore, retrospective studies investigating drugs which have known toxicological liability, particularly studies which require chronic exposure, are also hampered by currently available models lacking phenotypic similarity with the clinical situation, (Godoy et al., 2013). Much work is therefore required to develop these *in vitro* systems in order to increase the similarity to the *in vivo* situation and consequently the predictive and mechanistic endpoints required of toxicity studies.

This thesis describes our attempts to better understand and further develop currently available *in vitro* models of hepatotoxicity using innovative approaches with regard to proteomics, induced pluripotent stem cells and clustered regularly interspaced short palindromic repeats (CRISPR)/Cas9 technologies to investigate our hypotheses.

1.2.1 Adverse drug reactions and drug induced liver injury

Adverse drug reactions (ADRs) remain a considerable burden to clinicians, regulators and the pharmaceutical industry. These reactions may be split into two groups: predictable (type I) where there is a known dose-dependent toxicity, or idiosyncratic (type II) where the ADR is seen at therapeutic levels, often in a very small sub-population (Pirmohamed et al., 1998). However, while characterisation of the ADR type is relatively straightforward, understanding many of the underlying mechanisms and causes of toxicity remains an unsurmounted challenge, making ADR prediction and preventative measures difficult to develop or regulate.

Clinically, 6.7% of US hospital patients suffer serious ADRs, with 4.7% of these the initial cause of admission and 0.32% resulting in patient death (Lazarou et al., 1998). This was corroborated by a subsequent UK study, which reported that 6.5% of hospital admissions were related to ADRs (Pirmohamed et al., 2004). Furthermore, the financial burden to the NHS was estimated to be £466 million in 2004, with the majority of reactions suffered deemed avoidable (Pirmohamed et al., 2004). Once admitted, in-hospital ADRs were found to increase both with the number of medications taken by the patient and the length of time spent in hospital (Davies et al., 2009). A more recent study found that between 1999 and 2008 0.9% of English hospital admissions were related to ADRs; more concerning, however, was the admission trend over the examined period, with ADR-related admissions rising by 76.8% (Wu et al., 2010). ADRs are not only a burden in terms of admission to hospital, but also to the mortality rate. A Swedish study reported ADRs to be the 7th most common cause of death, accounting for 3.1% of total deceased study subjects and 6.4% of hospital fatalities (Wester et al., 2008).

Drug induced liver injury (DILI) is one of the most common ADRs. Two French studies provide the best estimate to the clinical burden of DILI, reporting an incidence of 13.9 per

100,000 (Sgro et al., 2002) and 1.4% (Meier et al., 2005), respectively. Both these reports state that the currently utilised measurements used by the French authorities likely under-estimate the true incidence of DILI, due to it often being asymptomatic in nature, and was not detected or noted in ~50% of initial diagnoses reported in the latter study (Meier et al., 2005). DILI is also the leading cause of acute liver failure (ALF) in the US and the UK (Ostapowicz et al., 2002). The rate of ALF as a result of acetaminophen overdose in particular showed a concerning upward trend between 1998 and 2003 from 23% to 51% of total ALF (Larson et al., 2005). As such, DILI places a huge burden on transplant units and was responsible for 15% of liver transplants between 1990 and 2002 in the US (Russo et al., 2004).

However, the impact of DILI is not limited to the clinic, with the pharmaceutical industry also suffering, mainly due to late stage clinical trial or post-market drug withdrawals as a consequence of hepatotoxicity (Watkins, 2005; Wilke et al., 2007). DILI is the largest cause of such post-marketing withdrawals (Wilke et al., 2007) and, given the costs to bring a drug to market, is an extremely expensive concern (Collier, 2009; Preziosi, 2004; DiMasi et al., 2003); thus, much effort is being placed on reducing the occurrence of DILI.

1.2.2 Liver anatomy, cell types and drug induced liver injury

To understand the mechanisms of DILI it is important to understand the architecture and functional roles of the liver. The liver is one of the most multi-functional organs in the body, with many unique feature, including: managing energy substrate levels (e.g. glucose and fatty acids), producing cholesterol and bile salts, metabolising xenobiotics, amino acid and ammonia, modulating hematopoietic, hormone and immune functions and storing vitamins (Fraczek et al., 2013). Furthermore, up to 40% of known genes are expressed in the liver, making it second-only to the brain in terms of transcriptomic complexity (Shackel et al., 2002).

Anatomically, the functional units of the liver are termed lobules which have a distinct hexagonal microstructure, incorporating several cell types with specific roles (Figure 1.1). Of these, hepatocytes account for the majority of cell number (60%) and mass (80%) and perform as the major metabolic unit of the liver (Godoy et al., 2013). Within the lobule, hepatocytes are arranged in cords, interconnected by tight junctions, running from the central vein, in the centre of the hexagon, to the portal triad, which includes the hepatic portal vein, hepatic artery and bile duct at the vertex. The hepatocytes are bordered by liver sinusoids which carry the blood from the portal vein to the central vein (Godoy et al., 2013).

Hepatocytes are remarkably versatile cells. The varying conditions to which they are subjected to along the porto-central lobule axis (e.g. oxygen tension), give rise to hepatocytes with specialised functions according to their location, termed zones 1-3 (Jungermann and Kietzmann, 1997; Allen and Bhatia, 2003). Zone 1 is found around the portal triad and is characterised by high oxygen tension, glycogen synthesis, β-oxidation, cholesterol biosynthesis and ureogenesis. Zone 3 is located around the central vein and is associated with low oxygen tension, glycolysis, xenobiotic metabolism, lipo- and keto-genesis and bile acid, glutamine and heme biosynthesis. Zone 2 incorporates a middle-ground between these two zones, demonstrating a gradient of function (Kietzmann et al., 2006; Godoy et al., 2013).

One of the most important roles of the hepatocyte is the detoxification and clearance of compounds and toxins which may be harmful to the body (Gomez-Lechon et al., 2003). These may be generated through endogenous homeostatic functions such as the various energy producing/storage pathways associated with the liver (Hodges and Minich, 2015), or exogenous sources, such as medicinal and recreational drugs and other inhaled or ingested toxins (Godoy et al., 2013). As a generalisation, these toxins are commonly

lipophilic and thus, for ease of excretion, the liver is required to alter the chemical properties of the compound to a water soluble product (Guengerich, 2001).

The compound is intially taken up by the hepatocyte via influx transporters. These consist of the organic anion transporting polypeptide (OAT), organic anion transporter (OATP) and organic cation transporter (OCT) families (Giacomini et al., 2010). The process of detoxification may then be split into three main phases. Phase I is orchestrated by cytochrome P450s (CYPs), alcohol dehydrogenases, aldehyde/xanthine oxidases, FAD-containing monooxygenases, monoamine oxidases, aldo-ketoreductases and epoxide hydrolases and esterases (Prakash and Vaz, 2008), and involves the oxidation, reduction, hydration, hydrolysis or dethioacetylation of the compound, resulting in neutralisation or the formation of an active intermediate (Guengerich, 2001; Jakoby and Ziegler, 1990; Fraczek et al., 2013).

Phase II enzymes neutralise these active intermediates through conjugation of the compound, reducing the potential for toxicity and increasing the water-solubility of the intermediate, allowing for excretion. The most commonly used phase II pathway is UDP-glucuronosyltransferase-mediated glucuronidation (Prakash and Vaz, 2008); however, glutathione S-transferases, sulfotransferases, N-acetyltransferases and methyltransferases also contribute through sulfation, acetylation, methylation and glutathione conjugation of the metabolite (Jakoby and Ziegler, 1990; Prakash and Vaz, 2008).

These water soluble compounds may then be removed from the hepatocyte by phase III transporters (Homolya et al., 2003; Konig et al., 1999) into the biliary (via BSEP, multiple drug resistance protein (MDR) 1, multidrug resistance-related protein (MRP) 2, breast cancer resistance protein and multidrug and toxin extrusion 1 transporters) or circulatory systems (via MRP3, MRP4, MRP6 transporters) and excreted from the body via bile or the kidneys, respectively (Giacomini et al., 2010).

Drug induced liver injury occurs when this process of metabolism and clearance becomes dysfunctional. In some instances, compounds undergo bio-activation and form chemically reactive metabolites, which can covalently bind to cellular proteins (Park et al., 2011). It has been estimated that ~85% of drugs withdrawn because of hepatotoxicity form chemically reactive metabolites (Nallani et al., 2008; Fraczek et al., 2013). These adducts negatively affect cell function, activating molecular initiating events (MIE) such as Nrf2 activation, mitochondrial perturbation, DNA damage, BSEP inhibition and the unfolded protein response. Although the toxicity profile is often drug-specific and ill-defined, through these MIEs, chemically reactive metabolites can result in cell death and the presentation of hepatotoxicity in the clinic (Park et al., 2011).

Hepatocytes are polarised cells, displaying varied functions at different membranes (Meier, 1988). One such function is bile acid section which takes place at the canalicular membrane of the hepatocyte and is associated with expression of the bile salt export pump (BSEP) (Hofmann, 2009; Meier and Stieger, 2002). This allows the export of bile salts into the bile canaliculi. The cells which line the bile canaliculi are termed cholangiocytes. Cholangiocytes secrete bicarbonate and water which, together with the bile salts, form bile. This is carried along the canaliculi towards the portal triad where it drains into the bile duct. This mechanism is important for the removal of many of the toxic products associated with normal liver function (Hofmann, 2009). The role of cholangiocytes in DILI remains largely unexplored. Research has previously shown that cholangiocytes can be damaged by parent compounds and hepatocyte-derived metabolite products (e.g. Flucloxacillin (Lakehal et al., 2001)) (Padda et al., 2011); however, further work has shown that they may be able to actively participate in DILI through the ability to detect (damage-associated molecular pattern) DAMPs released by damaged cells and secrete inflammatory cytokines, such as TNFα and IL-6 (O'Hara et al., 2013).

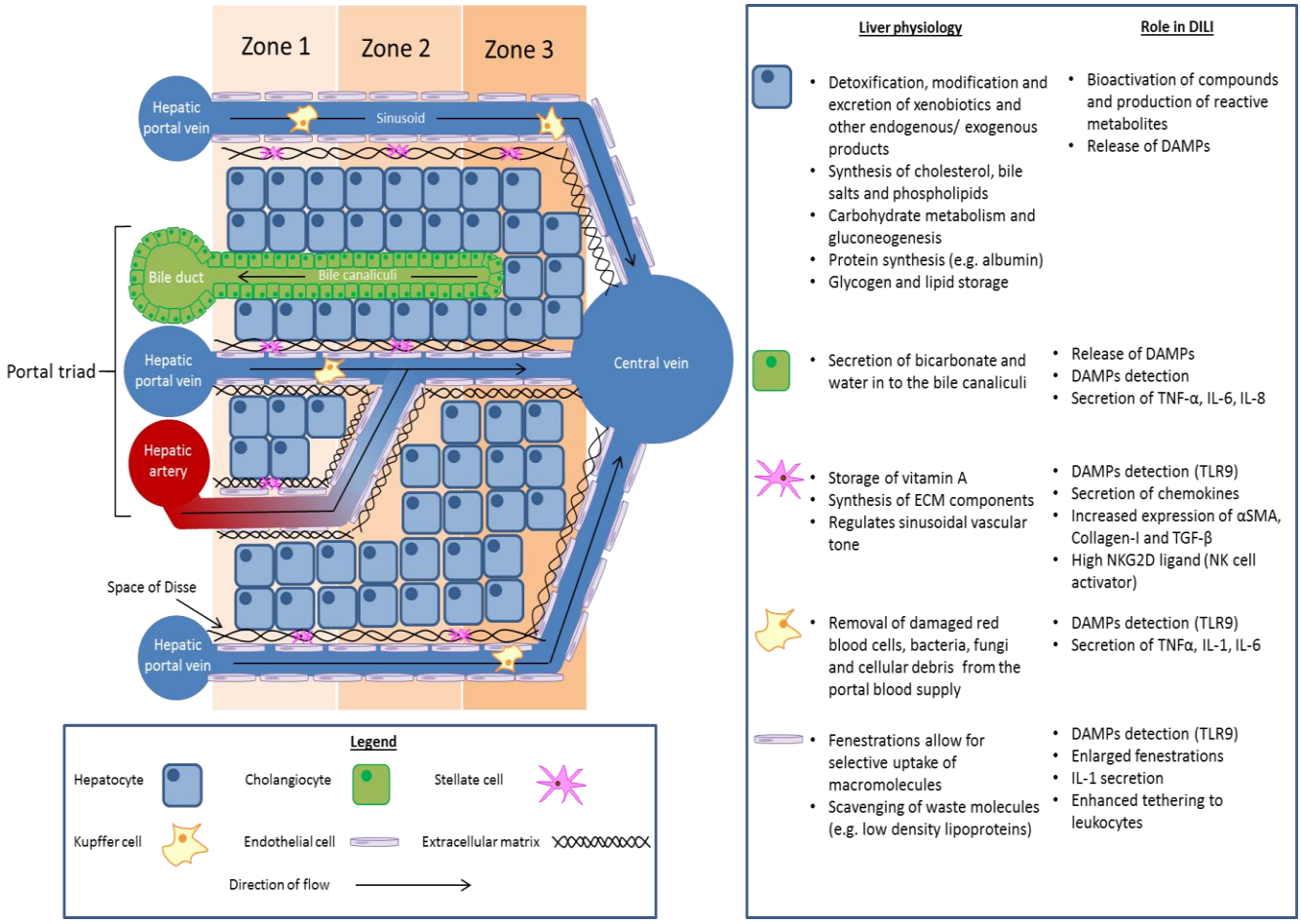

Figure 1.1: Schematic representation of the liver lobule highlighting the contribution of zonation, microvasculature and the native multi-cellular environment to hepatocyte function and the molecular initiating events leading to toxicity. Following injury, other non-native immune cells migrate to the liver (e.g. NK cells, leukocytes and macrophages) and can alleviate or potentiate the injury. These subsequent events are well reviewed by (Godoy et al., 2013).

Abbreviations: DAMPs: Damage-associated molecular pattern; TLR: Toll-like receptor; IL: Interleukin; TNF: Tumour necrosis factor; NK: Natural killer cell; α-SMA: alpha-smooth muscle actin; ECM: Extracellular matrix

The sinusoid and the surrounding area hold host to a multi-cellular environment and are key to maintaining healthy function of the liver. Liver sinusoidal endothelial cells (LSEC) line the lumen, forming a protective barrier between the lumen contents and the hepatocytes (Godoy et al., 2013). LSECs differ from other endothelial cells in their cytoplasmic projections contain fenestrations which are key to the selective uptake of molecules from the blood supply (Kmiec, 2001). Following insult to the liver, LSECs can detect DAMPs through toll-like receptors, (e.g. TLR9 detection of CpG-DNA released form damaged cells) (Martin-Armas et al., 2006) and consequently alter their phenotype, resulting in the enlargement or loss of fenestrations, IL-1 secretion and enhanced tethering of leukocytes (McCuskey et al., 2005; Neubauer et al., 2000). The changes permit the infiltration of leukocytes from the sinusoid to the site of injury and also result in the haemorrhage of erythrocytes into the space of Disse (McCuskey et al., 2005). LSECs are also thought to be important during post-injury regeneration, providing mitogenic growth factors (e.g. HGF) and a framework for the replacement hepatocytes (the origin of which is greatly contested) to grow in to (Hoehme et al., 2010; Ding et al., 2010).

Liver-resident macrophages, termed Kupffer cells, are located within the sinusoidal lumen adherent to the LSECs and are the first immune-defence point of contact with bacteria, endotoxins and micro-bacterial debris from the gastrointestinal tract (Bilzer et al., 2006; Fox et al., 1987). Kupffer cell roles and size are dependent on their location along the porto-central lobule axis, with those nearer the portal vein being grater in size, phagocytic capacity and secretion of inflammatory mediators such as TNF-α; whereas, mid and peri-central Kupffer cells secrete greater amounts of nitric oxide (Hoedemakers et al., 1995; Sleyster and Knook, 1982). Kupffer cells have been implemented in both liver injury and regeneration, and are thought to be key in the development and outcome of DILI (Tsutsui and Nishiguchi, 2014); however, the exact mechanisms are ill-defined. Reports have demonstrated that the inflammatory factors secreted by Kupffer cells following injury

results in the apoptosis of hepatocytes, increase fibrin deposition and the attraction of non-resident immune cells (Roberts et al., 2007). Notwithstanding these factors, depletion of Kupffer cells has been shown to exacerbate toxicity in a paracetamol injury model (Ju et al., 2002; Campion et al., 2008). This protective role of Kupffer cells is thought to be due to the secretion of the anti-inflammatory cytokine IL-10 and/or the induction of a protective phenotype in hepatocytes (Campion et al., 2008; Ju et al., 2002).

Between the endothelial cells and the hepatocytes lies the space of Disse, which contains a varied array of extracellular matrix, consisting of collagens, glycoproteins, proteoglycans and glycosaminoglycans (Godoy et al., 2013). The space of Disse also contains stellate cells, which are predominantly known to function as vitamin A storing cells (Kordes et al., 2009); however, upon injury stellate cells become activated and take on a myofibroblast-like phenotype, losing their vitamin A storage capacity (Reeves and Friedman, 2002). Stellate cell activation can occur through the detection of DAMPs released by damaged cells (Watanabe et al., 2007). The activated stellate cells up-regulate the production of collagen I and fibrogenic factors, such as TGF-β (Watanabe et al., 2007). In the short term, this limits the progression of injury, but in the longer term can lead to liver fibrosis (Bataller and Brenner, 2005). Moreover, it has been suggested that stellate cells are liver-resident mesenchymal stem cells, with the capacity to and secrete pro- and/or anti-inflammatory cytokines, modulating the progression of injury (Weiskirchen and Tacke, 2014), differentiate towards hematopoietic and osteogenic lineages (Castilho-Fernandes et al., 2011; Kordes et al., 2013) and influence liver regeneration (Kordes et al., 2012).

1.2.3 Models of drug induced liver injury

Much work is focussed on better understanding the mechanisms which underpin DILI, with the aim of identifying dangerous compounds at earlier stages of drug development and a consequent reduction in financial outlay and therapeutic burden.

To achieve this, there is a need for *in vitro* models which are readily available, stably encapsulate the unique metabolic competencies of the liver and, most importantly with regard to DILI, correlate with the toxicity seen in man. However, despite continued efforts, a model which possesses the physiological, pharmacological and toxicological phenotypes of the liver has yet to be achieved. Furthermore, whilst it is clear that the non-parenchymal cell types of the liver are key to the manifestation of DILI, the hepatocyte remains central to the toxicity profile of the majority of known hepatotoxic compounds, either through direct hepatocyte toxicity or through the production of metabolites which damage other cell types. As a consequence, the development of *in vitro* models of DILI has, in the main, focused on the production of hepatocytes or hepatocyte-like cell models to understand the molecular initiating events of toxicity.

Immortalised cell lines

Cell lines offer a readily available, easy to culture and reproducible model for the investigation of hepatotoxicity *in vitro*. Various cell types are currently used throughout academia and in pharmaceutical drug safety testing, including HepG2s and Huh7s (Castell et al., 2006); however, these cell types lack many of the key enzymes required for the effective modelling of DILI (Godoy et al., 2013; Castell et al., 2006). Some groups have attempted to overexpress selected enzymes or hepatic nuclear factors (Nibourg et al., 2010; Kuang et al., 2015); however, this represents a model which differs in both physiological and pharmacological phenotype to the liver (Castell et al., 2006). Thus, whilst

the compound of interest may show turnover and reactive metabolite production, the resulting effect on cell and the toxicological phenotype is likely to differ greatly from what is found *in vivo*.

The HepaRG is a bipotent cell line isolated from a hepatocellular carcinoma and represents a more metabolically competent cell type (Marion et al., 2010). These cells are thought to be equivalent to progenitor cells with their capacity to divide and become quiescent upon confluence; this, in tandem with dimethyl sulfoxide (DMSO) and other growth factors, induces hepatic differentiation allowing for the investigation of hepatotoxicity (Marion et al., 2010). However, these cells also exhibit higher expression of certain absorption, distribution, metabolism, and excretion (ADME) functions, increasing resistance to toxicity and reducing their translatability to the clinical situation (Sison-Young et al., 2015).

Most importantly for the modelling of DILI, cell lines represent a single, albeit unstable, genotype. Given the large variance in metabolic competence across the population and that idiosyncratic reactions are often incredibly rare, a single-genotype model is highly unlikely to be predicative of DILI in all situations (Pirmohamed et al., 1998). Using a panel of cell lines to increase the diversity of toxicity screens is one option; however, the variation in derivation technique (i.e. how the cell was immortalised), cancer-vs-liver phenotype and the cell type of origin would likely add large degrees of variability to the assays. Therefore a model which is phenotypically similar across a panel of selectable genotypes would be an invaluable resource.

Primary human hepatocytes

The current gold standard for investigating DILI is the primary human hepatocyte (PHH). These cells are usually isolated from waste tissue following liver resection or donor livers

which are unsuitable for transplant and demonstrate the highest metabolic competency of the available models (Bhogal et al., 2011).

PHH also have limitations as a model. The aforementioned supply of liver tissue is a major bottleneck to PHH application. Due to the nature of surgery and transplants, the supply is often unpredictable in frequency and yield, making experimental planning and high throughput investigations difficult (Bhogal et al., 2011). Furthermore, the quality of the liver tissue is also variable. As these specimens are either not suitable for transplant or resected from 'healthy' sections of diseased tissue, it is unlikely that any PHH used are truly representative of the normal condition. Furthermore, variation can be attributed to donor genotype and lifestyle which can have major effects on the experimental outcome (Bhogal et al., 2011). Whilst these concerns are common in many human-derived primary cells, it is particularly pertinent in PHH as they do not divide in culture and rapidly lose their metabolic competence following isolation (Elaut et al., 2006).

Such characteristics make genotype-controlled repeats reliant on cryopreserved hepatocytes. Hepatocytes are known to suffer from poor resuscitation following cryopreservation, which has led to the development of specialist techniques to improve the yield and reproducibility of plating efficiency following thawing (Alexandre et al., 2002). These developments have allowed for cryopreserved hepatocytes to be used as part of drug development with the advantage of a pre-determined knowledge of cell yield and repeatable genotypic/phenotypic characteristics. Whilst cryopreservation removes some of the concerns with availability, resources will always remain finite and consequently expensive. Additionally, these cells are known to have a reduced metabolic capacity when compared to freshly isolated PHH and still undergo the process of dedifferentiation following thawing and plating (Richert et al., 2006).

Dedifferentiation is a phenomenon that has been well described in hepatocytes (Elaut et al., 2006; Fraczek et al., 2013). Following isolation the cells lose their essential hepatic phenotype, rapidly down-regulating many of the key metabolic enzymes required for modelling DILI. Understanding this process has been a key area of research with the aim of improving hepatic culture conditions and the stability of the hepatic phenotype and consequently the relevance to DILI. The main driving forces behind the loss-of-phenotype are thought to be inflammatory and proliferative responses, particularly NF-κB and MAP kinase associated pathways (Fraczek et al., 2013). However, as yet, the underlying mechanisms of the global process remain incompletely understood. Hepatocyte dedifferentiation is investigated further in chapter 5.

The most successful method of reducing the impact of dedifferentiation has been through the development of culture systems which better model the hepatic niche. The most widely adopted of these is the sandwich culture, i.e. the overlaying of cells with an extracellular matrix mimicking substrate, such as Matrigel or collagen. This has been shown in numerous studies to improve cell polarisation, maintenance of metabolic competence and enhanced survival in culture (Fu et al., 2013; Kim et al., 2010b; Rowe et al., 2010).

Further recapitulation and enhancement of phenotype has been achieved using 3D or co-culture systems. As demonstrated in figure 1.1, the hepatic niche is a highly organised, multi-cellular environment with variable environmental conditions depending on the location of the cell (e.g. oxygen concentration, xenobiotic exposure, etc.) (Godoy et al., 2013).

Spheroid culture allows for the relatively simple formation of 3D clusters of hepatocytes with or without non-parenchymal or other non-liver stromal cells (No et al., 2012; Tostoes et al., 2012; Abu-Absi et al., 2004; Lu et al., 2005; Brophy et al., 2009; Ambrosino et al., 2005). In all cases, these papers report an enhancement in phenotype, most commonly

determined via increased and/or better maintained albumin secretion and phase I metabolism. This enhanced phenotype is thought to be due to the restoration of cell polarity and close cell-to-cell contact (Ambrosino et al., 2005). Further advancements in spheroid technology has led to the development of nanopillar-based culture systems (Takahashi et al., 2010). However, the inconsistent use of comparators means that any improvements between different spheroid systems are hard to quantify (Kia et al., 2013). In comparison to other 3D culture techniques, such as bioreactors (Tostoes et al., 2011), spheroids allow for an improved cost-efficiency and would consequently allow for scale-up possibilities (Goldring et al., 2015).

The effect of non-parenchymal and stromal cells has also been studied in non-spheroid culture systems. Micropatterned culture allows the maintenance of hepatocytes in various 'islands' of cells across the well, with stromal fibroblasts cultured in the surrounding spaces (Bhatia et al., 1997; Ukairo et al., 2013). This culture system has been shown to support albumin secretion, ADME functions and cell polarity for up to four weeks (Ukairo et al., 2013) and has the capacity for scale-up culture for use in high content screening (Trask et al., 2014). Furthermore, inflammatory conditions using co-culture with Kupffer cells have also been modelled, demonstrating a physiological-like reaction to perturbation, with inflammatory cytokines detected and subsequent loss of CYP3A4 expression described (Nguyen et al., 2015).

A move towards an increasingly physiological-like culture environment may therefore hold great promise in terms of better replicating the pharmacological and toxicological mechanisms of DILI. For example, the use of 3D bio-printing has the potential to fully replicate the complexity of the hepatic niche in terms of cell type and cell locations (Murphy and Atala, 2014). Notwithstanding this potential, complex 3D and multicellular models are likely to remain prohibitively expensive/complex for the large-scale screening of

compound libraries required by pharmaceutical companies (Goldring et al., 2015). Thus understanding the mechanisms by which these techniques improve phenotype and developing small molecules and other supplements/inducers to mimic their effects may be more cost effective. A high-throughput screen by Shan et al., demonstrated that a select number of the compounds tested could boost hepatic phenotype and also encourage proliferation (Shan et al., 2013), a characteristic which remains elusive in standard *in vitro* culture systems. Such results point towards the possibility of using the knowledge gained from more complex culture systems to enhance the simpler and more cost-effective *in vitro* models, bridging the gap between the requirements of academia and industry (Goldring et al., 2015).

Pluripotent stem cells

Pluripotent stem cells offer a scalable, reproducible and genotypically normal cell model combining cell line-like availability and the potential for producing physiologically-relevant cell types. There are two main types of human pluripotent stem cell available to researchers: embryonic stem cells (ESCs) and induced pluripotent stem cells (iPSCs). The relative advantages and disadvantages to these cell types are presented in table 1.1.

Human ESCs were first isolated from the blastocyst of human embryos in 1998 by James Thompson (Thomson et al., 1998); this process uses discarded fertilised eggs leftover from *in vitro* fertilisation treatment and is consequently limited by ethical constraints in certain countries and a restricted genotypic range. The isolation of human ESCs owed much to the techniques developed during the isolation and culture of embryonic carcinoma cells (Evans and Kaufman, 1981; Martin and Evans, 1974; Martin and Evans, 1975; Kleinsmith and Pierce, 1964; Stevens, 1958) and mouse ESCs (Evans and Kaufman, 1981; Martin, 1981). Much of the culture conditions and differentiation protocols described in this thesis were

first optimised using ESCs; however, whilst ESCs are used as a positive control in some instances, the main body of work regards iPSCs.

iPSCs were first reported in 2006 by Shinya Yamanaka, demonstrating the reprogramming of somatic cells from mice (Takahashi and Yamanaka, 2006) and later humans (Takahashi et al., 2007), using 4 retrovirally inserted transcription factors: Oct4, Sox2, Klf4 and c-Myc (OSKM).

Since the first reports, a range of techniques have been demonstrated for generating iPSCs. Traditional techniques relied on genomic integrations using retroviruses or lentiviruses for the insertion of the OSKM factors (Sommer et al., 2009; Takahashi et al., 2007; Yu et al., 2007). However, these insertions bring concerns with regard to the potential phenotypic alterations associated with genomic disruptions. The development of non-integrative reprogramming techniques, utilising direct transfection of proteins (Kim et al., 2009) or mRNAs (Warren et al., 2010), Sendai viruses (Fusaki et al., 2009) or episomal plasmids (Yu et al., 2009), or through the use of small molecules (Hou et al., 2013) has reduced concerns regarding incomplete promoter silencing and genomic disruptions of traditional techniques.

Some have also replaced the potentially oncogenic OSKM reprogramming factors with microRNAs to reprogram somatic cells (Miyoshi et al., 2011; Anokye-Danso et al., 2011). These techniques used the embryonic stem cell enriched microRNA cluster 302/367 either alone, or in combination with others to reprogram somatic cells, reporting the negation of OSKM factors and either an enhanced efficiency or integration-free reprogramming. These techniques are investigated in chapter 3.

Cell type	Derivation	Tumorigenicity	Pluripotency	Immunogenicity	Disease modelling	Phenotypic range
hESCs						
hiPSCs						

Table 1.1: Assessment of the inherent properties of hiPSCs and hESCs relative to each other. Green indicates that the cell type is thought to have greater capacity/less risk in the given category relative to the other cell type; Red indicates that the cell type has a reduced capacity/greater risk in the given category relative to the other cell type. The differences between the cell types is further reviewed by (Heslop et al., 2015)

Given that ESCs, unlike iPSCs, are derived directly from human embryos without need for genetic or phenotypic manipulation, they are often considered to be a more accurate representation of development. Comparisons between these two cell types have found differences in the genetic and epigenetic landscapes (Mallon et al., 2014; Guenther et al., 2010; Chin et al., 2009); however, despite slight differences required in some protocols, these do not appear translate to major functional differences in the differentiated products (Jozefczuk et al., 2011; Sullivan et al., 2010).

The major advantage of iPSCs over ESCs is the ability to capture the genotype of the donor cell, consequently allowing for the modelling of complex conditions, such as Alzheimer's disease (Kondo et al., 2013) or Down's syndrome (Chang et al., 2015), without the need for invasive and dangerous biopsies. With regard to DILI, this also allows for the creation of iPSC lines from patients who have suffered idiosyncratic reactions or a condition of interest, with the aim of replicating the reaction *in vitro,* and to create a panel of hepatocyte-like cells with a range of phenotypes to better represent the population during early compound screens (Takayama et al., 2014; Kia et al., 2013).

Once exogenously expressed within the cell, the OSKM factors set off a chain of events which lead to a pluripotent stem cell-like state; however, the mechanisms which underlie these changes and the specific roles that each OSKM factor plays are far from understood,

with the process appearing to be partly stochastic in nature (Buganim et al., 2012) and others describing it as an ordered probabilistic process (Chung et al., 2014).

Single cell PCR analysis has aimed to investigate the reprogramming process in greater detail (Buganim et al., 2012). These studies have shown a three-stage dynamic process. c-Myc has been shown as a key determinant of reprogramming efficiency but not reprogramming outcome i.e. the transcriptional effect of c-Myc is non-essential for reprogramming, but allows for increased efficiency through the generic enhancement of gene expression during the first initiation stage of reprogramming (Nakagawa et al., 2008). This stage is supported by Klf4 and, to a lesser degree, Oct4 and Sox2 which bind to openly accessible chromatin, activating or repressing the corresponding gene (Polo et al., 2012; Schmidt and Plath, 2012). The binding of the reprogramming factors drives increased proliferation, mesenchymal-to-epithelial transition, histone mark changes, activated DNA repair and RNA processing (Sancho-Martinez and Belmonte, 2013; Buganim et al., 2013). These changes appear to be stochastic, showing no conventional or conserved route to the acquisition of these characteristics (Buganim et al., 2012).

This is also true of the intermediate phase of reprogramming in which pluripotency and developmental regulators, along with glycolysis are activated through interactions with Oct4, Sox2 and Klf4 (Buganim et al., 2013). During the final two stages of reprogramming there is a gradual increase in the expression of Oct4 and Sox2 target genes (Buganim et al., 2012). The final stage of reprogramming has a more defined pattern of activation. This is instigated by the transcription factor Sox2 and leads to the expression of pluripotency-associated genes including Lin28, Sall4 and Esrrb, inducing the core endogenous pluripotency circuit (e.g. Oct4, Sox2, Nanog) and silencing of the exogenous transgene promoters (Buganim et al., 2012).

During reprogramming, the epigenetic landscape of the cells changes dramatically. These changes are brought about by a complex and incompletely understood set of mechanisms which reset the somatic epigenome to that of an embryonic stem cell-like state (Papp and Plath, 2013). Much of the epigenetic changes found during the reprogramming of somatic cells are related to the over-expression of the OSK factors, but not c-Myc which is thought to enhance the transcription at sites of already open chromatin (Rahl et al., 2010). These OSK factors are 'pioneer factors' and have the capacity to bind to unmarked and closed chromatin (Soufi et al., 2012). Binding to closed chromatin within nucleosomes makes up 70% of OSK binding in the early stages of fibroblast reprogramming (Soufi et al., 2012). This is proposed to be achievable by OSK due to their 3D structure, which allows binding to one side of the DNA helix and through a capacity to interact with nucleosome DNA (Soufi et al., 2012). This binding is thought to alter the chromatin state at enhancer regions from closed to either open or poised, a necessary pre-requisite for gene expression changes. In fact, a greater amount of histone modifications are found when compared to gene expression changes during the first stages of reprogramming, particularly in the enhancer and, to a lesser degree, promoter regions of genes which are not yet active, but are required in the later stages of reprogramming (Koche et al., 2011).

Methylation is another epigenetic mechanism and key determinant of gene expression. Interestingly, whilst changes to histone modifications and gene expression occur throughout the reprogramming process, Koche et al., reported that the respective hyper- and hypo-methylation changes to the somatic and pluripotency genes occurs very late in the reprogramming process and may in fact be non-essential to the induction of pluripotency (Koche et al., 2011). The regions of DNA which combine a shift from closed to OSK bound and methylation changes were also found to contain nearly all 20 reported hotspots for differences between iPSC and ESC methylation status; suggestive of an

incomplete process of epigenome reprogramming and that a 'memory' of the cell type of origin may remain imprinted (Lister et al., 2014).

In most cases, incomplete reprogramming of the epigenetic landscape would be detrimental, with studies using iPSCs attempting to recapitulate development for various endpoints; however, some have investigated whether this incomplete reprogramming, termed 'epigenetic memory' can be used as an advantage. Research has revealed an altered differentiation propensity, favouring the cell type or lineage of origin, depending on the source of the iPSCs. This heightened differentiation capacity was first described in 2010 using mouse iPSCs (Polo et al., 2010; Kim et al., 2010a), with different cell types showing enhanced differentiation to different lineages. This was also to be found to be true of the spontaneous differentiation propensity of pancreatic beta cells in comparison to non-beta pancreatic iPSCs, non-pancreatic iPSCs and ESCs (Bar-Nur et al., 2011). The influence epigenetic memory has on hepatocyte-like cell differentiation is investigated in chapter 4.

Differentiation of pluripotent stem cells to hepatocyte-like cells

By definition, a pluripotent stem cell can be expanded indefinitely and differentiate into cell types from all three germ layers, including fully functional hepatocytes. Therefore, pluripotent stem cells offer an attractive combination of availability and the capacity for metabolic competence.

To generate hepatocyte-like cells *in vitro*, most differentiation protocols attempt (selected examples are presented in table 1.2) to recapitulate the conditions found during the normal developmental process (Summarised in figure 1.2 (Baxter et al., 2010)). Whilst the nomenclature varies across the literature, the process is usually divided into 3 main checkpoints: definitive endoderm, hepatic endoderm and hepatocyte-like cells. Early techniques relied upon embryoid body formation, i.e. culturing the pluripotent stem cells in

suspension, encouraging the initiation of differentiation. These embryoid bodies were formed in conditions which promoted specification towards definitive endoderm; however, a relatively poor differentiation efficiency of 6-15% was reported across various studies (Lavon et al., 2004; Duan et al., 2007). Subsequent work used monolayer differentiation, demonstrating a slightly improved differentiation efficiency of 20% (Hay et al., 2007); however, larger increases in efficiency were found utilising Activin A and Wnt3A for differentiation of ESCs and iPSCs towards definitive endoderm (70-90%) (D'Amour et al., 2005; Hay et al., 2008b; Hay et al., 2008a; Sullivan et al., 2010). Interestingly, it has also been suggested that the differentiation to definitive endoderm is also influenced by the expression of expression of Wnt3, with higher endogenous expression significantly correlated with enhanced differentiation purity (Jiang et al., 2013).

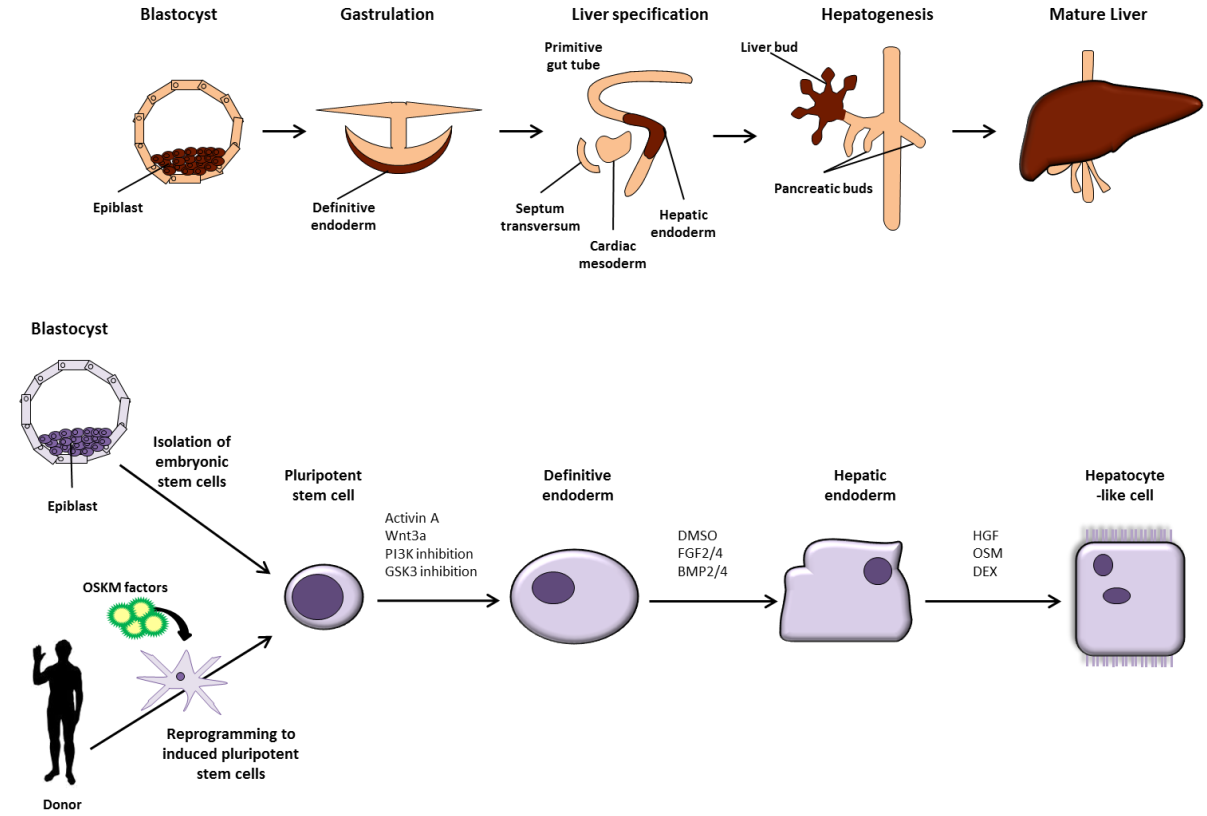

Figure 1.2: Schematic diagram demonstrating *in vitro* attempts to recapitulate liver development and the factors and cell types which are used to generate HLCs from pluripotent stem cells.

Abbreviations: Wnt: Wingless-type MMTV integration site family; DMSO: Dimethyl sulfoxide; HGF: Hepatocyte growth factor; Dex: Dexamethasone; OSM: Oncostatin M; BMP: Bone morphogenetic protein; FGF: Fibroblast growth factor; PI3K: Phosphoinositide 3-kinase; GSK3: Glycogen synthase kinase 3

The commitment to hepatic endoderm has been achieved using a much greater range of growth factor/compound variations and combinations. In general this stage is attempting to replicate the factors derived from the cardiac mesoderm during differentiation, most commonly with the factors which are known to play a role in this stage of development: fibroblast growth factor 2 and 4 (FGF2/4) and bone morphogenetic protein 2 and 4 (BMP2/4)(Si-Tayeb et al., 2010). Other groups have used dimethyl sulfoxide (DMSO) (Sullivan et al., 2010), which has been shown to enhance pregnane X receptor (PXR), constitutive androstane receptor (CAR), hepatic nuclear factor (HNF) -4α and CCAAT/enhancer binding protein (C/EBP) -α expression (Su and Waxman, 2004; Mizuguchi et al., 1998) and inhibit cell division, encouraging differentiation towards a hepatic lineage (Mizuguchi et al., 1998).

The specification and maturation of hepatocyte-like cells is the final stage of differentiation. This is widely achieved using the growth factors hepatocyte growth factor and oncostatin M; however, the concentrations used vary greatly between protocols (Sullivan et al., 2010; Hannan et al., 2013). Further variation between protocols at this point of differentiation is the time taken for maturation. Some have reported peaks at days 18-22 (Sullivan et al., 2010), followed by a loss of phenotype, whilst others have reported continued maturation up to day 35 and beyond (Hannan et al., 2013; Sjogren et al., 2014).

Despite large improvements in efficiency, the development of an *in vitro* protocol that can produce hepatocyte-like cells with a mature metabolic phenotype has yet to be achieved and, despite incremental improvements, the field is currently limited to an immature differentiation product more comparable to a foetal rather than a mature hepatic phenotype (Baxter et al., 2015). Furthermore, it is made harder to identify any step-wise change in phenotypic maturity by the inconsistency between comparators used. Kia *et al.,* compared a selection of available protocols in terms of reported differentiation efficiency,

hepatic expression and functional capabilities and demonstrated the difficulty in comparing between these protocols when the comparators used vary so greatly (Kia et al., 2013).

Given the lack of a clear step-wise change in phenotype using traditional methods, groups have attempted numerous new methods for identifying improvements to protocols. Recently, a report was published describing the stem cell derived formation of a liver bud (Takebe et al., 2013). By combining HLCs differentiated from iPSCs with mesenchymal stem cells and human umbilical vascular endothelial cells (HUVECs), the cells self-organised into a vascularised 3D structure with significantly improved function over 2D comparators (Takebe et al., 2013). Others have shown the benefit of small molecules with a high-throughput screen looking for enhancement of albumin secretion showed beneficial effects in HLC differentiation (Shan et al., 2013). However, the caveat remains with the screens is that it is often unclear which mechanisms are being activated and supressed to enhance the phenotype. More recently, microbial-derived lithocholic acid and vitamin K2 was shown to further boost HLC phenotype through activation of PXR (Avior et al., 2015) and exploring the effect of the microbiome and other external influences may lead to further enhancements of the hepatic phenotype. Together with co-culture and 3D models discussed with relation to primary hepatocyte culture, these novel approaches represent the current best attempts to boost HLC maturity (figure 1.3).

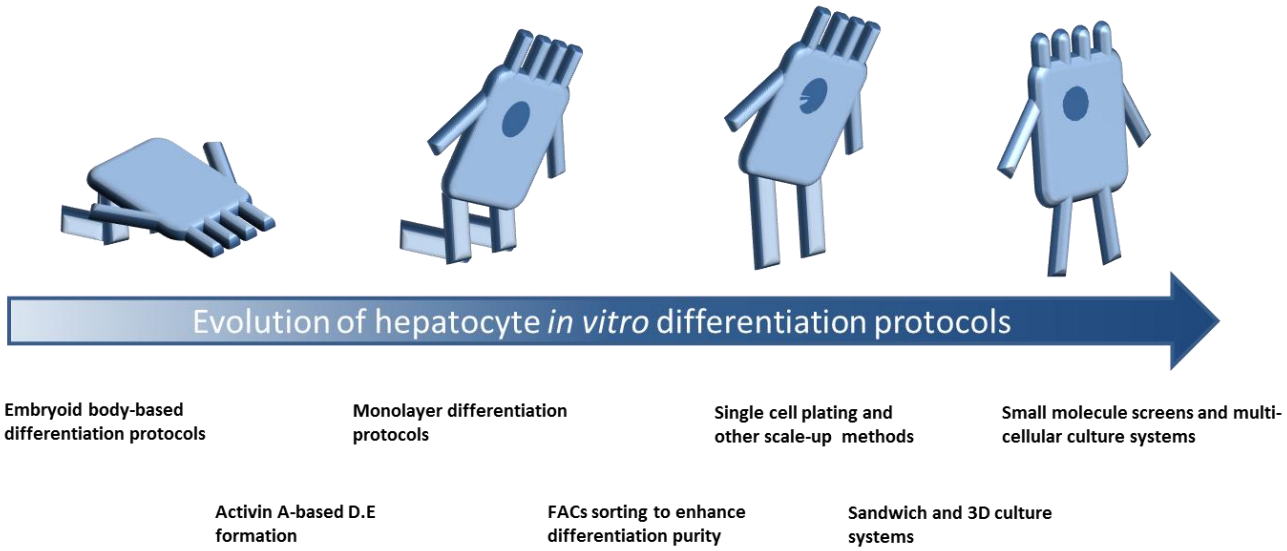

Figure 1.3: The development of hepatocyte-like cell differentiation protocols. Timeline showing the advances reported in the generation of protocols to enhance differentiation efficiency, maturity and scalability of HLC production.

Ref. (Author/year)	Stem cell Type ESC/iPSC	Differentiation method (EB, monolayer, co-culture)	Differentiation factors used (HGF, DMSO, etc.)	Differentiation efficiency % Albumin positive cells (method)
(Cai et al., 2007)	ESC (H1 and H9)	Monolayer and EB	AA, ITS, BMP2, FGF4, HGF, OSM, Dex	70% (ICC)
(Ek et al., 2007)	ESC (SA002, SA002.5 and SA167)	Monolayer	FGF2, VitroHES medium	-
(Hay et al., 2008a)	ESC (H1 and H9)	Monolayer	AA, Wnt3A, sodium butyrate, DMSO, HGF, OSM, hydrocortisone 21-hemisuccinate, Insulin	90% (ICC)
(Shiraki et al., 2008)	ESC (Khes-1)	Monolayer (Previously coated with feeder cells)	AA, FGF2, DMSO, HGF, Dex, BMP4, LY294002	9% (ICC)
(Agarwal et al., 2008)	ESC (H1, H9 and WA09)	Monolayer	AA, FGF4, HGF, OSM, Dex	67.4% (ICC)
(Moore and Moghe, 2009)	ESC (H1)	Monolayer and EB	AA, Wnt3A, Dex, OSM, HGF	72.8% (ICC)
(Basma et al., 2009)	ESC (H1)	Monolayer and EB	AA, FGF2, DMSO, HGF, Dex	55% (ICC)
(Song et al., 2009)	iPSC	Monolayer	AA, ITS, FGF4, BMP2, KGF, OSM, Dex	60% (ICC)
(Duan et al., 2010)	ESC (H9)	Monolayer	AA, sodium butyrate, FGF4 , HGF, BMP2, BMP4, DMSO	90% (FACs/ICC)
(Synnergren et al., 2010)	ESC (SA002, SA167, and SA461)	Monolayer	AA, FGF2, FGF1, BMP2, BMP4, HGF, ITS, Dex, OSM	-
(Touboul et al., 2010)	ESC (H9)	Monolayer	Ly294002, AA, FGF2, BMP4, FGF10, Retonic acid, SB431542, FGF4, HGF, EGF	-
(Brolen et al., 2010)	ESC (SA001, SA002, SA002.5 and SA167)	Monolayer	AA, FGF1/2, Wnt3A, BMP2/4, Dex, HGF, OSM	-
(Bone et al., 2011)	ESC (Shef1 and 3)	Monolayer	GSK-3 inhibitor, OSM, Dex, HGF, FGF4	-
(Ghodsizadeh et al., 2010)	iPSC	EB	AA, FGF-2, DMSO, HGF, Dex	50% (FACS)
(Liu et al., 2010a)	iPSC	Monolayer	AA, HGF, FGF4, Dex, OSM	-
(Si-Tayeb et al., 2010)	iPSC	Monolayer	AA, FGF2, BMP4, OSM	80% (FACS)
(Sullivan et al., 2010)	iPSC	Monolayer	AA, Wnt3A, DMSO, HGF, OSM, hydrocortisone 21-hemisuccinate, Insulin	70%-90%(ICC)

(Rashid et al., 2010)	iPSC	Monolayer	CHIR99021, Ly294002, AA, FGF2, BMP4, HGF, OSM	83% (FACS)
(Zhang et al., 2011)	iPSC	Monolayer	AA, OSM, BMP2, FGF4, HGF, KGF, Dex,	60-80% (ICC and FACS)
(Chen et al., 2012)	ESC (H9), iPSC	Monolayer	AA, ITS, HGF, Wnt3A, OSM, DMSO, DEX	–
(Cayo et al., 2012)	iPSC	Monolayer	AA, BMP4, FGF2, OSM	–
(Schwartz et al., 2012)	iPSC	Monolayer	AA, BMP4, FGF2, HGF, OSM	80 (ICC)
(Takayama et al., 2012)	ESC (H9), iPSC	Monolayer	AA, HEX, BMP4, FGF4, HNF1α, FOXA2, HGF, OSM, DEX	–
(Choi et al., 2013)	iPSC	Monolayer	AA, FGF4, HGF, OSM, DEX	–
(Ramasamy et al., 2013)	ESC (H1)	Monolayer & 3D culture	AA, DMSO, HGF, OSM	–
(Gieseck III et al., 2014)	iPSC	Monolayer, 3D-single cell or Clump culture	AA, FGF2,BMP4, LY-294002, lipid concentrate, insulin, transferrin, HGF, OSM	–
(Jia et al., 2014)	iPSC	Monolayer, EB formation	AA, FGF4, BMP2, HGF, KGF, OSM, DEX	64 (FACS)
(Avior et al., 2015)	ESC (I3)	Monolayer	AA, Wnt3A, HGF, DMSO, DEX, OSM, FGF2, LCA, MK4	83 (FACS)
(Chien et al., 2015)	iPSC	Co-culture with MEF, EB formation	AA, FGF4, BMP2, HGF, KGF, OSM, DEX, miR122	–
(Siller et al., 2015)	ESCs (H1 and 207) iPSC	Monolayer	CHIR99021, DMSO, Dihexa, Dex	72% and 79% (ICC)

Table 1.2: Selected hepatocyte-like cell differentiation protocols and reported differentiation efficiencies. Adapted from (Kia et al., 2013).

Abbreviations: EB: Embryoid body; AA: Activin A; FGF: Fibroblast growth factor; BMP: Bone Morphogenetic Protein; HGF: Hepatocyte growth factor; ITS: Insulin-transferrin-selenium; Dex: Dexamethasone; OSM: Oncostatin M; LCA: Lithocholic acid; MK4: Vitamin K; KGF: Keratinocyte growth factor; DMSO: dimethyl sulfoxide; HNF: Hepatocyte nuclear factor; FOX: Forkhead Box; ICC: Immunocytochemistry

1.2.4 Cytochrome P450s

Despite continued efforts, no *in vitro* model of hepatotoxicity has comparable phase I metabolism with that seen in man, most notably with regard to CYP expression. The majority of phase I xenobiotic metabolism (~75%) is performed by CYPs, a key family of phase I enzymes which contribute to the metabolic competence of the hepatocyte (Zanger and Schwab, 2013; Guengerich, 2008). CYPs are the terminal oxidase enzymes of the membrane-bound microsomal monooxygenase system that catalyse the oxygenation of both exogenous and endogenous substrates (Zangar et al., 2004). CYPs can also lead to the formation of chemically reactive metabolites, a key component in many forms of DILI and therefore a necessity in any model of hepatotoxicity.

In humans, CYPs may be grouped based on their structure into 18 distinct families. Families are grouped by number if they have ≥40% homology in structure and by letter if the homology is ≥55%. The CYP families 1, 2 and 3 are responsible for 70-80% of drug detoxification (Figure 1.3)(Prakash and Vaz, 2008). Of these, ~30% of clinically-available drugs are metabolised by CYP3A4/5 (Zanger and Schwab, 2013).

CYP-dependent oxygenation requires an input of electrons. These are provided by cytochrome b5, or more commonly by the oxidation of NADPH by NADPH-P450 reductase (Zangar et al., 2004). The transfer of electrons is often inefficient, usually ~50% but has been reported to be as low as 0.5%, and causes substantial oxidative stress on the cell as a result (Gruenke et al., 1995; Kuthan and Ullrich, 1982). This production of ROS continues even when the CYPs are not bound by substrates (Bondy and Naderi, 1994).

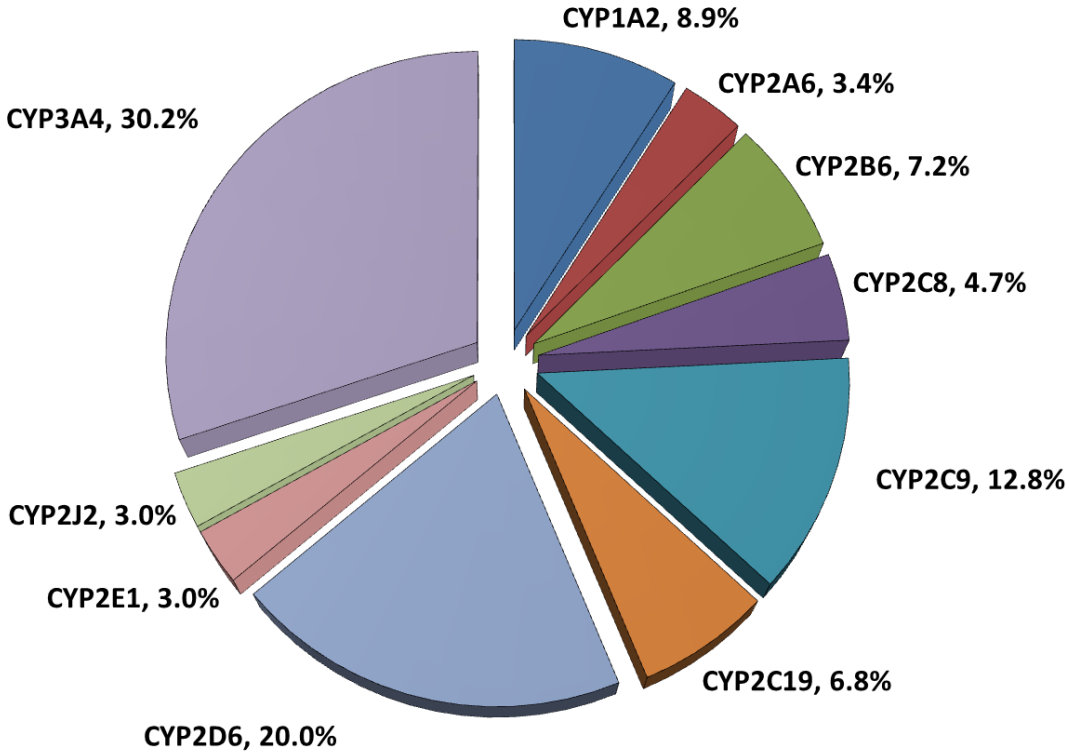

Figure 1.3: Pie chart representing the percentage of drugs which are metabolised by each of the CYPs. Adapted from (Zanger and Schwab, 2013)

Regulation of Cytochrome P450s

An effective *in vitro* model of DILI requires an *in vivo*-like ADME expression profile; however, as discussed, no current *in vitro* model has the capacity to fully acquire or maintain a mature metabolic phenotype which has PHH-comparable CYP expression. Therefore, understanding the regulatory mechanisms governing the expression of these essential enzymes is a key component of any strategy aiming to enhance CYP expression.

CYPs are a substantial source of oxidative and toxicological stress upon the cell and are therefore tightly regulated by numerous mechanisms (Zangar et al., 2004). Transcription (no known ligands) and nuclear (ligand-based activation) factors have the capacity to modulate CYP expression. Of particular importance are the liver enriched transcription factors (LETFs), such as HNF1α and HNF4α and C/EBPα, which have been shown to exert

regulatory control over a number of CYPs (Akiyama and Gonzalez, 2003). These factors are constitutively expressed and bind directly to the promoter regions which contain their specific binding sites. Of the nuclear receptor family, the PXR, aryl hydrocarbon receptor (AhR) and CAR have particular relevance to xenobiotic metabolism-related CYPs (Czekaj and Skowronek, 2012; Xu et al., 2005). Once activated by ligand binding, nuclear receptors migrate from the cytosol to the nucleus and form heterodimers, most commonly in the case of PXR and CAR with retinoid X receptor (RXR), and bind to the corresponding binding site, driving transcription (Xu et al., 2005).

The transcription of CYPs is multi-faceted and each individual factor does not act alone to drive CYP expression, with multiple transcription/nuclear factors thought to influence the expression of each CYP. Table 1.3 shows the binding sites for transcription factors which exist within each of the CYPs according to the BIObase database. The extensive number of different transcription factors associated with each CYP demonstrates the intricate and tightly controlled mechanisms which govern CYP expression. A further layer of complexity is added by the capacity of these factors to form heterodimers, altering the target and function of the factor (Xu et al., 2005).

The LETFs and nuclear factors are also known themselves to be susceptible to transcription modulation, as demonstrated in table 1.4, further highlighting the complex nature of cross-regulation which exists within the LETFs and associated factors. In addition, the expression of nuclear factors in particular can be modulated by a range of stimuli and ligands. For example, the presence of bile acids increases farnesoid X receptor (FXR) expression, causing down-regulation of CYP7A1, an enzyme which converts cholesterol into bile acids preventing the build-up of bile acids in the hepatocyte (Akiyama and Gonzalez, 2003). Such tightly controlled feedback loops are vital for homeostasis *in vivo*; however, these same

mechanisms likely contribute to the poor CYP expression in *in vitro* culture systems due the disruption of important processes, such as bile acid removal.

CYPs are also thought to be regulated by microRNAs (miRNA). miRNAs bind to the transcribed mRNA of the gene and inhibit the translation to protein and/or target the mRNA for degradation (Shruti et al., 2011). However, these are not specific for a single mRNA and therefore one miRNA may have hundreds of targets and thus a wide-ranging effect on cell function (Shruti et al., 2011). Specific miRNAs have been shown to target CYPs, for example, CYP1A2 is targeted by miR-762, whilst CYP1B1 and CYP3A4 are targets of miR-27b (Betel et al., 2008; Pan et al., 2009; Tsuchiya et al., 2006). Furthermore, transcription and nuclear factors are also controlled via miRNA activity, with miR-34a shown to be target HNF4α (Takagi et al., 2010) and miR-148a found to target pregnane X receptor (PXR) (Takagi et al., 2008).

Epigenetic control of CYP expression is far from understood. *In silico* work predicting the potential methylation sites of the promoter regions of CYPs has revealed little evidence of CpG islands within these genes, suggesting little-to-no direct involvement of methylation in CYP gene regulation (Ingelman-Sundberg et al., 2007). Notwithstanding these findings, studies investigating differences in gender have shown changes in methylation patterns of CYP2E1, CYP1A1 and CYP7B1 in response to different hormones (Penaloza et al., 2014). The use of a histone deacetylation inhibitor Trichostatin A has been demonstrated to improve the maintenance of the hepatic miRNA global phenotype *in vitro* (Bolleyn et al., 2011), although it is as yet unclear if this improvement is through epigenetic associated mechanisms or how this relates to CYP expression. A study using stem cell derived hepatocytes has shown that the lack of expression of CYP1A1, CYP1A2, CYP1B1, CYP2D6, and CYP2E1 in these cells may be explained by hypermethylation of the promoter regions

of these genes; whereas, the same regions are hypomethylated in primary hepatocytes (Park et al., 2015).

Oxidative stress can also repress the expression of CYPs. This has been shown to be particularly true of CYP2E1 and CYP1A1. A study of promoter activity of these two CYPs demonstrated a down-regulation when oxidative stress was induced by the addition of H_2O_2 or glutathione depletion (Morel et al., 2000). Furthermore, the oxidative stress produced by the CYPs themselves also has consequences; the same study showed an increase in CYP1A1 resulted in a down-regulation of CYP2E1 promoter activity (Morel et al., 2000). Thus, as CYP expression basally produces oxidative stress (Bondy and Naderi, 1994), the cell must tightly control and finely tune the expression to ensure homeostatic levels of oxidative stress are maintained during perturbation.

Inflammation is another key determinant of CYP expression. Studies have shown a strong correlation between inflammatory cytokines, such as IL-6 and TNF-α, and the alteration of CYP expression (Aitken et al., 2006). A recent study found a reduction in CYP1A, 2C, 2D, 2E and 3A families expression (mRNA and protein) in an inflammatory model. These effects were associated with an up-regulation of NFκB nuclear translocation and reduction in CAR/PXR nuclear expression (Kusunoki et al., 2014). The type and pathway of inflammation also seems to determine the CYP response, with LPS-, but not anaphylaxis-induced inflammation, resulting in a down-regulation of CYP1A2 and CYP3A4 protein expression (Moriya et al., 2014).

Post-translation, CYPs are continually degraded when inactive. This is exemplified by CYP2E1, which is bound and chaperoned to degradation by HSP90 when inactive; however, this mechanism is inhibited when CYP2E1 is active (Morishima et al., 2005). Such mechanisms provide a dynamic response which reduces cellular stress during times of low perturbation, but can react quickly upon exposure to a given compound.

The expression of CYPs, and consequently the capacity for PHH to metabolise the majority of xenobiotics, is tightly regulated by numerous complex and interacting variables. Therefore, any *in vitro* model of hepatotoxicity needs to recapitulate *in vivo* conditions, or successfully manipulate the discussed influencing factors, to ensure that the system is amenable and permissive to CYP expression. Without these, the model is likely to be poor in the prediction of hepatotoxicity and in the identification of the mechanisms underlying it.

Cytochrome P450	Transcription factors with binding sites in the gene
CYP1A2	AhR(h), AhR(m), RXR-alpha(h):CAR(h), AhR(h),
CYP2A6	ER-alpha(h), Nrf2(h), POU2F1(h), POU2F1(r), C/EBPalpha(r), C/EBPalpha(r):C/EBPbeta(r), C/EBPbeta(r), HNF-4alpha(r), HNF-4alpha(m.s.), HNF-4alpha(h), HNF-4alpha(h):GR(h), POU2F1(h),
CYP2C8	POU2F1(h), PXR(h):RXR(h), CAR(h):RXR(h), PXR(h):RXR(h), CAR(h):RXR(h), RORalpha1(h), RORgamma-isoform1(m), RORalpha-4(m), RORalpha1(h), RORgamma-isoform1(m), RORalpha-4(m), HNF-4alpha(h), HNF-4(h),
CYP2C19	PXR(h):RXR(h), CAR(h):RXR(h), HNF-4alpha(h), GATA-6(h), GATA-4(h), ER-alpha(h), HNF-4alpha(h),
CYP2D6	HNF-4alpha(h), HNF-4(h), HNF-4(r), COUP-TF1(h),
CYP2E1	CYP2E1GATA-4(h), NF-AT5(h), NF-AT5c(h),
CYP3A4	HNF-4alpha(h), HNF-1alpha-A(h), HNF-4alpha(h), AP-1(h), USF1(h), HNF-4alpha2(h), COUP-TF2(h), RXR-alpha(h):PPARalpha-isoform1(h), HNF-4alpha(h), HNF-4alpha(r), RXR-alpha(h):PPARalpha-isoform1(h), PXR-isoform1A(h):RXR-alpha(h), PXR(h):RXR-alpha(h), RXR-alpha(h):T3R-alpha1(h), (COUP-TF2(h), 2FXR(h):RXR-alpha(h), VDR(h):RXR-alpha(h), RXR-alpha(h):LXR-alpha(h), (COUP-TF1(h),), 2PXR(h):RXR-alpha(h), RXR-alpha(h):T3R-beta1(h), RXR-alpha(h):CAR(h), RXR-alpha(h):COUP-TF2(h), CAR(h), VDR(h):RXR-alpha(h), VDR(h):RXR-alpha(m.s.), C/EBPbeta(m.s.), C/EBPbeta(m.s.), C/EBPbeta(m.s.), RXR-alpha(h):PPARalpha-isoform1(h), RXR-alpha(h):PPARalpha-isoform1(h), HNF-3gamma(h), C/EBPalpha(r), C/EBPalpha(r), NFI/CTF(h), HNF-4alpha2(h), C/EBPalpha(h), HNF-3alpha(m.s.), HNF-3(h), PXR(h), CAR2(m):RXR-alpha(m), SXR(h):RXR-alpha(h), PXR-isoform1A(h):RXR-alpha(h), PXR-isoform1A(h):RXR-beta(h), PXR-isoform1(m):RXR-alpha(m), CAR(h):RXR-alpha(h), PXR(h):RXR-alpha(h), RXR-alpha(h):CAR(h), PXR(m), (RXR-alpha(h),), 2CAR(h):RXR-alpha(h), VDR-isoform1(h):RXR-alpha(m.s.), PXR(h):RXR-alpha(h), PXR(h):RXR(h), PXR(h):RXR-alpha(h), PXR-isoform1(m):RXR-alpha(m), VDR(h):RXR(h), RXR(m.s.):PXR(h), PTS1R(m.s.), PXR(h), VDR(h), VDR(h):RXR-alpha(h), PXR(h):RXR-alpha(h), RXR-alpha(h):T3R-alpha1(h), VDR(h):RXR-alpha(m.s.), (T3R-beta1(h),), 2FXR(h):RXR-alpha(h), VDR(h):RXR-alpha(h), RXR-alpha(h):LXR-alpha(h), (COUP-TF1(h),), 2RXR-alpha(h):T3R-beta1(h), RXR-alpha(h):CAR(h), RXR-alpha(h):COUP-TF1(h), NF-1C(h), C/EBPalpha(r), C/EBPalpha(h), C/EBPalpha(m.s.), Sp1(m.s.), Sp1(h), USF1(h), DEC1(m.s.), DEC1(h), Sp1(h), Sp3(h), PXR(h):RXR-alpha(h), VDR(h):RXR-alpha(h), PXR(h):RXR-alpha(h), PXR(h):RXR-alpha(h),
CYP27A1	PXR(h):RXR-alpha(h), PXR(h):RXR-alpha(h), GR-alpha(h), GR-alpha(h), CREB-H(h), Sp1(h), Sp3(h), HNF-4alpha(m), HNF-4alpha(h), HNF-4alpha(h), PXR(h):RXR-alpha(h), Sp1(h), Sp3(h), Sp1(h), Sp3(h),
CYP2B6	CAR(h):RXR-alpha(h), PXR(h):RXR-alpha(h), CAR(h):RXR-alpha(h), PXR(h):RXR-alpha(h), RXR-alpha(h):CAR(h), c-Fos(h):c-Jun(h), PXR-isoform1A(h):RXR-alpha(h), CAR(h):RXR-alpha(h), T3R-alpha(c):RXR-alpha(h), VDR(h):RXR-alpha(h), PXR-isoform1A(h):RXR-alpha(h), PXR-isoform1(m):RXR-alpha(m), CAR(h):RXR-alpha(h), CAR(m):RXR-alpha(m), VDR(h):RXR-alpha(m.s.), PXR(h), CAR(h):RXR-alpha(h), PXR(h):RXR(h), CAR(h):RXR(h), CAR(m):RXR(h), PXR(h):RXR-alpha(h), CAR(h), Egr-1(h), Egr-1(h), Egr-1(h), SMC1(h), Egr-1(h), HNF-4alpha(h), POU2F1(h),
CYP2C9	PXR(h):RXR-alpha(h), PXR(h):RXR(h), CAR(h):RXR(h), CAR(m):RXR(h), PXR(h):RXR(h), CAR(h):RXR(h), CAR(m):RXR(h), PXR(h):RXR-alpha(h), CAR(m):RXR(h), PXR-isoform1A(h):RXR-alpha(h), CAR(h):RXR-alpha(h), VDR(h):RXR-alpha(m.s.), GR(h), HNF-4alpha(r), HNF-4alpha2(m), HNF-4alpha(h), GATA-6(h), GATA-4(h), ER-alpha(h), HNF-4alpha2(m), HNF-4alpha(h), HNF-4(h), HNF-4(r), POU2F1(h),
CYP2J2	Nrf2(m.s.):c-Jun(m.s.), Nrf2(h):c-Jun(h), c-Fos(h), c-Jun(h), c-Jun(h), POU2F1(h),
CYP4F2	NR1B1(h):RXR-alpha(h), SREBP-1(m.s.), SREBP-1(m.s.),
CYP4F3	SIP1-isoform1(h),
CYP7B1	Sp1(h), Sp1(h), Sp3(h),
CYP51A1	CREB1(r), CREM(r), CREMtau(m.s.), CREB (h), CREM(r), ATF-1(h), SREBP-1(m.s.), SREBP(pg), SREBP-1(h), SREBP-1a(h), Sp1(h), Sp3(h),

Table 1.3: Transcription factors with binding sites within selected CYP genes.

Abbreviations: (h): human; (ms) mouse; (r): rat; CYP: cytochrome P450; AhR: aryl hydrocarbon receptor; RXR: retinoid X receptor; CAR: constitutive androstane receptor; ER: estrogen receptor; Nrf2: nuclear factor (erythroid-derived 2)-like 2; POU2F1: POU Class 2 homeobox 1; HNF: hepatic nuclear receptor; GR: glucocorticoid receptor; PXR: pregnane X receptor; ROR: RAR-related orphan receptor; GATA: GATA binding protein; COUP-TF1: chicken ovalbumin upstream promoter-transcription factor; NF-AT: Nuclear Factor Of Activated T-Cells; AP-1: activator protein 1; USF1: upstream transcription factor; PPAR: peroxisome proliferator-activated receptors; T3R: thyroid hormone receptor; FXR: farnesoid X receptor; VDR: vitamin D receptor; C/EBP: CCAAT/enhancer binding protein; CREB: cAMP responsive element-binding protein; Egr: early growth response protein; SMC1: structural Maintenance of Chromosomes; NR1B1: retinoic acid receptor alpha; SREBP: sterol regulatory element-binding proteins; CREM: CAMP Responsive Element Modulator; ATF: activating transcription factor.

Transcription factor	Transcription factors with binding sites in the gene
HNF1a	RXR-alpha(h), HNF-4alpha(h), (HNF-4alpha(r),), 2HNF-4alpha(r), HNF-4alpha(h), HNF-4alpha1(h),
HNF4a	NF-AT(h), GATA-6(r), GATA-6(h), HNF-6alpha(r), HNF-6(h), SREBP-2(m.s.), RXR-alpha(h), COUP-TF(h), COUP-TF(r), NR1B1(r):RXR-alpha(r), HNF-4alpha(r), COUP-TF2(h), HNF-4alpha(m), HNF-4alpha(h), HNF-4alpha(r), HNF-1alpha(m), HNF-1alpha(m), HNF-1alpha(h), HNF-1alpha(r), ipf1(r), Sp1(h), Sp1(r), HNF-1alpha(h), HNF-1alpha-A(h), HNF-1alpha(r), Sp1(h), SREBP-2(m.s.),
HNF6	-
FOXA1	-
FOXA2	HNF-6(r), HNF-6(m), HNF-6(m), HNF-6(gl), HNF-6(HA), Smad3(m.s.), Smad3(h),
FOXA3	-
CEBPa	HNF-1(h), HNF-4(h), HNF-3(h), USF2(m.s.), usf1(m.s.), USF2(m.s.), usf1(m.s.), HIF-1alpha(h), HIF-1alpha(h), HIF-1alpha(h), USF1(h), AP-2alphaA(h), AP-2alpha(m), Gfi1(r), Gfi1(r),
CEBPb	XBP-1(h), ATF-6(m.s.), FOXO1A(m), FOXO1A(m),
PXR	HNF-4alpha(h), PPARalpha(m.s.), PPARalpha(h),
CAR	GR(h), HNF-4alpha1(h), HNF-4alpha7(h), HNF-4alpha(r), NR1B1(h):RXR-alpha(h),
RXRa	-
FXR	HNF-1alpha(h), STAT1(h), STAT1(h),
LXR	RXR-alpha(h):LXR-alpha(h), RXR-alpha(h):LXR-beta(h), RXR-alpha(h):LXR-alpha(h), RXR-alpha(h):LXR-alpha(h), LXR-alpha(h):RXR-alpha(h), LXR-beta(h):RXR-alpha(h), RXR-alpha(m.s.):LXR-alpha(h), RXR-alpha(h):LXR-alpha(h), PPARgamma(m):RXR-alpha(m),
LXRb	c-Ets-1(m.s.), c-Ets-1(r), Elk-1(m.s.), Elk-1(h), Elk-1(r), SRF(m.s.), SRF(r),
VDR	Cdx-2(m), Cdx-2(h), C/EBPalpha(m.s.), ICER-IIgamma(m.s.), Pit-1(h), JunB(h), c-Jun(h), Fra-1(h), Fra-2(h), FOSB(h), ATF-2(h),
RARa	AR(h), Sp1(h), Sp1(m.s.), Sp1(h), Sp1(h), ER(h), ER(m), NR1B1(m):RXR-beta(m),
LRH-1	ER-alpha(h), ipf1(m), ipf1(m), HNF-1(m.s.), SF-1(r), LRH-1(h), LRH-1(r), SF-1(h), Sp1(h), Sp3(h), Sp3(r), Sp1(r), ipf1(m), ipf1(m), ipf1(m), ipf1(m),

Table 1.4: Transcription factors with binding sites within selected liver enriched transcription factor genes.

Abbreviations: (h): human; (ms) mouse; (r): rat; LXR: liver X receptor; RXR: retinoid X receptor; HNF: hepatic nuclear receptor ; NF-AT: nuclear factor of activated T-cells; GATA: GATA binding protein; SREBP: sterol regulatory element-binding proteins; COUP-TF: chicken ovalbumin upstream promoter-transcription factor; NR1B1: retinoic acid receptor alpha; ipf1: insulin promoter factor 1; Smad3: mothers against decapentaplegic homolog; USF: upstream transcription factor, C-Fos Interacting; HIF-1: hypoxia-inducible factor; Gfi1: growth factor independent 1 transcription repressor; ATF: Activating transcription factor; FOX: Forkhead Box; PPAR: peroxisome proliferator-activated receptors; GR: glucocorticoid receptor; Elk-1: ETS domain-containing protein; SRF: serum response factor; ICER-II: inducible cAMP early repressor; Pit-1: growth hormone factor 1; Fra-1: Activator Protein 1 transcription factor Fos-related antigen 1; AR: androgen receptor; ER: estrogen receptor; SF-1: steroidogenic factor 1.

Aims of thesis

Drug induced liver injury remains a considerable burden on the health sector and pharmaceutical industry. Models which are able to predict these reactions are not currently available, with many large toxicological screens *in vitro* performed in cells with little translational relevance.

Induced pluripotent stem cells have the inherent capacity to form all cells of the human body, including fully functional hepatocytes, thus providing a uniquely expandable and potentially metabolically relevant phenotype for toxicology screens; however, despite incremental improvements using a myriad of differentiation techniques, the caveat remains that this inherent capacity has yet to be 'unlocked' *in vitro*. Given the incomplete epigenetic remodelling which occurs during reprogramming and the various reports of enhanced differentiation capacity in other cell types, the investigation of altered differentiation propensity towards hepatocyte-like cells in iPSCs derived from hepatocytes and other cell types is an area of interest which has yet to be fully assessed is an isogenic context.

The current gold standard for toxicology screening is primary human hepatocytes; however, these cells have several drawbacks, most pertinently, the rapid loss of metabolic phenotype, termed dedifferentiation. Understanding how to culture hepatocytes to best maintain their functional capacity is an area of research which has been ongoing for many years; however, whilst improvements have been reported, the mechanistic understanding of the process remains incompletely understood. The advent of omics technology allows for a global investigation of this process, allowing for novel insights into whole cell changes. Moreover, by further understanding the process of dedifferentiation, the same information may then be used to inform advances in the differentiation protocols used to derive hepatocyte-like cells from pluripotent stem cells.

Another emerging concept in the differentiation of hepatocyte-like cells is the roles of previously non-associated transcription factors, such as Nrf2. The targeting of traditional LETFs during differentiation is well-described; however, emerging evidence points towards additional roles of these non-liver specific/enriched factors, which may have particular relevance to *in vitro* differentiation protocols. Understanding how these can influence the hepatic phenotype is another key question which has not been addressed with regard to hepatocyte-like cells.

Therefore, given the aims outlined above, this thesis will set out to assess the following hypotheses:

Hypothesis 1:

The use of primary human hepatocyte-derived iPSCs to generate hepatocyte-like cells yields an improved maturity in hepatocyte-like cell maturity when compared to HDF-derived iPSCs from the same donor.

Hypothesis 2:

Mechanistic evaluation of the primary human hepatocyte proteome during monolayer culture will yield novel information and hypotheses regarding the dedifferentiation and differentiation of hepatocytes.

Hypothesis 3:

Nrf2 regulates the hepatocyte phenotype during differentiation and dedifferentiation

Chapter 2

Methods

2.1. Methods

Cell type	Media composition	Derived in Liverpool?	Company	Use in thesis	Other
Primary human hepatocytes	Williams E medium 1x Insulin-Transferrin-Selenium 100nM Dexamethasone 2mM L-Glutamine 1x Penicillin/Streptomycin	Yes	N/A	Studying dedifferentiation, Nrf2 in the hepatic phenotype and cellular reprogramming	-
Human dermal fibroblasts	DMEM 10% FBS 2mM L-Glutamine 1x Penicillin/Streptomycin	Yes	N/A	Cellular reprogramming	-
Juvenile dermal fibroblasts	Fibroblast growth medium 2	No	Promocell	Cellular reprogramming	Kind gift from Dr. Michael Cross
Neonatal dermal fibroblasts	DMEM 10% FBS 2mM L-Glutamine 1x Penicillin/Streptomycin	No	ATCC	Cellular reprogramming	-
Mouse embryonic fibroblasts	DMEM 15% ESC-qualified FBS 2mM L-Glutamine 1x Penicillin/Streptomycin	No	GlobalStem	Pluripotent stem cell culture	-
Hues7 (hESCs)	Essential 8 media	No	WiCell	Pluripotent stem cell comparator	Kind gift from Dr. Patricia Murray
iPSCs	Essential 8 media OR DMEM/F12 20% KnockOut Serum replacement 1x Non-essential amino acids 50μM β-mercaptoethanol 0.5x Penicillin/Streptomycin 4ng/ml Basic-FGF	Yes	N/A	Starting cell type comparisons for HLC differentiation and Nrf2 during HLC differentiation	-
HepG2s	DMEM 10% FBS 1x Penicillin/Streptomycin	No	ATCC	Viral titre assessment	-
293FTs	DMEM 10% FBS 1x Penicillin/Streptomycin	No	Life technologies	Virus production	-

Table 2.1: Information regarding the cell types used to generate the data presented in this thesis. Further information regarding the use of these cells and the companies from which the materials were purchased can be found in the text.

2.1.1 Primary cell isolation techniques

Primary human hepatocyte and dermal fibroblast isolation and culture

Liver and skin resections were received as surgical waste (Aintree hospital, Liverpool, United Kingdom) with full patient consent and ethical approval from the relevant institutional review boards (National Research Ethics Service REC ref: 11/NW/0327).

Primary human hepatocytes were isolated using a modified version of the previously described 2-step collagenase method (LeCluyse et al., 2005). Briefly, liver resections were received as surgical waste. The resections were perfused with 4-(2-hydroxyethyl)-1-piperazineethanesulfonic acid (HEPES)-buffered saline (HBS; 10mM HEPES (Sigma Aldrich, St. Louis, MO), 5mM KCl, 136mM NaCl, 0.5% (w/v) glucose (Thermo Fisher Scientific, Pittsburgh, PA), followed by digestion with 0.5mg/ml Collagenase IV (400-600 collagenase digesting units/mg; Sigma Aldrich) in HBS containing 700µM $CaCl_2$ (Thermo Fisher scientific). The capsule was then opened and the digested cells separated using nylon monofilament 125µm (Clarcor UK, Warrington, United Kingdom). The cell suspension was centrifuged twice at 80 x g for 5 minutes at $4^{o}C$, and resuspended in Williams E medium (Sigma Aldrich). Cells were plated onto Collagen-I coated plates (Corning, Corning, NY) at $2.5x10^5$ cells/cm^2 to achieve full confluency in Williams E supplemented with 1% (v/v) insulin-transferrin-selenium (ITS; Life Technologies, Carlsbad, CA), 2mM L-glutamine (Sigma Aldrich), 100nM dexamethasone (Sigma-Aldrich) and 1% (v/v) penicillin (final concentration: 100units/ml)/streptomycin (final concentration: 100µg/ml) (Sigma Aldrich). After 3 hours, non-attached cells were washed away and the culture medium was replaced.

Human dermal fibroblasts (HDFs) were isolated using a previously published protocol (Aasen and Belmonte, 2010). Skin biopsies were cut using scalpel and forceps into approximately $1cm^2$ pieces and placed into a 6 well plate (3 pieces/well). Two drops of

Dulbecco's modified Eagle's medium (DMEM; Sigma Aldrich) supplemented with 10% (v/v) foetal bovine serum (FBS; Life technologies), 2mM L-glutamine and 1% (v/v) penicillin/streptomycin (HDF media) were placed on top of each segment and left to attach overnight. Drops of HDF media were replaced daily to keep the pieces submerged. After 7 days, 1ml of media added/well and changed every 48 hours. After 2 weeks HDF outgrowths were observable. Once confluent, HDFs were detached with 0.05% trypsin (Sigma Aldrich) and expanded for reprogramming and cryopreservation.

2.1.2. hiPSC generation from different somatic cells

Sendai virus reprogramming

PHH were plated on embryonic stem cell (ESC)-qualified Matrigel (Corning) at a density of $1x10^5$ – $5x10^5$ cells/well in a 6 well plate. Cells were cultured in Williams E medium supplemented with 2.5% (v/v) FBS, 50ng/ml hepatocyte growth factor (HGF; Promokine, Heidelberg, Germany), 50ng/ml epidermal growth factor (EGF Life technologies), 15mM HEPES buffer (Sigma-Aldrich), 100nM dexamethasone, 0.2% (v/v) insulin-transferrin-selenium and 0.5% (v/v) penicillin/streptomycin (PHH reprogramming media). Following 3 days of culture, Sendai viruses containing Oct4, Sox2, Klf4 and c-Myc transcription factors (Life technologies) were added at multiplicities of infection (MOI) 3-10. After 24 hours, media was replaced with non-virus containing PHH reprogramming media and culture continued for a further 2 days. Subsequently, cells were then cultured in Essential 6 media (Life technologies) containing basic fibroblast growth factor (bFGF; 100ng/ml; Life technologies) and 0.5% (v/v) penicillin/streptomycin for 25-30 days, replacing the media every 24 hours.

BJ neonatal fibroblasts (CRL-2522, ATCC, Middlesex, United Kingdom) or HDFs were plated in a 6 well plate at $5x10^6$ cells/well or $3x10^5$ cells/ well, respectively. After 48 hours of

culture, cells were transduced with Sendai viruses containing Oct4, Sox2, Klf4 and c-Myc at MOI 3 or 5. After 24 hours, media was replaced and changed every 48 hours for 7 days. On day 7 of reprogramming, cells were trypsinised (0.05% trypsin) and replated onto 10cm^2 dishes coated with mouse embryonic fibroblasts (MEFs; Globalstem, Rockville, MD) or 6 well plates coated with Matrigel. Cells were plated in HDF media which was replaced with either DMEM/F12 media supplemented with 20% (v/v) KnockOut serum replacement media, 1x non-essential amino acids, 50μM 2-mercaptoethanol (Life technologies) and 0.5% (v/v) penicillin/streptomycin on MEF cultures or Essential 6 media supplemented 100ng/ml basic-FGF (Life technologies) for Matrigel cultures. Media was changed daily and colonies formed from day 21 onwards.

iPSC clone isolation, expansion and culture

Colonies from PHH and fibroblast cultures formed between days 25 and 40 and were picked using a dissection microscope (EVOS XL Core Cell Imaging System; Life technologies). Clones expanded and maintained on either Matrigel with Essential 8 media (Life technologies) or MEFs with DMEM/F12 supplemented with 20% (v/v) KnockOut serum replacement media, 1x non-essential amino acids, 50μM 2-mercaptoethanol and 0.5% (v/v) penicillin/streptomycin.

Cells were split using gentle cell disassociation reagent (GCD; Stem cell technologies; Vancouver, Canada) according to the manufacturer's protocol. Briefly, differentiated cells were removed using a dissection microscope. Cells were then washed once with 1ml GCD and then incubated in 1ml GCD at room temperature for 5-8 minutes. Once breaks in cell adhesion were observable using light microscopy, GCD was removed and 2mls stem cell media added. Cells were then removed from the plate and suspended in the media using a cell scraper (Greiner bio-one, Monroe, NC). For feeder-free, cells were transferred directly to Matrigel coated plates; for feeder dependent cultures, cells were transferred to 15ml

tube (Greiner bio-one) and iPSCs and feeder cells separated by allowing the larger MEFs to settle to the bottom of the tube and transferring the remaining cell suspension to freshly plated MEFs. Depending on cell confluence and line, iPSCs were split 1:3 to 1:10.

MEFs were plated 24 hours prior to iPSC splitting. For 6 well plates, 1ml attachment factor (Life technologies) was added to each well and incubated at 37^{o}C for 30 minutes. MEFs were taken from liquid nitrogen storage and submerged in a 37^{o}C water bath until vial contents were mostly defrosted. Subsequently, the vial contents was transferred to a 15 ml tube and 5ml MEF medium (DMEM, 15% (v/v) ESC-qualified FBS (Life Technologies), 2mM L-glutamine and 1% (v/v) penicillin/streptomycin) was added drop-wise. Cells were centrifuged at 200 x g for 5 minutes. The cell pellet was resuspended and counted using trypan blue exclusion. Cells were plated at 3x10^{4} cells/cm^{2}.

miR302/367 lentivirus production and transduction

PCR reactions were performed using forward and reverse primers for miR-302/367 sequence (Forward: TGG CTT AAC AAT CCA TCA CCA TTG; Reverse: GGG TAA AAG GCA GGG ACT TCA GCC; Eurofins, Luxembourg), and template DNA isolated from Hues8 and Panc2 cell lines. These reactions were performed using the GeneAmp PCR system 9700 thermal cycler system (Applied biosystems, Waltham, MA) using the following conditions: 94^{o}C for 5 minutes followed by 35 cycles of: 94^{o}C for 1 minute, 57^{o}C for 1 minute, 72^{o}C for 2 minutes and 72^{o}C for 8 minutes, followed by a 4^{o}C hold.

Once amplified, the samples were separated by ethidium bromide agarose gel electrophoresis (1% (w/v) agarose (Thermo Fisher Scientific) gel, 70pM ethidium bromide (Sigma-Aldrich)) and visualised using a EC3 gel imaging system with transilluminator (Ultra-Violet Products, Cambridge, United Kingdom). The sample was then manually extracted from the gel using a UV light box and cleaned using the gel extraction kit (QIAgen Venlo,

Netherlands), following the manufacturer's protocol. The following steps were then performed using the pCR8/GW/TOPO TA Cloning Kit (Life technologies). Briefly, 3' overhangs were added to the PCR product using TAQ polymerase at 72^{o}C for 10 minutes. The product was then immediately incubated for 5 minutes at room temperature for insertion into the TOPO entry vector.

The TOPO vector was then used to transform one shot competent E.coli. Briefly, a mix of TOPO vector containing the miR302/367 PCR product and E. coli was heat shocked for 30 seconds at 42^{o}C. 250µl of SOC medium was then added and incubated at 37^{o}C and 200rpm in a rotating incubator for 1 hour. Transformed E. coli was then spread across 100µg/ml spectinomycin (Sigma-Aldrich) containing agar plates and incubated at 37^{o}C overnight. Following growth, 10 colonies were picked and grown in spectinomycin (100µg/ml) containing Lysogeny broth (LB) broth (Sigma-Aldrich) overnight at 37^{o}C, rotating at 200rpm.

Plasmids were extracted using QIAgen extraction kit and assessed by restriction digest by incubating the plasmid at 37^{o}C for 2 hours with the ECOR1 and KPN1 enzymes (Promega, Madison, WI). The digested samples were then run on a 1% (w/v) agarose gel containing ethidium bromide for assessment of integration. Plasmids with the correct digestion patterns were sent for sequencing (Eurofins).

Plasmids with greatest homology to the target sequence (>99%) were chosen and subsequently transferred to the pLenti6/V5-DEST entry vector (Life technologies). Briefly, chosen clones were incubated with the entry vector at 37^{o}C for 90 minutes. Transformed E. coli was derived as previously described and then spread across (100µg/ml) ampicillin (Sigma-Aldrich) agar plates. Clones were then picked and incubated at 37^{o}C in a rotating incubator at 200rpm overnight in LB broth containing 100µg/ml ampicillin. Plasmids were subsequently isolated using the QIAgen extraction kit.

The extracted plasmids were then subjected to restriction digest analysis using the enzymes Xho I and Afl II (Promega) in and incubated at 37^{o}C for 90 minutes. The resulting products were assessed using an ethidium bromide containing 1% (w/v) agarose gel and the correct digestion patterns identified. Selected plasmids were then sent for sequencing analysis (Eurofins) and the correctly sequenced plasmids then further expanded and isolated using QIAgen MaxiPrep kit.

Production of lentiviral particles

Lentivirus particles were produced in accordance with commercially available ViraPower™ Lentiviral Expression Systems kit (Life technologies). 293FT cells were cultured in DMEM supplemented with 10% (v/v) FBS, 2mM L-glutamine 1% (v/v) penicillin/streptomycin and 1x non-essential amino acids. Briefly, 293FT cells were plated in a 10cm^2 plate at 5x10^6 cells/plate. The following day, cells were transfected 9µg of packaging plasmid and 3µg of plasmid with Lipofectamine 2000. After 24 hours, media replaced and cultured for a further 24 hours before collection of virus containing media. Viral supernatant was concentrated using a 45µm PVDF filter with centrifugation (Merck Millipore, Billerica, MA).

Blasticidin (Life technologies) and polybrene (Sigma-Aldrich) toxicity assays were performed using concentrations ranging from 0-10µg/ml. Cells were plated at 2.5x10^4 cells/well in a 24 well plate. Following 24 hour culture, media was changed to polybrene and blasticidin containing growth media respectively. polybrene was examined following 1 and 3 days of culture. Blasticidin toxicity was examined over 14 days with media replenished every 3-4 days.

HepG2s were used to titre the viral supernatant and were cultured in DMEM supplemented with 10% (v/v) FBS and 1% (v/v) penicillin/streptomycin. Cells were plated at 2x10^5 cells/well in a 6 well plate. 24 hours later, cells were transduced with the virus at 10^{-2}, 10^{-3},

10^{-4}, 10^{-5} and 10^{-6} with 6µg/ml polybrene. Following 24 hour incubation, the virus containing media was removed and replaced with normal growth media and cultured for a further 24 hours. Subsequently, cells were cultured in media containing 4µg/ml blasticidin. These cells were cultured for 14 days and the media was changed every 3-4 days. After 14 days, media was removed and 1% (w/v) crystal violet (Sigma Aldrich) in 10% (v/v) ethanol was added to the cells for 10 minutes. Stained wells were washed with Dulbecco's phosphate-buffered saline (DPBS) and colonies forming units (CFU) counted and multiplicity of infection (MOI) was determined using the formula below:

MOI = the volume of the virus used (ml) x virus titre (CFU/ml) / cell number

miR302/367 lentivirus reprogramming followed a previously published protocol (Anokye-Danso et al., 2011). Briefly, PHH and human neonatal fibroblasts in their corresponding media and juvenile dermal fibroblasts (jHDFs; a kind gift from Dr. Michael Cross; C-12300, Promocell, Heidelberg, Germany) in fibroblast growth medium 2 (Promocell) were plated at $1x10^5$ cells/well in 6 well plates. The following day, cells were transduced in the presence of polybrene (6µg/ml). Following 2 days of transduction, viral media was removed and cells trypsinised, centrifuged, resuspended in stem cell medium and placed onto MEF coated 6 well plates. Media was changed every 24 hours.

Reprogramming using the direct transfection of miRNAs

Optimising transfection conditions using BlockIT fluorescent oligonucleotide

HepG2s, jHDFs and PHH were plated at a range of densities/conditions and transfected with 100nM BlockIT fluorescent transfection reagent (Life technologies) for between 4 and 24 hours with Lipofectamine RNAimax (Life technologies). Fluorescence was detected using Axio Observer Z1 fluorescence microscope (Carl Zeiss) 24 hours after transfection. Transfection efficiency was estimated using ImageJ cell counting (Schneider et al., 2012).

Transfecting cells with miR-302a/b/c/d, miR-369-3p/5p and miR-200

Transfections were performed as previously described by Miyoshi *et al.,* (Miyoshi et al., 2011). Briefly, cells were plated at $1x10^5$ cells/well in a 24 well plate in standard culture media. Following culture for 24 hours, cells were transfected with each of the 7 microRNAs (10-30nm; Thermo Fisher Scientific) using Lipofectamine RNAiMAX (Life technologies) for either 4 or 24 hours. This was repeated every 48 hours for 4 cycles. After 8 days, cells were transferred to stem cell culture and maintained for up to 40 days. Any changes in morphology were monitored closely using light microscopy.

Embryonic stem cell comparator

The embryonic stem cell line, Hues7 was a kind gift from Dr. Patricia Murray. These cells were cultured on Matrigel coated plates in Essential 8 media and used as a positive control for the characterisation and embryoid body studies.

2.1.3 Hepatocyte-like cell differentiation

Optimisation of single cell plating and definitive endoderm generation

The neonatal fibroblast-derived iPSC line Liv1W was cultured on Matrigel in Essential 8 media. Cells were disassociated using Accutase (Life technologies) and plated at $5x10^4$, $1x10^5$ and $1.5x10^5$ cells/cm^2 onto Matrigel coated 48 well plates in RPMI media (Life technologies) supplemented with 1x B27 (Life technologies), 100ng/ml Activin A and 50ng/ml Wnt3a (RnD systems, McKinley Place, MI) and 10 μM Y-27632 Rho-associated protein kinase inhibitor (ROCK inhibitor; Merck Millipore). After 24 hours, cells were cultured in the plating media without ROCK inhibitor for three to five days in various combinations of Activin A and Wnt3a. Cells were then fixed and examined for SOX17 expression by immunofluorescence. The differentiation efficiency was estimated by

ascertaining the percentage of positive cells using ImageJ cell counting plugin across 10 images taken of each condition.

Optimisation of hepatocyte-like cell differentiation

Cells were cultured on Matrigel in Essential 8 media. Upon confluence, cells were washed once with DPBS and disassociated with Accutase at 37^{o}C for ~5 minutes (until cell detachment was observed). Accutase was then diluted with RPMI media supplemented with 0.5% (v/v) penicillin/streptomycin and 1x B27 supplement. Cells were then centrifuged at 200 x g for 5 minutes and re-suspended in RPMI media supplemented with 1x B27, 0.5% (v/v) penicillin/streptomycin and 10µM ROCK inhibitor. Cells were the counted and plated at 1.5x10^{5} cells/cm^{2} on Matrigel coated 24 well plates in RPMI media supplemented with 1x B27, 0.5% (v/v) penicillin/streptomycin, 10µM ROCK inhibitor, 100ng/ml Activin A and 50ng/ml Wnt3a. At this point, several protocols were adapted and compared for the differentiation of iPSCs to HLCs for comparison (figure 2.1) (Chen et al., 2013; Kajiwara et al., 2012; Sullivan et al., 2010).

Sullivan protocol: following overnight plating, cell media was replaced daily with RPMI

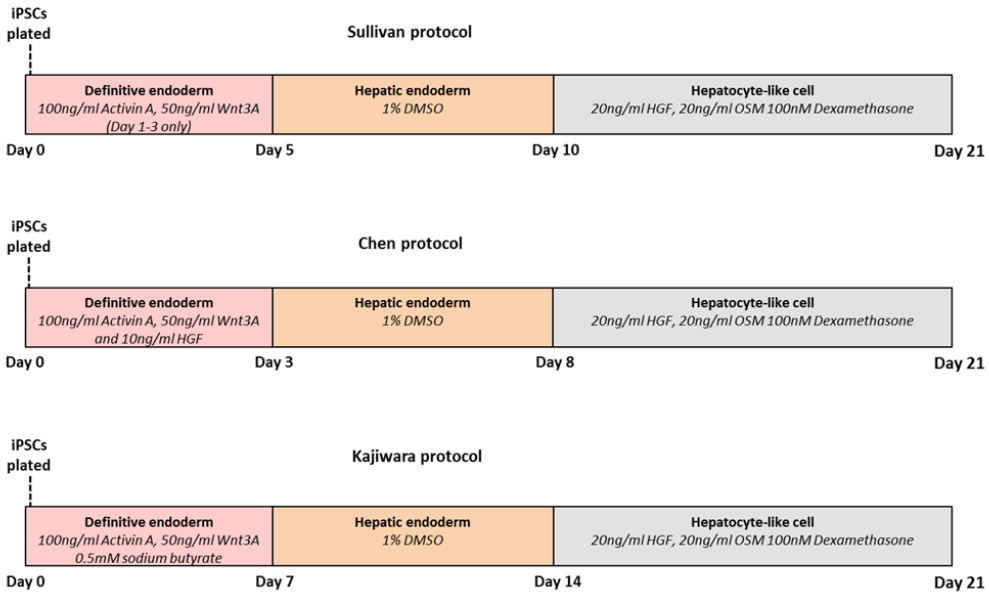

Figure 2.1: Schematic representation of the protocols used to compare HLC differentiation.

media containing 1x B27, 100ng/ml Activin A and 50ng/ml Wnt3a. After 3 days, Wnt3a was omitted from the media for a further 2 days. At day 5, media was replaced with KnockOut DMEM (Life technologies) containing 20% (v/v) KnockOut serum, 1mM L-glutamine, 0.5% (v/v) penicillin/streptomycin, 1x non-essential amino acids, 100µM 2-mercaptoethanol and 1% (v/v) dimethyl sulfoxide (DMSO; Thermo fisher scientific). Media was changed every 48 hours for 5 days. At day 10, media was replaced with Hepatozyme culture media (Life technologies) supplemented with 0.5% (v/v) penicillin/streptomycin, 20ng/ml HGF, 20ng/ml oncostatin M (OSM; Promokine) and 100nM dexamethasone.

Chen protocol: HGF (10ng/ml) included during the three day definitive endoderm culture. The differentiation conditions were then the same as the Sullivan protocol, with the exception of a 14 day maturation phase.

Kajiwara protocol: sodium butyrate (0.5mM; Sigma Aldrich) was added for a 7 day definitive endoderm differentiation stage. Both the hepatic endoderm and maturation stages used the same conditions as the Sullivan and Chen protocols; however, both stages were 7 days. Media was changed and collected every 48 hours before lysing for comparisons at day 22.

Differentiation to hepatocyte-like cells

Cells were transferred to Matrigel culture 1:1 from MEF culture and cultured in Essential 8 media. Upon confluence, cells were washed once with DPBS and disassociated with Accutase at 37^{o}C for ~5 minutes (until cell detachment is observed). Accutase was then diluted with RPMI media supplemented with 0.5% (v/v) penicillin/streptomycin and 1x B27 supplement. Cells were then centrifuged at 200 x g for 5 minutes and re-suspended in RPMI media supplemented with 1x B27 and 10µM ROCK inhibitor. Cells were then counted and plated at 1.5x10^{5} cells/cm^{2} on Matrigel coated 24 well plates in RPMI media supplemented

with 1x B27, 0.5% (v/v) penicillin/streptomycin, 10μM ROCK inhibitor, 100ng/ml Activin A and 50ng/ml Wnt3a. Following overnight plating, cell media was replaced daily with RPMI media containing 1x B27, 0.5% (v/v) penicillin/streptomycin, 100ng/ml Activin A and 50ng/ml Wnt3a. After 3 days, Wnt3a was omitted from the media for a further 2 days. At day 5 media was replaced with KnockOut DMEM media containing 20% (v/v) KnockOut serum, 1mM L-glutamine, 0.5% (v/v) penicillin/streptomycin, 1x non-essential amino acids, 100μM 2-mercaptoethanol and 1% (v/v) DMSO. Media was changed every 48 hours for 7 days. At day 12, media was replaced with HepatoZyme culture media supplemented with 2mM L-glutamine, 0.5% (v/v) penicillin/streptomycin, 20ng/ml HGF, 20ng/ml OSM and 100nM dexamethasone. At day 22, cells were lysed for HLC comparisons. Samples were also taken at definitive endoderm (day 5) and hepatic endoderm (day 12) stages.

Spontaneous differentiation assays

Cells in 6 well plate format were disassociated using gentle cell disassociation reagent and scraped in to DMEM/F12 media supplemented with 20% (v/v) KnockOut serum, 1x non-essential amino acids, 100μM 2-mercaptoethanol, 0.5% (v/v) penicillin/streptomycin and 10μM ROCK inhibitor. MEFs were removed by gravitational separation and cells plated in 12 well non-tissue culture treated plates (Corning) in triplicate (1:1 ratio). After 24 hours cells were resuspended and transferred to a new plate to reduce attachment. Media changed every 48 hours without ROCK inhibitor. For gene expression comparisons, cells were cultured for 16 days before lysing in QIAzol (QIAgen). For characterisation experiments, cells were cultured for 7 days, before transfer to attachment factor-coated 48 well tissue-culture treated plates for re-attachment. Cells were cultured for a further 7 days, before fixing with 4% (v/v) PFA for immunofluorescence assessment.

2.1.4 Proteomic assessment of PHH during culture

Isobaric tags for relative and absolute quantitation (iTRAQ) analysis

Freshly isolated PHH samples were collected directly after isolation, before cells were plated. Samples were centrifuged at 80 x g for 5 minutes and lysed in 100µl iTRAQ buffer. 24, 72 and 168 hour timepoints were collected directly from 6 wells of a 24 well plate in a total of 100µl iTRAQ buffer. Protein concentration was determined by Bradford assay. Protein lysates derived from five donors were labelled according to the manufacturer's instructions (Applied Biosystems, Foster City, CA). 100µg protein in 20µl of iTRAQ buffer was denatured and the protein cysteine residues reduced with tris(2-carboxyethyl)phosphine for 1 hour at 60°C, and subsequently capped with methylmethanethiosulfate, before overnight digestion with reconstituted trypsin at 37°C. Isopropanol was then added to each sample, before labelling with differentially-weighted isobaric tags for 2 hours, at room temperature. The labelled samples were then pooled and made up to 5ml with 10 mM potassium dihydrogen phosphate/25% (w/v) acetonitrile. The pH was then adjusted using concentrated phosphoric acid to <pH3, before cation-exchange chromatography, followed by tandem mass spectrometry (MS/MS) of peptide-rich fractions was performed on a QSTAR Pulsar I hybrid mass spectrometer (AB Sciex, Framingham, MA) (Rowe et al., 2013; Rowe et al., 2010). Samples were run across three 8-plex iTRAQ runs and results obtained relative to each donor's fresh sample to control for inter-donor variation.

Transcription factor binding analysis

Mapper$_2$ online software was used to compare the predicted transcription factor binding sites (Marinescu et al., 2005). Analysis was completed using the collated database, analysing the sequence of each gene 2000 base pairs upstream of the transcription start

site. The number of proteins of interest which interacted with each predicted transcription factor was then compared to determine the significance of each factor. Those factors which demonstrated enriched predicted binding within a subset of proteins (≥4 proteins) were classed as factors of interest.

2.1.5 Mitochondrial assessment of PHH during culture

Seahorse functional mitochondrial assay

PHH were cultured on collagen-I coated (Life Technologies; 50 µg/ml in 0.02M acetic acid), XF 96-well cell culture microplates (Seahorse biosciences, North Billerica, MA; $2.5x10^4$ cells/ well). OXPHOS stress test medium (Seahorse biosciences) was supplemented with 25mM D-glucose, 2mM L-glutamine and 1mM sodium pyruvate. The glycolytic stress test medium (Seahorse biosciences) was prepared by adding 2mM L-glutamine. Both media were pre-warmed to 37°C. PHH culture medium was removed and replaced with OXPHOS or glycolytic stress test medium. Cells were incubated in a CO_2 free incubator at 37°C for 1 hour. 1µM oligomycin, 0.25µM Carbonyl cyanide-p-trifluoromethoxyphenylhydrazone (FCCP) and 1µM rotenone-antimycin-A (OXPHOS stress test) and 25mM glucose, 1µM oligomycin, and 100mM 2-deoxyglucose solutions (glycolytic stress test) were prepared. Prior to the rate measurements, the XFe96 Instrument (Seahorse biosciences) allowed the oxygen partial pressure to reach equilibrium. The oxygen consumption rate (OCR) and extracellular acidification rate (ECAR) were measured simultaneously three times to establish a baseline rate. After each compound injection, conditions were allowed to return to normal oxygen tension and pH. The OCR and ECAR measurements for each well were recorded and reported as pmol/min and mpH/min, respectively by XF Wave software (Seahorse biosciences). Results were displayed as a percentage of maximal OCR and ECAR or as relative fold change of each parameter between time points.

Rotenone assay

PHH were plated at $1x10^5$ in 96 well Collagen-I coated plates. At 24 and 168 hours, serial concentrations (0-20mM) of rotenone (Sigma Aldrich) were made in DMSO. Then the compound solutions were added to culture media at 1/200 (v/v) ratio to make final dosing concentrations of 0-100µM (0.5% (v/v) DMSO). Culture media was removed and replaced with the media containing rotenone. Following incubation for 2 hours (37°C, 5% CO_2), ATP content was assessed using the Cell-titre glo assay (Promega), according to the manufacturer's instructions. Briefly, 30µl of ATP reagent was added to each well containing 100µl of media. The plate was shaken (1 minute), then 100µl of the well content was transferred to a white 96 well plate and the ATPase luminescence was measured using a plate reader (Varioskan, Thermo Fisher Scientific). Results were presented as percentage of control.

2.1.6 Pyrosequencing of PHH and iPSCs

DNA was extracted using the QIAamp DNA mini kit (QIAgen). Briefly, samples were defrosted and lysed with 300µl lysis buffer and 5µl RNAse (QIAgen). Samples were then heated 56^{o}C for 15 minutes in a heat shaker followed by the addition 30µl protease and heated at 56^{o}C for a further 15 minutes. 300µl of ETOH (Sigma-Aldrich) was then added and the samples vortexed, transferred to spin columns and centrifuged 14000 x g for 2 minutes at room temperature. Flow through was discarded and columns washed with supplied buffers. Extracted DNA was then eluted by placing filter into 1.5ml collection tube and adding 100µl of AE buffer. The filter was left to soak for 5 minutes before spinning at 14000 x g for 2 minutes. Samples were then transferred to 500µl PCR tube and analysed using a NanoDrop spectrophotometer (Thermo Fisher Scientific).

Each sample was adjusted to 250ng sample DNA in 20µl distilled H_2O. Samples were then bisulphite converted using the EZ DNA Methylation-Gold kit (Zymo, Irvine, CA) according to manufacturer's protocol. Briefly, 130µl CT conversion reagent was added to each sample before briefly spinning and heating at 96°C for 10 minutes and 56°C for 5 hours using a GeneAmp PCR system 9700 thermal cycler. Upon completion, 600µl binding buffer was added to 1.5ml tubes and the conversion mix added. The sample-binding buffer mix was then added to columns attached to a vacuum pump to pull the mix through the column filter. The filter was washed with 500µl wash buffer and then soaked for 20 minutes in 200µl desulphonation buffer at room temperature before being washed twice with 500µl wash buffer. Samples were then eluted by adding 25µl elution buffer directly onto the spin column membrane and soaking for 15 minutes. Samples were then spun at 14000 x g for 5 minutes and transferred to PCR tubes.

Genes with CpG islands within the promoter region were ascertained using the NCBI gene information and the online tool CpG island searcher (http://cpgislands.usc.edu/) using the default search settings. PCR and pyrosequencing primers (sequencing, biotinylated and non-biotinylated) were designed using the QIAgen pyrosequencing primer design tool and purchased from Eurofins (table 2.2). These primers were reconstituted to 100pmol/µl (10mM Tris-HCl pH 8.0, 1mM Ethylenediaminetetraacetic acid (EDTA) and 50% (v/v) Glycerol; Sigma Aldrich) and optimised using multiple annealing temperatures and assessed by 2% (w/v) agarose gel with 3µl/100ml SafeView (NBS Biologicals, Huntingdon, United Kingdom). PCR reactions products were then generated for all primer sets using the optimised conditions. Briefly, 3µl 10x Coral load buffer, 1.2µl 5nM DNTPs, 0.15µl Taq polymerase (All QIAgen) and 1.5µl primer mix (7.5µl non-biotinylated primer, 3.5µl biotinylated primer and 88.75µl ddH_2O) was made up to 27µl with 21.15µl PCR-grade H_2O per reaction. 3µl of each sample was then added and the PCR run on a GeneAmp PCR system 9700 thermal cycler as follows: 95°C for 10 minutes then 40 cycles of 94°C for 30

seconds, 50-55^{o}C for 30 seconds, 72^{o}C for 30 seconds followed by 72^{o}C for 10 minutes, then a hold at 4^{o}C. Samples were then checked for correct size and specificity using a 2% (w/v) agarose gel with SafeView. Images were taken using a EC3 gel imaging system with transilluminator. (Ultra-Violet Products, Cambridge, United Kingdom).

Successfully generated PCR products were then subjected to pyrosequencing using reagents from QIAgen. Briefly, 75µl of binding buffer containing streptavidin beads (50µl binding buffer, 1.25µl streptavidin beads, 23.75µl dH_2O/sample) were added to each sample and the resulting mixture transferred to a 96 well plate and vortexed for 10 minutes. The sequencing primer mix was then made (43.5µl annealing buffer and 1.5µl 10µM sequencing primer) and put into another 96 well plate (QIAgen). Samples were then run through the Pyromark q96 workstation (QIAgen) vacuum system to wash the beads-PCR complexes through a sequence of 70% (v/v) ETOH, 0.2M NaOH and 10mM Tris acetate. The resulting samples were then added to the 96 well plate (QIAgen) containing the sequencing primer-annealing buffer mix and heated at 80^{o}C for 2 minutes. The samples are allowed to cool for 2 minutes before placing into the PyroMark Q96 ID pyrosequencing (QIAgen) machine and running the assay designed with the primer design software (QIAgen).

	Name	Sequence 5-3	Modification
↘	CYP2E1meth-Fb	ATATGGATATTAGTAGGAGGAAGG	5’ biotin
←	CYP2E1meth-R	TCCCTTTCCACAAAATTATC	
←	CYP2E1meth-S	TTTCCACAAAATTATCTC	
↘	HNF1ameth-Fb	TTAGTTTGGTTAATATGGTGAA	5’ biotin
←	HNF1ameth-R	CCAATAAAACAATCTTAACTCACTAC	
←	HNF1ameth-S	AATAAAACAATCTTAACTCAC	
↘	HNF4ameth-F	TGGGTGATTAGAAGAATTAATAAG	
←	HNF4ameth-Rb	CAACACAACCACCAAAAAC	5’ biotin
→	HNF4ameth-S	TGATTAGAAGAATTAATAAGATA	
↘	C/ebpameth-F	TTGGAGATTAGAGTTAGGAGA	
←	C/ebpameth-Rb	AACCAAAACCAAACCTATC	5’ biotin
→	C/ebpameth-S	GGAGATTAGAGTTAGGAG	
↘	FOXA2meth-F	TGTGATTGAAAAGTAATTTTGAA	
←	FOXA2meth-Rb	CAAACAACCCCTCTAACAAC	5’ biotin
→	FOXA2meth-S	GAAAAGTAATTTTGAAATA	
↘	CK18meth-F	TTTAGGTGGAGGAGGTGT	
←	CK18meth-Rb	CCCAAAATACTAAAATTACAAAC	5’ biotin
→	CK18meth-S	TTAGGTGGAGGAGGTGTT	
↘	HNF6meth-F	GTAATAGAGTTATGGTTTAAGTTG	
←	HNF6meth-Rb	GTTCTTAAAATTCTAAAATCTCC	5’ biotin
→	HNF6meth-S	AGTTATGGTTTAAGTTGGT	
↘	HNF1a-new-F	GTTTGGAGTGTAGTGGAGTAA	
←	HNF1a-new-Rb	ACCTATAATCCCAACTACTCC	5’ biotin
→	HNF1a-new-S	TAATTTTGGTTTATTGTAA	
→	CYP2E1meth-S2	TCCACAAAATTATCTC	

Table 2.2: Primer sequences used for pyrosequencing analysis.

→: Sequencing primer; ↘: Forward primer; ←: Reverse primer; ←/↝: Biotinylated primer.

2.1.7 Manipulation of Nrf2 in PHH and HLCs

Non-Liverpool derived cell types were supplied as part of various consortia for collaborative work. The University of Bath supplied Shef3 ESC cells and corresponding HLCs generated as previously described (Bone et al., 2011) as part of the Stem Cells for Safer Medicines consortium (SC4SM). Cellectis supplied the ChiPSC-18 iPSC line and HLCs differentiated using a proprietary protocol as part of the MIP-DILI consortium.

CDDO-me supplementation of PHH during culture

PHH were isolated as described previously. For media supplementation, 100nM bardoxolone methyl (CDDO-me; Cayman Chemical, Ann Arbor, MI) was added to media at plating whereas control conditions were cultured as normal. Media, with or without CDDO-me supplementation, was replaced every 24 hours and samples taken at 24, 48, 72 and 168 hours in RIPA buffer (Sigma Aldrich).

Inducing naïve PHH with CDDO-me at set timepoints during culture

PHH isolated and plated as previously described. At 24, 48, 72 and 168 hours cells were dosed with 100nM CDDO-me or 0.5% (v/v) DMSO respectively for 2 hours. Cells were subsequently lysed with RIPA buffer.

siRNA transfection during HLC differentiation

Liv1W iPSCs were differentiated using the optimised HLC differentiation protocol described previously. At the hepatic endoderm stage cells were transfected with 20nM Nrf2 siRNA SMARTpool (Dharmacon, Lafayette, CO). For reverse transfection Lipofectamine RNAiMAX-siRNA complexes were prepared and added to Matrigel coated plates. H.E cells were then detached using sequential incubation with 0.02% (v/v) EDTA (Sigma Aldrich) for 5 minutes followed by AccuMAX (Merck Millipore) for 20 minutes at 37^{o}C. Detached cells were then

centrifuged at 100 x g. The resulting cell pellet was resuspended, counted using trypan blue exclusion and replated at $2x10^5$ cells/cm^2 in the HLC maturation media with 10μM ROCK inhibitor. Forward transfection complexes were prepared as described and added directly to H.E cells. Lipofectamine RNAiMAX only conditions used as a vehicle control. Media was replaced after 24 hours and cells lysed with RIPA buffer 48 hours later. For multiple transfections during HLC maturations, cells were forward transfected as described above on day 12 and 17 (for x 2 transfections) or day 12, 15 and 18 (for 3x transfection). Samples were collected for comparison at day 22 of culture.

CRISPR/Cas9 knockout of Nrf2 in A549s and iPSCs

A549 cells were cultured in DMEM supplemented with 10% (v/v) FBS and 1% (v/v) penicillin/streptomycin. iPSCs were cultured on Matrigel as previously described. Puromycin concentration for selection was established by plating the iPSCs and A549s at 80-90% confluence in 24 well plates. 24 hours after plating, 0, 0.5, 1, 1.5, 2, 4, 6, 8 and 10μg/ml puromycin concentrations were tested in triplicate and cell viability assessed by phase contract light microscopy.

Optimisation of clustered regularly interspaced short palindromic repeats (CRISPR)/Cas9 transfection was achieved using a non-coding CRISPR/Cas9 plasmid (Santa Cruz) using the manufacturer's protocol. Briefly, A549s were plated at ~80% confluency. The following day, cells were transfected with 250ng of the control plasmid using UltraCruz transfection reagent. 48 hours later, cells were visualised by fluorescence microscopy to confirm transfection via the expression of the GFP tag. iPSCs were plated at $1x10^5$ and $1.25x10^5$ cells/cm^2 and transfected with 250ng plasmid with or without 1% (v/v) DMSO using three different methods: forward-transfection, reverse-transfection and modified reverse-transfection. Modified reverse transfection protocol involved plating the transfection complexes at the same time as the Matrigel to immobilise the complexes and plating the

iPSCs 1 hour later. In all conditions, cells were plated on Matrigel in the presence of 10µM ROCK inhibitor. UltraCruz and Lipofectamine 3000 reagents were used according to the manufacturer's protocols with plasmid transfection (Santa Cruz) or Opti-MEM (Life technologies) media, respectively. Transfection efficiency was estimated 48 hours later using fluorescence microscopy to investigate the expression of the GFP reporter tag.

For Nrf2 knockdown, A549s were plated at 80% confluence in a 6 well plate. 24 hours later, cells were transfected with 2.5µg CRISPR/Cas9 and 2.5µg of the homology directed repair (HDR) plasmid using UltraCruz transfection reagent. Media was replaced after 48 hours. 96 hours after transfection 1.5µg/ml puromycin was added to the A549s. After 20 days of culture colonies of cells were notable throughout the well. These were picked using a dissection microscope out of the well and placed into 24 well plate wells for expansion.

For iPSC knockdown, cells were plated on Matrigel in a 6 well plate at $1x10^5$ and $1.25x10^5$ cells/cm^2 in Essential 8 flex media (Life technologies) supplemented with 10µM ROCK inhibitor. After 24 hours, cells were transfected with 2.5µg Nrf2 CRISPR/Cas9 plasmid and 2.5µg HDR plasmid. Media was replaced after 48 hours. 96 hours after transfection, 0.5µg/ml puromycin was added to the media and light microscopy used to determine if any successfully generated clones were derived. After 30 days, immunofluorescence live staining with Tra-1-60 was used to determine if any clones were visible.

2.1.8 Sample end-point analysis

Immunofluorescence

Cells were fixed with 4% (w/v) paraformaldehyde (Sigma Aldrich) for 15 minutes and subsequently washed three times with DPBS buffered with $MgCl_2$ and $CaCl_2$ (DPBS+; Life technologies). Fixed cells were blocked with DPBS+ supplemented with 10% (v/v) donkey serum (Sigma Aldrich) and 0.01% (v/v) Triton X-100 (Sigma Aldrich) for 30 minutes. Primary

antibodies were diluted (table 2.3) in DPBS+ containing 1% (v/v) donkey serum 0.01% (v/v) Triton X-100 and incubated overnight at 4^{o}C. Cells were washed three times with DPBS+ and alexafluor secondary antibody diluted 1:750 in DPBS+ supplemented with 1% (v/v) donkey serum with 0.01% (v/v) triton X-100 added and incubated at room temperature for 2 hours. Cells were washed three times and Hoechst 33342 stain (1mg/ml; Sigma Aldrich) added at a 1:7500 dilution in DPBS+ (final concentration: 133.3ng/ml) for 10 minutes. Cells washed three times and imaged using the Axio Observer Z1 fluorescence microscope with the AxioCam MR digital camera. Images processed using Zen lite software (Carl Zeiss).

For albumin staining, 10x blocking buffer (Abcam, Cambridge, United Kingdom) was used to replace donkey serum. Staining with Tra-1-60 and SSEA-4 conjugated antibodies performed without triton x-100 and with a single 90 minute incubation at room temperature following blocking with 10% (v/v) donkey serum in DPBS+.

Western blotting

Samples collected in iTRAQ or RIPA buffer were quantified by Bradford assay and assessed by western blot to validate iTRAQ results. Briefly, 5-40µg samples were denatured at 80^{o}C in Laemmli sample buffer (Sigma Aldrich), separated in 10% hand-cast polyacrylamide gels (running buffer: Tris: 15mM, glycine: 115mM and sodium dodecyl sulphate (SDS): 2mM; Thermo Fisher Scientific) and then transferred (transfer buffer: glycine: 200mM, tris: 25mM, 20% (v/v) ETOH) to nitrocellulose membranes (G.E Healthcare, Buckinghamshire, United Kingdom). Following 1 hour blocking in 10% (w/v) milk (Bio-Rad, Hercules, CA), primary antibodies (table 2.3) were added overnight or for 15 minutes (β-actin). Following washing, secondary antibodies (table 2.3) were subsequently added for 1 hour. Membranes were then washed and visualised using chemiluminescence. Washing, block and antibodies were made up in Tris buffered saline (NaCl: 150mM, KCl: 3mM, Tris: 25mM; Thermo Fisher Scientific) with 0.1% (v/v) tween-20 (Thermo Fisher Scientific). Samples were

normalised against β-actin wherever possible; however, during differentiation and dedifferentiation, ponceau red (Sigma-Aldrich) was used to confirm equal loading as β-actin showed differential expression.

Nrf2 western blots were performed as above with the following alterations. 4-12% pre-cast NuPAGE gels (Life technologies) were loaded with samples denatured in NuPAGE LDS sample buffer (Life technologies) and NuPAGE sample reducing reagent (Life technologies) in a 7:3 ratio. Gels were run in MOPs buffer (MOPs: 50mM, Tris: 50mM, SDS: 3.5mM, EDTA: 1mM; Thermo Fisher Scientific). The membrane was blocked overnight and the primary antibody (table 2.3) incubated for 3 hours.

Use	Antibody	Company	Dilution	Secondary	Dilution
Immunofluorescence	Oct4	Abcam	1:100	Anti-rabbit alexafluor 488	1:750
	Sox2	Abcam	1:100		
	Nanog	Abcam	1:100		
	AFP	Dako	1:100		
	α-SMA	Abcam	1:100		
	TUJ1	Abcam	1:500		
	HNF4α	Santa-Cruz	1:50		
	Albumin	Abcam	1:20		
	Sox17	RnD systems	1:20	Anti-goat alexafluor 568	1:750
	Tra-1-60	BD Gentest	1:10	Conjugated 488	N/A
	SSEA-4	BD Gentest	1:10	Conjugated 568	
Western blot	CYP1A2	Abcam	1:3000	Anti-mouse	1:10,000
	CYP2D6	BD Gentest	1:1000	Anti-mouse	1:10,000
	CYP2E1	Abcam	1:5000	Anti-rabbit	1:5000
	CYP3A4	Santa Cruz	1:2000	Anti-mouse	1:10,000
	Nrf2	Abcam	1:400	Anti-rabbit	1:5000
	NQO1	Abcam	1:5000	Anti-Goat	1:10,000
	ENTDP5	Abcam	1:2000	Anti-rabbit	1:5000
	HO-1	Abcam	1:5000	Anti-rabbit	1:5000
	Keap1	Santa Cruz	1:1000	Anti-goat	1:2000
	β-actin	Abcam	1:10,000	Anti-mouse	1:10,000

Table 2.3: Antibodies used for immunofluorescence and western blotting

qRT-PCR analysis of gene expression

Primers for use in quantitative reverse transcription polymerase chain reaction (qRT-PCR) gene expression studies were designed using the NCBI Primer BLAST tool (http://www.ncbi.nlm.nih.gov/tools/primer-blast/). Briefly, the mRNA RefSeq annotation associated with the gene of interest was used as the search term, with exon-exon spanning the only parameter which differed from the default settings. Primer quality was assessed using OligoCalc with regard to the estimated self-complementary scores and melting temperatures. Primers were purchased from Eurofins and the sequences are provided in table 2.4.

Samples were collected in 700µl QIAzol (QIAgen), vortexed for 1 minute and stored at -80^{o}C. Total RNA was extracted using the miRNeasy extraction kit according to the manufacturer's protocol (QIAgen) and partly automated using a QIAcube system (QIAgen). In brief, samples were defrosted and 140µl of chloroform (Thermo Fisher Scientific) added. Samples were then mixed by repeated inversion and left at room temperature for 3 minutes, followed by centrifugation at 4^{o}C for 15 minutes at 12000 x g. The upper aqueous phase was removed (350µl), placed into collection tubes and inserted into the QIAcube for automated extraction using the protocol: Purification of total RNA, including small RNAs, from animal tissues and cells (aqueous phase). This protocol involves the following steps. 525µl of 100% (v/v) ETOH added the sample and transferred to the spin column containing the aqueous phase. The column is subsequently washed with the buffers supplied and eluted in 30µl PCR-grade water by centrifugation at 10000 x g for 1 minute. Extracted RNA content was measured using the NanoDrop spectrophotometer.

RNA was reverse transcribed to complementary DNA (cDNA) using the ImProm-II reverse transcription kit (Promega). Briefly, 1µl of oligo DT was added to 1µg of RNA and heated to 70^{o}C for 5 minutes and cooled on ice. The mixture was subsequently added to a reaction

mix consisting of RT buffer, $MgCl_2$, dNTPS, PCR-grade H_2O and reverse transcriptase. Samples were heated at 25°C for 5 minutes, 42°C for 1 hour and 70°C for 15 minutes using a GeneAmp PCR system 9700 thermal cycler.

Due to low RNA yield following extraction, whole transcriptome amplification was performed on selected samples using the QuantiTect Whole Transcriptome Kit (Qiagen), following the manufacturer's protocol. Briefly, 100ng of starting RNA from each sample was mixed with reverse transcriptase kit component and incubated at 37°C for 30 minutes and 95°C for 5 minutes. Ligation mix was then added to each samples and incubated for 2 hours at 22°C. Finally, the amplification mix was added and incubated for 8 hours at 30°C and 5 minutes at 95°C. Temperature controlled steps were carried out using the GeneAmp PCR system 9700 thermal cycler system and amplification confirmed using the NanoDrop spectrophotometer.

Gene expression analysis was performed using the SYBERGreen JumpStart Taq ReadyMix (Sigma Aldrich). Briefly, 10-100µg of cDNA was mixed with a reaction mix consisting of: 10µM forward and reverse primers, SYBERGreen and Rox (Sigma Aldrich). Loading of samples in duplicate in 368 well plates was performed using QIAgility (QIAgen), an automated pipetting machine. qRT-PCR was performed as follows: 95°C for 10 minutes, then 40 cycles for 95°C 15 seconds and 60°C for 60 seconds using the ViiA7 qRT-PCR machine (Applied biosystems). Results were calculated using the C_t values generated, normalised against GAPDH or glyceraldehyde 3-phosphate dehydrogenase (GAPDH) and succinate dehydrogenase (SDHA) and calculated relative to a calibrator sample (e.g. PHH) using $2^{-\Delta\Delta}C_t$ method (Livak and Schmittgen, 2001).

Sendai virus expression analysis of iPSCs was conducted using the TaqMan iPSC Sendai Detection Kit (Life technologies) according the manufacturer's instructions. Results were

normalised using GAPDH and calculated relative to the reprogramming plate using $2^{-\Delta\Delta}C_t$ method.

Primer		Sequence (5' to 3')
ALB	F	CCTGTTGCCAAAGCTCGATG
	R	ATCTCCATGGCAGCATTCGC
A1AT	F	TCCGATAACTGGGGTGACCT
	R	AGACGGCATTGTCGATTCACT
CYP1A2	F	AGCACCTGCCTCTACAGTTGG
	R	TGGTGGACTTTTCAGGCCTTT
CYP3A4	F	AGAAATCTGAGGCGGGAGC
	R	GGAATGGAAAGACTGTTATTGAGAG
CYP2E1	F	ACCCTGAGATCGAAGAGAAGC
	R	AAATGGTGTCTCGGGTTGCT
CYP2D6	F	TTCCCAAGGGGTGTTCCTGG
	R	TCACGGCTTTGTCCAAGAGA
CK18	F	ACATCCGGGCCCAATATGAC
	R	GGTGCTCTCCTCAATCTGCT
GAPDH	F	CTATAAATTGAGCCCGCAGCC
	R	GCCCAATACGACCAAATCCGT
HNF4α	F	GTTGACGATGGGCAATGACAC
	R	TCTTTGTCCACCACGCACTG
AFP	F	GCGGCCTCTTCCAGAAACTA
	R	AATAATGTCAGCCGCTCCCT
SOX17	F	GGATACGCCAGTGACGACCA
	R	GACTTGCCCAGCATCTTGCTC
FOXA2	F	ATTGCTGGTCGTTTGTTGAGG
	R	TTCATGCCGTTCATCCCCAG
GATA4	F	CGACACCCCAATCTCGATATG
	R	GTTGCACAGATAGTGACCCGT
CXCR4	F	GAAACCCTCAGCGTCTCAGT
	R	AGTAGTGGGCTAAGGGCACA
WNT3	F	GAGCCCAGAGATGTGTACTGC
	R	CTTCTAATGGAGCCCCACCT
PDX1	F	CAAAGCTCACGCGTGGAAAG
	R	TTTTTCCACTTCATGCGGCG
ISL1 (Insulin)	F	ACAAGCAGCCGGAGAAGAC
	R	TGGATATTAGTTTTGTCATTGGGCT
SDHA	F	TGGTTGTCTTTGGTCGGG
	R	GCGTTTGGTTTAATTGGAGGG

Table 2.4: Primer sequences used for qRT-PCR analysis.

Metabolism studies

Cells were incubated for 15 minutes at 37°C (5% CO_2) in standard culture media with a final substrate cocktail concentration of 1mM testosterone (CYP3A4) and 0.25mM dextromethorphan (CYP2D6) (Sigma Aldrich) in MeOH or H_20, respectively (Thermo Fisher Scientific). 0.5µM Phenacetin (Sigma Aldrich) in 100% MeOH was then added to the incubation media (1:1 v/v) as a stop solution and an internal standard for LC-MS-MS analysis. The media containing the respective metabolites, 6β-OH-testosterone and dextrorphan, was then filtered using 96-well filter plates (Merck Millipore).

The samples were analysed using a quadrupole linear ion trap mass spectrometer (AB Sciex 4000 QTrap) coupled to a Dionex Ultimate 3000 HPLC system (Thermo Fisher Scientific). 10mL of each sample was separated using a Phenomenex Luna 5 µ C18(2) 100A 100 x 2.00mm column and a gradient consisting of 0.1% formic acid in water (mobile phase A) and methanol (mobile phase B) with a 200ml/minute flow rate. The column oven and auto-sampler were maintained at 30°C and 4°C respectively. The mass spectrometer was operated using the multiple reaction monitoring mode and the analytes detected and quantified using the most abundant transitions obtained during direct infusion of standards. Results were normalised by protein content of the well following quantification by Bradford assay.

Albumin ELISA

The albumin concentration was measured by ELISA following the manufacturer's protocol (Bethyl laboratories, Montgomery, TX) protocol. Briefly, 96-well high-affinity binding plates (Thermo Fisher Scientific) were coated with coating antibody in coating buffer for 1 hour and subsequently blocked with 1% (w/v) bovine serum albumin (BSA; Sigma Aldrich) for 30 minutes. Cell supernatants were added to wells at appropriate dilutions and incubated at

room temperature for 1 hour. Horseradish peroxidase detection antibody was then added to each well at a 1:50,000 concentration. Following a 1 hour incubation, 3,3',5,5'-Tetramethylbenzidine substrate solution was added, incubated for 20 minutes and the reaction stopped with a 0.18M sulphuric acid (Thermo Fisher Scientific). Plates were read at 450nm using MRX^{e} Revelation plate reader (Dynex Technologies, Chantilly, VA).

Bradford assay

Samples for protein quantification were collected in RIPA- or iTRAQ buffer. Briefly, samples were diluted between 1:20 and 1:100 with distilled H_2O and 20µl of each sample loaded into a 96 well plate in duplicate. Standards were made up using a stock of 0.5mg/ml BSA to generate standard concentration of 0.25, 0.2, 0.15, 0.1, 0.05, 0.025 and 0mg/ml. A 1:5 dilution of Bradford reagent (BioRad) was made using distilled H_2O and 200µl of diluted Bradford reagent was added to each well. Plates were read at 570nm using MRX^{e} Revelation plate reader.

Phase contrast light microscopy

Phase contrast light microscopy (ECLIPSE TS100/100-F; Nikon, Tokyo, Japan) was used to examine cell morphology. Images of the cells were taken using the digital camera attachment (DS-Vi1, Nikon) and stand-alone control unit DS-L3 (Nikon).

2.1.9 Data handling and statistical analysis

Proteomic data analysis

Following iTRAQ analysis, only proteins which were present in all samples, identified with 95% confidence (2 or more peptides) or 99% confidence (single peptide) with a false detection rate (FDR) of less than 1% were statistically analysed using R open-source software (http://www.r-project.org/). The iTRAQ output was analysed and differentially

expressed proteins (DEPs) identified using the linear models for microarray data (LIMMA) and t-test (multtest) modules as described previously (Rowe et al., 2010). Statistical outputs (p-value, Benjamini-Hochberg and log fold change) of these modules were presented as volcano plots and proteins detected in all samples were subjected to hierarchical clustering and heatmap analysis.

Individual trend analysis of CYPs and transporters detected in ≥3 donors were assessed by one-way ANOVA. Co-efficient of variance (CV) was calculated as (standard deviation/mean). The most variable proteins were defined as CV>1.3 and the most stable proteins were defined as CV<0.3 and a mean relative fold change >0.8 and <1.25. PANTHER analysis was used to categorise differential subsets of proteins into biological functional groups and displayed as a pie chart (Mi et al., 2013).

Significant DEPs ($p<0.05$) were uploaded to the Ingenuity platform IPA (QIAgen) to investigate the associated pathways, networks and regulators. IPA uses a database of known protein interactions from scientific publications to associate and group the uploaded DEPs with pathways (Thomas and Bonchev, 2010). Using IPA algorithms, the software generates a p-value which relates to the likelihood that a particular pathway or network is linked to the DEPs in the dataset. Only pathways which were altered by $p<0.05$ (Thermo Fisher exact T-test) were classed as significantly altered or linked. The Z-activation score, which additionally takes into account the directional change of the proteins, was used for biological function and upstream regulator analysis. Using the IPA algorithm, functions or regulators which have a Z-score of ≥2 are predicted to be activated and ≤-2 are predicted to be inhibited.

Non-proteomic data analysis

Statistics were performed using the StatsDirect software package (Cheshire, United Kingdom). For direct comparisons, non-dependent and dependent samples were analysed using unpaired and paired T-tests, respectively. In comparisons of three or more groups, significance was calculated by one-way or two-way ANOVA. Correlations were assessed using linear regression correlation. In all cases $P<0.05$ was classed as significant.

Chapter 3

Development of iPSC reprogramming and differentiation protocols.

3.1 Introduction

The use of pluripotent stem cells is growing rapidly and the associated techniques and protocols are subject to constant development and improvements (Kia et al., 2013; Gonzalez et al., 2011). Pluripotent stem cells hold great potential for the development of better cell models and treatments for debilitating conditions. One potential use is a source of hepatocyte-like cells for assessing the toxicological profile of small compounds during drug development programmes (Kia et al., 2013).

Induced pluripotent stem cells (iPSCs) were first described by Yamanaka *et al.,* in 2006 and 2007 and represent a step-forward in terms of phenotypic coverage of the population when compared to embryonic stem cells (ESCs) (Takahashi et al., 2007; Takahashi and Yamanaka, 2006). iPSCs may be reprogrammed from any donor of interest using readily available adult somatic cells, such as those derived from skin or blood samples. This allows for the possibility of personalised therapies, large coverage of HLA types in immune-related studies and, with relation to drug induced liver injury, panel-based assessment of the phenotypic variation seen in the population and, in the longer term, personalised toxicology studies (Krueger et al., 2014).

Before these applications can be realised, iPSCs must first be generated and differentiated. Since the first report of cellular reprogramming using the retroviral insertion of Oct4, Sox2, Klf4 and c-Myc (OSKM), several different techniques have been published (Gonzalez et al., 2011). These have focussed on delivering these transcription factors at higher efficiency and in a greater range of cell types or without genome insertion, e.g. direct transfection of mRNA or protein, episomal plasmids or non-integrating viruses such as adeno- or Sendai virus (Warren et al., 2010; Yu et al., 2009; Fusaki et al., 2009; Kim et al., 2009). Other groups have gone further and attempted to use alternative transcription factors, such as

Nanog or Lin28 (Yu et al., 2007), or even replace the OSKM factors completely with small molecules or microRNAs (Miyoshi et al., 2011; Anokye-Danso et al., 2011; Hou et al., 2013).

Of those techniques using the OSKM factors, the Sendai virus offers a unique trade-off between high efficiency genome insertion-based techniques and low efficiency non-insertion-based techniques (Fusaki et al., 2009). It is capable of delivering the OSKM factors at efficiencies similar or greater than lentiviral or retroviral techniques in a wide-range of cell types (Fujita et al., 2006) and, as it has an RNA-based viral cycle, no genome integration or disruption occurs (Fusaki et al., 2009).

MicroRNA-based techniques offer a capacity to remove the oncogenic transcription factors associated with OSKM-based reprogramming. The use of the miR-302/367 cluster has been widely reported to enhance reprogramming efficiency when used in conjunction with OSKM factors (Subramanyam et al., 2011; Liao et al., 2011; Hu et al., 2013); however, in 2011, Anokye-Danso *et al*., reported a microRNA only reprogramming technique (Anokye-Danso et al., 2011). The authors demonstrated that the lentiviral transduction of miR302/367 had a 30% greater reprogramming efficiency (as measured by OCT4-GFP positive colonies) than standard OSKM factors in mouse cells, whilst human neonatal fibroblasts were reprogrammed at efficiencies ~2800 times greater than OSKM-techniques, as measured by counting colonies with ESC-like morphologies (Anokye-Danso et al., 2011).

In the same issue of the journal, Miyoshi et al., found that reprogramming could be achieved via the direct transfection of seven microRNAs: miR302a/b/c/d, miR200c and miR369-3p/5p (Miyoshi et al., 2011). The authors reported a very low efficiency compared to previously reported viral methods; however, the lack of a need to introduce OSKM factors or use integrating-based techniques which may have negative effects on genome integrity is highly attractive for many groups wishing to generate iPSCs.

As a consequence of the great number of options available, choosing the correct reprogramming technique for the chosen application can prove difficult (Gonzalez et al., 2011). Therefore, as part of this chapter, we assessed the three described techniques for the ability to reprogram both fibroblasts and hepatocytes required for the experiments described in chapter 4. Whilst fibroblasts are generally reported to be readily reprogrammable, very few publications have shown successful reprogramming of human hepatocytes (Hansel et al., 2014; Liu et al., 2010a). One potential cause of this is that human hepatocytes are known to become cell cycle arrested in current culture systems (Xu et al., 2013b); therefore, we required a reprogramming technique which is capable of delivering the required factors to a range of cell types, including a non-dividing cell type.

The differentiation of iPSCs to hepatocyte-like cells has also been described using numerous techniques (Kia et al., 2013). Many different protocols have been published with regard to the production of HLCs and deciding which method best suits the requirements of the researcher is an imperative consideration. Therefore, within this chapter we also investigate three different protocols for HLC differentiation and assess which is most likely to allow for the differentiation of a wide number of cell types, as required in chapter 4.

3.2 Results

Lentiviral transduction of miR302/367 to reprogram somatic cells to iPSCs

We first looked to reproduce the work reported by Anokye-Danso *et al,* who demonstrated reprogramming at higher efficiency than OSKM-based techniques (Anokye-Danso et al., 2011). In addition, the use of lentiviral constructs allows integration into a wider number of cell types, including non-dividing cells, than more traditional retroviral-based techniques (Gonzalez et al., 2011). Together, this suggests that a wide range of cell types may be amenable to this novel microRNA reprogramming technique.

Generation of a lentivirus vector containing miR302/367

To asses this novel technique, we generated a lentivirus construct encoding the miR302/367 cluster. Figure 3.1 shows the production of this virus. Firstly, the vector sequence was successfully amplified by PCR (Figure 3.1a.i). We then transferred this amplified product into a TOPO entry vector and confirmed that the correct sequence had been transferred using restriction digest analysis (Figure 3.1a.ii). The sequence was then transferred to the destination vector and again verified by restriction digest analysis (Figure 3.1a.iii). The results from Figure 3.1a.iii were further assessed by sequencing analysis (Eurofins), confirming the correct sequence was present within the destination vector. Plasmids with the correct sequence and orientation were then expanded and viral particles produced using 293FT cells.

Titration of lentiviral particles

Once the viral particles were produced, the titre of the supernatant was then assessed. This was achieved using HepG2s, as this is a clonally expandable and non-migratory cell line, both of which are required for colony forming unit-based titration. HepG2s were transduced with viral particles at serial dilutions 10^{-2} -10^{-6} and subsequently selected out

using blasticidin. Following 2 weeks of selection, crystal violet analysis suggested that the initial titre was relatively low: $1.52x10^3$, colony forming units (CFU). Therefore, the virus was concentrated using a centrifugal filtration method, resulting in an improved titre of $8.9x10^5$ CFU. It has been reported that miRNA-based lentiviruses produce lower titres as a result of various mechanisms (Liu et al., 2010b). We therefore compared our miRNA plasmid with a control plasmid to see if the miRNA was impacting on the viral titre. Following centrifugal concentration, the results demonstrated a large difference in viral concentration: $2.6x10^5$ and $1.95x10^6$ CFU for the miRNA (Figure 3.1c.i) and control plasmids (Figure 3.1c.ii), respectively. Consequently, the analysis of the miRNA lentivirus technique sequence across a single batch of virus was limited.

Reprogramming of cells with the lentivirial vector

Subsequently, cells were transduced with the viral particles. Analysis demonstrated successful integration and production of the miRNA-encoded sequence in HepG2s, as part of the titration experiment (Figure 3.2a) and in neonatal fibroblasts (Figure 3.2b and c). Interestingly, despite the cell morphology suggesting increased toxicity at the higher viral loads, particularly at MOI 10 (figure 3.2b); no increase in miR302b expression was observed (Figure 3.2c).

Reprogramming of cells using this virus was then attempted at MOI 5 using the protocol described in the original publication (Anokye-Danso et al., 2011) (Figure 3.3a). However, despite numerous attempts in neonatal and juvenile fibroblasts and PHH, little to no colony formation was noted (Figure 3.2b and c). Of those colonies which did form, none displayed the morphological or growth characteristics associated with iPSCs. Some colonies were noted from the juvenile dermal fibroblasts (jHDFs); however, these had a different morphology than expected. Analysis of these colonies revealed high Sox2 expression, whereas Nanog and Oct4 were undetectable (Figure 3.3d).

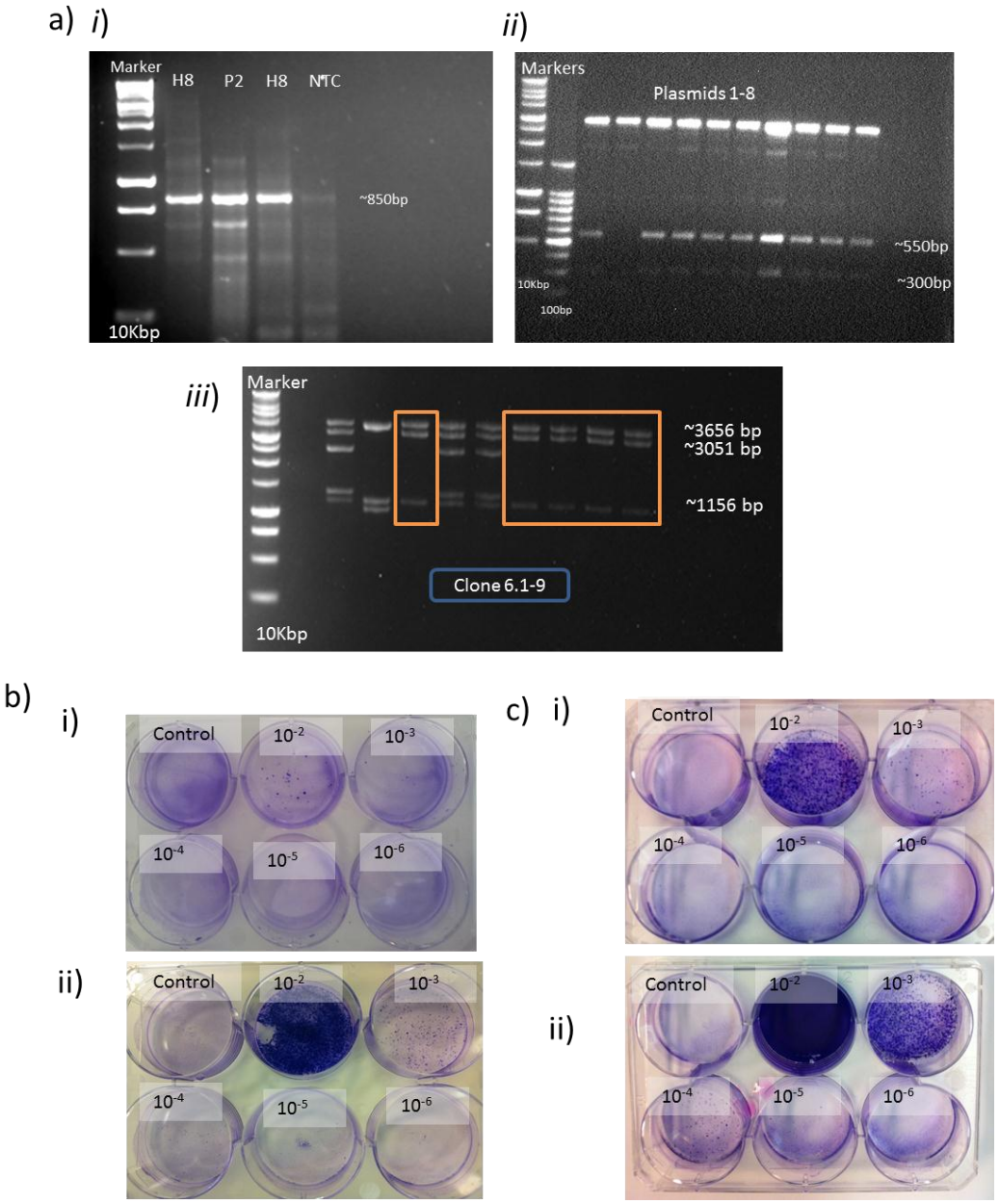

Figure 3.1: Lentiviral miR302/367 construct production.

a) Ethidium bromide gels. *i)* PCR amplicons of miR-302/367 sequence in cells lines Hues8 (H8), and Panc2 (P2) and no template control (NTC); *ii)* Restriction digest with ECOR1 and KPN1 of the miR-302/367 cluster inserted into the entry TOPO vector; *iii)* Restriction digest using Afl II and Xho I of the expression plasmid following enzymatic transfer from the entry TOPO vector. Highlighted in orange are the correctly inserted plasmids as determined by expected fragment size. **b)** Viral titre of transduced, Blasticidin selected and crystal violet stained HepG2s using serially diluted viral stock. *i)* non-concentrated viral titre; *ii)*: concentrated virus. **c)** Viral titre of transduced, Blasticidin selected and crystal violet stained HepG2s using serially diluted viral stock *i)* miRNA-encoding virus; *ii)* Control virus.

Abbreviations: H8: Hues8 (ESCs), P2: Panc 2 cell line

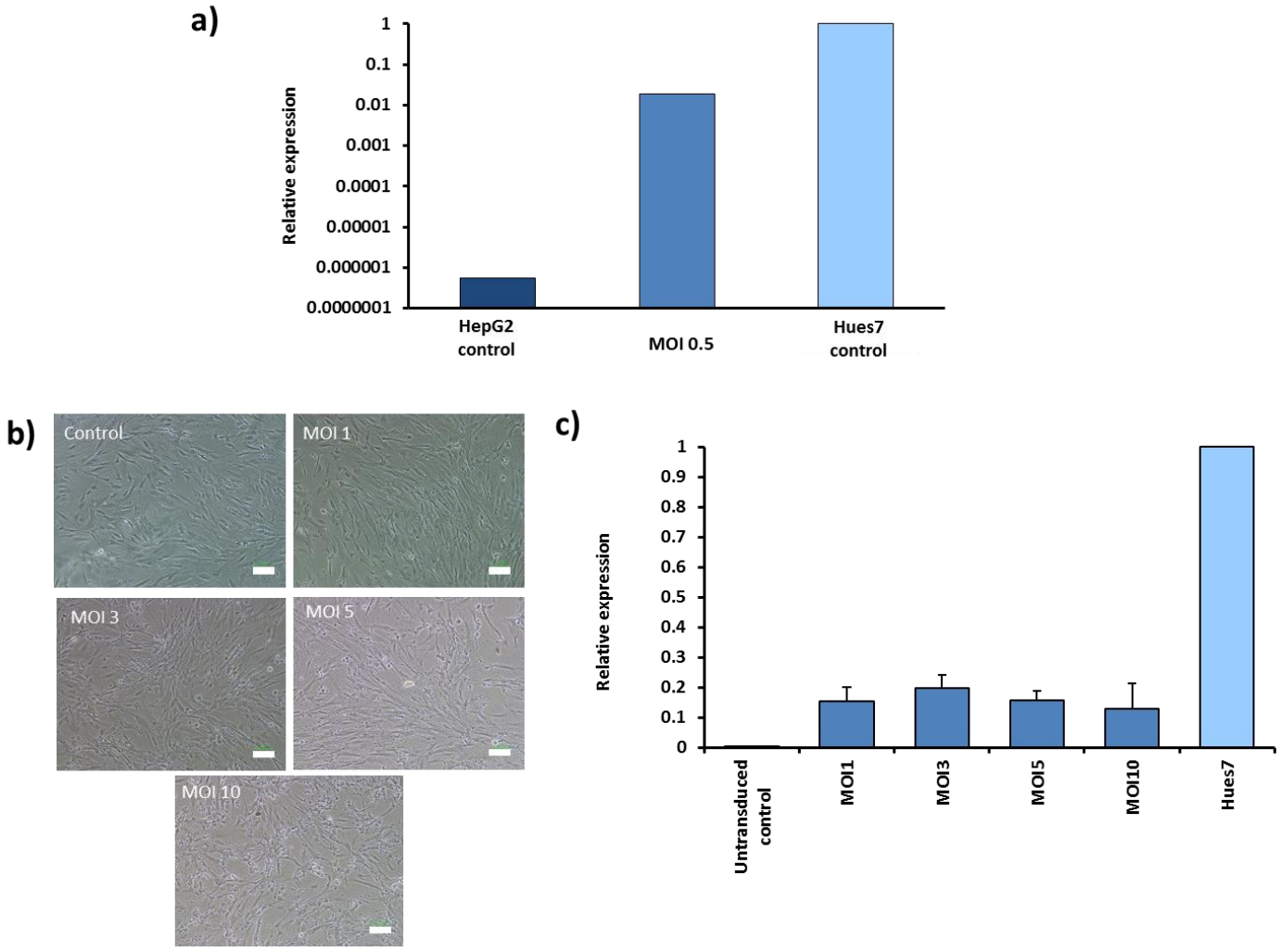

Figure 3.2: Successful lentiviral miR302/367 transduction of cells.

a) Relative expression of miR302b expression following transduction of HepG2s (MOI 0.5) with lentiviral particles as detected by q-PCR. Results normalised to U6 and shown relative to Hues7, a ESC control of endogenous pluripotent levels of miR302b; n=1. **b)** Morphology of BJ fibroblasts 24 hours post-transduction with miR302/367 lentivirus at MOI 1, 3, 5 and 10. Magnification x1000, scale bar: 100µm **c)** Relative expression of miR302b expression following transduction of BJ fibroblasts (MOI 1-10) with lentiviral particles as detected by q-PCR. Results normalised to U6 and shown relative to Hues7, an ESC control of endogenous pluripotent levels of miR302b; n=2. Error bars: SEM.

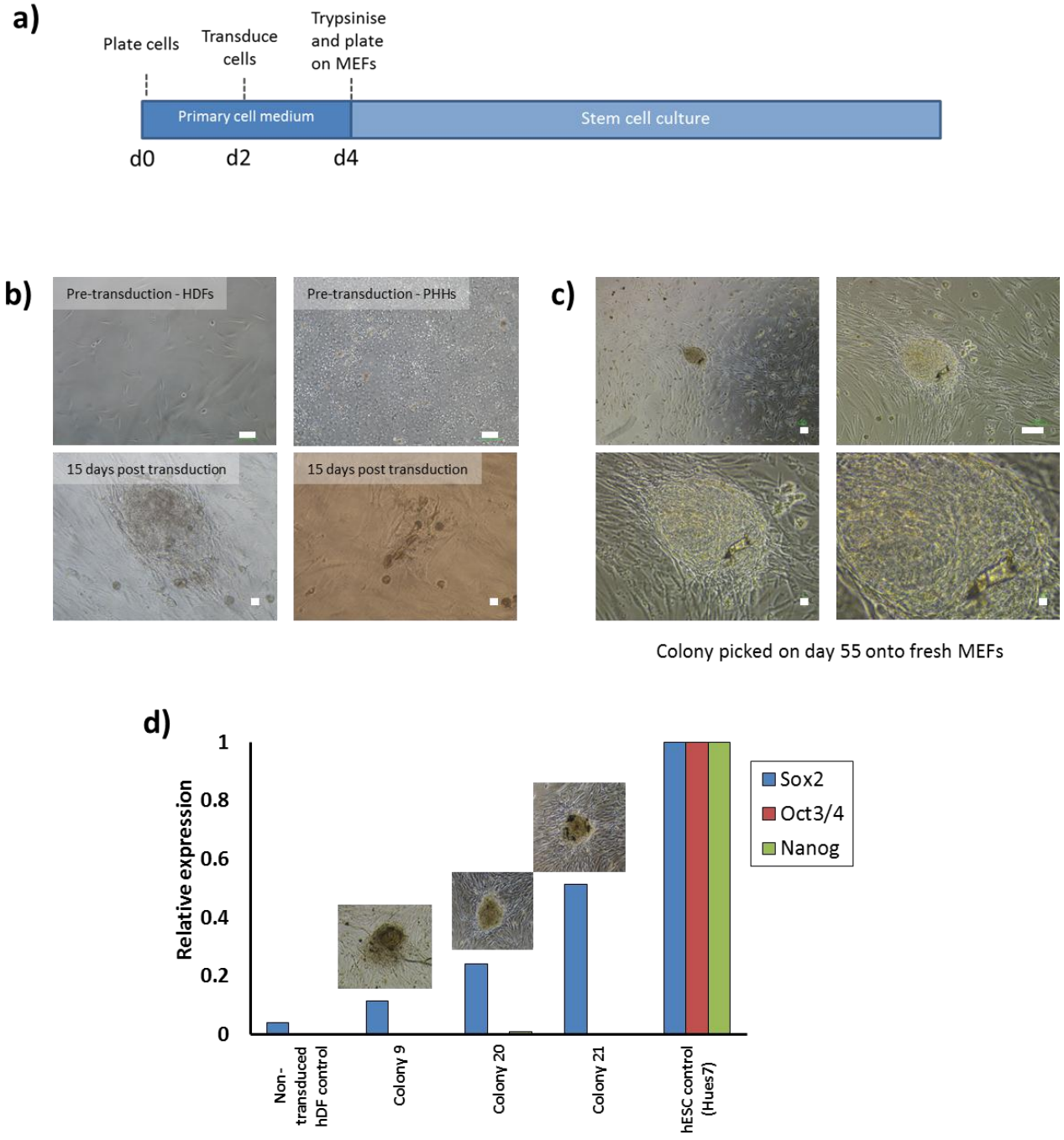

Figure 3.3: Lentiviral miR302/367 reprogramming of cells does not yield iPSCs.

a) Schematic diagram of the protocol used to transduce primary cells using the miR302/367 lentivirus. **b)** Lentiviral transduction of PHH and jHDFs (MOI 1) pre-transduction (magnification x100, scale bar: 100µm) and potential colonies (magnification x200, scale bar: 10µm) forming 15 days post transduction. **c)** Attachment of jHDF colonies picked onto fresh MEFs at day 55 post transduction (magnification: x40, x100, x200, x400; scale bar: 100µm, 100µm, 10µm, 10µm, respectively). **d)** Q-PCR analysis of 3 picked colonies. Gene expression of pluripotency markers Sox2, Oct3/4 and Nanog shown relative to Hues7 control and against a non-transduced HDF culture. Each sample n=1 and run in duplicate.

Abbreviations: Oct4: Octamer-binding transcription factor 4; Sox2: SRY (sex determining region Y)-box 2

Direct transfection of miRNA to reprogram somatic cells to iPSCs

The use of direct transfection is an attractive method of reprogramming as it avoids the use of integrative vectors such as lenti- or retroviruses. Within our laboratory, we have shown that it is possible to manipulate hepatocytes with siRNA, a synthetic oligonucloetide which works in a similar way to mature miRNAs (unpublished data).

Optimising the transfection efficiency

To assess this reprogramming technique, we first optimised our transfection conditions for all cells used with a fluorescently labelled oligonucleotide. Our results suggested that HepG2s (Figure 3.4a.i) and dermal fibroblasts (figure 4a.ii) showed relatively high transfection efficiency. Interestingly, for hepatocytes, sandwich cultures incorporating a Matrigel overlay were not amenable to transfection, whereas monolayer cultures were (Figure 3.4a.iii). Furthermore, lower plating densities increased transfection efficiency (Figure 3.4a.vi). We then assessed the relative expression of a single miRNA to confirm successful transfection. Our results showed a large increase in the miRNA expression in the transfected fibroblasts which was ~15-fold above non-transfected cells and also above the levels of Hues7 ESCs (Figure 3.4b).

Reprogramming using microRNA transfection

Using the optimised conditions, we then plated neonatal and juvenile fibroblasts at the pre-determined densities and transfected them with the seven microRNAs every 48 hours over 4 cycles (Figure 3.5a). Following the final transfection, cells were transferred to feeder-dependent stem cell culture. After extended culture of 50 days, no typical-iPSC colonies were detected in any of the cell types investigated (Figure 3.5b). Attempts to reprogram primary human hepatocytes were also unsuccessful, yielding no colonies which were demonstrative of an iPSC-like phenotype (Figure 3.5b).

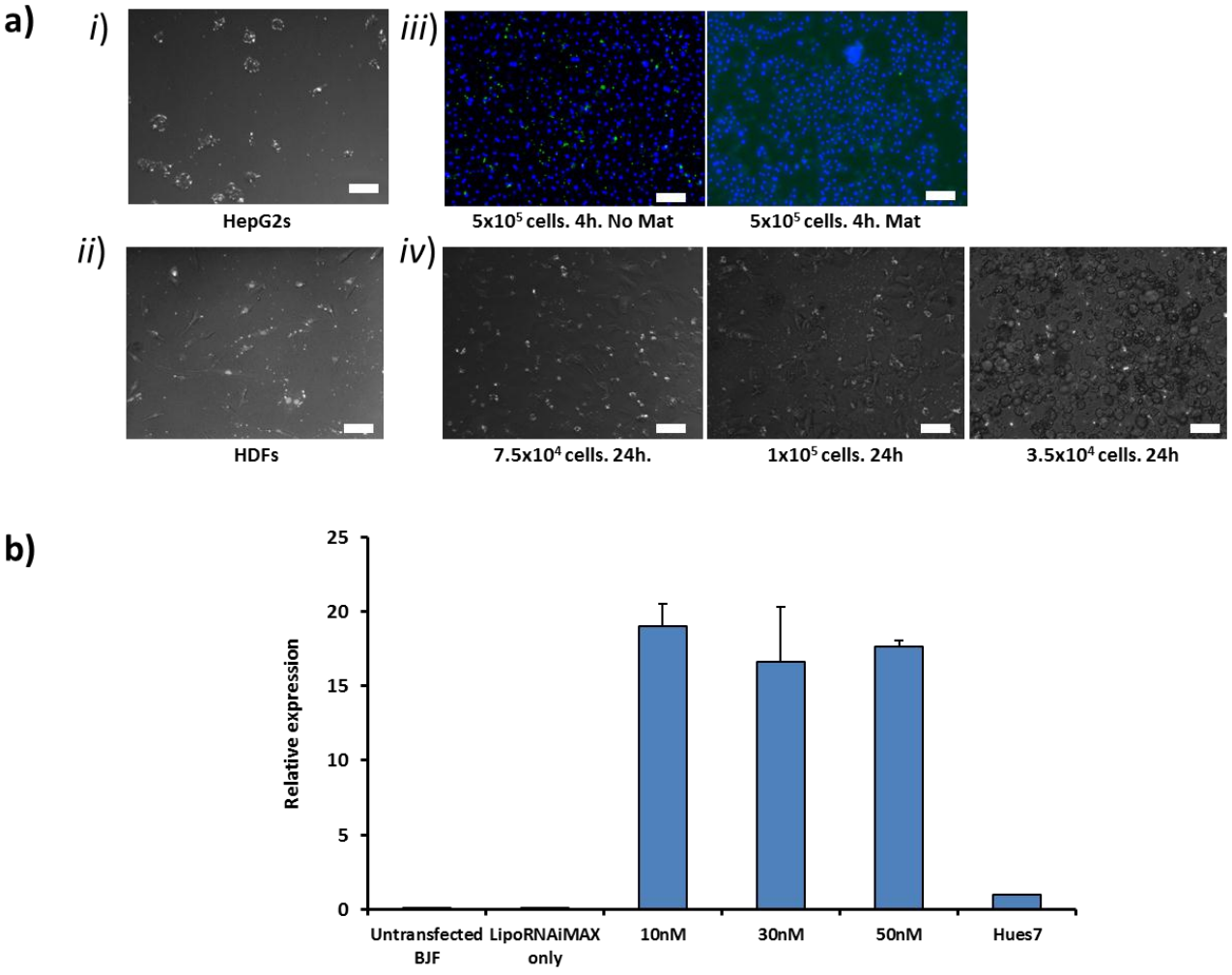

Figure 3.4: Optimising transfection conditions with BlockIT fluorescent oligo and qRT-PCR

a) Merged light and fluorescent microscopy of *i)* Low density HepG2s transfected with BlockIT (white) at 100nM; *ii)* Low density jHDFs transfected with BlockIT at 100nM *iii)* Fluorescence comparison of BlockIT accumulation in Matrigel overlaid and non-overlaid primary hepatocytes (green: BlockIt reagent); *iv)* Comparison of BlockIT accumulation in primary human hepatocytes plated at different cell densities. Magnification x100, scale bar: 100µm. **b)** Confirmation of transfection in BJ fibroblast cultures at various concentrations of miRNAs. miR302b relative expression measured by q-PCR and shown relative to Hues7; n=2 wells of a single experiment, error bars: SEM.

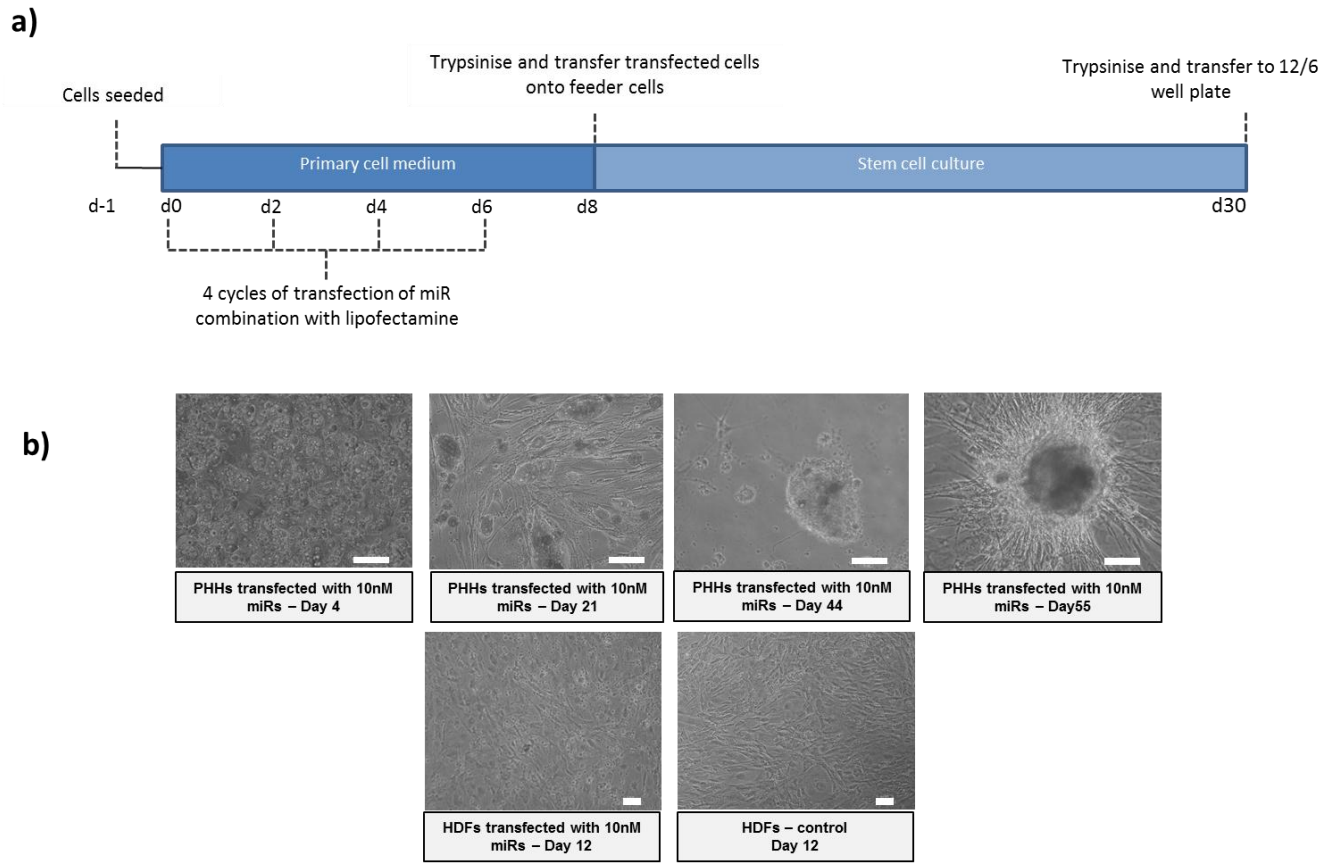

Figure 3.5: Reprogramming primary cells with direct transfection of miRNAs.

a) Schematic of the protocol used for the transfection of primary cells. **b)** *i)* Primary human hepatocytes transfected with 7xmiRs and the subsequent culture and attempted expansion. Images taken at various points of culture. Magnification x200, scale bar: 100µm; *ii)* HDFs transfected with 7xmiRNAs. Images represent the different morphology of transfected and control cells taken at day 12 post initial transfection. Magnification x100, scale bar: 100µm

Use of Sendai virus to reprogram somatic cells to iPSCs

As neither microRNA approach yielded iPSC colonies, we then attempted a more traditional approach using the OSKM factors delivered via Sendai virus. According to the manufacture's suggestions, we first attempted reprogramming in the BJ neonatal (Figure 3.6a). Using viral loads of MOI 3 in duplicate we were able to successfully generate iPSCs using the Sendai virus technique (Figure 3.6b). In total, 26 colonies were picked onto either feeder-dependent or feeder-independent culture and labelled Liv1A-Z (Figure 3.6c).

Following expansion, two feeder-free (Liv1W and Liv1R) and 2 feeder-dependent (Liv1E and Liv1N) lines were characterised using a panel of ESC-associated markers Oct4, Sox2, Nanog, Tra-1-60 and SSEA-4 (Figure 3.7a). To functionally characterise the iPSCs we then formed embryoid bodies from the clones with all lines forming spheroid-like structures in non-tissue culture coated plates (Figure 3.7b). Following re-plating, pluripotency was confirmed in all four lines based on expression of endoderm (AFP), ectoderm (TUJ1) and mesoderm (alpha-SMA) specific markers using immunofluorescence (Figure 3.7c).

We then confirmed a switch from exogenous to endogenous OSKM expression through the loss of Sendai virus expression. As this virus does not integrate, it is reported to be lost at passages >10. To examine residual Sendai virus expression we used a qRT-PCR assay directed to specific tags on the 4 viruses used for reprogramming (Figure 3.8a). Our results showed almost complete loss of Sendai virus expression in Liv1E, Liv1R and Liv1W lines. The residual expression of c-Myc and Klf4 in Liv1N is still very low, ~333 fold less than the reprogramming plate, and would likely dissipate with further time in culture. The high endogenous gene expression levels of Oct4, Sox2 and Nanog (Figure 3.8b) further demonstrated the commitment to a pluripotent phenotype in the absence of viral expression.

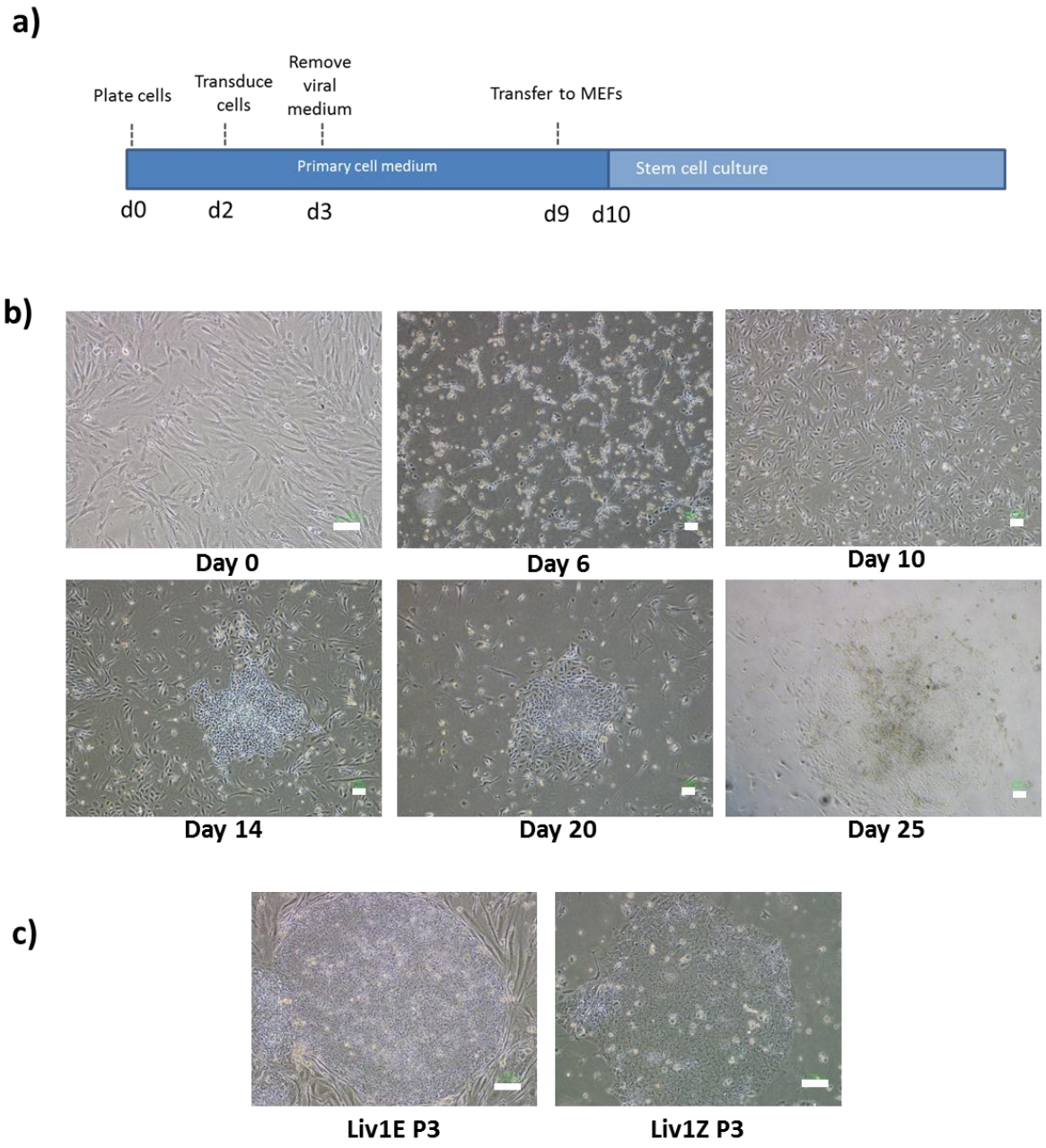

Figure 3.6: Sendai virus BJ fibroblast reprogramming yields fully reprogrammed iPSCs.

a) Schematic diagram of the Sendai virus protocol. **b)** Images taken of cells pre-transduction and at various stages of culture up to the emergence of picked colonies: day 1: magnification x100, scale bar 100µm; day 6-25: x40, scale bar 100µm. **c)** Examples of colonies successfully picked onto feeder-dependent (Liv1E) and feeder-free (Liv1Z) culture systems. Magnification: x100, scale bar 100µm.

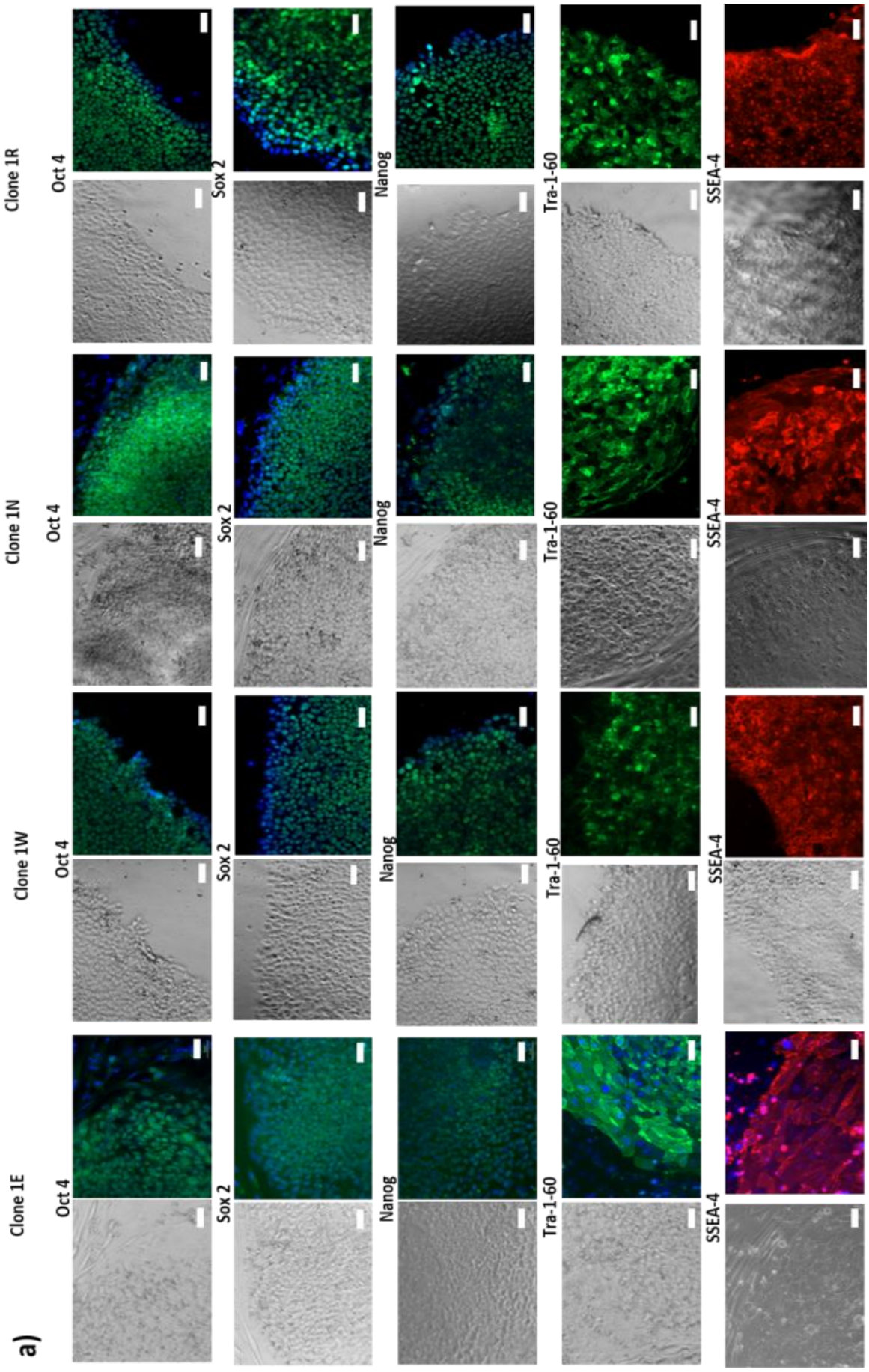
a)
Clone 1E
Clone 1W
Clone 1N
Clone 1R
Oct 4
Sox 2
Nanog
Tra-1-60
SSEA-4

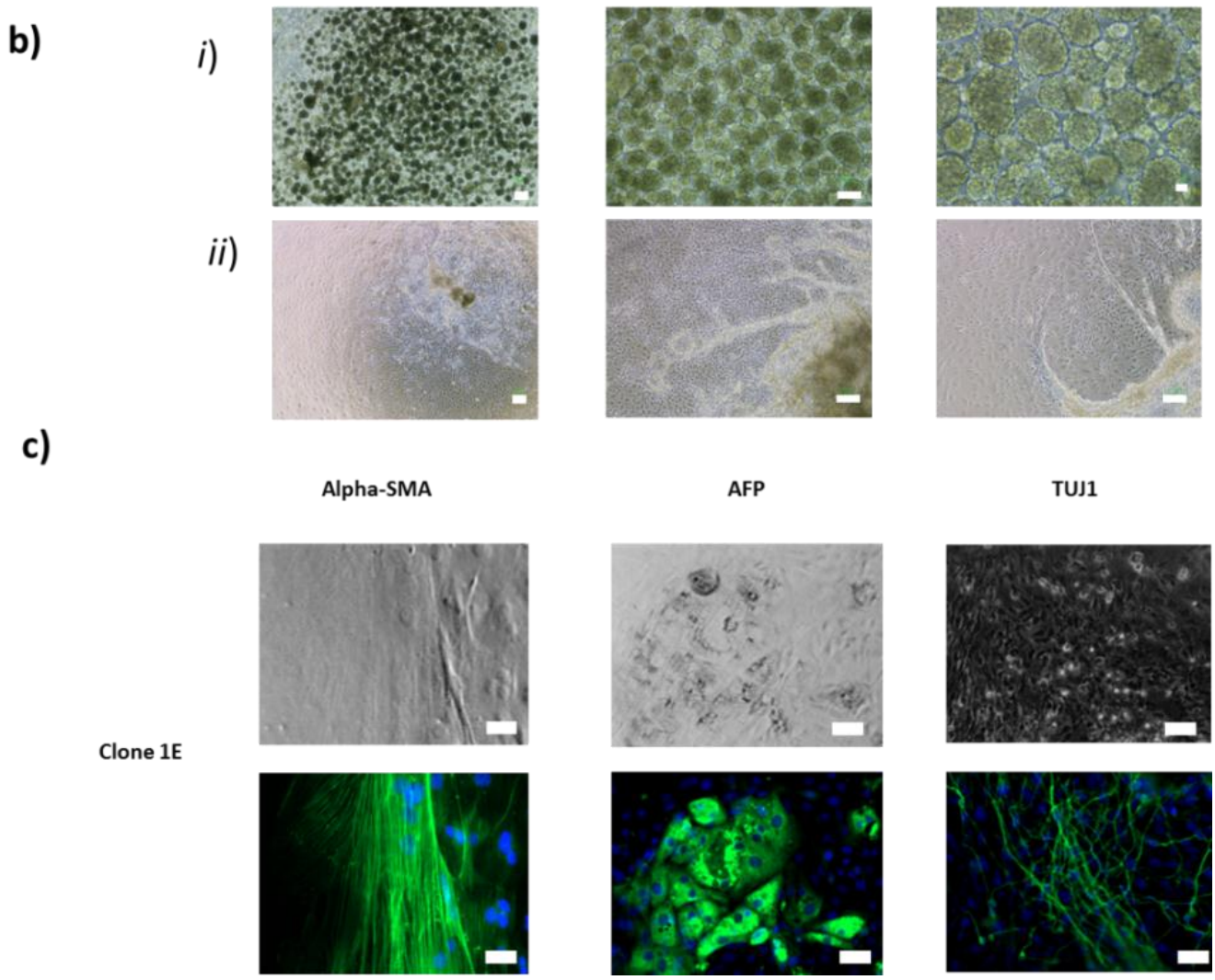

Figure 3.7: Characterisation of BJ fibroblast-derived iPSCs using embryoid bodies.

a) BJ fibroblast-derived iPSC colony characterisation. 4 clones characterised using panel of markers: Oct4, Sox2, Nanog, Tra-1-60 and SSEA-4. Magnification x200, scale bar 50µm. **b)** i) Embryoid bodies formed for assessment of spontaneous differentiation capacity. ii) Embryoid bodies replated for staining analysis. Images present a representative well with multiple cell morphologies present. Magnification x40, x100, x200, scale bar: 100µm, 100µm and 10µm **c)** Immunofluorescence images taken of 3 markers of germ layers: Alpha smooth muscle actin (mesoderm), alpha fetoprotein (endoderm) and TUJ1 (Ectoderm). All lines presented at 20x with corresponding bright-field images. Magnification x200, scale bar 50µm. 4 lines characterised using EB assays with 1 shown as an example.

Abbreviations: AFP: Alpha-Fetoprotein; α-SMA: alpha smooth muscle actin; Tuj1: Neuron-specific class III beta-tubulin; Oct4: Octamer-binding transcription factor 4; Sox2: SRY (sex determining region Y)-box 2; Tra-1-60: Tumour-related antigen (TRA)-1-60; SSEA-4: Stage-specific embryonic antigen-4

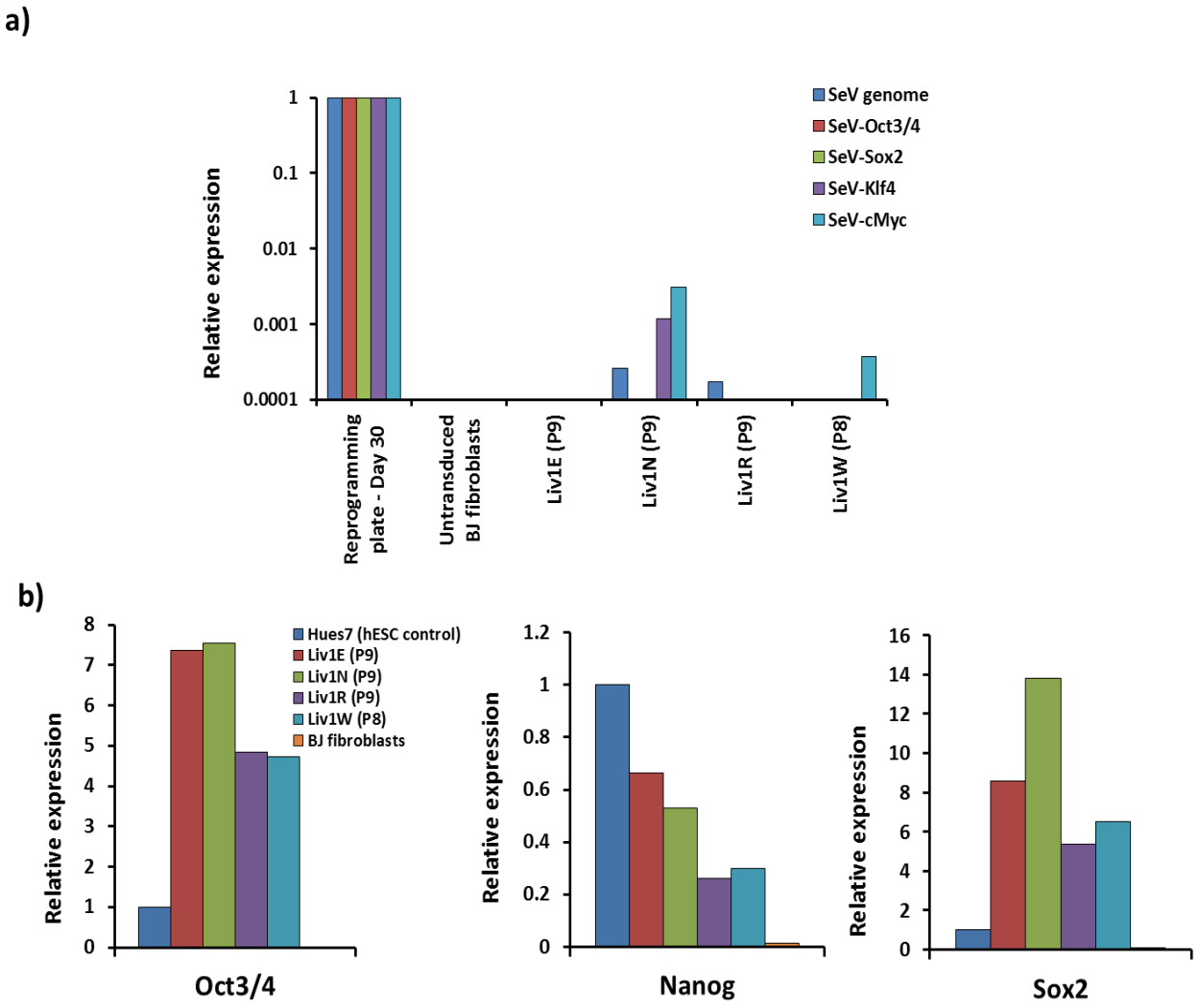

Figure 3.8: Characterisation of BJ fibroblast-derived iPSCs using qRT-PCR.

a) Confirmation that the Sendai virus expression has been removed through multiple passaging. Relative expression compared to the original reprogramming plate 30 days post-transduction. All samples n=1 run in duplicate **b)** BJ fibroblast-derived iPSC colony characterisation. 4 clones characterised using a panel of markers: Oct4, Sox2, Nanog by qRT-PCR. Results presented as relative to hESC control. N.B at time of sample derivation hESC culture was of low quality and contained numerous areas of differentiation. All samples n=1, run in duplicate.

Abbreviations: Oct4: Octamer-binding transcription factor 4; Sox2: SRY (sex determining region Y)-box 2; SeV: Sendai virus

Differentiation of iPSCs towards HLCs

Once characterised, we then developed a protocol for differentiating iPSCs to hepatocyte-like cells. The requirement, discussed further in chapter 4, was for a protocol which can be used in a wide range of iPSC lines; therefore we investigated one of the most widely established protocols used in the literature and the different variants which have been published.

In an attempt to improve inter-donor, inter-clone and inter-experiment reproducibility we developed a single cell method for plating the iPSCs before differentiation. Initial experiments focussed on the survival rate and subsequent growth characteristics when plated in standard Essential 8 media culture media (Figure 3.9a). The results suggested high plating efficiency was found in the presence of ROCK inhibitor, with the cells quickly reforming colony-like structures when maintained in stem cell maintenance media.

We then compared different methods of differentiation towards definitive endoderm using single cell differentiation model to enhance intra-line reproducibility and reduce inter-line variability. Depending on the cell type and line, groups have reported slightly altered protocols to generate the purist population of definitive endoderm cells. We therefore compared various combinations of Activin A and Wnt3A at several different single cell plating densities. Densities were chosen based on Kajiwara *et al*., which reported a plating density of $1x10^5$ cells/cm^2. Our results suggest that higher plating densities enhance definitive endoderm differentiation in single cell plating models (Figure 3.9b). Estimations of population purity were made by counting and comparing the number of Sox17 positive cells across 10 representative pictures of the well. This data suggested that there was little difference between the higher densities in these conditions; however, the use of Activin A and Wnt3a for 3 days followed by Activin A alone for 2 days was noted as being the most efficient by eye (Figure 3.9c).

As the only significant difference in definitive endoderm differentiation efficiency was seen with different cell densities, further conditions were used as part of a comparison of full differentiation protocols seeded at $1.5x10^5$ cells/cm^2. These protocols used were adapted from published protocols: Sullivan, Kajiwara and Chen, respectively (Chen et al., 2012; Kajiwara et al., 2012; Sullivan et al., 2010). Both the Kajiwara and Chen protocols are modified versions of the Sullivan protocol. Using two of our iPSCs lines, we differentiated these cells, following each protocol as closely as possible (Figure 3.10).

Our results demonstrated the variation that can be found between lines and that the Sullivan protocol was much more effective at producing HLCs in our iPSCs than the Chen protocol, as determined by albumin secretion (Figure 3.11a). The use of sodium butyrate in the Kajiwara protocol was found to cause toxicity during the earliest stages of culture in Liv1W. Both the Kajiwara and Sullivan protocol successfully yielded cells which had a hepatocyte-like morphology and had detectable secretion of albumin. Interestingly, the Kajiwara protocol was able to induce albumin secretion in Liv1R, which was not possible in the Sullivan or Chen protocols.

We also investigated the gene expression of HLCs produced using the Sullivan protocol. In-keeping with current literature, the cells showed detectable expression of several hepatic-associated genes, such as HNF4α, albumin, CK18 and A1AT; however, the expression of several CYP450s was below the level of detection (Figure 3.11b).

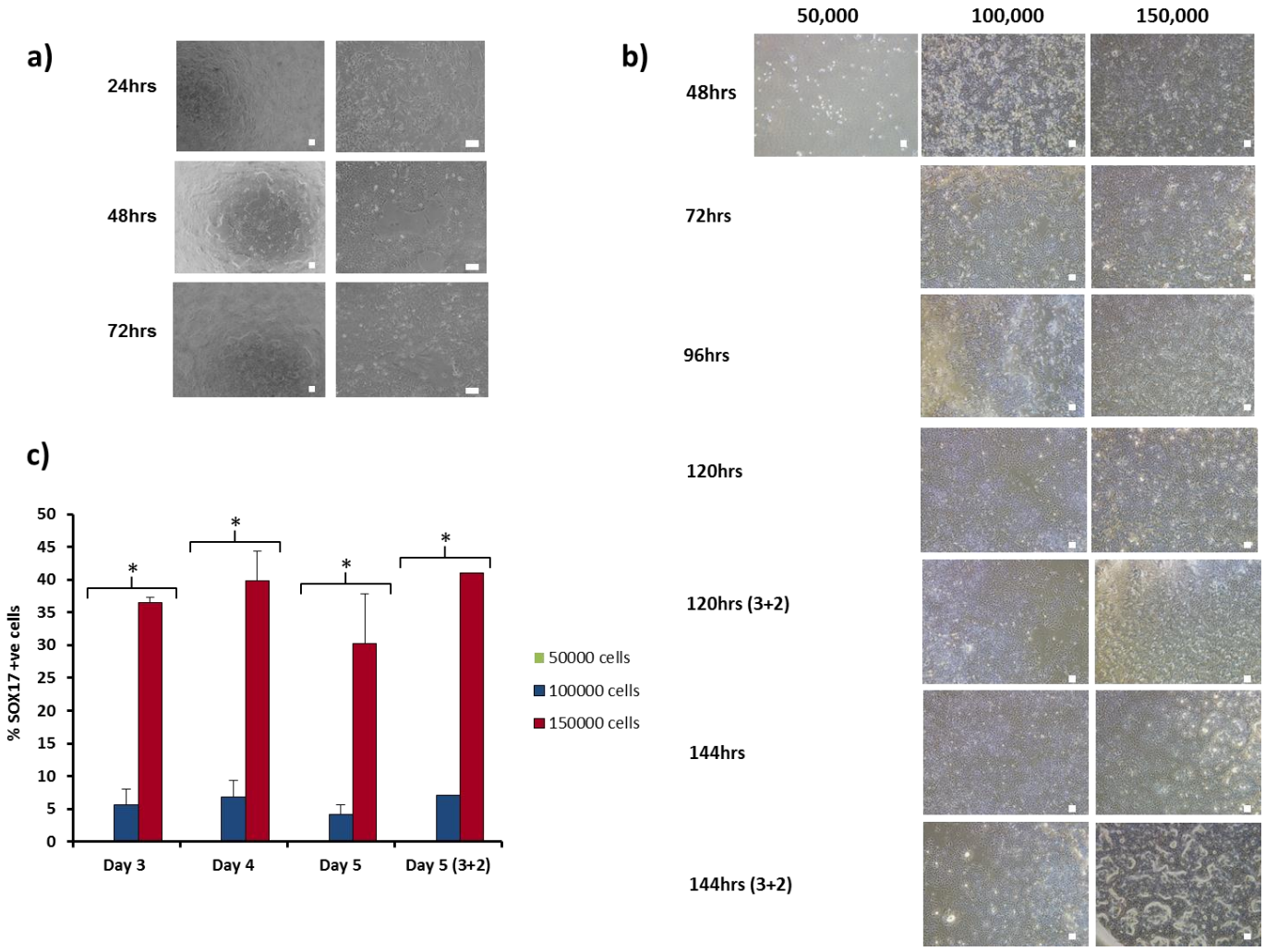

Figure 3.9: Optimising the single cell plating and differentiation of iPSCs to definitive endoderm.

a) Single cell plating of iPSCs in Essential 8 Media. Magnification x40 and x100, scale bar: 100µm and 100µm. **b)** Plating and differentiation of iPSCs at $5x10^4$, $1x10^5$ and $1.5x10^5$ cells/cm^2 at different stages of differentiation. No cells survived beyond 48 hours in the $5x10^4$ cells/cm^2 condition. 3+2 refers to 3 days of 100ng/ml Activin A and 50ng/ml WNT3a followed by 2 days of 100ng/ml Activin A only. All other conditions have 100ng/ml Activin A and 50ng/ml Wnt3a throughout the differentiation period. Magnification x40, scale bar: 100µm **c)** Results of 10 images taken from each well in duplicate. Percentage of Sox17+ve cells ascertained using the cell count function in imageJ. Error bars represent SD. (*) $p<0.05$ paired T-test.

Abbreviations: Sox17: SRY (sex determining region Y)-box 17.

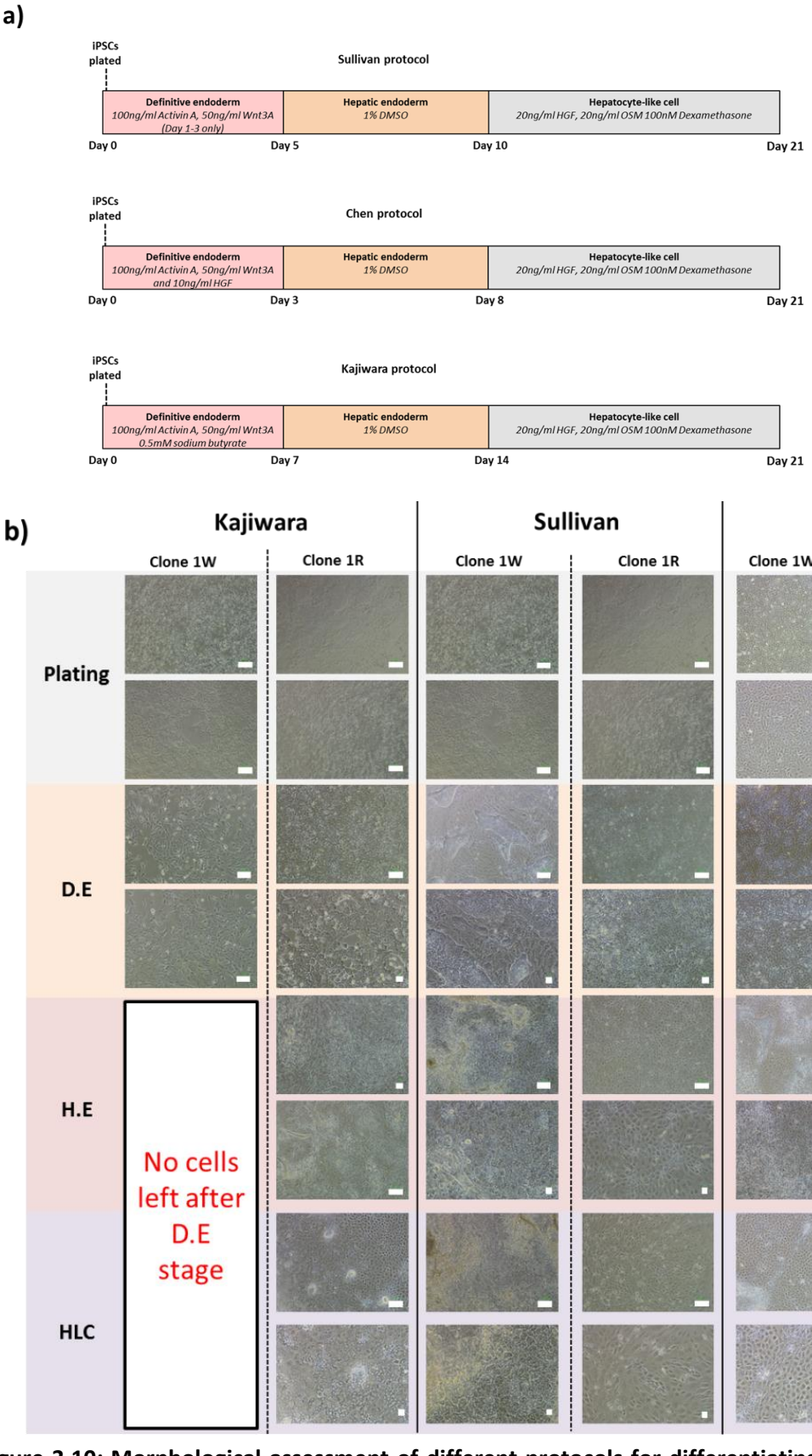

Figure 3.10: Morphological assessment of different protocols for differentiating iPSCs to Hepatocyte-like cells.

a) Schematic diagrams of the various protocols used for HLC differentiation. **b)** Morphological changes of two iPSC lines differentiated using three different HLC protocols at each stage of differentiation. No cells were left in Liv1W following the D.E stage of the Kajiwara protocol. Magnification: x40, x100, x200, x400; scale bar: 100µm or 10µm.

Abbreviations: Wnt3A: wingless-Type MMTV Integration Site Family, Member 3A; HGF: Hepatocyte growth factor; DMSO: dimethyl sulfoxide; OSM: oncostatin M

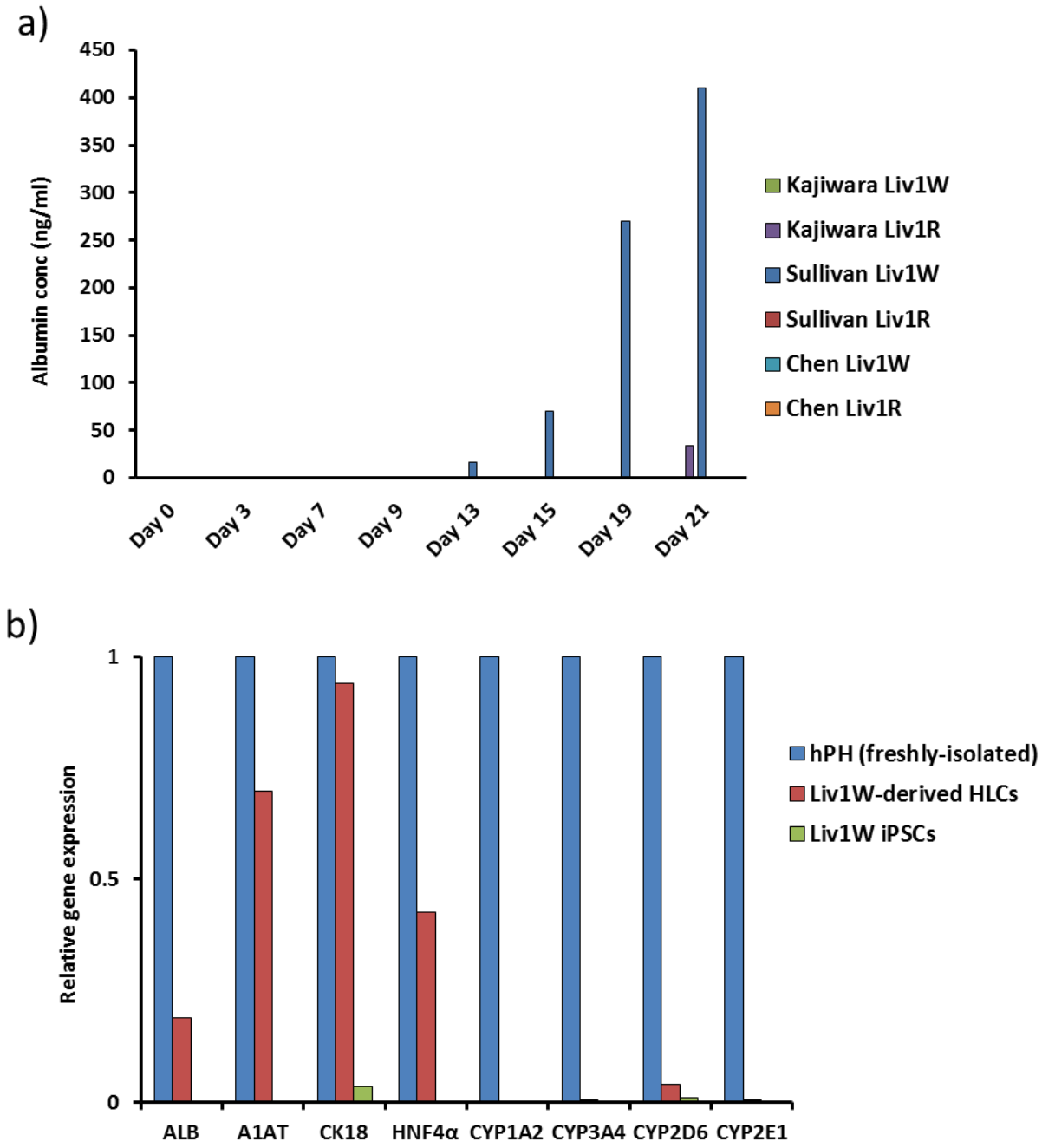

Figure 3.11: Phenotyping of iPSCs differentiated to Hepatocyte-like cells using albumin ELISA and qRT-PCR

a) Albumin secretion of each protocol during the differentiation protocols. Albumin concentration measured using ELISA. **b)** Gene expression of key hepatic genes. The expression of mRNA copies was normalised against GAPDH expression, and the expression of freshly-isolated human primary hepatocytes was set to 1 for each gene. All samples n=2, run in duplicate.

Abbreviations: ALB: albumin; A1AT: alpha-1-anti-tryspin; CK18: cytokeratin-18; HNF4α: hepatic nuclear factor 4 alpha; CYP: cytochrome P450

Use of Sendai virus to reprogram human hepatocytes

To compare iPSCs derived from fibroblasts and hepatocytes, we required a protocol capable of reprogramming human hepatocytes.

Our first attempts at reprogramming used viral MOIs of 3 and 5 and followed the Sendai virus protocol as closely as possible, allowing for cell type restrictions, including a re-plating step at day 7. This protocol did not generate any clones; however, encouraging cuboidal, dividing cells were noted, similar to those seen at the early stage of fibroblast reprogramming (Figure 3.12).

Hepatocytes are known not to respond well to trypsinisation and re-plating, therefore we hypothesised that developing a protocol which did not require re-plating would be the most successful route. Further, given that the cell cycle is a vital component of reprogramming (Xu et al., 2013b), we also decided to use the media composition described by Liu et al., (Liu et al., 2010a) which contains high levels of HGF and EGF, known mitogenic factors.

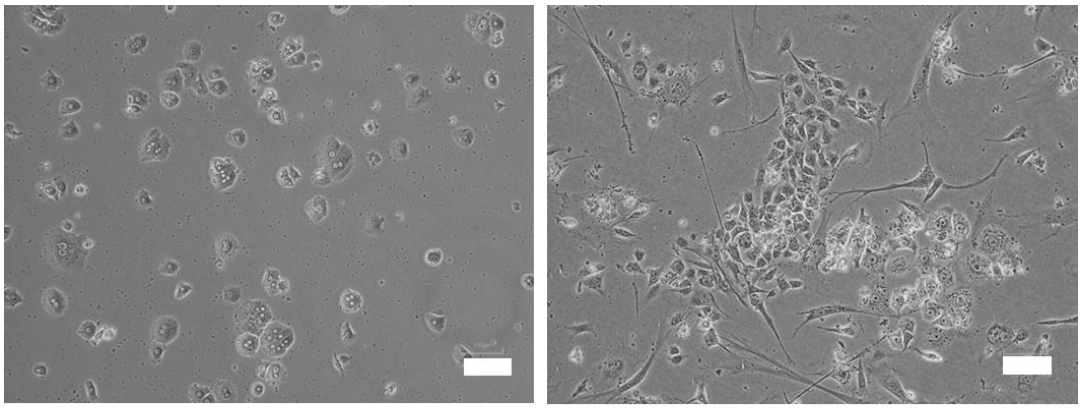

Figure 3.12: Sendai virus-based reprogramming of PHH using the standard protocol did not yield iPSC colonies.

PHH pre-transduction and at day 17 post transduction following transfer to MEF-based culture. Magnification x100, scale bar: 100µm.

To assess if these conditions were feasible, we plated freshly-isolated hepatocytes onto ESC-qualified Matrigel coated plates in hepatocyte reprogramming media at low densities. The cells were then cultured and the morphology of the cells noted over a seven day period, representing the conditions the cells would face during the initial stages of reprogramming. The changes in the cells were marked, with the sub-confluent, mitogenic culture conditions inducing cell flattening and spreading of the hepatocytes with much greater survival than those cells in standard hepatocyte culture media (Figure 3.13a). The maintenance of the hepatic phenotype was confirmed with albumin staining, demonstrating that despite these morphological changes, a key hepatic marker was still present (Figure 3.13b).

The optimised culture conditions appeared ideally suited for the reprogramming of hepatocytes. Therefore, the cells were transduced with Sendai virus at MOI 5 and MOI 10 and examined during for the reprogramming period for colony formation (Figure 3.14). Toxicity was noticeable between Sendai and control wells, with greater toxicity seen at MOI 10. At day 20, the first colonies were noted with similar, but incomplete iPSC-like morphology. These colonies appeared to be heterogeneous and underwent growth arrest during the culture period (Figure 3.15a). At day 24, one colony was noted which did represent the hallmark features of an iPSC colony. After tracking the colony over several days, the colony remained homogenous and continued to expand. This colony was picked onto MEF-coated plates for expansion (Figure 3.15b). Following successful attachment, the clone was expanded and characterised using the panel of pluripotency markers (Figure 3.16a) and functional embryoid body analysis confirming the capacity to differentiate to all 3 germ layers (Figure 3.16b).

As it is difficult to ascertain any true differences between starting cell types if only one clone is compared, we then sought to enhance our reprogramming technique. To increase

the number of clones generated from subsequent donors, we increased the plating density from $1x10^5$ to $5x10^5$. Interestingly, the increased number of starting cells resulted in an increase in the number of clones that were successfully generated; from one iPSC clone in donor 1 to five and ten in donors 2 and 3, respectively. Figure 3.17 demonstrates examples of the iPSC lines which were generated from the PHH cultures of each donor. The generation of these clones allowed for the comparison between PHH- and HDF-derived iPSCs, presented in chapter 4.

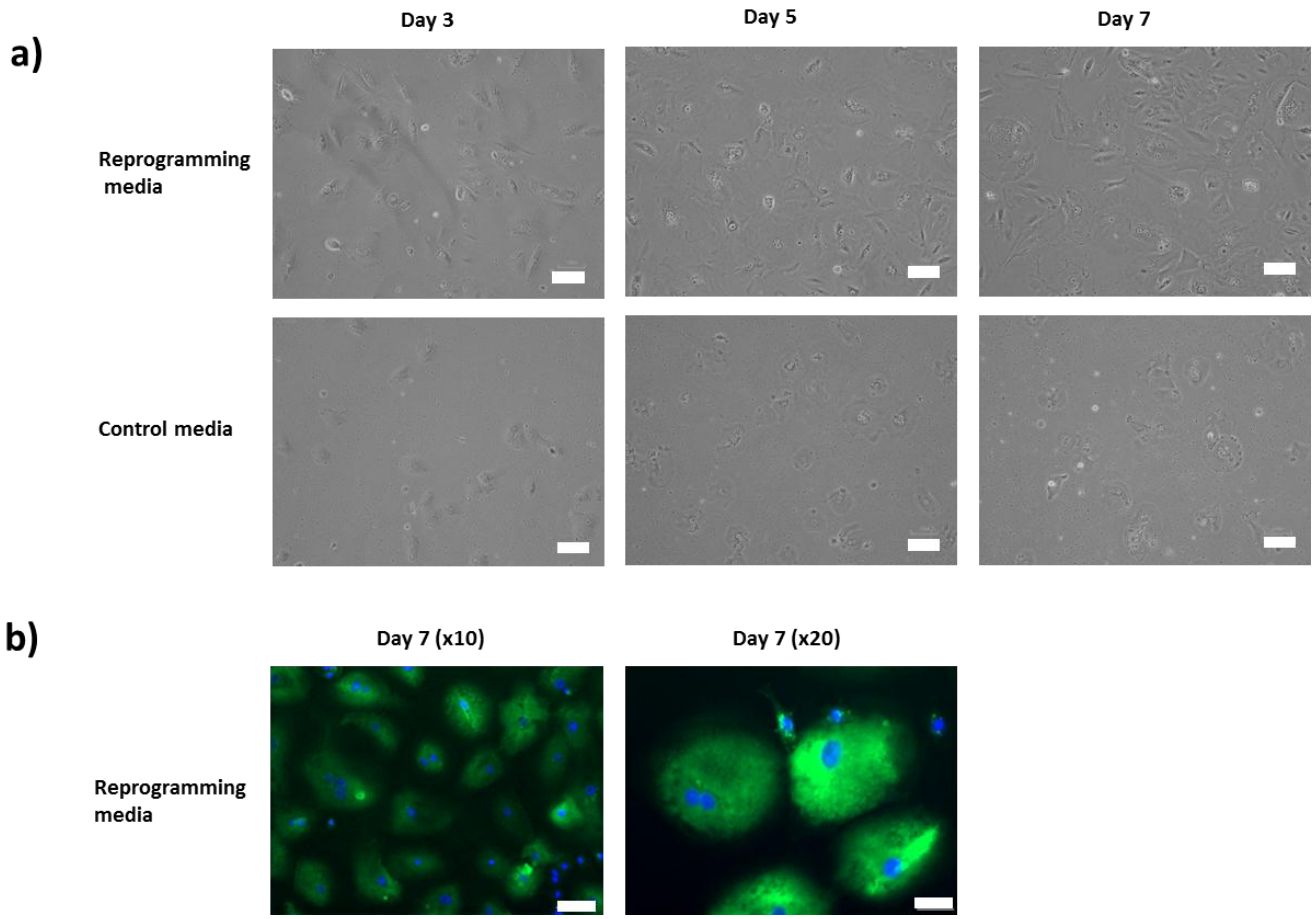

Figure 3.13: Developing a technique to reprogram PHH using a high growth factor-based culture medium.

a) Comparison of morphology and cell survival in PHH cultured in reprogramming media and standard media over a period of 7 days to replicate reprogramming conditions. Magnification x100, scale bar: 100µm. **b)** Immunofluorescence staining for albumin expression in PHH following 7 days of culture in reprogramming media. IF: Magnification x100 and x200, scale bar: 100µm and 50µm.

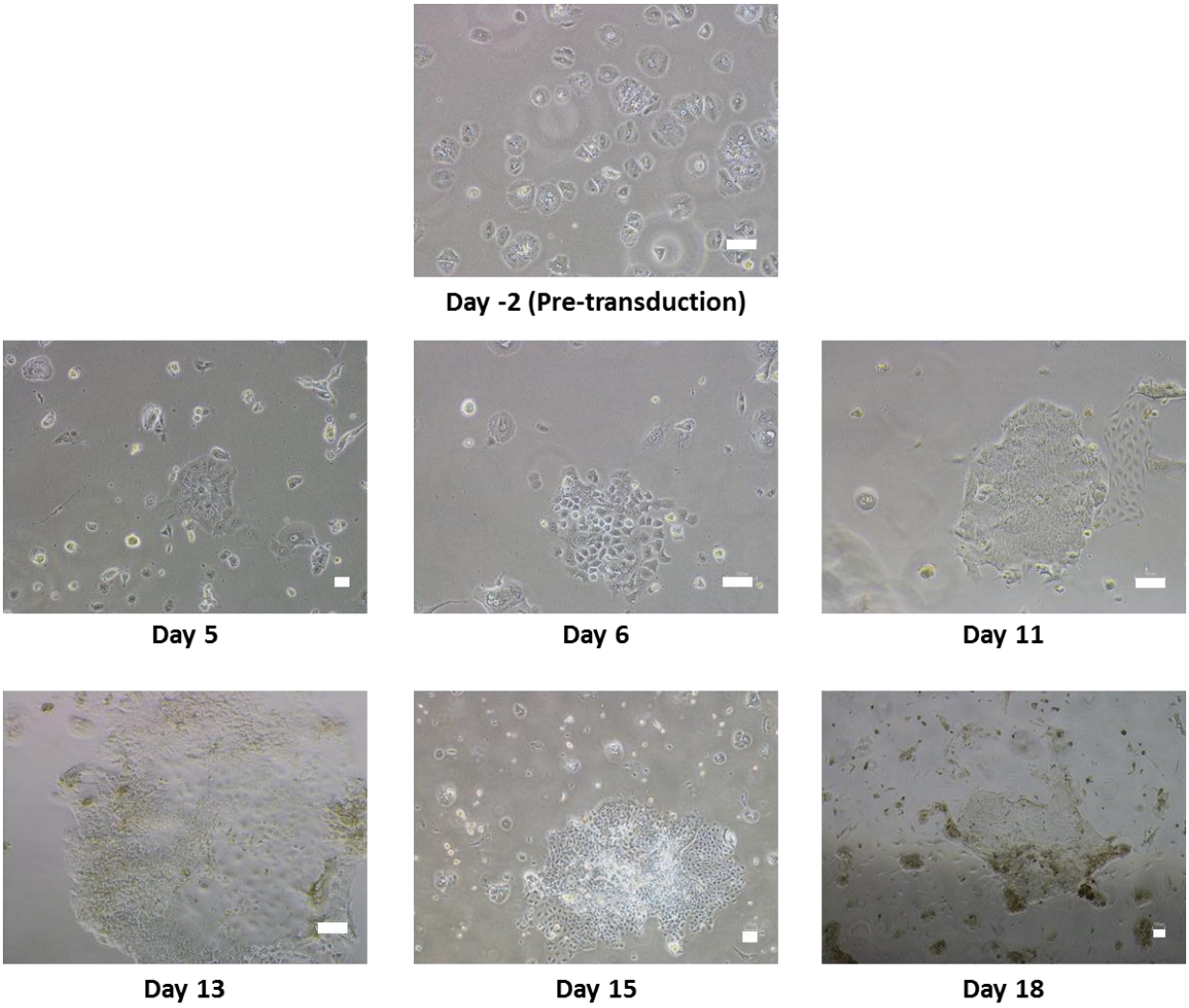

Figure 3.14: The development of partially reprogrammed clones following Sendai virus PHH reprogramming in optimised conditions.

Images taken of PHH pre-transduction and at various stages of culture prior to the emergence of picked colonies. Magnification: x40 (day 5 and 15) and x100, scale bar: 100µm

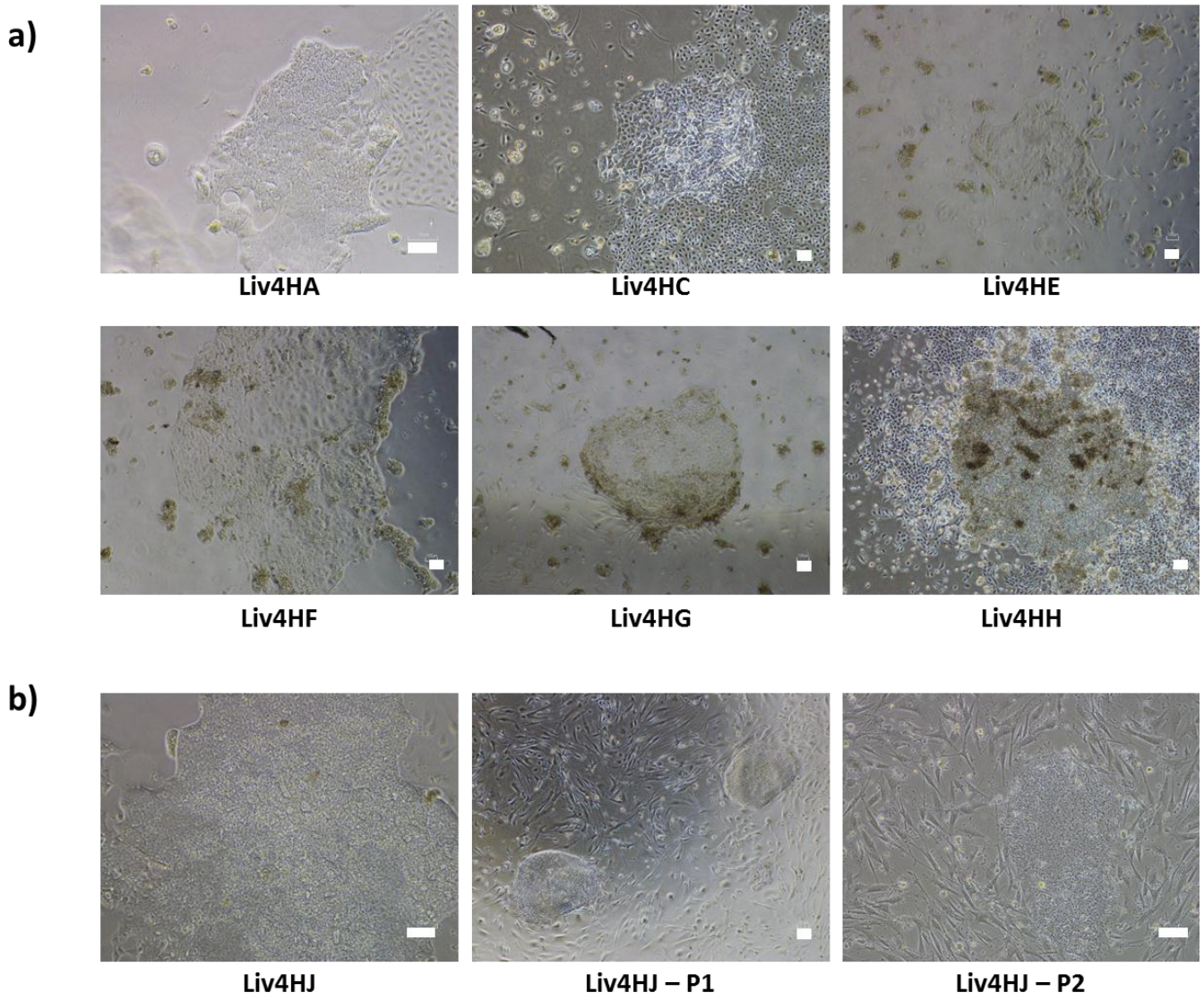

Figure 3.15: Sendai virus PHH reprogramming in optimised conditions generates a single iPSC clone.

a) Images taken of PHH-derived clones which displayed some morphological similarity to iPSCs. Cells were picked but no expansion was noted. **b)** Liv4HJ displayed all characteristics of an iPSC clone and was successfully picked and expanded. Magnification x40 and x100, scale bar: 100µm

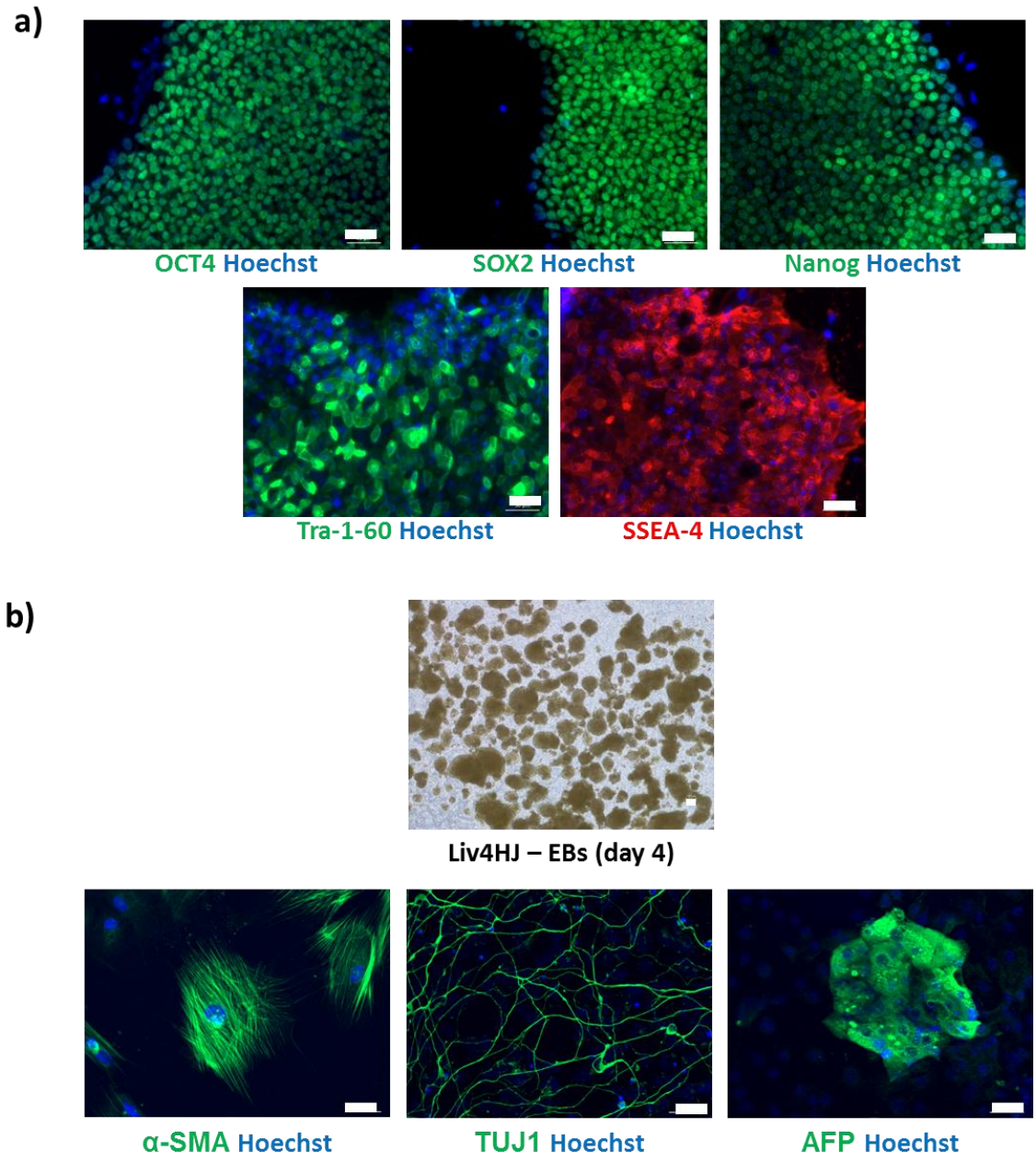

Figure 3.16: Characterisation of PHH-derived iPSCs.

a) Liv4HJ characterised using panel of markers: OCT4, SOX2, Nanog, Tra-1-60 and SSEA-4. **b)** Embryoid bodies formed for assessment of spontaneous differentiation capacity; Immunofluorescence images taken of 3 markers of germ layers: α-smooth muscle actin (mesoderm), TUJ1 (Ectoderm) and alpha fetoprotein (endoderm). IF images: magnification x200, scale bar: 50µm. Light microscopy: magnification x40, scale bar: 100µm.

Abbreviations: AFP: Alpha-Fetoprotein; α-SMA: alpha smooth muscle actin; Tuj1: Neuron-specific class III beta-tubulin; Oct4: Octamer-binding transcription factor 4; Sox2: SRY (sex determining region Y)-box 2; Tra-1-60: Tumour-related antigen (TRA)-1-60; SSEA-4: Stage-specific embryonic antigen-4

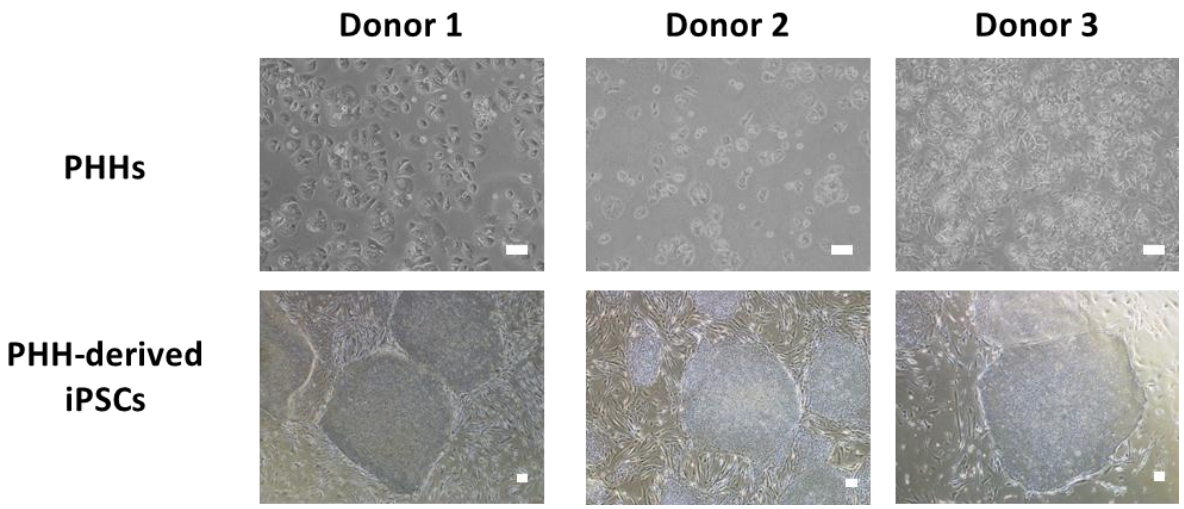

Figure 3.17: Characterisation of PHH-derived iPSCs.

Isolation and reprogramming of somatic cells. The morphology of PHH from each donor prior to reprogramming and selected examples of the iPSCs which were generated from each of these starting cell types/donors. PHH: magnification: x100, scale bar: 100µm; iPSCs: magnification x40, scale bar: 100µm.

3.3 Discussion

The data presented in this chapter demonstrates the multiple steps and optimisation undertaken to develop a working protocol for hepatocyte reprogramming and differentiation.

Despite using two published techniques of microRNA-based cell reprogramming (Anokye-Danso et al., 2011; Miyoshi et al., 2011), we were unable to replicate successful iPSC generation in any of the cell types used. Whilst no fully reprogrammed clones were found within our culture systems, colonies of interest did form in the cells transduced with the lentiviral miR-302/367 construct. Upon analysis, these colonies had detectable expression of the pluripotency marker Sox2, but no expression of other markers, such as Oct4 and Nanog. This suggests that the technique yielded partially reprogrammed colonies which have resulted ectoderm-like cells, based on the Sox2 expression in the absence of Oct4 and Nanog (Puligilla et al., 2010). Our results are in-keeping with current literature as, at the time of writing, no subsequent reports of miRNA-based reprogramming have been published (Lüningschrör et al., 2013). In contrast to the reported high efficiency of reprogramming of the lentiviral method, our results suggest that the technique has a very low efficiency of reprogramming and/or works in conditions specific to the laboratory of origin.

Our investigations of the lentivirus-based technique were hampered by low viral yields which could not be enhanced sufficiently using concentration methods, preventing multiple high MOI repeats in large numbers of cells. The enhanced viral titre in the control virus compared to the miRNA virus suggests that the reports describing mechanisms, such as Drosha targeting and cytomegalovirus (CMV) promoter interference, which reduce miRNA viral loads in lentiviral preparations, may have been the causative factor in our low viral titres (Liu et al., 2010b). The same publication suggested that the replacement of the CMV

promoter with an inducible promoter can restore the titre levels (Liu et al., 2010b); however, due to the lack of positive results from the pilot experiments and the success of the Sendai virus, this was not pursued.

Direct transfection of microRNAs was repeated numerous times using a variety of different conditions and cell types. Despite this, no reprogrammed colonies and only small differences in cell morphology were observable with the fibroblast cells appearing to 'ball up', perhaps representative of the mesenchymal-to-epithelial transition associated with reprogramming (Sancho-Martinez and Belmonte, 2013), although this may also represent cytotoxicity.

Following the successful reprogramming of BJ fibroblasts using the Sendai virus delivery method, we used these resulting cell lines to optimise the differentiation to hepatocyte-like cells, assessing numerous techniques and protocols. The plating density and growth factor combination used to derive the definitive endoderm cell population was assessed using the definitive endoderm marker, Sox17. The results suggested that it was the plating density which had the greatest effect on the resulting differentiation efficiency, with the highest cell density yielding the greatest number of Sox17+ve cells. The requirement for high cell numbers appears to be a consequence of single cell plating as confluences as low as 50% have been reported in the literature previously, when differentiation is initiated using colony-based protocols (Sullivan et al., 2010). This is perhaps indicative that high cell density and paracrine factors, as seen in colony-based cultures, are required to commence endodermal differentiation; however, a recent paper reported a plating density of 3-4x10^4 cells/cm^2 (Asplund et al., 2015). This work was performed using cells which were routinely cultured as a monolayer and using a single cell method for passaging; therefore, the change from colony-based to single cell plating may be detrimental to definitive endoderm efficiency.

Of interest, plating cells at the density reported by Kajiwara *et al.,* ($1x10^5$cells/cm^2) did not yield high definitive endoderm differentiation efficiency (Kajiwara et al., 2012); this may be due to differences in laboratory conditions or iPSC line variability as we followed the same plating methodology as reported in this paper. However, we did use a different stem cell media (Essential 8 as opposed to MEF-conditioned media) to convert our iPSCs to feeder free culture before differentiation. To improve batch-to-batch reproducibility, Essential 8 media does not contain bovine serum albumin (BSA) (Chen et al., 2011); consequently, the differentiation capacity of the cells may be affected as removal of BSA also removes fatty acids and other molecules which are bound to the albumin and have as yet undefined roles in differentiation processes. In support of this hypothesis, subsequent to the work presented in this thesis being completed, Stem Cell Technologies have developed an additional pre-treatment media to use with their definitive endoderm differentiation kits (product code: 05115) for those using Essential 8-based culture systems.

Furthermore, the areas towards the edge of the culture demonstrated the greatest differentiation efficiency, with the central regions proving to be refractory to differentiation. This may be partially explained by a recent report of spatial patterning which is evident within ESC colonies when cultured on micro-patterned plates, used to define colony size and shape (Warmflash et al., 2014). Within these colonies paracrine factors are thought to influence the differentiation propensity of the different areas of the colony, with those closest to the centre associated with ectodermal markers, encircled by a ring of mesodermal/primitive streak-like cells and then further encircled by SOX17+ve endodermal cells, following BMP4 induced differentiation (Warmflash et al., 2014). This patterning is remarkably similar to the results seen within the differentiation of cells seeded at $1.5x10^5$ cells/cm^2 with a clear enrichment of Sox17+ve cells towards the edge of the well. Subsequent work suggested using plating densities up to $2x10^5/cm^2$ reduces the

zonation of the culture and further increases the differentiation efficiency (data not shown).

When cells were differentiated towards and hepatic phenotype, our results suggested that the Kajiwara and Sullivan protocols allowed for the differentiation of albumin producing cells, whereas the Chen protocol did not. Furthermore, Liv1R appeared refractive to HLC differentiation secreting little-to-no detectable albumin across the three protocols. This is in-keeping with the majority of literature which demonstrate line-to-line variation with regard to hepatocyte differentiation potential (Jiang et al., 2013). However, the Kajiwara protocol was able to induce small amounts of albumin secretion in Liv1R, whereas the Sullivan protocol did not; therefore, for the experiments described in chapter 4, we used an adapted version of the Sullivan protocol with a 7, rather than 5, day hepatic endoderm stage.

The transition of the Sendai virus reprogramming conditions to PHH was successful, producing a single clone from $1x10^5$ cells. At the time of the experiment, this was the first PHH-derived iPSC to be produced using a non-integrative method; however, Takayama *et al.,* have since reported a similar technique with the Sendai virus (Takayama et al., 2014).

During the design of the experiment, we compared the two published reports of PHH reprogramming. Whilst Hansel *et al*., repeated a very low reprogramming efficiency which was only achievable using the OSKM factors plus Lin28 and Nanog in relatively young donors (Hansel et al., 2014), Liu *et al*., reported a relatively high efficiency which was equal to, if not greater than, HDF reprogramming techniques (Liu et al., 2010a). As a consequence, we closely followed the Liu *et al*., protocol, particularly with regard to the media composition, which contained high levels of mitogenic factors hepatocyte growth factor (HGF) and epidermal growth factor (EGF). Our initial results suggest that PHH reprogramming occurs at a very low efficiency, which is in agreement with Hansel *et al*. The

discrepancy between the efficiencies is likely the result of multiple factors regarding the quality of hepatocytes, which can vary dramatically between donors (Bhogal et al., 2011). Another likely factor is the age of the patient. Hansel *et al*., reported that reprogramming was only achievable from very young donor hepatocytes; whereas the donor age of the Liu *et al*., paper is not reported. The donor used for this initial experiment was 66 years old at the time of surgery and therefore the low efficiency may be a consequence of donor age (Trokovic et al., 2015). This hypothesis was strengthened as we were subsequently able to generate clones from two further donors of different ages in slightly enhanced reprogramming conditions (i.e. higher plating density). Interestingly, by increasing the starting cell density five-fold, we were able to generate 5 fold clones from donor 2 (63 years old), suggesting the reprogramming efficiency was directly proportional to the starting cell number. However, in the same enhanced conditions, 10 clones were derived from donor 3 (27 years old). These data point towards an enhancement of hepatocyte reprogramming efficiency in younger donors. Thus, it is possible that the protocols described may have allowed reprogramming of donor hepatocytes which would have been refractory in the conditions reported by Hansel *et al*.

Furthermore, as primary human hepatocytes are highly sensitive following isolation and, to the best of our knowledge, lack any truly discriminative cell surface markers, they cannot be sorted effectively to enhance purity. Therefore, it is not possible to rule out the potential that the resulting iPSC has been derived from a different cell type from the PHH-enriched population. The aforementioned study by Takayama *et al.,* claimed to be able to demonstrate PHH as the source using short tandem repeat analysis (Takayama et al., 2014); however, whilst this confirms the cells are from the correct donor, it is unclear how they can distinguish between different cell types using this technique.

In summary, this chapter encapsulates the work done to establish the protocols required to undertake the isogenic comparison of PHH and HDF-derived iPSCs in the production of HLCs. This comparison is presented in chapter 4.

Chapter 4

Isogenic comparison of hepatocyte-like cells differentiated from human primary hepatocyte- and dermal fibroblast-derived induced pluripotent stem cells

Introduction

Drug induced liver injury (DILI) remains incompletely understood. This is in part due to the lack of a predictive *in vitro* model to allow the identification of compounds which go on to cause DILI during clinical trials or post-marketing authorisation. The gold standard for investigating DILI remains primary human hepatocytes (PHH); however, PHH dedifferentiate rapidly in culture (investigated in chapter 5) and vary greatly between donors (Fraczek et al., 2013). Therefore, a metabolically relevant, reproducible and physiologically normal source of cells would be invaluable to the pharmaceutical industry and academia investigating DILI.

The development of stem cells as a source of hepatocyte-like cells (HLCs) has been an area of intense research since the first differentiation protocols were described in 2004 by Lavon *et al* (Lavon et al., 2004). In the intervening years, incremental improvements have seen enhancements in both efficiency of differentiation and phenotype maturity. Despite these improvements, the hepatic phenotype still remains closer to a foetal rather than an adult phenotype (Kia et al., 2013). This has led to researchers to look elsewhere for improvements in the differentiation of stem cells towards HLCs.

One potential area of interest has been to investigate the cell of origin. Previous work has shown that during the reprogramming process, the hypermethylation of the genes associated with the somatic cell phenotype occurs at a relatively late stage of induced pluripotency (Koche et al., 2011). Consequently, induced pluripotent stem cells (iPSCs) maintain a memory of the cell from which they were derived, which can influence the differentiation propensity of the cell towards the lineage of origin (Lister et al., 2014).

This phenomenon, termed epigenetic memory, was first described in two separate studies in 2010 (Kim et al., 2010a; Polo et al., 2010). This was subsequently found to be true of

other cell types, such as pancreatic β cells, which demonstrated increased PDX1 and insulin gene expression in spontaneously differentiated iPSCs-derived from β cells when compared to non-β cell-derived iPSCs and ESCs (Bar-Nur et al., 2011).

Epigenetic memory has also been investigated using hepatocytes (table 4.1); however, no study has provided definitive proof of whether the starting cell type significantly impacts upon the hepatic differentiation capacity of iPSCs. Genotype-controlled experiments in mice have shown a transient advantage in HLC gene expression of albumin and CK18 in hepatic-derived iPSCs compared to MEF-derived iPSCs (Lee et al., 2012). However, this advantage was greater when derived from hepatoblasts than hepatocytes and dissipated with time in culture. Liu *et al*., published the first human comparison in 2011, (Liu et al., 2011), demonstrating no significant advantage in hepatic phenotype when PHH-derived iPSCs were compared to iPSCs derived from other cell types derived from different donors, as measured by albumin secretion, CYP3A activity assays; however, a similar but distinct global epigenetic profile was reported (Liu et al., 2011). More recently Takayama et al., corroborated the report from Lee et al., in human cells, demonstrating a small but significant advantage between hepatocytes and other cell types; however, the cells were sourced from different donors and the advantage was again found to dissipate with time in culture (Takayama et al., 2014). The importance of donor-dependent genetic differences were further highlighted by Kajiwara *et al.,* who showed that donor differences were the largest determinant of hepatocyte-like cell quality, rather than the cell of origin, albeit without the investigation of PHH-derived iPSCs (Kajiwara et al., 2012). These donor-dependent differences are likely to be driven by the transcriptional variation derived from the genetic background of the donor influencing differentiation propensity (Rouhani et al., 2014).

Authors	Species	Starting cell types	Assays used	Improved phenotype?
(Liu et al., 2011)	Human	Hepatocytes Fibroblasts Keratinocytes BM-MSCs	Albumin secretion CYP3A4 activity	Yes, but non-significant
(Lee et al., 2012)	Mouse	Mouse ESCs Fibroblasts Hepatoblasts Hepatocytes	Albumin secretion HLC gene expression	Yes, but transient
(Kajiwara et al., 2012)	Human	PBMCs Fibroblasts	Albumin/Urea secretion	No, donor dependent
(Takayama et al., 2014)	Human	Hepatocytes Fibroblasts PBMCs HUVECs	Albumin secretion CYP3A4 activity TAT expression	Yes, but transient

Table 4.1: Summary of the previously published investigations of starting cell type for hepatocyte-like cell differentiation

Abbreviations: PBMCs: Peripheral blood mononuclear cells; HUVECs: Human umbilical vein endothelial cells; BM-MSCs: Bone marrow mesenchymal stem cells; ESCs: embryonic stem cells

Therefore, investigation of epigenetic memory in hepatocyte-derived HLCs for the study of human iPSCs can only be truly assessed using a thorough comparison of human, genotype-controlled iPSCs derived from hepatocytes and non-hepatocytes isolated from the same donor. Herein, using the protocols established in chapter 3, we describe the comparison of isogenic PHH- and dermal fibroblast derived iPSCs and the hepatic differentiation potential of these cells.

Hypothesis: The use of primary human hepatocyte-derived iPSCs to generate hepatocyte-like cells yields an improved maturity in hepatocyte-like cell maturity when compared to HDF-derived iPSCs from the same donor.

Results

Generation of iPSCs derived from PHH and HDFs of multiple donors.

In order to compare the hepatic differentiation capacity of iPSCs derived from different donors, we first needed to reprogram both PHH and HDFs. The reprogramming of human hepatocytes has been reported as relatively inefficient compared to more traditional cell types, such as fibroblasts (Hansel et al., 2014). Therefore, we first developed a protocol capable of reprogramming human hepatocytes (chapter 3).

Using this protocol, we successfully generated iPSCs from hepatocyte cultures from three separate donors (table 4.2). Subsequent to successful PHH-reprograming, the dermal fibroblasts of the corresponding donors were also reprogrammed using a well-established dermal fibroblast protocol, the isolation and characterisation of these cells is described in R. Kia's PhD thesis (Kia, 2014). Pictures of the PHH and HDFs derived from each donor and schematic diagrams of the techniques used for reprogramming are shown in Figure 4.1.

Pluripotency was assessed using a panel of embryonic stem cell-enriched markers: Oct4, Sox2, Nanog, Tra-1-60 and SSEA-4 (Figure 4.2). All lines examined demonstrated expression of each of the markers, indicating that they had established a pluripotent phenotype.

The functional differentiation capacity of these lines was also assessed using embryoid body (EB) assays. This assay allows the cells to differentiate without endogenous growth factors in the media and, if truly pluripotent, should result in differentiation towards cell types from all three germ layers: ectoderm, mesoderm and endoderm. Following EB culture, the presence of each of these germ layers within differentiated cell population was investigated by immunofluorescence, using the markers TUJ1 (Neuron-specific class III beta-tubulin; ectoderm), α-SMA (alpha smooth muscle actin; mesoderm) and AFP (Alpha-

Fetoprotein; endoderm) (Figure 4.3). All of the iPSC lines generated stained successfully for the markers, indicating that every line was functionally pluripotent.

	DONOR 1	DONOR 2	DONOR 3
Age at surgery	66	63	27
BMI	27.9	31.2	32.1
Sex	Male	Female	Male
Diagnosis	Colorectal carcinoma with liver metastases	Colorectal carcinoma with liver metastases	focal nodular hyperplasia
Co-morbidity	Type II diabetes mellitus	Hypertension Chronic liver disease Type II diabetes mellitus	None
No. of PHH-derived clones	1	5	10

Table 4.2: **Details of the donors from which the cells used for reprogramming were derived, including key parameters such as age, co-morbidities and the number of iPSC clones derived from each donor PHH.**

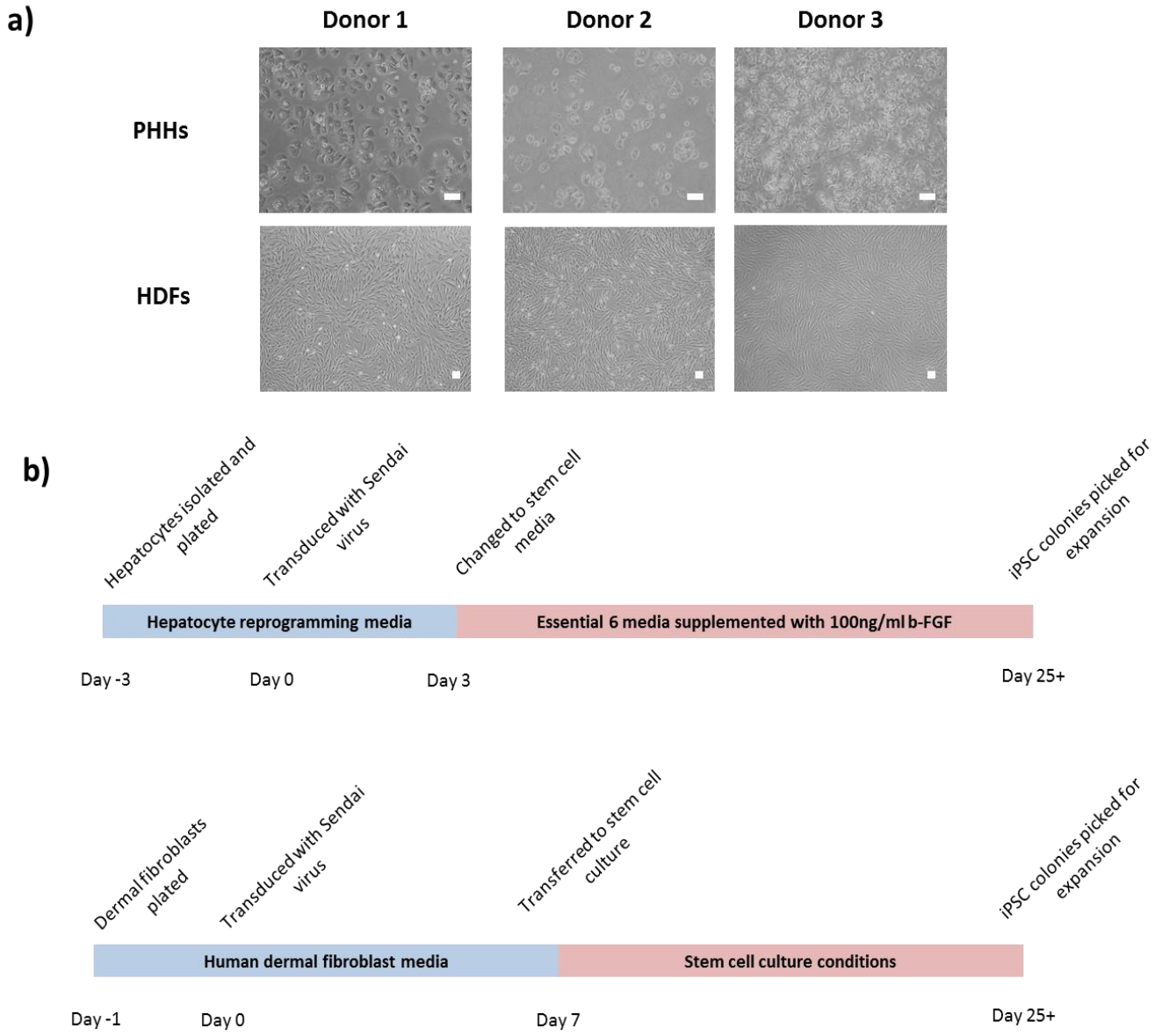

Figure 4.1: Isolation and reprogramming of somatic cells.

a) The morphology of PHH and HDFs from each donor prior to reprogramming. PHH: Magnification: x100, scale bar: 100µm; HDFs: magnification x40, scale bar: 100µm. **b)** Schematic diagram of the protocols used to reprogram each cell type. PHH: Primary human hepatocytes; HDFs: Human dermal fibroblasts; b-FGF: basic fibroblast growth factor

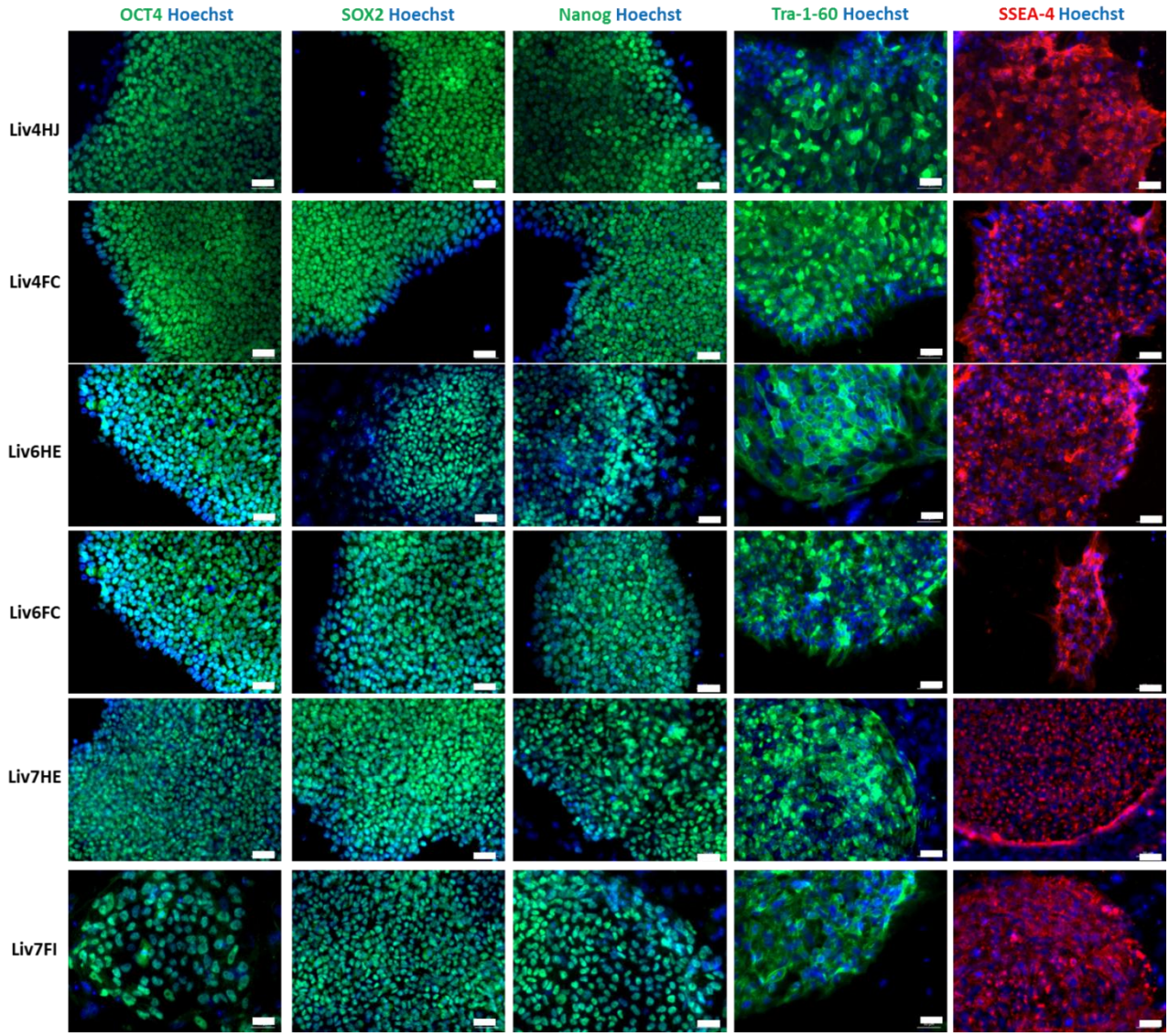

Figure 4.2: Generation and characterisation of each iPSC line confirmed by morphology and immunofluorescence.

Morphology of selected lines from each donor and starting cell type is shown next to the immunofluorescence images of nuclear pluripotency markers Oct4, Sox2 and Nanog and surface markers Tra-1-60 and SSEA-4. Immunofluorescence images: x200 magnification, 50µm scale bar. Light microscopy images: x100 magnification, 100µm scale bar. For each line: F – derived from HDF; H-derived from PHH; 4: donor 1; 6: Donor 2; 7: Donor 3.

Abbreviations: Oct4: Octamer-binding transcription factor 4; Sox2: SRY (sex determining region Y)-box 2; Tra-1-60: Tumour-related antigen (TRA)-1-60; SSEA-4: Stage-specific embryonic antigen-4

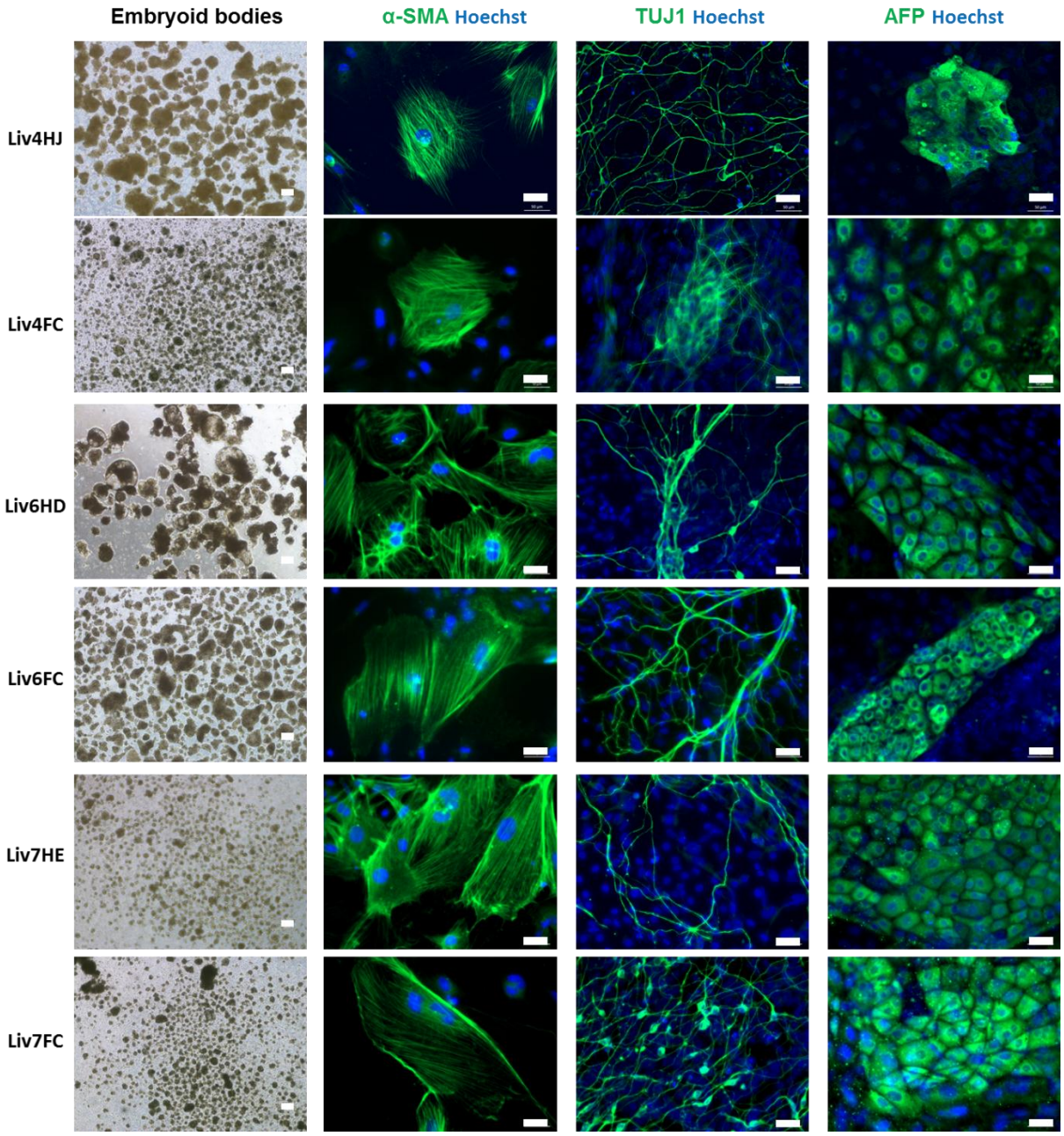

Figure 4.3: Functional pluripotency characterisation using embryoid body assay confirmed by immunofluorescence.

Embryoid bodies generated from each iPSC line and stained for markers of the three germ layers associated with pluripotency, selected lines from each donor and starting cell type presented: Endoderm (AFP), Mesoderm (α-SMA) and Ectoderm (Tuj1). Immunofluorescence images: x200 magnification, 50µm scale bar. Light microscopy images: x40 or x100 magnification, 100µm scale bar. . For each line: F – derived from HDF; H-derived from PHH; 4: donor 1; 6: Donor 2; 7: Donor 3.

Abbreviations: AFP: Alpha-Fetoprotein; α-SMA: alpha smooth muscle actin; Tuj1: Neuron-specific class III beta-tubulin

Comparing PHH and HDF-derived iPSCs gene expression and methylation status

To fully compare the iPSCs generated from PHH and HDFs, comparisons were required at all stages of culture and differentiation. Therefore, we first compared the expression of important pluripotency-associated genes for differences in expression. Across these markers, Oct4 and Nanog showed similar levels of expression between both cell types of origin. Sox2 expression was significantly greater in the PHH-derived lines for donor 3; however, this was not true of donors 1 and 2. Furthermore, analysis of Wnt3, which has been proposed as an iPSC marker of definitive endoderm potential (i.e. high Wnt3 expression correlates with high purity D.E formation) (Jiang et al., 2013), again showed no significant differences between PHH and HDF-derived iPSCs.

As the inherent memory of iPSCs is reported to be a consequence of incomplete epigenetic reprogramming, we then investigated the potential differences in methylation patterns between PHH and HDF-derived lines at the iPSC stage. We therefore compared the methylation status of key hepatic genes, HNF4α and FOXA2, which would likely influence the differentiation status of the HLCs should they be differentially methylated. During the process of reprogramming, the methylation status of HNF4α in PHH is significantly increased by 65.8%. A significant change in HNF4α methylation during reprogramming also occurs in HDFs, which increased from 82.6% in HDFs to 90.6% methylation in HDF-derived iPSCs. FOXA2 methylation was also seen to significantly increase between both starting cell types and iPSCs, albeit to a lesser degree.

Our results suggested very little difference in methylation status between the PHH and HDF-derived lines. Across the five CpG sites examined within the HNF4α promoter region, each site was consistently ~1% less methylated in the PHH-derived lines when compared to the HDF-derived lines. Across all lines and CpG sites investigated a mean of 1.22% less methylation was observed in PHH-derived samples. No differences were noted between

the FOXA2 iPSCs derived from PHH and HDFs. The trend noted in the HNF4α analysis was found to dissipate with time in culture as direct comparison of early and late passage PHH-derived lines showed increasing levels of methylation to become more comparable to the status of the HDF-derived lines, with a difference of 0.42% methylation between late passage PHH-derived and HDF-derived iPSCs. FOXA2 also shows an increase in methylation (1.22%) between early and late passage PHH-derived IPSCs.

No noticeable difference in Line1 (Line 1: Long interspersed nuclear elements retrotransposable element 1) methylation, a sequence which is repeated throughout the genome and often used as a surrogate marker of whole genome methylation status, was observed across the early passage iPSCs (passage <10). In fact, Line1 methylation showed remarkable similarity between PHH- and HDF-derived clones, which had mean methylation statuses of 65.35% of 65.43%, respectively.

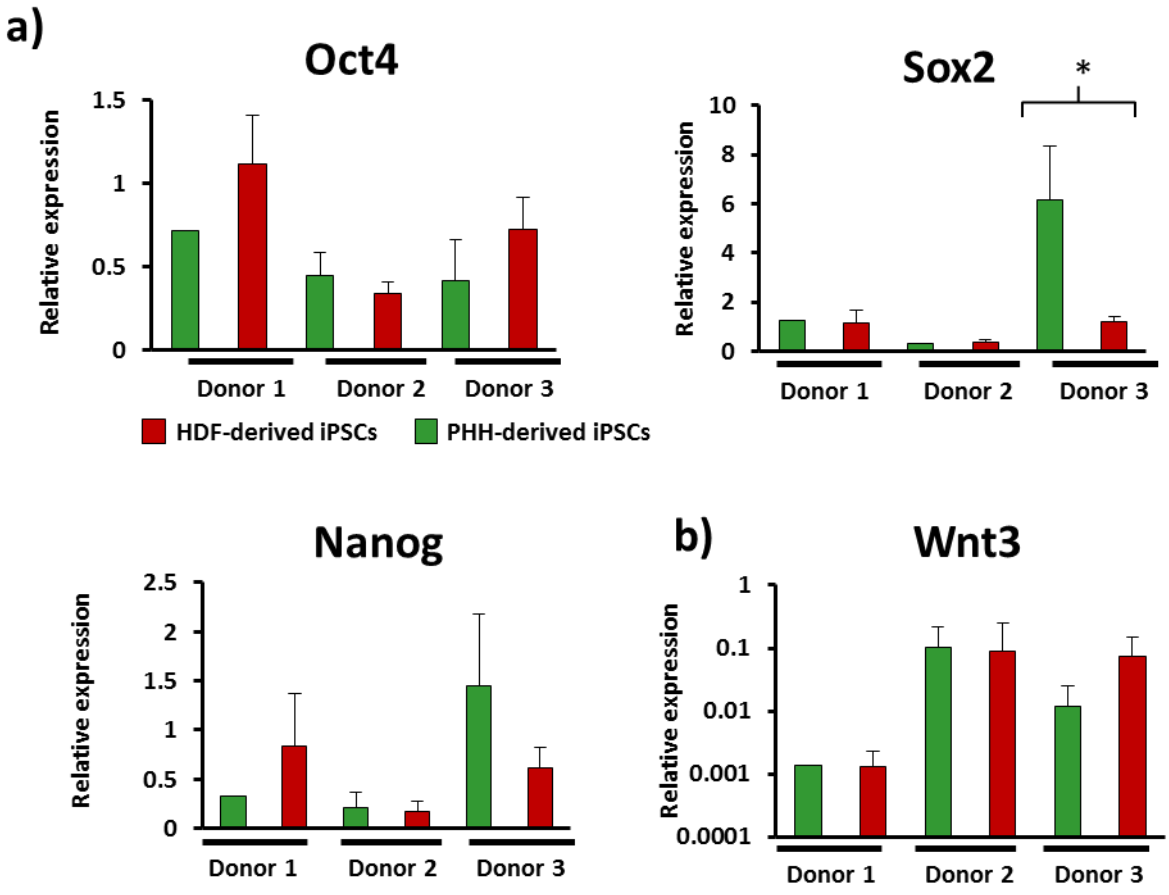

Figure 4.4: Comparison of iPSC gene expression by qRT-PCR.

a) Nanog, Sox2 and Oct4 gene expression determined by qRT-PCR and presented as $2^{-\Delta\Delta}$CT relative to ESC comparator and normalised with GAPDH. **b)** Wnt3 gene expression determined by q-PCR and presented as $2^{-\Delta\Delta}$CT relative to ESC comparator and normalised with GAPDH. Error bars represent standard deviation between the means of each PHH-/HDF-derived iPSC line which were derived from three individual differentiation cultures. Each sample tested by qRT-PCR was loaded in duplicate. (*) denotes p>0.05 unpaired T test.

Abbreviations: Oct4: Octamer-binding transcription factor 4; Sox2: SRY (sex determining region Y)-box 2; Wnt3: Wingless-Type MMTV Integration Site Family, Member 3

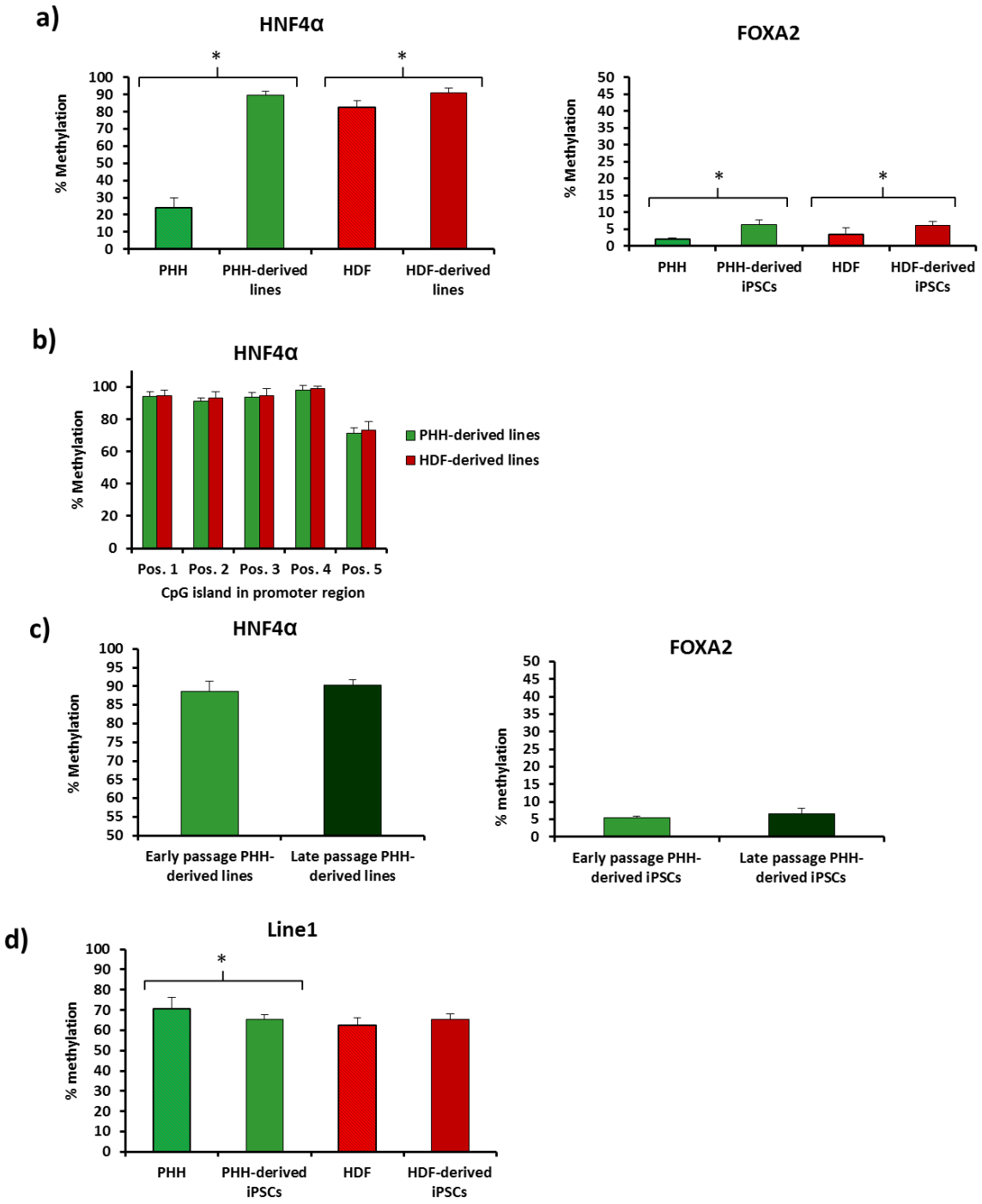

Figure 4.5: Comparison of methylation status using pyrosequencing analysis of HNF4α and Line1 promoter regions.

a) The changes in methylation status of HNF4α and FOXA2 in PHH (48hrs culture) and HDFs pre- and post-reprogramming; **b)** the difference in HNF4α methylation status of the PHH- and HDF-derived iPSCs across the 5 CpG sites located in the analysed sequence; **c)** The methylation status of HNF4α and FOXA2 which occur following repeat passaging of the cells during standard culture procedures. **d)** The changes in methylation status of Line1 in PHH and HDFs pre- and post-reprogramming. (*) denotes p>0.05 One way ANOVA. Error bars represent standard deviation between the mean values of each line for iPSCs and between donors for PHH and HDFs

Abbreviations: HNF4α: Hepatic nuclear factor 4 alpha: Line1: Line 1: Long interspersed nuclear elements retrotransposable element 1; FOXA2: Forkhead box protein A2

Spontaneous differentiation comparisons of PHH and HDF-derived iPSCs

To investigate if the cell of origin influences the inherent differentiation propensity of iPSCs, the endoderm-enriched gene expression of embryoid bodies were compared (Figure 4.3). Using a previously published method for comparing iPSCs of different origins (Bar-Nur et al., 2011), we generated EBs and cultured them in suspension for 16 days and then compared the gene expression of known endoderm and hepatic markers.

Our results suggested a very slight trend towards the enhancement of hepatic-associated gene expression in PHH-derived EBs in five of the genes tested, i.e. Albumin, AFP, SOX17, FOXA2 and CXCR4. However, GATA4 and HNF4α showed a trend towards higher expression in the HDF-derived clones. Despite these trends, only Sox17 showed significantly greater expression in PHH-derived iPSCs, although this difference was only observed in one of the three donors. Taken together there was very little difference in the spontaneous differentiation propensity of PHH and HDF-derived iPSCs across the investigated hepatic and endodermal-associated genes. Indeed, the greatest determinant of gene expression appeared to be the donor, rather than the starting cell type.

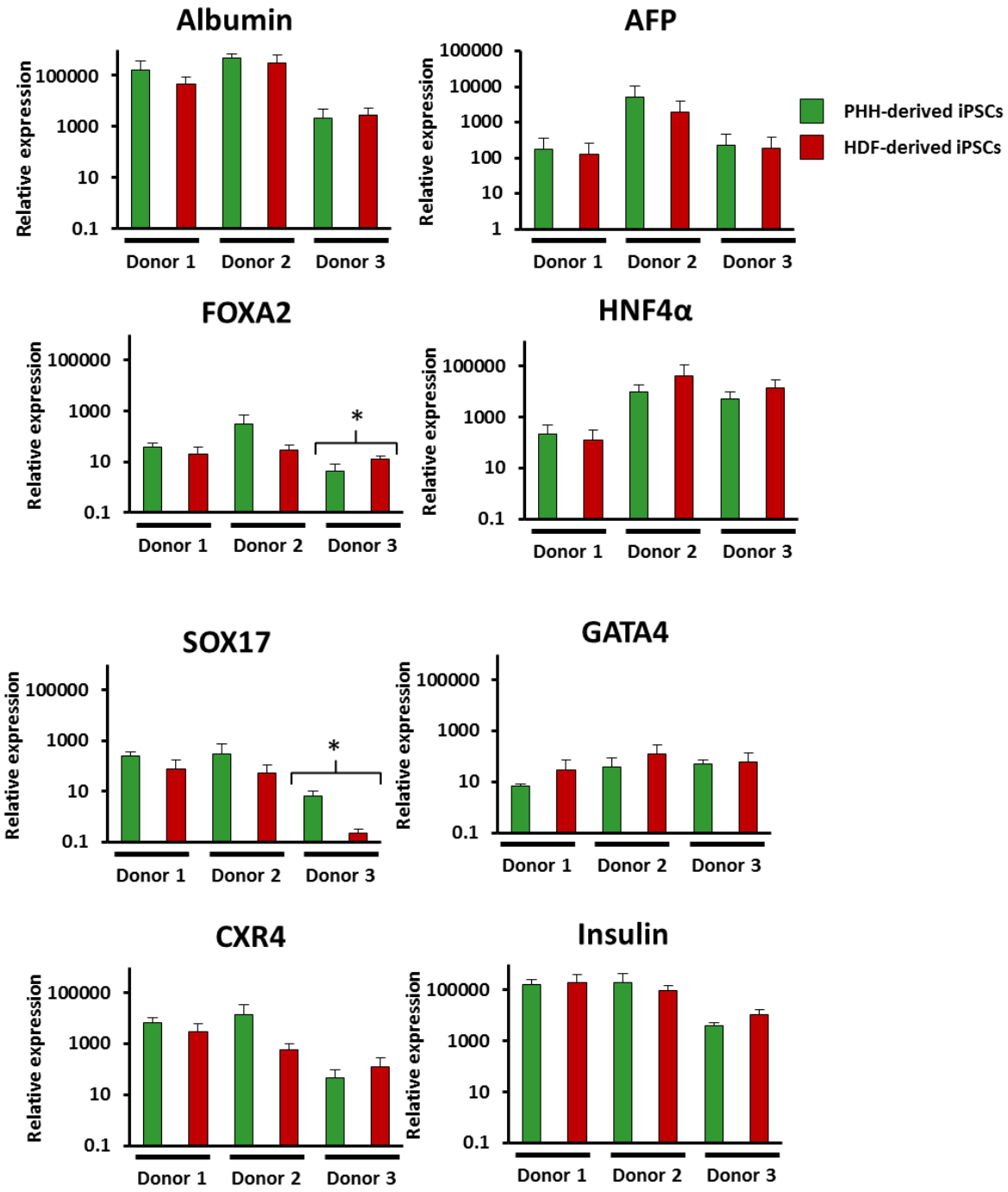

Figure 4.6: Comparison of endoderm and hepatic associated gene expression in PHH- and HDF derived embryoid bodies using qRT-PCR.

All genes shown as $2^{-\Delta\Delta}$CT relative to a ESC-derived EB comparator and normalised to GAPDH and Succinate dehydrogenase. Error bars represent standard deviation between the means of each PHH-/HDF-derived iPSC line which were derived from three individual differentiation cultures. Each sample tested by qRT-PCR was loaded in duplicate. (*) denotes p>0.05 unpaired T test.

Abbreviations: AFP: Alpha-Fetoprotein; SRY (Sex Determining Region Y)-Box 17; FOXA2: Forkhead Box A2; HNF4α: Hepatic nuclear factor 4 alpha: GATA4: GATA Binding Protein 4; CXCR4: Chemokine (C-X-C Motif) Receptor 4.

Comparison of gene expression during hepatocyte differentiation from PHH and HDF-derived iPSCs

The differentiation of iPSCs towards hepatocyte-like cells was achieved using the protocol established in chapter 3 (Figure 4.7a) and successful differentiation was confirmed by immunofluorescence at each stage: definitive endoderm (Sox17), hepatic endoderm (HNF4α) and HLCs (Albumin) (Figure 4.7b).

To fully evaluate the differentiation procedure and to assess for any inherent advantage as a result of the different starting cell types, we compared the gene expression at each stage of differentiation. Figure 4.8 demonstrates a comparison of several key markers of definitive endoderm. The results followed a similar pattern to previous analysis, demonstrating no significant differences between starting cell types when the gene expression of FOXA2, SOX17, GATA4 or CXCR4 was compared. Interestingly, FOXA2, SOX17 and CXCR4 showed a larger dependence on the donor of origin than starting cell type; whereas, GATA4 demonstrated greater consistency in expression between donors.

Similar analysis was also undertaken for the hepatic endoderm stages, using markers AFP and HNF4α as stage-specific markers. Despite a trend towards enhanced levels of both markers in the PHH-derived iPSCs, only HNF4α in donor 2 demonstrated significantly enhanced gene expression in PHH-derived hepatic endoderm ($p>0.05$).

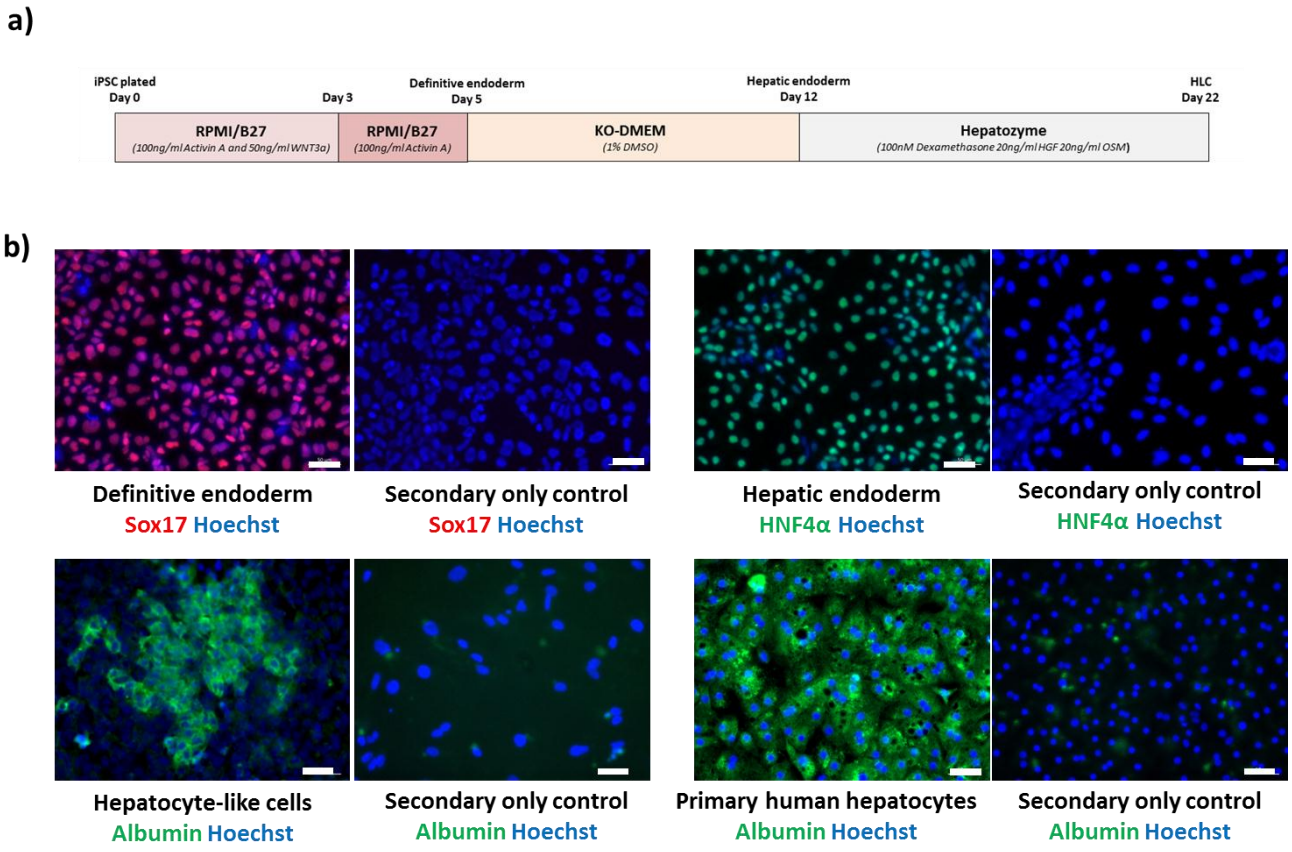

Figure 4.7: Differentiation of all lines to hepatocyte-like cells and confirmation by immunofluorescence.

a) A schematic diagram of the protocol used for the differentiation experiments, including the growth factors/small molecules used at each stage of differentiation. **b)** Immunofluorescence analysis of iPSCs during each stage of differentiation: Definitive endoderm (Sox17), Hepatic endoderm (HNF4α) and hepatocyte-like cells/primary human hepatocytes (albumin). Immunofluorescence images: x200 magnification, 50µm scale bar. Light microscopy images: x100 magnification, 100µm scale bar.

Abbreviations: Wnt3a: Wingless-Type MMTV Integration Site Family, Member 3A; DMSO: Dimethyl sulfoxide; HGF: Hepatocyte growth factor; OSM: Oncostatin M; SRY (Sex Determining Region Y)-Box 17; HNF4α: Hepatic nuclear factor 4 alpha.

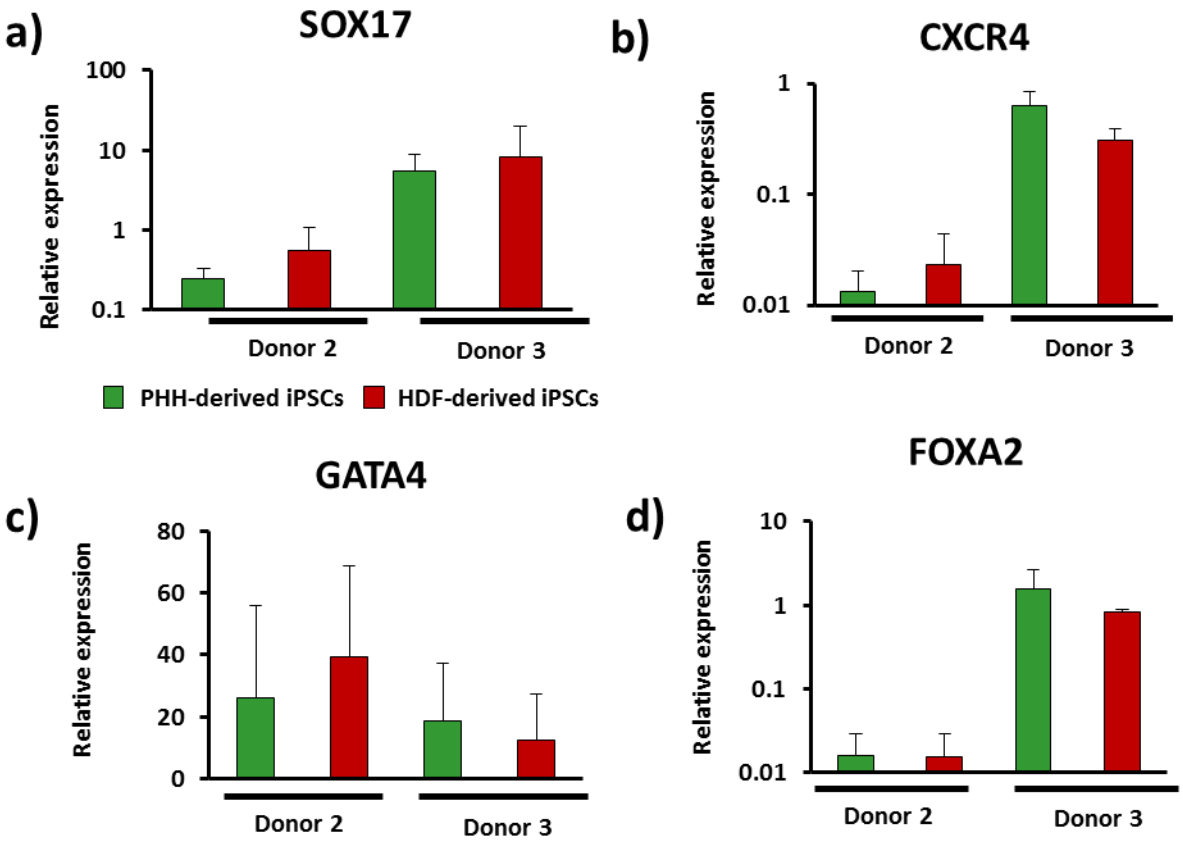

Figure 4.8: Comparison of definitive endoderm-associated gene expression measured by qRT-PCR.

All genes shown as $2^{-\Delta\Delta}$CT relative to a ESC-derived control and normalised using GAPDH and Succinate dehydrogenase gene expression. Error bars represent standard deviation between the means of each PHH-/HDF-derived iPSC line which were derived from three individual differentiation cultures. Each sample tested by qRT-PCR was loaded in duplicate. (*) denotes p>0.05 unpaired T test.

Abbreviations: GATA4: GATA Binding Protein 4; SRY (Sex Determining Region Y)-Box 17; CXCR4: Chemokine (C-X-C Motif) Receptor 4; FOXA2: Forkhead Box A2

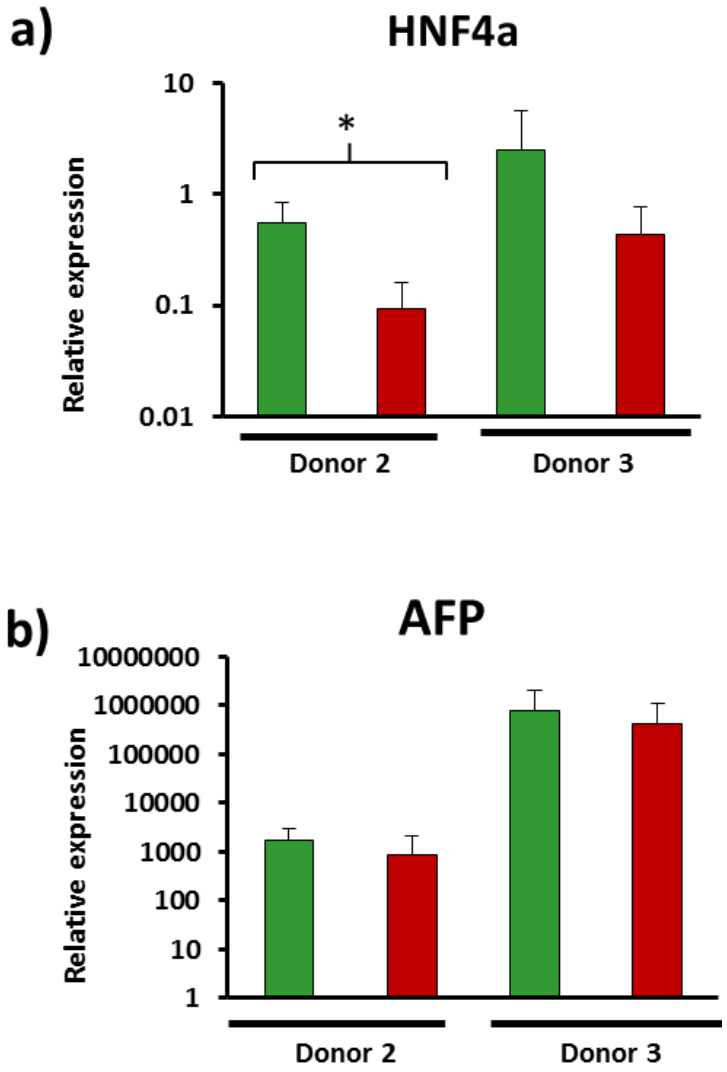

Figure 4.9: Comparison of hepatic endoderm-associated gene expression measured by qRT-PCR

a) HNF4α and **b)** AFP shown as $2^{-\Delta\Delta}$CT relative expressed relative to PHH of the same donor and normalised using GAPDH and Succinate dehydrogenase. Error bars represent standard deviation between the means of each PHH-/HDF-derived iPSC line which were derived from three individual differentiation cultures. Each sample tested by qRT-PCR was loaded in duplicate. (*) denotes $p>0.05$ unpaired T test.

Abbreviations: AFP: Alpha-Fetoprotein; HNF4α: Hepatic nuclear factor 4 alpha.

Comparison of the phenotype of hepatocyte-like cell differentiated PHH and HDF-derived iPSCs

To establish a full phenotypic comparison between the starting cell types, we used both gene expression and functional analysis-based assays.

Fully-differentiated HLCs were compared using a panel of mature and immature hepatic markers. The gene expression of these markers demonstrated very little difference between the lines generated from different cell types. Despite this, there is a general trend towards an improved gene expression in five of the eight genes examined in the PHH-derived clones for the majority of genes examined (figure S6). The enhanced expression of HNF4α, AFP and CYP2D6 in PHH-derived HLCs is conserved between donors; whereas, the other markers lack conformity, with the greater expression of the marker gene differing between PHH and HDF-derived HLCs across the assessed donors.

Of particular interest, CYP3A is close to the levels of PHH; however, this is most likely due to the combined presence of the foetal CYP3A7 and CYP3A5, rather than the mature CYP3A4 isoform alone. The enhanced expression of HNF4α, AFP and CYP2D6 in PHH-derived HLCs is conserved between donors; whereas, the other markers lack conformity, with the greater expression of the marker gene differing between PHH and HDF-derived HLCs across the assessed donors.

We also assessed the albumin secretion function of the HLCs to establish a functional comparison between the lines. Figure 4.11a demonstrates the increasing albumin secretion seen during the 22 day differentiation period. When compared at day 22 (figure 4.11b), our results demonstrated a non-significant trend pointing towards PHH-derived clones having slightly higher, but non-significant, albumin secretion in two of the three donors. The first donor contained Liv4FA which had exceptionally high albumin gene expression and albumin

secretion. When examined together, the difference between PHH- and HDF-derived iPSC HLCs albumin secretion is not significantly different; however, when Liv4FA is removed from the data analysis, the difference between PHH and HDF-derived HLCs does become significant (figure 4.11c).

CYP3A and CYP2D6 activity was also assessed using probe substrates testosterone and dextromethorphan, respectively (Figure 5c and d). No significant differences were found between the HLCs derived from the different starting cell types. Interestingly, despite the slightly greater CYP3A gene expression found in PHH-derived HLCs, a trend of greater CYP activity in the HDF-derived clones was observed. As testosterone is a substrate for all CYP3A isoforms (3A4/3A5/3A7), gene expression was analysed using primers which target the same CYP3A isoforms; however, the isoforms have known differences in their capacity to metabolise testosterone (Williams et al., 2002), potentially explaining the disparity between the CYP3A gene expression and activity.

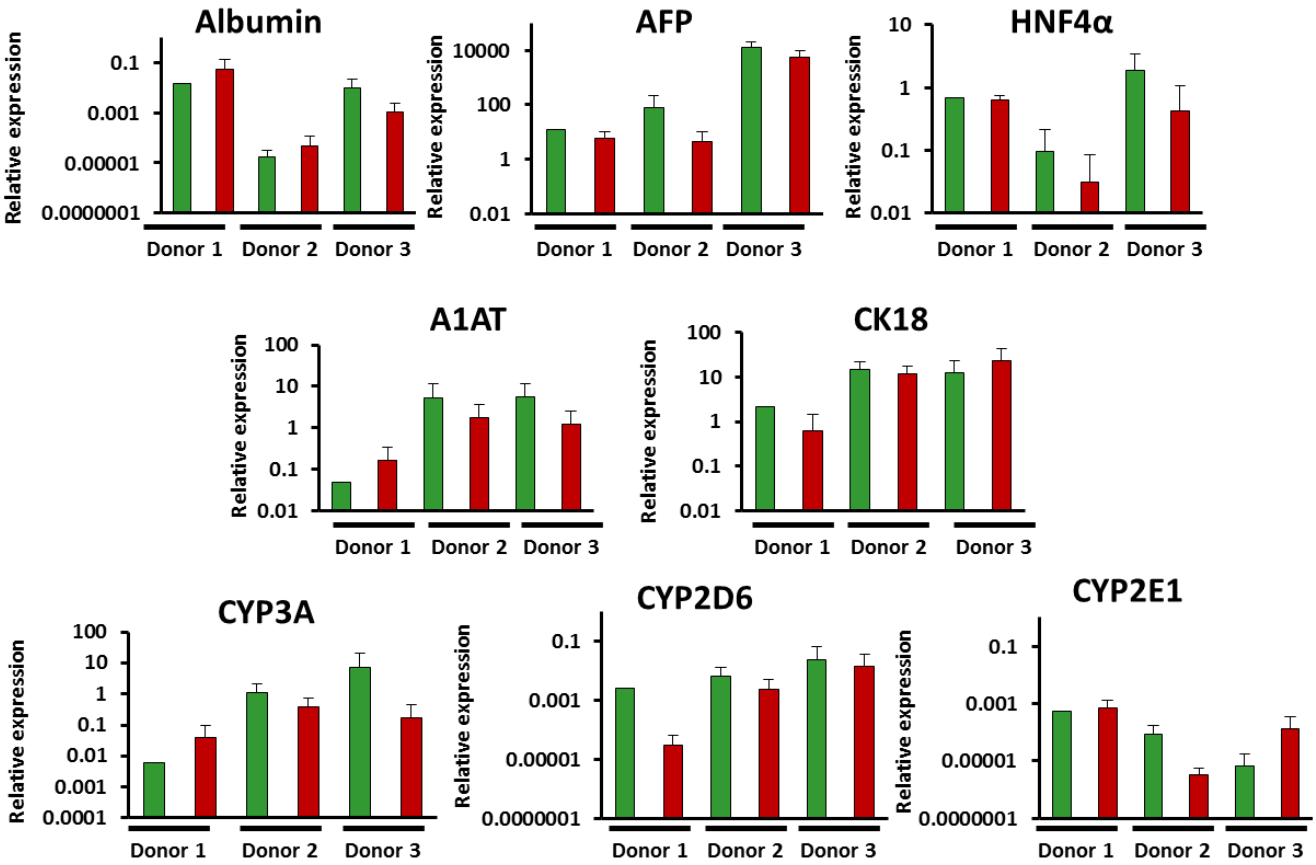

Figure 4.10: Comparison of hepatocyte-like cell-associated gene expression measured by qRT-PCR.

Gene expression of key hepatic genes obtained by q-PCR analysis and displayed as $2^{-\Delta\Delta}$CT relative to PHH of the corresponding donor. Results normalised using GAPDH and Succinate dehydrogenase. Error bars represent standard deviation between the means of each PHH-/HDF-derived iPSC line which were derived from three individual differentiation cultures. Each sample tested by qRT-PCR was loaded in duplicate. (*) denotes p>0.05 unpaired T test.

Abbreviations: AFP: Alpha-Fetoprotein; HNF4α: Hepatic nuclear factor 4 alpha; A1AT: Alpha-1 Antitrypsin; CK18: Cytokeratin 18; CYP: Cytochrome P450

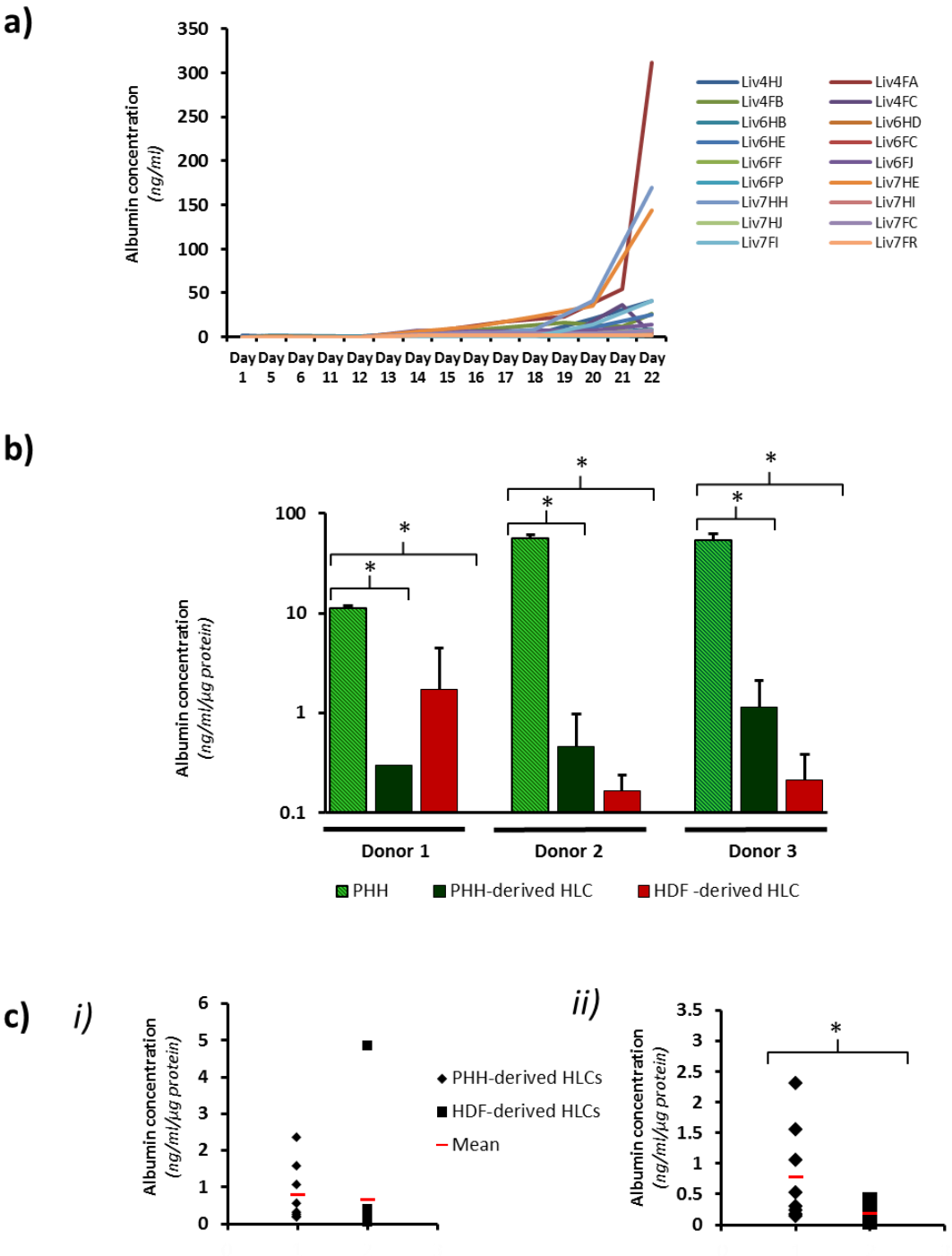

Figure 4.11: Albumin secretion of hepatocyte-like cells using ELISA

a) Albumin secretion during hepatocyte-like cell differentiation at each stage of differentiation and every 48 hours for the final stage of differentiation. **b)** Isogenic comparison of albumin secretion in PHH and PHH- and HDF-derived HLCs at the final stage of differentiation normalised using total protein content of corresponding well. * denotes p>0.001 one-way ANOVA. Error bars: SD. **c)** *i)* Comparison of PHH and HDF-derived HLCs from all three donors and *ii)* with Liv4FA omitted from the results *p>0.05 unpaired T test.

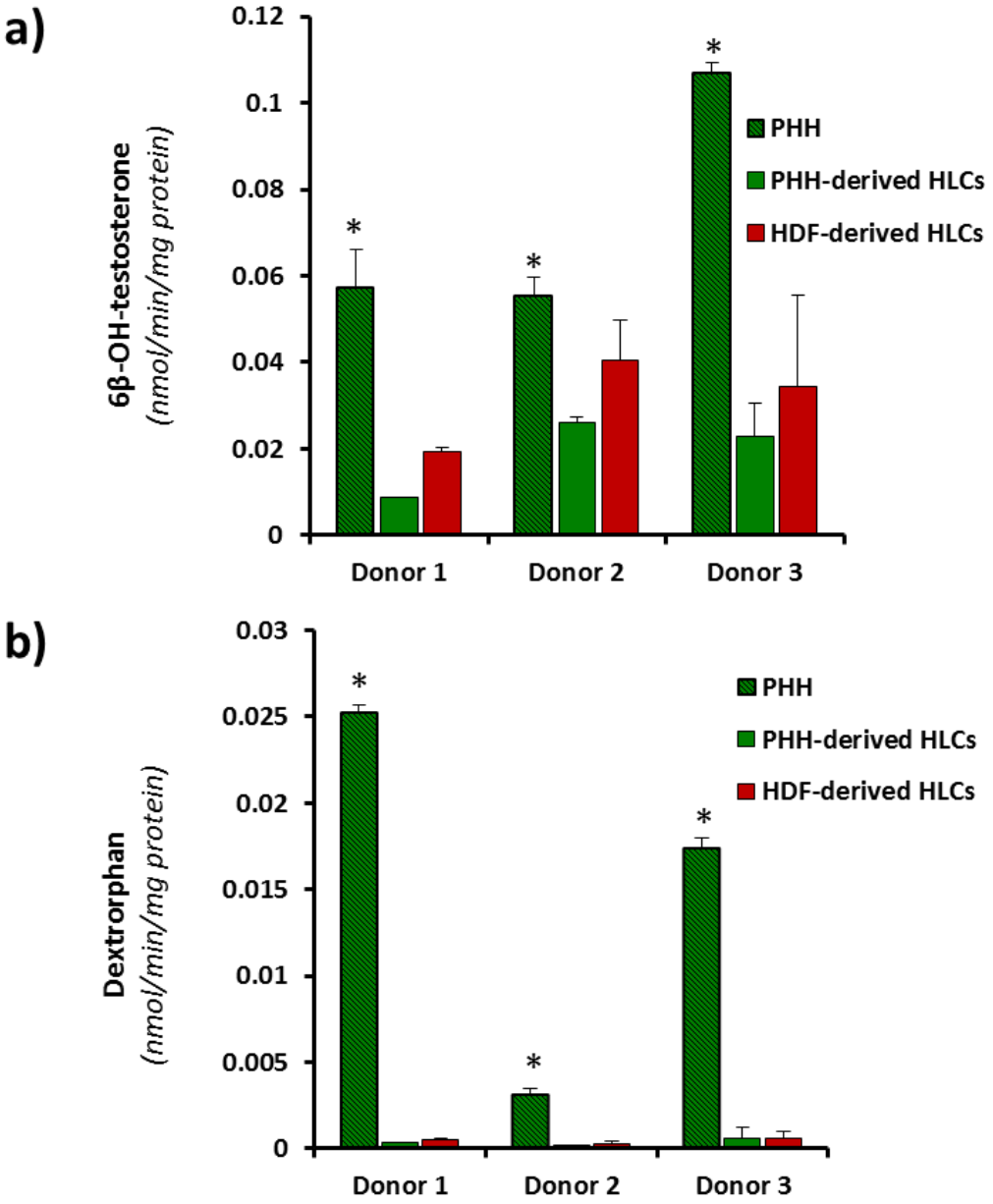

Figure 4.12: CYP activity of PHH and HDF derived HLCs

a) and **b)** CYP activity as detected using LC-MS method analysing the turnover of probe substrates and quantification of metabolites for **a)** 6β-OH-testosterone (CYP3A) and **b)** Dextrorphan (CYP2D6). (*) denotes p>0.05 one-way ANOVA. Error bars: SD.

Discussion

In this chapter we have investigated the benefit of starting with primary human hepatocytes when deriving iPSCs for hepatocyte-like cell differentiation, using HDFs derived from the same donor as the gold standard comparator. We have investigated the PHH- and HDF-derived iPSCs potential for hepatocyte differentiation in a multi-faceted panel of assays to give a thorough comparison of iPSC differentiation potential.

Our main hypothesis, that the starting cell type may influence the differentiation capacity of the cell, was driven by the reported epigenetic memory which remains from the somatic cell following reprogramming (Kim et al., 2010a; Polo et al., 2010). Our results suggested a slight but non-significant epigenetic memory may be found in the HNF4α promoter region. Throughout the analysis, a general trend towards a slight, non-significant advantage, to starting with primary human hepatocytes, when compared to dermal fibroblasts, was noted. This was perhaps most evident with HNF4α expression at the hepatic endoderm stage of differentiation. Therefore, the slight trend of enhanced phenotype in PHH-derived iPSCs at the HLC stage may be caused by the reported small, but conserved differences in hepatic-associated genes methylation patterns. Our findings that the noted differences in HNF4α methylation dissipate with time in culture are in-keeping with previous literature, which has demonstrated that the distinct epigenetic patterns and enhanced phenotype in a given cell type-derived iPSC are lost following repeat passaging (Lee et al., 2012; Takayama et al., 2014; Kim et al., 2010a; Polo et al., 2010).

The albumin secretion of the HLCs also showed a trend towards enhanced albumin secretion in PHH-derived clones. Despite this, when all lines were compared, no significant differences were seen between PHH- and HDF-derived lines. This was in part due to the HDF-derived line, Liv4FA, which displayed much greater albumin secretion and gene expression than all other lines. If Liv4FA is not included in the analysis, there is significantly

greater HLC albumin secretion in lines derived from PHH. This highlights the inherent inter-clone variability derived from other undefined variables can be a greater influence of HLC phenotype than the starting cell type. It has long been established that individual clones have unique characteristics; however, recent studies have suggested that this is mainly due to donor variations (Kajiwara et al., 2012). Our results suggest that despite iPSCs being derived from the same donor, inter-clone variation is still prominent.

With the exception of Liv4FA, the variation in albumin secretion appeared to be greatest between PHH-derived clones, with the HDF-derived clones being relatively consistent. One potential explanation for this may be the source of the cells. The isolation of PHH is relatively well-established; however, the lack of a *bona fide* cell surface marker and the sensitivity of the cells during the isolation process mean that, to the best of our knowledge, a homogenous population of hepatocytes is not currently achievable. Previous work has shown that our isolation process achieves an enrichment of hepatocytes from the 60% of cells in the liver, to ~90% of cells isolated, as determined by albumin positive cells using flow cytometry (Kia, 2014). Therefore, there remains a possibility that not all of the iPSC clones derived from the PHH-enriched population were derived from hepatocytes, thus causing the variability seen between PHH-derived clones. However, if PHH-derived clones were to be used in future experiments, the inability to guarantee a homogenous starting population of hepatocytes will likely remain; therefore, this work is also representative of the practical limitations associated with PHH as a starting cell source.

It must also be acknowledged that the slight enhancements seen in PHH-derived clones may well be limited by the restricted differentiation maturity which is currently achievable in simple HLC culture systems. Previous work in mice has shown that the greatest advantage in HLC differentiation was achieved reprogramming hepatoblasts, rather than adult hepatocytes (Lee et al., 2012). This may be a consequence of the relatively immature

phenotype of HLCs. Therefore, future investigations into the starting cell type would require the development of protocols which produce a more mature phenotype; however, this in itself remains a major bottleneck in the field of HLCs (Kia et al., 2013).

As part of our analysis, we attempted to generate CYP activity data to further compare the functional capacity of the HLCs. Despite the results presented demonstrating an increase from iPSC to HLC, the detectable amounts of metabolites were close to the assays limit of detection in most cases. The assay used was based on a 15 minute exposure to each substrate, as developed using PHH to prevent metabolite saturation; however, this may be insufficient time for the HLCs to turnover more readily detectable levels of the respective metabolite. Other groups have used exposure times of between 1 and 48 hours for metabolism studies and this may allow for the generation of more reliable data (Szkolnicka et al., 2013; Asplund et al., 2015; Ulvestad et al., 2013; Siller et al., 2015). The comparable CYP3A gene expression in HLCs and PHH would suggest that our HLCs should have a more similar level of CYP3A activity in response the probe substrate testosterone, when compared to PHH. However, this is not the case and the discrepancy most likely arises through the differences in the isoforms present in both cell types and that CYP mRNA has not been adequately translated into functional protein (Schwanhausser et al., 2011). Further work is also required to investigate the isoforms which make up the CYP3A expression (i.e. CYP3A4, CYP3A5 and CYP3A7) and if these genes have been translated to protein.

Taken together, the lack of any major advantage to PHH-derived iPSCs is of significance to the field of iPSC-derived HLCs, suggesting that any trend towards enhanced expression in PHH-derived clones is not greater than the inter-clone variation derived from other non-defined influencing factors. Furthermore, the access and phenotypic range of available PHH samples is very restricted in comparison to the easily accessible skin or blood samples used

in the majority of current studies. Therefore, the similarity between the cell types in all tested parameters is reassuring for current and future studies, particularly those which require specific genotypic backgrounds, i.e. for disease studies, or a large phenotypic range for population-representative studies.

Chapter 5

Mechanistic evaluation of *in vitro* primary human hepatocyte culture using global proteomic analysis

5.1 Introduction

Primary human hepatocytes (PHH) are an important tool for studying human liver disease and drug-induced liver injury (DILI), with other models, such as rat hepatocytes, hepatic cell lines and stem cell-derived hepatocyte-like cells failing to offer metabolically-competent and species-relevant alternatives (Godoy et al., 2013). However, accessing and culturing PHHs remains difficult due to inconsistent supply and an inability to stimulate sufficient division for *in vitro* expansion. Furthermore, following isolation, primary human hepatocytes undergo a rapid dedifferentiation process in which many unique hepatocyte characteristics are lost, reducing the physiological relevance of the model (Fraczek et al., 2013; Godoy et al., 2013).

It is thought that dedifferentiation is caused by inflammatory and proliferative-associated responses to both PHH isolation and subsequent *in vitro* culture (Elaut et al., 2006; Fraczek et al., 2013; Godoy et al., 2009; Zellmer et al., 2010). Current models of dedifferentiation hypothesise that these responses result in the down-regulation of important liver-enriched transcription factors (LETFs) such as hepatic nuclear factors (HNFs) HNF1α and HNF4α which control many of the ADME processes (absorption, distribution, metabolism, and excretion) and other features unique to PHHs, resulting in a loss of hepatic phenotype (Godoy et al., 2009; Zellmer et al., 2010); however, the exact mechanisms which govern these changes remain incompletely understood.

Several approaches have been adopted to maintain the hepatocyte phenotype in culture, including co-culture and 3D models such as sandwich cultures, bioreactors, liver buds and spheroids which attempt to better replicate the *in vivo* hepatic environment (Darnell et al., 2012; No et al., 2012; Tostoes et al., 2012). In addition, a wide range of growth factors, cytokines and small molecules have also been used to target and maintain the hepatic phenotype, such as those shown recently by Shan *et al* (Shan et al., 2013). Many of these

strategies have been thoroughly reviewed by both Godoy *et al* and Fraczek *et al* (Fraczek et al., 2013; Godoy et al., 2013).

Despite these continued improvements and advances towards complex culture conditions which can maintain an improved phenotype over a period of weeks, the full *in vivo* phenotype has not yet been achieved. Therefore, there remains a real need to improve the understanding of the underlying causes of this process, and to identify novel strategies/targets for intervention. Moreover, as complex models reduce the effects of dedifferentiation, analysis of these systems may result in the underlying causes being difficult to fully ascertain. Therefore, studies of more rudimentary models which result in more pronounced dedifferentiation may consequently provide a greater insight into the partially understood and currently unknown causes of dedifferentiation.

Crucially, increased understanding of dedifferentiation is also likely to be useful in guiding attempts to direct and maintain a hepatic phenotype from pluripotent cells *in vitro*. Current efforts worldwide have not taken a cell beyond a relatively immature hepatocyte (chapters 3 and 4) (Kia et al., 2013) and it can be hypothesised that an integral part of this challenge is how we can capture the hepatic phenotype and prevent its loss.

Global studies offer an insight into how cells react in a holistic sense to a particular condition, and whilst efforts have been made to map changes in the hepatocyte transcriptome during dedifferentiation (Kim et al., 2010b; Lasher et al., 2011), many changes key to the mature phenotype of the hepatocyte are not properly represented in such analysis. This is exemplified by the recent results showing that only ~40% of the variation in cell protein levels can be explained by differences in the corresponding mRNA levels (Schwanhausser et al., 2011). We have previously shown that the use of a global proteomic approach to phenotype rat hepatocytes can provide novel information on

dedifferentiation (Rowe et al., 2010) and here look to build on that study using human cells.

We have therefore now followed PHHs over the first 7 days of monolayer culture, chosen specifically to exacerbate the effects of dedifferentiation. Using iTRAQ-based stable isotope labelling and pathway analysis we have identified the key changes in the PHH proteome during dedifferentiation and the inter-donor variability which exists not only in donor phenotype, but also in the subsequent dedifferentiation profile.

Hypothesis: Mechanistic evaluation of the primary human hepatocyte proteome during monolayer culture will yield novel information and hypotheses regarding the dedifferentiation and differentiation of hepatocytes.

5.2. Results

Global proteomics reveals donor-dependent variation as a major influence on dedifferentiation

iTRAQ quantitative global proteomic analysis was used to assess the changes which occur in PHH at different time points during a 168 hour monolayer culture. Dedifferentiation and loss of characteristic hepatocyte morphology were confirmed by microscopy. Figure 5.1a shows images of the cells taken at 24, 72 and 168 hours and clearly demonstrates the maintenance of confluency and the loss of the typical hepatocyte polygonal morphology (24 hours), towards a culture with flatter and less defined epithelial characteristics at 72 and 168 hours.

A total of 3430 unique proteins were detected across three iTRAQ runs, with 1117 identified across all samples (raw data is provided with the electronic version of the thesis). Statistical analysis using a linear model yielded significantly differentially-expressed proteins (DEPs) at each time point relative to freshly isolated cells. These changes highlight a dynamic and escalating process; 40 DEPs are seen after 24 hours, 118 after 72 hours and 272 after 168 hours in culture ($P < 0.05$). When displayed as volcano plots (log fold-change versus P value), the increasing dispersion and direction of change of the proteins over time in culture is strikingly evident (Figure 5.1b); interestingly, at both 24 and 72 hours of culture the majority of DEPs increased in expression. Despite the large number of changes detected within our analysis, not all functions were affected over the culture period. Figure 5.1c demonstrates the relative stability of albumin secretion over the 168 hour culture period.

Hierarchical clustering of the entire dataset shows that the dominant factor in determining how the samples are related is in fact the original source of the cells, rather than time in

culture (Figure 5.2a). This is particularly pronounced at the 24 and 72 hour time points, which cluster according to donor in every case. The separation from the other donors is still evident at 168 hours for donors 2 and 5, although these samples cluster away from the earlier time points; whereas, by this time the other three donors (1, 3 and 4) cluster together, demonstrating a convergence towards a dedifferentiated phenotype which is more reflective of time in culture than the cell source.

Thus, these data suggest that phenotypic characteristics of the donor have a greater impact on the protein dedifferentiating expression profile of the hepatocytes than does the length of time in culture, particularly over the first 72 hours of culture. The variability between donor proteomic profiles during dedifferentiation is further shown by the heatmap in Figure 5.2b.

Donors	Gender	Age	Reason for surgery	Underlying diseases	Medication	iTRAQ run	No. of proteins detected
Donor 1	M	67	Colorectal liver metastases	Hypertension Asthma Hypercholesterolemia Gout	Omeprazole Atorvastatin Tramadol Allopurinol Amlodipine Lisinopril	1	2439
Donor 2	M	74	Colorectal liver metastasis	Deep venous thrombosis Benign prostatic hyperplasia	Citirizine Finasteride Terazosin Paracetamol		
Donor 3	F	61	Cholangiocarcinoma	Severe pancreatitis	Diclofenac Paracetamol Omeprazole	2	2944
Donor 4	M	58	Primary hepatocarcinoma	Hypertension	Atenadol Allopurinol		
Donor 5	M	66	Colorectal liver metastases	Diabetes	Meiformin Glicazide Simvastatin	3	2347

Table 5.1: iTRAQ proteomic analysis.

Details of the donors analysed in each iTRAQ run and the number of proteins detected in each separate analysis.

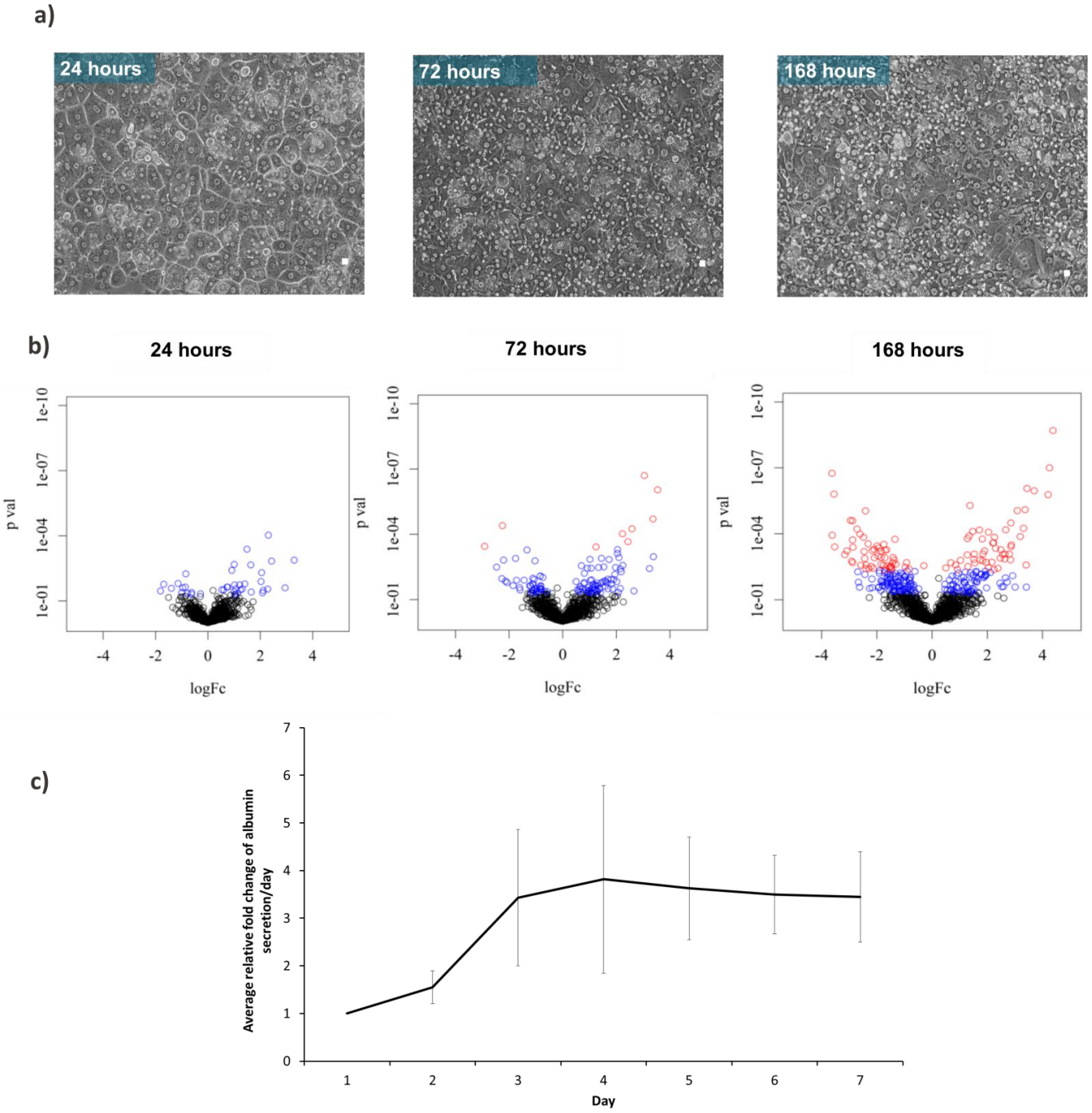

Figure 5.1: Changes in PHH morphology, proteome and function during culture

a) Morphological changes in primary human hepatocytes over 168 hours in monolayer collagen I-coated plate culture. Magnification: x200, scale bar represents 10µm; **b)** Volcano plot analysis of the iTRAQ detected proteins log fold change vs p-value at 24, 72 and 168 hours. Blue: significantly altered proteins (n=5; p≤0.05) and red: significantly altered after multiple testing correction (n=5; Benjamini-Hochberg ≤0.2) **c)** Albumin secretion during culture measured by albumin ELISA (n=4; errors bars: SD).

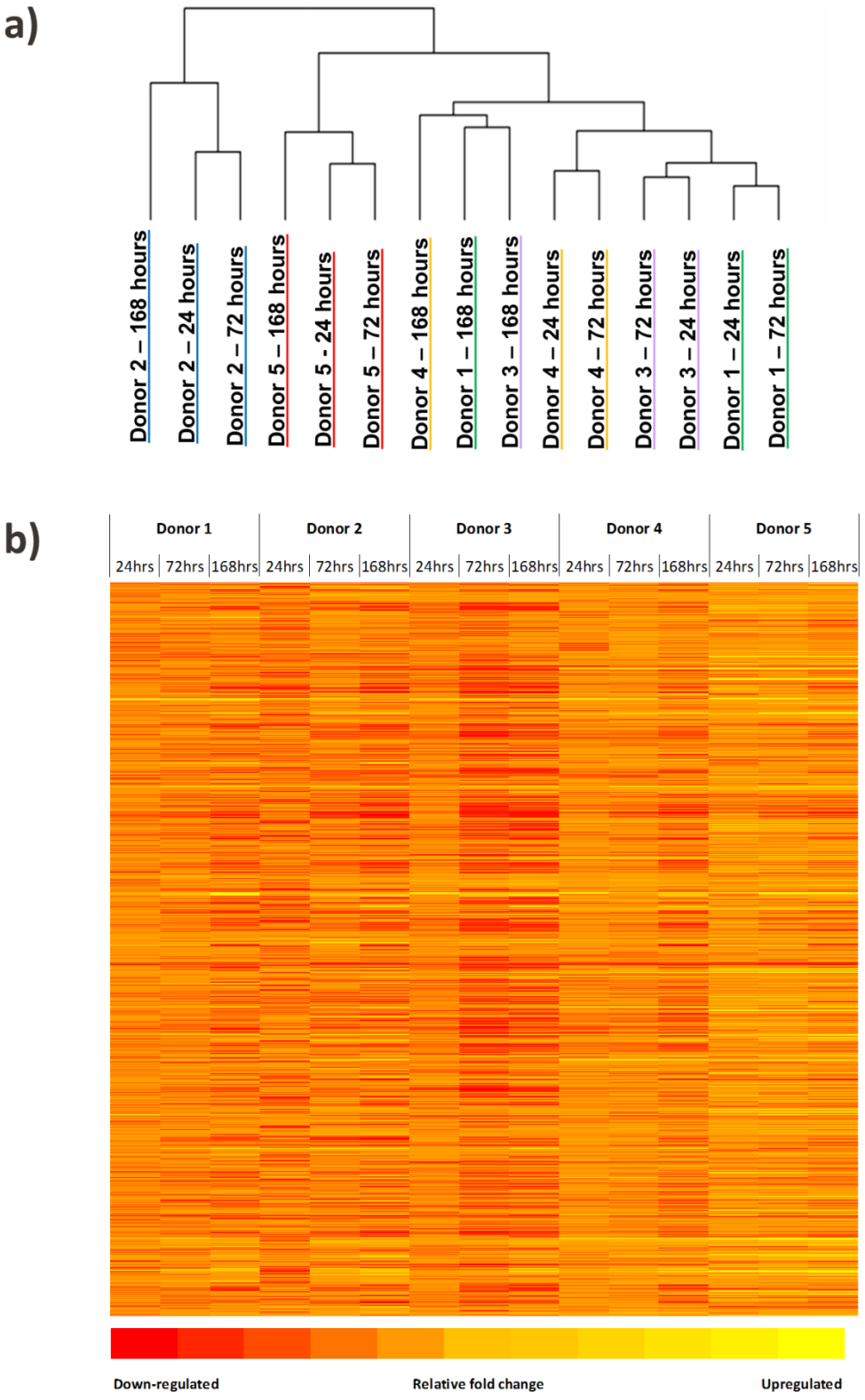

Figure 5.2: Hierarchical clustering and heatmap analysis of the proteomic data

a) Hierarchal clustering analysis showing the relationship between donors and timepoints (n=5); **b)** Heatmap of each donor's proteome during dedifferentiation relative to the freshly isolated sample. Red indicates down-regulation, yellow up-regulation. The intensity of colour reflects the degree of change.

Analysis of the dedifferentiation proteome reveals the most variable and the most stable proteins between donors and timepoints

To identify the proteins with the greatest variability across the 5 donors at the different time points, co-efficient of variance (CV) analysis was then used (Table 5.1). This criterion highlights a number of proteins, including CYP2C9, which is known to vary in expression between individuals (Sistonen et al., 2009), and glutamine synthetase, which is associated with differential expression according to liver zonation (Jungermann and Kietzmann, 1996). In fact, zonation appears to be a large influencing factor on variation during culture as our pathway analysis of the most variable proteins revealed significant association with ketogenesis, cholesterol biosynthesis, fatty acid β oxidation and glutamine synthesis (Table 5.2), all of these are related to the porto-central axis gradient of the lobule (Godoy et al., 2013).

The most stable proteins during dedifferentiation were also investigated (Table 5.3). These included several mitochondrial proteins within the ten most stable proteins. Thus, while many proteins show conserved differential expression or high levels of inter-donor variability, a subset of proteins remain relatively stable and consequently may retain *in vivo*-like functionality and also serve as useful normalisers for protein expression changes. This is particularly pertinent for hepatocyte dedifferentiation as β-actin increases in expression during culture (demonstrated later in the chapter, figure 5.12b).

The proteins with the greatest up- or down-regulation at each timepoint demonstrate a similarity in expression to hepatocyte-like cells derived from stem cells.

Table 5.5 highlights the most up and down-regulated DEPs at each time point, as assessed by $\log_2$ fold change relative to the fresh sample. Interestingly, the first noticeable effects at 24 hours are an increase in stress-related mediator superoxide dismutase and a decrease in

histone proteins. Of note, hepatic-associated proteins are not universally down-regulated, as exemplified by alpha-1-antitrypsin and cytokeratins 8 and 18, which are up-regulated throughout the analysis. Interestingly, these proteins are readily detectable in hepatocyte-like cells derived from stem cells (Rambhatla et al., 2003), whereas many of the down-regulated proteins are not, demonstrating that simple *in vitro* culture systems may support similar expression patterns during both hepatic dedifferentiation and differentiation.

Uniprot Accession Number	Name	*Co-efficient of variance*		
		24 hours	*72 hours*	*168 hours*
P0DJI9	Serum amyloid A-2 protein	2.083909	2.078728	2.073038
Q9NUJ1	Mycophenolic acid acyl-glucuronide esterase, mitochondrial	1.707109	1.882177	1.986591
Q969Z3	MOSC domain-containing protein 2, mitochondrial	1.693348	1.414446	1.810794
P15374	Ubiquitin carboxyl-terminal hydrolase isozyme L3	1.817535	1.672397	1.692353
P26599	Polypyrimidine tract-binding protein 1	1.603233	1.62981	1.683913
O15260	Surfeit locus protein 4	1.570576	1.70747	1.643518
O14756	17-beta-hydroxysteroid dehydrogenase type 6	1.087739	1.350166	1.635544
P25398	40S ribosomal protein S12	1.647474	1.709673	1.605359
P01011	Alpha-1-antichymotrypsin	0.69682	0.419842	1.58037
P11712	Cytochrome P450 2C9	1.199075	1.424764	1.573942
Q96EK6	Glucosamine 6-phosphate N-acetyltransferase	1.737418	1.608963	1.542857
Q99714	3-hydroxyacyl-CoA dehydrogenase type-2	1.296856	1.47145	1.539702
Q96IJ6	Mannose-1-phosphate guanyltransferase alpha	1.667729	1.352937	1.514543
Q6YN16	Hydroxysteroid dehydrogenase-like protein 2	1.467704	1.601775	1.504808
P24752	Acetyl-CoA acetyltransferase, mitochondrial	1.136518	1.483382	1.503606
Q16134	Electron transfer flavoprotein-ubiquinone oxidoreductase, mitochondrial	1.079149	1.394389	1.491195
P35914	Hydroxymethylglutaryl-CoA lyase, mitochondrial	1.127576	1.404124	1.4818
O43708	Maleylacetoacetate isomerase	1.402363	1.518733	1.47866
Q16222	UDP-N-acetylhexosamine pyrophosphorylase	1.577758	1.634465	1.468517
O75643	U5 small nuclear ribonucleoprotein 200 kDa helicase	1.442048	1.330621	1.440199
Q08AH3	Acyl-coenzyme A synthetase ACSM2A, mitochondrial	1.079716	1.288258	1.392047
P15104	Glutamine synthetase	0.346635	1.048488	1.385288
Q14558	Phosphoribosyl pyrophosphate synthase-associated protein 1	1.170621	1.090732	1.381804
O75521	Enoyl-CoA delta isomerase 2, mitochondrial	1.328238	1.486261	1.379483
Q15366	Poly(rC)-binding protein 2	1.700238	1.408374	1.375921
Q9BRX8	Redox-regulatory protein FAM213A	1.179568	1.360546	1.370182
P78329	Leukotriene-B(4) omega-hydroxylase 1	1.35427	1.396285	1.368089
Q04446	1,4-alpha-glucan-branching enzyme	1.147705	1.039434	1.361002
P62330	ADP-ribosylation factor 6	1.469331	1.574059	1.33387
Q93088	Betaine--homocysteine S-methyltransferase 1	0.849564	0.876841	1.323588
Q02338	D-beta-hydroxybutyrate dehydrogenase, mitochondrial	1.376122	1.416189	1.319087
Q68CK6	Acyl-coenzyme A synthetase ACSM2B, mitochondrial	1.385784	1.368136	1.317599
Q99624	Sodium-coupled neutral amino acid transporter 3	1.357665	1.157176	1.315244
Q9BWD1	Acetyl-CoA acetyltransferase, cytosolic	1.57992	1.445088	1.291763
P30084	Enoyl-CoA hydratase, mitochondrial	0.997547	0.988534	1.291622
Q92820	Gamma-glutamyl hydrolase	1.219966	1.4691	1.278405
P05141	ADP/ATP translocase 2	1.200215	1.420541	1.260025
P02042	Hemoglobin subunit delta	1.419209	1.129662	1.243176
Q02978	Mitochondrial 2-oxoglutarate/malate carrier protein	1.109218	1.354909	1.214753
P18085	ADP-ribosylation factor 4	1.505917	1.29611	1.204037
Q3LXA3	Bifunctional ATP-dependent dihydroxyacetone kinase/FAD-AMP lyase (cyclizing)	1.404937	1.220907	1.196514
Q6NVY1	3-hydroxyisobutyryl-CoA hydrolase, mitochondrial	1.384332	1.649482	1.183856
O95394	Phosphoacetylglucosamine mutase	1.371555	1.306498	1.16418
P09417	Dihydropteridine reductase	1.479465	1.19829	1.159391
P37837	Transaldolase	1.519568	1.516419	1.147909
Q96LJ7	Dehydrogenase/reductase SDR family member 1	1.382342	1.468168	1.146213
P16219	Short-chain specific acyl-CoA dehydrogenase, mitochondrial	1.453542	1.142062	1.113124
P07339	Cathepsin D	1.300016	1.508745	1.084154
P07437	Tubulin beta chain	1.613412	1.035572	0.978595
P11766	Alcohol dehydrogenase class-3	1.322958	1.114523	0.916866
P02753	Retinol-binding protein 4	1.079394	1.343397	0.846919
Q8TC12	Retinol dehydrogenase 11	1.451007	0.867983	0.843923
Q13885	Tubulin beta-2A chain	1.545352	1.057663	0.821749

Table 5.2: The most variable proteins during PHH dedifferentiation.

Co-efficient of variance analysis used to assess the variability between proteins. Those with a CV>1.3 at any timepoint are listed with their corresponding CV values at each timepoint.

Canonical Pathways	-log(p-value)
Ketogenesis	8.15
Isoleucine Degradation I	7.48
UDP-N-acetyl-D-glucosamine Biosynthesis II	6.54
Ketolysis	5.92
UDP-N-acetyl-D-galactosamine Biosynthesis II	5.92
Glutaryl-CoA Degradation	5.5
Tryptophan Degradation III (Eukaryotic)	4.73
Fatty Acid β-oxidation I	4.21
Mevalonate Pathway I	3.33
Remodeling of Epithelial Adherens Junctions	3.19
Superpathway of Geranylgeranyldiphosphate Biosynthesis I (via Mevalonate)	3.09
Valine Degradation I	3.04
Superpathway of Cholesterol Biosynthesis	2.66
Glutathione-mediated Detoxification	2.63
Glutamine Biosynthesis I	2.6
Glutamate Removal from Folates	2.6
Ethanol Degradation II	2.52
Noradrenaline and Adrenaline Degradation	2.47
Estrogen Biosynthesis	2.4
Formaldehyde Oxidation II (Glutathione-dependent)	2.3

Table 5.3: Pathway analysis of the most variable proteins during dedifferentiation.

The canonical pathways ($p<0.05$, Fisher exact T-test) significantly associated the most variable proteins

Uniprot Accession Number	Name
O75600	2-amino-3-ketobutyrate coenzyme A ligase, mitochondrial
P31327	Carbamoyl-phosphate synthase [ammonia], mitochondrial
Q5SRE7	Phytanoyl-CoA dioxygenase domain-containing protein 1
O95202	LETM1 and EF-hand domain-containing protein 1, mitochondrial
O14818	Proteasome subunit alpha type-7
P35606	Coatomer subunit beta'
Q16531	DNA damage-binding protein 1
Q07954	Prolow-density lipoprotein receptor-related protein 1
P55735	Protein SEC13 homolog
O96008	Mitochondrial import receptor subunit TOM40 homolog
P62249	40S ribosomal protein S16
P56556	NADH dehydrogenase [ubiquinone] 1 alpha subcomplex subunit 6
P62847	40S ribosomal protein S24
P30533	Alpha-2-macroglobulin receptor-associated protein
Q13586	Stromal interaction molecule 1
Q13131	5'-AMP-activated protein kinase catalytic subunit alpha-1
Q8NC51	Plasminogen activator inhibitor 1 RNA-binding protein
Q8NI60	Chaperone activity of bc1 complex-like, mitochondrial
Q16706	Alpha-mannosidase 2
O75131	Copine-3
Q86UE4	Protein LYRIC
Q9H0R4	Haloacid dehalogenase-like hydrolase domain-containing protein 2
A1L0T0	Acetolactate synthase-like protein
Q9H0E2	Toll-interacting protein
P35637	RNA-binding protein FUS
P51580	Thiopurine S-methyltransferase
Q96HS1	Serine/threonine-protein phosphatase PGAM5, mitochondrial
P10155	60 kDa SS-A/Ro ribonucleoprotein
O95340	Bifunctional 3'-phosphoadenosine 5'-phosphosulfate synthase 2
Q9Y6B6	GTP-binding protein SAR1b
O14841	5-oxoprolinase
P23246	Splicing factor, proline- and glutamine-rich
O95486	Protein transport protein Sec24A
O75531	Barrier-to-autointegration factor
Q969X5	Endoplasmic reticulum-Golgi intermediate compartment protein 1
Q9Y2T3	Guanine deaminase
O43390	Heterogeneous nuclear ribonucleoprotein R
P14868	Aspartate--tRNA ligase, cytoplasmic
P62753	40S ribosomal protein S6

Table 5.4: The most stable proteins during PHH dedifferentiation.

Proteins which had a co-efficient of variance of <0.3 and a mean relative fold change >0.8 and <1.2 throughout the analysis were described as stable.

24 hours						72 hours						168 hours					
Up-regulated			Down-regulated			Up-regulated			Down-regulated			Up-regulated			Down-regulated		
Uniprot Accession Number	Name	Log_2 fold change	Uniprot Accession Number	Name	Log_2 fold change	Uniprot Accession Number	Name	Log_2 fold change	Uniprot Accession Number	Name	Log_2 fold change	Uniprot Accession Number	Name	Log_2 fold change	Uniprot Accession Number	Name	Log_2 fold change
P01011	Alpha-1-antichymotrypsin	3.293	P62805	Histone H4	-1.809	P04179	Superoxide dismutase [Mn], mitochondrial	3.54	Q71DI3	Histone H3.2	-2.914	P07355	Annexin A2	4.377	P11509	Cytochrome P450 2A6	-3.628
P01009	Alpha-1-antitrypsin	2.947	Q71DI3	Histone H3.2	-1.689	P01011	Alpha-1-antichymotrypsin	3.383	O14832	Phytanoyl-CoA dioxygenase, peroxisomal	-2.465	P04179	Superoxide dismutase [Mn], mitochondrial	4.249	P10632	Cytochrome P450 2C8	-3.616
P02679	Fibrinogen gamma chain	2.432	P10412	Histone H1.4	-1.395	P10909	Clusterin	3.367	P62805	Histone H4	-2.27	P10909	Clusterin	4.204	Q02928	Cytochrome P450 4A11	-3.551
P04179	Superoxide dismutase [Mn], mitochondrial	2.307	P36957	Dihydrolipoyllysine-residue succinyltransferase component of 2-oxoglutarate dehydrogenase complex, mitochondrial	-1.140	P43490	Nicotinamide phosphoribosyltransferase	3.24	P11509	Cytochrome P450 2A6	-2.248	P37802	Transgelin-2	3.699	P11168	Solute carrier family 2, facilitated glucose transporter member 2	-3.528
P43490	Nicotinamide phosphoribosyl transferase	2.283	Q96CM8	Acyl-CoA synthetase family member 2, mitochondrial	-1.001	P07355	Annexin A2	3.046	P10412	Histone H1.4	-2.204	P35579	Myosin-9	3.439	P54868	Hydroxymethylglutaryl-CoA synthase, mitochondrial	-3.159
P02671	Fibrinogen alpha chain	2.115	P11509	Cytochrome P450 2A6	-0.959	P01009	Alpha-1-antitrypsin	2.654	P11168	Solute carrier family 2, facilitated glucose transporter member 2	-2.137	P60903	Protein S100-A10	3.412	P31513	Dimethylaniline monooxygenase [N-oxide-forming] 3	-3.088
P02763	Alpha-1-acid glycoprotein 1	2.086	P05386	60S acidic ribosomal protein P1	-0.866	P37802	Transgelin-2	2.583	P05177	Cytochrome P450 1A2	-2.076	P43490	Nicotinamide phosphoribosyl transferase	3.407	P07099	Epoxide hydrolase 1	-2.955
P02675	Fibrinogen beta chain	2.054	P46777	60S ribosomal protein L5	-0.845	P26038	Moesin	2.431	P22307	Non-specific lipid-transfer protein	-1.851	P26038	Moesin	3.370	P45954	Short/branched chain specific acyl-CoA dehydrogenase, mitochondrial	-2.911
P08107	Heat shock 70 kDa protein 1A/1B	2.028	P14920	D-amino-acid oxidase	-0.776	P02679	Fibrinogen gamma chain	2.243	O43772	Mitochondrial carnitine/acylcarnitine carrier protein	-1.760	P21333	Filamin-A	3.314	P49326	Dimethylaniline monooxygenase [N-oxide-forming] 5	-2.880
P07602	Proactivator polypeptide	1.653	P62750	60S ribosomal protein L23a	-0.625	P35579	Myosin-9	2.23	P08684	Cytochrome P450 3A4	-1.724	P09493	Tropomyosin alpha-1 chain	3.194	P04040	Catalase	-2.879

Table 5.5: The most differentially expressed proteins during PHH dedifferentiation.

The 10 most up and down-regulated proteins by log_2 fold change at each timepoint 24, 72 and 168 hours relative to freshly isolated PHH.

Pathway analysis reveals the key changes and dynamic profile of dedifferentiation

Pathway enrichment analysis was used to identify the affected functions and pathways which underlie dedifferentiation.

Heatmap analysis of the biological functions at the three post-isolation time points (Figure 5.3) revealed the differential dynamics of the pathway groups. Many of the pathways follow a linear pattern of increasing activation or inhibition; however some, such as the cell survival pathways, display different dynamics, as they are predicted to be activated at 72 hours, but not at 24 or 168 hours. Figure 5.4 displays the canonical pathways at the assessed time points. Whilst metabolic pathways display a trend of increasing significance during culture, acute phase response signalling and ROS/NOS production are significantly affected at 24 hours, but not at 168 hours.

Upstream regulation analysis (i.e. transcription factors, cytokines, growth factors and receptors) was then used to predict which regulators were activated or inhibited (Figure 5.5). The results suggest an activation of proliferative and inflammatory regulators and inhibition of metabolic-associated factors. Moreover, many energy production-associated factors are down-regulated at 168 hours including PPARα, insulin receptor, KLF15 and the mitochondrial transcription factor TFAM. A list of the most significantly perturbed pathways and functions at the three time points is shown in Table 5.6.

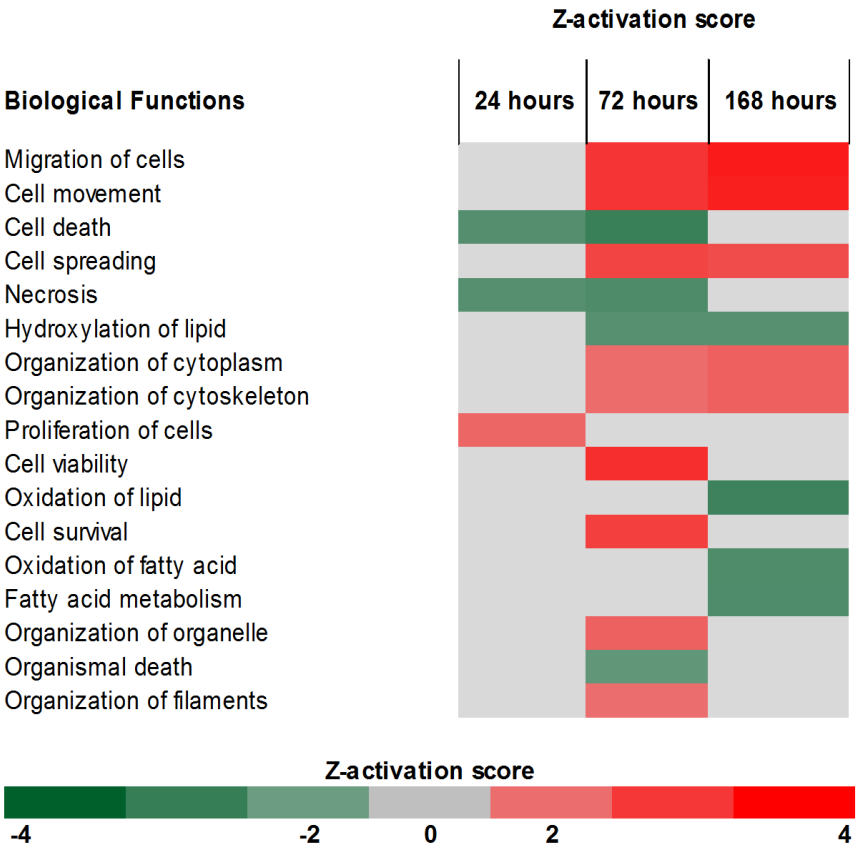

Figure 5.3: Biological functions associated with the dedifferentiation by pathway analysis

Pathway analysis of DEPs. If score 2 ≥ Z-score ≤ -2 the function is predicted to be activated or inhibited, respectively. Red: up-regulated, green: down-regulated. Intensity of colour correlates with greater Z-activation score.

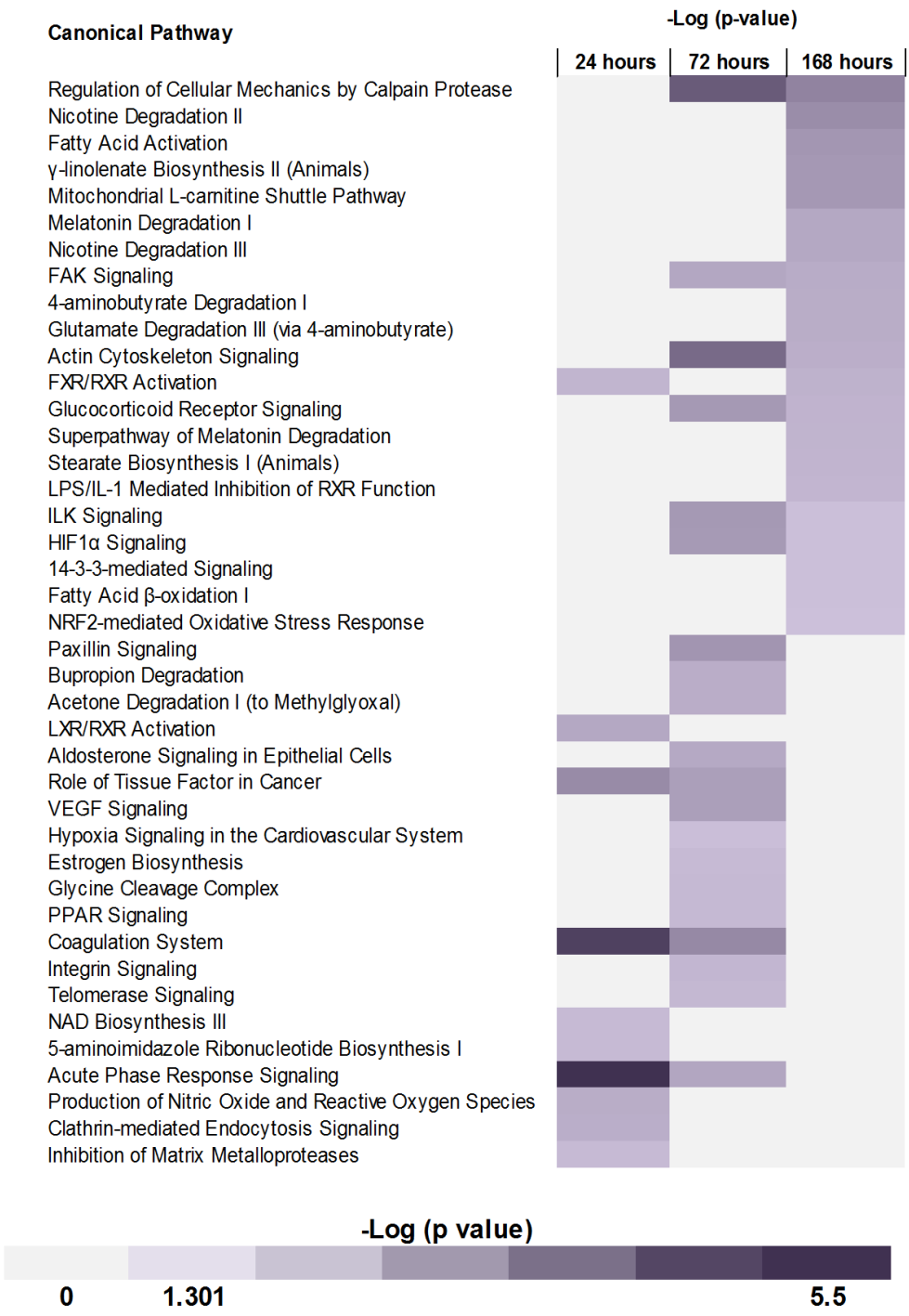

Figure 5.4: Canonical pathways perturbed during dedifferentiation.

Results displayed as –Log (P values), pathway included if p<0.05 at any of the assessed timepoints. Colour Intensity corresponds to the significance value

Abbreviations: RXR: retinoid X receptor; PPAR: peroxisome proliferator-activated receptors; FXR: farnesoid X receptor Nrf2: nuclear factor (erythroid-derived 2)-like 2; HIF-1: hypoxia-inducible factor; FAK: focal adhesion kinase; LPS: lipopolysaccharide; interleukin-1; LXR: liver X receptor; VEGF: vascular endothelial growth factor.

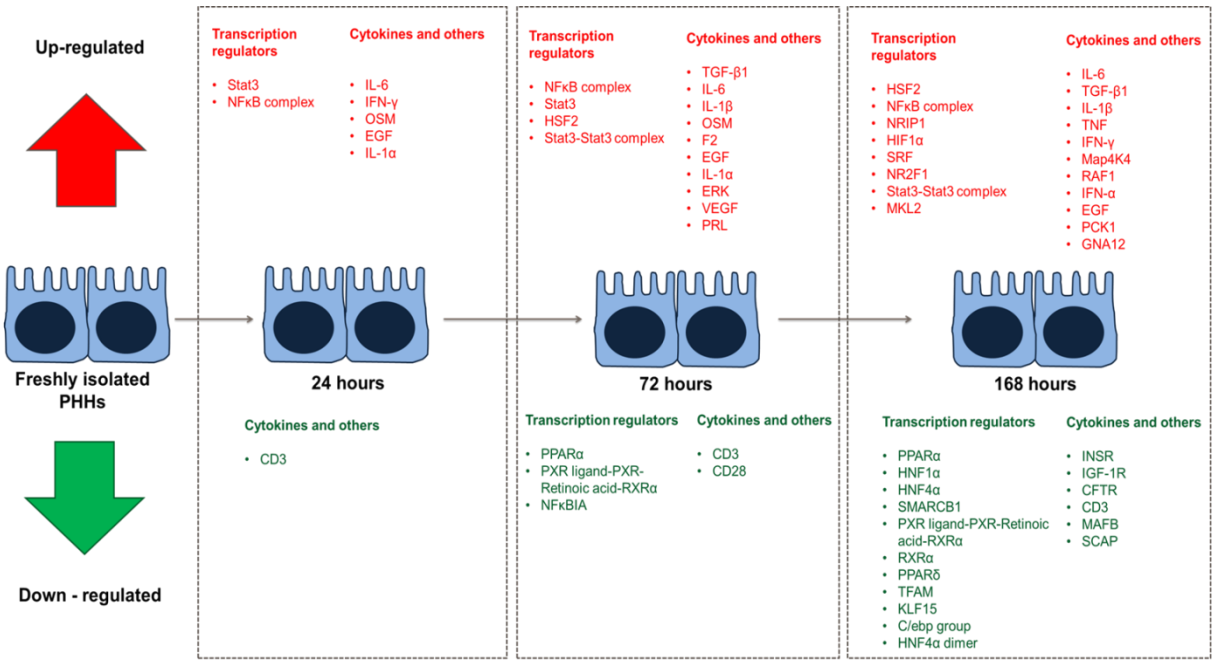

Figure 5.5: Upstream regulation analysis of PHH during dedifferentiation.

Upstream regulators predicted to be either activated or inhibited by Z activation score (2 ≥ Z-score ≤ -2). Red: activated, green: inhibited, in order of significance.

Abbreviations: MAPKs: mitogen-activated protein kinases; NFκB: nuclear factor kappa-light-chain-enhancer of activated B cells; IL: Interleukin; IFN: Interferon; OSM: Oncostatin M; EGF: Epidermal growth factor; INSR: Insulin receptor; IGF-1R: Insulin growth factor receptor 1; HSF2; Heat shock factor protein 2; PPAR: Peroxisome proliferator-activated receptor; ERK: Extracellular signal-regulated kinase; HNF: Hepatic nuclear factor; TGF-β: Transforming growth factor β; TNF: Tumour necrosis factor; VEGF: Vascular endothelial growth factor; PRL: Prolactin; NFκBIA: NFκB inhibitor; PXR: Pregnane X receptor; RXR: Retinoid X receptor; NRIP1: Nuclear receptor-interacting protein 1; HIF1α: Hypoxia-inducible factor 1-alpha; SRF: Serum response factor; NR2F1: nuclear receptor subfamily 2, group F, member 1; MKL2: MKL/Myocardin-Like 2; PCK1: Phosphoenolpyruvate carboxykinase 1; GNA12: Guanine nucleotide binding protein (G protein) alpha 12; SMARCB1: WI/SNF-related matrix-associated actin-dependent regulator of chromatin subfamily B member 1; TFAM: Mitochondrial transcription factor A; KLF15: Krüppel-like factor 15; CFTR: Cystic fibrosis transmembrane conductance regulator; MAFB: V-maf musculoaponeurotic fibrosarcoma oncogene homolog B; SCAP: Sterol regulatory element-binding protein cleavage-activating protein; CD: Cluster of differentiation; F2: Coagulation factor II (thrombin)

24 hours	72 hours	168 hours
Cellular and molecular pathways		
• Cellular Movement • Cell-To-Cell Signalling and Interaction • Cellular Growth and Proliferation • Cellular Development • Cellular Assembly and Organization	• Cell Death and Survival • Cellular Movement • Cellular Assembly and Organization • Cellular Function and Maintenance • Cell Morphology	• Energy Production • Lipid Metabolism • Small Molecule Biochemistry • Cellular Function and Maintenance • Cell Morphology
Toxicity pathways		
• Positive Acute Phase Response Proteins • LXR/RXR Activation	• Positive Acute Phase Response Proteins • NRF2-mediated Oxidative Stress Response • CYP450 Panel - Substrate is a Xenobiotic (Human) • Aryl Hydrocarbon Receptor Signaling • Hypoxia-Inducible Factor Signalling	• NRF2 oxidative stress response • Fatty acid metabolism • LPS/IL-1 mediated inhibition of RXR function • Xenobiotic metabolism signalling • Positive acute phase response proteins • CYP450 panel – substrate is Xenobiotic (Human)
Networks		
• Developmental Disorder, Hematological Disease, Hereditary Disorder • Lipid Metabolism, Small Molecule Biochemistry, Molecular Transport • Cellular Assembly and Organization, Amino Acid Metabolism, Small Molecule Biochemistry	• Post-Translational Modification, Protein Folding, Drug Metabolism • Cellular Assembly and Organization, Cellular Function and Maintenance, Cell Morphology • Protein Synthesis, Cell Death and Survival, Cellular Assembly and Organization • Drug Metabolism, Developmental Disorder, Hematological Disease • Nucleic Acid Metabolism, Small Molecule Biochemistry, Drug Metabolism	• Cell Death and Survival, Neurological Disease, Cancer • Small Molecule Biochemistry, Drug Metabolism, Nucleic Acid Metabolism • Lipid Metabolism, Molecular Transport, Small Molecule Biochemistry • Lipid Metabolism, Small Molecule Biochemistry, Vitamin and Mineral Metabolism • Cellular Assembly and Organization, Cell Morphology, Cellular Function and Maintenance

Table 5.6: Pathway/network analysis.

Top 5 most significantly altered ($p<0.05$; Fisher exact T test) cellular and molecular functions, canonical pathways, toxicity functions and networks associated with the DEPs at 24, 72 and 168 hours by Ingenuity pathway analysis.

Analysis of mitochondrial functional profile reveals donor-variation in the bio-energetic profile

Pathway analysis predicted a perturbation of energy production and mitochondrial mechanics; therefore, we investigated the mitochondrial proteome in further detail. The expression of proteins with known mitochondrial associations demonstrated a general downward trend of the DEPs (bold) with time in culture, particularly at 168 hours, with superoxide dismutase II being a notable exception (Figure 5.6). However, a number of key mitochondrial proteins, such as mitochondrial import receptor subunits, remained largely unchanged (Table 5.4). This indicates that the large-scale down-regulation of mitochondrial proteins represents an alteration in function between freshly isolated cells and 168 hours rather than a generalised loss of mitochondrial mass between these time points.

Pathway analysis was then used to assess the mitochondrial proteomic dataset DEPs. This analysis revealed predicted roles for 5' AMP-activated protein kinase (AMPK) signalling, a master regulator of energy metabolism, which increases in significance during time in culture (Figure 5.7a). Furthermore, a negative regulator of mitochondrial fusion, OMA-1 is also predicted to be down-regulated (Figure 5.7b).

To assess how these changes impacted mitochondrial function, oxygen consumption rate (OCR) and extracellular acidification rate (ECAR) at 24 and 168 hours were investigated. Across 5 donors, a clear variation in individual bioenergetic OCR profiles is observed at 24 hours (Figure 5.8a), with the 168 hour profile showing greater dependence on the 24 hour profile, rather than time in culture. Analysis of glycolytic consumption, as measured by ECAR, shows much greater donor-dependent variation (Figure 5.8b), which may be attributable to the known gradient of glycolysis across the porto-central axis, and is consistent with our findings regarding the most variable proteins. Despite this variation, a trend emerges: basal glycolysis shows an increase during culture in donors with lower basal

glycolysis, whereas those with higher basal levels at 24 hours decrease; suggestive of a convergence towards a culture-dependent level of basal glycolysis.

Furthermore, many of the tested OCR parameters remain remarkably stable between 24 and 168 hours (Figure 5.8c), despite the large-scale changes to the mitochondrial proteome. ECAR measurements showed similar stability; however, there was a general trend of increased glycolytic parameters, including the only significantly altered factor, namely glycolytic reserve (Figure 5.8d).

Further investigation of the proteomic data revealed a significant down-regulation of three complex I subunits, whereas the remaining nine detected subunits were not significantly differentially expressed. To assess the functional consequence of these changes, rotenone was used as a model of complex I mitochondrial perturbation. A significant increase in PHH resistance to rotenone toxicity in all donors at 168 hours regardless of background bio-energetic (OCR/ECAR) profile (Figure 5.9) was found. Together these data suggest that, despite the variability seen between donors, a conserved change in essential mitochondrial function is observed as a result of time in culture.


Name
24 hours
72 hours
168 hours
Superoxide dismutase [Mn], mitochondrial
Hydroxyacyl-coenzyme A dehydrogenase, mitochondrial
Glutamate dehydrogenase 1, mitochondrial
Apoptosis-inducing factor 1, mitochondrial
Glycine dehydrogenase [decarboxylating], mitochondrial
Hydroxymethylglutaryl-CoA synthase, mitochondrial
Dimethylglycine dehydrogenase, mitochondrial
ES1 protein homolog, mitochondrial
Short/branched chain specific acyl-CoA dehydrogenase, mitochondrial
10 kDa heat shock protein, mitochondrial
Fumarate hydratase, mitochondrial
Carbamoyl-phosphate synthase [ammonia], mitochondrial
Sterol 26-hydroxylase, mitochondrial
ATPase inhibitor, mitochondrial
Succinyl-CoA ligase [GDP-forming] subunit beta, mitochondrial
Carnitine O-palmitoyltransferase 2, mitochondrial
mitochondrial carnitine/acylcarnitine carrier protein
Ornithine carbamoyltransferase, mitochondrial
NADH dehydrogenase [ubiquinone] iron-sulfur protein 4, mitochondrial
Alanine--glyoxylate aminotransferase 2, mitochondrial
Succinate-semialdehyde dehydrogenase, mitochondrial
GrpE protein homolog 1, mitochondrial
Sulfite oxidase, mitochondrial
Methylmalonyl-CoA epimerase, mitochondrial
ATP synthase-coupling factor 6, mitochondrial
Sarcosine dehydrogenase, mitochondrial
Cytochrome b-c1 complex subunit 2, mitochondrial
Glutaminase liver isoform, mitochondrial
Dihydrolipoyllysine-residue acetyltransferase component of pyruvate dehydrogenase complex, mitochondrial
Coproporphyrinogen-III oxidase, mitochondrial
GTP:AMP phosphotransferase, mitochondrial
Enoyl-CoA hydratase domain-containing protein 2, mitochondrial
Acyl-CoA synthetase family member 2, mitochondrial
Medium-chain specific acyl-CoA dehydrogenase, mitochondrial
4-aminobutyrate aminotransferase, mitochondrial
Cytochrome c oxidase subunit 4 isoform 1, mitochondrial
Methylmalonate-semialdehyde dehydrogenase [acylating], mitochondrial
Ferrochelatase, mitochondrial
Adenylate kinase 2, mitochondrial
Methylmalonyl-CoA mutase, mitochondrial
Heat shock protein 75 kDa, mitochondrial
Acyl-coenzyme A synthetase ACSM3, mitochondrial
Phosphoenolpyruvate carboxykinase [GTP], mitochondrial
Dihydrolipoyl dehydrogenase, mitochondrial
Sulfide:quinone oxidoreductase, mitochondrial
NADH dehydrogenase [ubiquinone] 1 alpha subcomplex subunit 10, mitochondrial
Glycine amidinotransferase, mitochondrial
Agmatinase, mitochondrial
Aldehyde dehydrogenase, mitochondrial
Isoleucine--tRNA ligase, mitochondrial
Dynamin-like 120 kDa protein, mitochondrial
Dihydrolipoyllysine-residue succinyltransferase component of 2-oxoglutarate dehydrogenase complex, mitochondrial
Choline dehydrogenase, mitochondrial
Very long-chain specific acyl-CoA dehydrogenase, mitochondrial
Cytochrome c oxidase subunit 5B, mitochondrial
Succinate dehydrogenase [ubiquinone] iron-sulfur subunit, mitochondrial
Enoyl-CoA delta isomerase 1, mitochondrial
ATP synthase subunit alpha, mitochondrial
3-ketoacyl-CoA thiolase, mitochondrial
Malonyl-CoA decarboxylase, mitochondrial
Adenylate kinase isoenzyme 4, mitochondrial
NADH dehydrogenase [ubiquinone] 1 alpha subcomplex subunit 5
Complement component 1 Q subcomponent-binding protein, mitochondrial
2,4-dienoyl-CoA reductase, mitochondrial
Acylpyruvase FAHD1, mitochondrial
ATP synthase subunit b, mitochondrial
NADH dehydrogenase [ubiquinone] 1 alpha subcomplex subunit 6
Aspartate aminotransferase, mitochondrial
Kynurenine/alpha-aminoadipate aminotransferase, mitochondrial
Pyruvate carboxylase, mitochondrial
Probable 2-oxoglutarate dehydrogenase E1 component DHKTD1, mitochondrial
Leucine-rich PPR motif-containing protein, mitochondrial
Aldehyde dehydrogenase X, mitochondrial
NAD(P) transhydrogenase, mitochondrial
3-hydroxyisobutyrate dehydrogenase, mitochondrial
Peptidyl-prolyl cis-trans isomerase F, mitochondrial
Propionyl-CoA carboxylase alpha chain, mitochondrial
Cytochrome b-c1 complex subunit 6, mitochondrial
2-oxoglutarate dehydrogenase-like, mitochondrial
Isochorismatase domain-containing protein 2, mitochondrial
Adrenodoxin, mitochondrial
[3-methyl-2-oxobutanoate dehydrogenase [lipoamide]] kinase, mitochondrial
Citrate lyase subunit beta-like protein, mitochondrial
Cytochrome b-c1 complex subunit Rieske, mitochondrial
mitochondrial fission 1 protein
Acyl-CoA synthetase short-chain family member 3, mitochondrial
mitochondrial ornithine transporter 1
NADH dehydrogenase [ubiquinone] 1 alpha subcomplex subunit 4
Calcium-binding mitochondrial carrier protein Aralar2
2-oxoglutarate dehydrogenase, mitochondrial
Glutaredoxin-related protein 5, mitochondrial
2-methoxy-6-polyprenyl-1,4-benzoquinol methylase, mitochondrial
Delta(3,5)-Delta(2,4)-dienoyl-CoA isomerase, mitochondrial

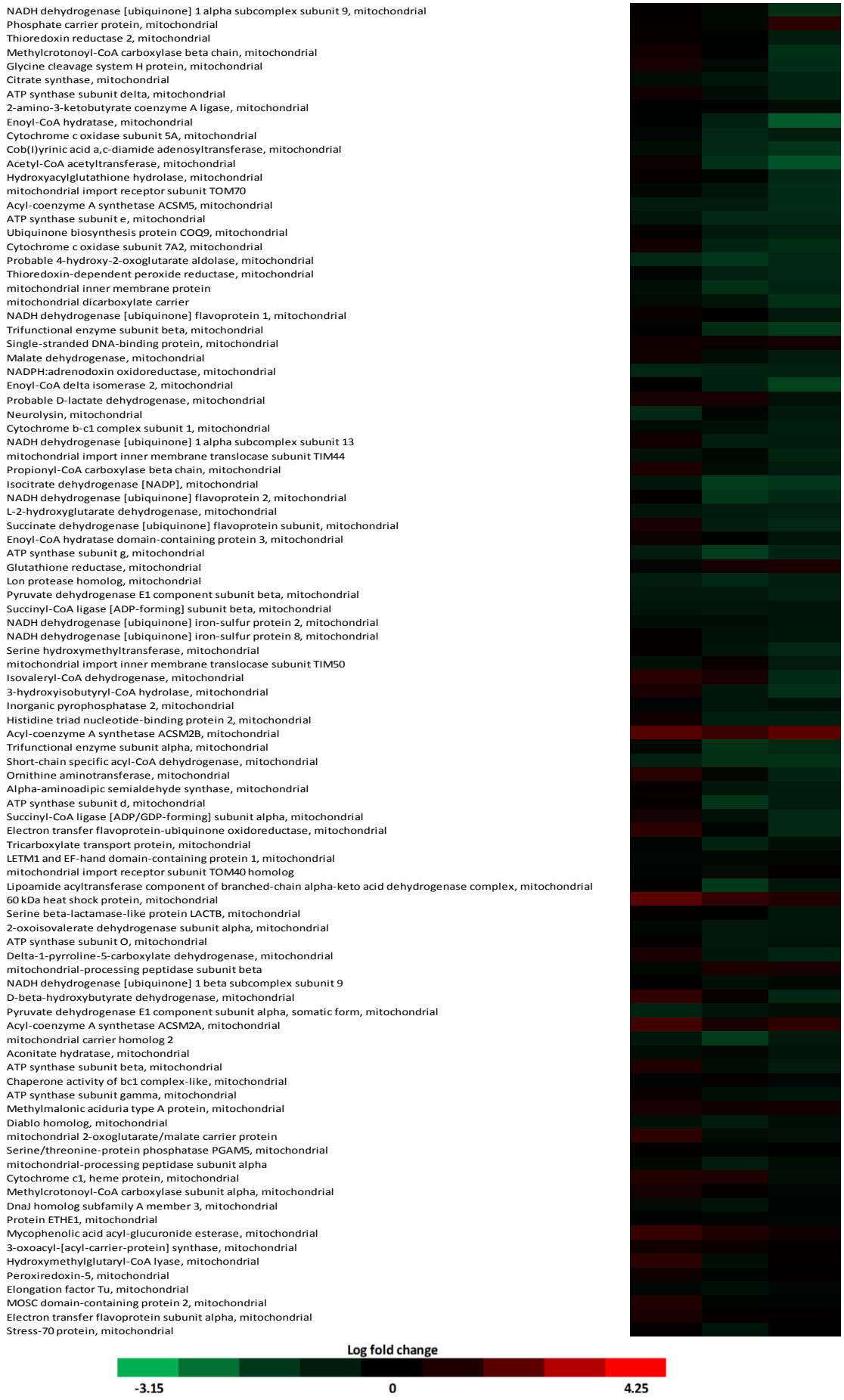

Figure 5.6: Mitochondrial changes during dedifferentiation.

Log_2 fold change of mitochondrial proteins. Red: up-regulated, green: down-regulated. Intensity of colour: log_2 fold change. Bold proteins: differentially expressed at 168 hours ($p<0.05$).

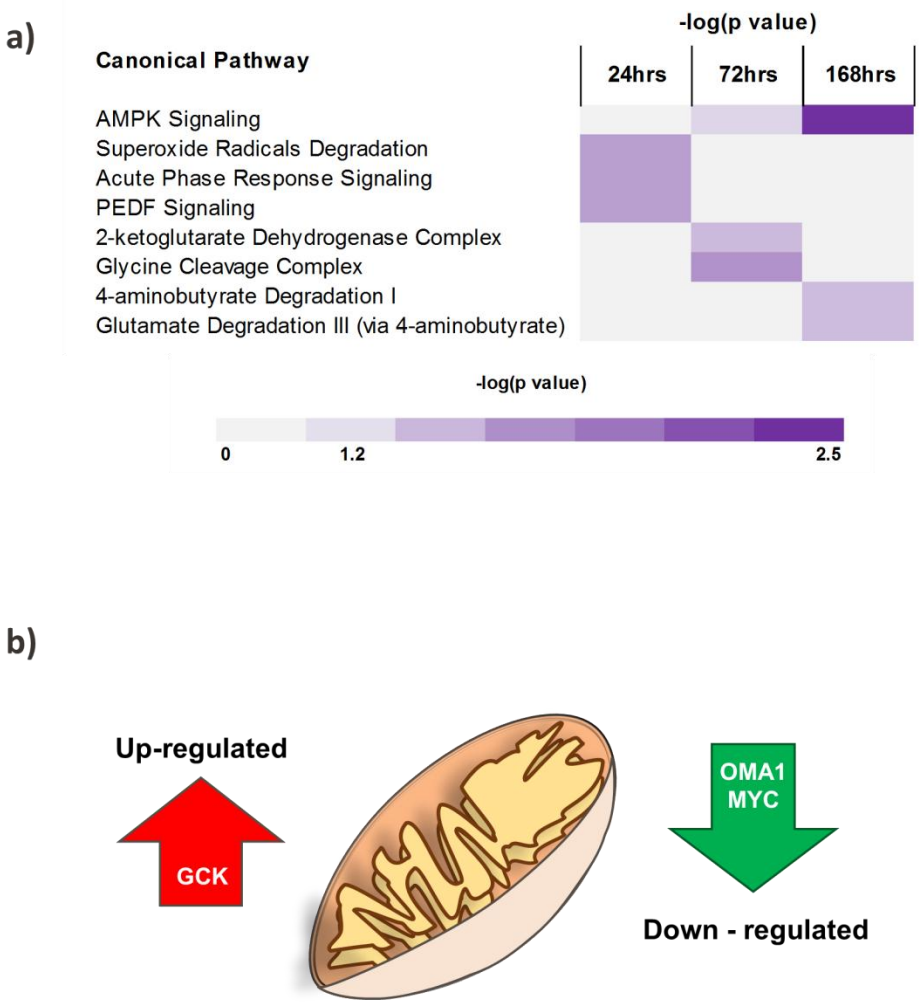

Figure 5.7: The Pathway analysis of mitochondrial DEPs during dedifferentiation

a) Canonical pathway analysis of mitochondrial proteins Results displayed –Log (P values), pathway included if $p<0.05$ at any of the assessed timepoints. Intensity of purple corresponds to the significance value; **b)** Upstream regulators of mitochondrial changes predicted to be activated or inhibited by IPA software displayed. Red regulators are up-regulated, green regulators are down-regulated. Upstream regulators were included if Z activation scores ($2 \geq$ Z-score ≤ -2).

Abbreviations: GCK: Glucokinase; OMA1: Metalloendopeptidase OMA1. AMPK: 5' AMP-activated protein kinase; PEDF: Pigment epithelium-derived factor.

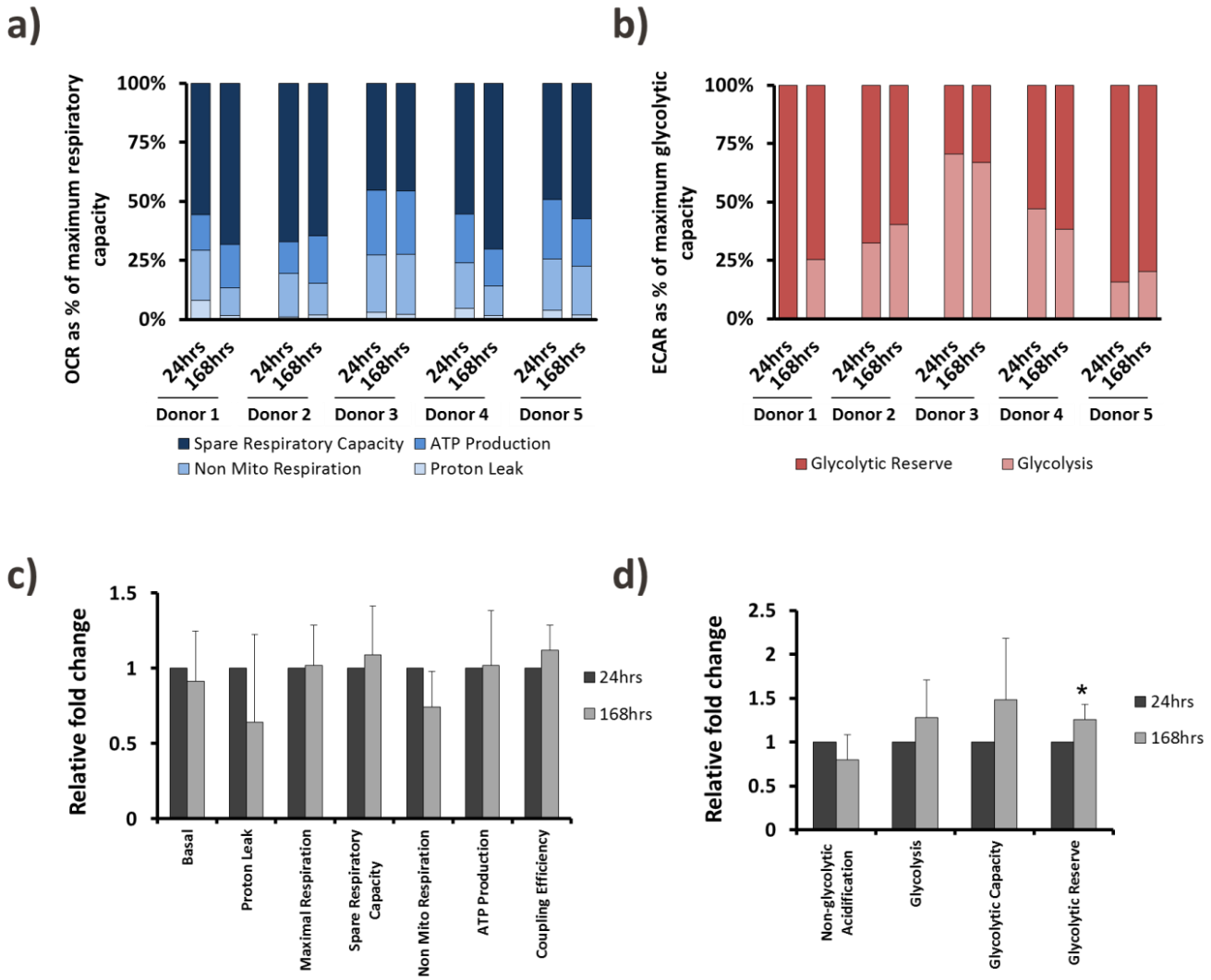

Figure 5.8: Seahorse analysis of the bioenergetic profile of PHH during culture

a) Oxidative phosphorylation and **b)** glycolysis parameters as percentages of maximal oxygen consumption rates and extracellular acidification rate, respectively; Relative fold change of **c)** oxidative phosphorylation and **d)** glycolysis parameters. (*) $p<0.05$ paired T-test.

Abbreviations: OCR: Oxygen consumption rate; ECAR: Extracellular acidification rate

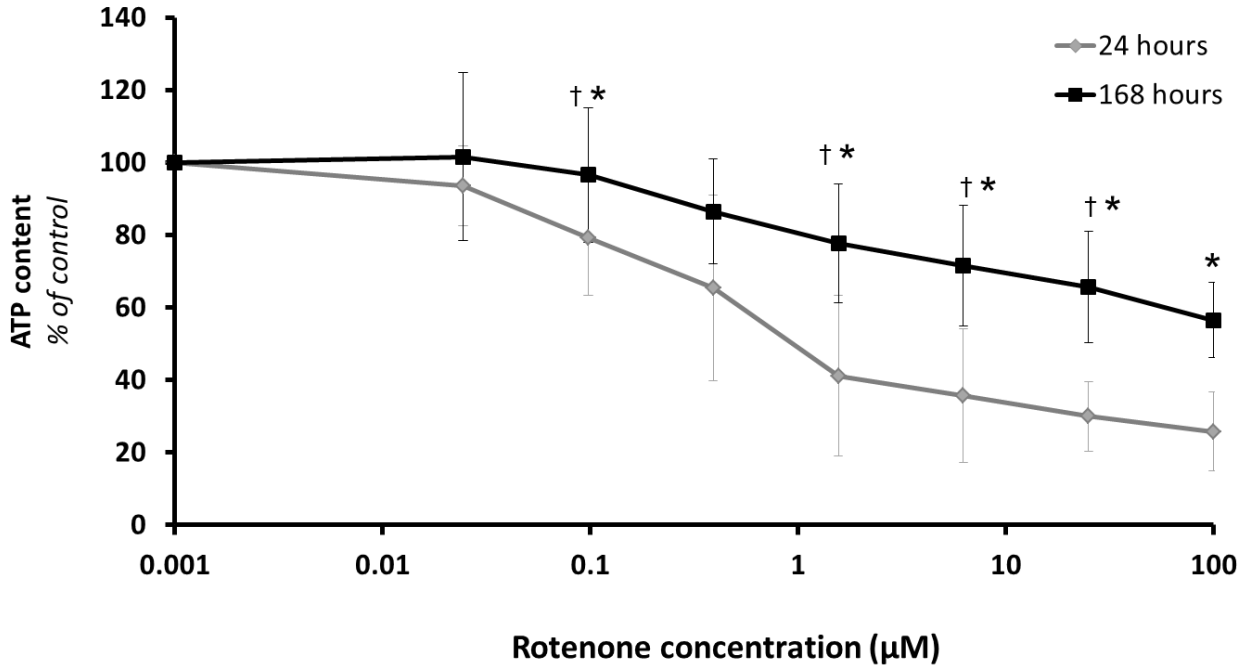

Figure 5.9: Assessing changes in mitochondrial sensitivity to Complex I inhibitor Rotenone over time in culture

ATP levels at 24 (♦) and 168 hours (■) following rotenone treatment. Results: percentage of control, (*) $p<0.05$ two tailed paired T-test and (†) $p<0.05$ Wilcoxson test signed rank test (n=5).

Assessment of ADME proteins during dedifferentiation reveals selective protein down-regulation

A well-known feature of hepatocyte dedifferentiation is the loss of the metabolic phenotype. To distinguish whether this is a selective or global loss of metabolic competence, several protein subsets generated in this analysis were compared: 168 hour DEPs, 168 hour non-DEPs, most stable proteins and the most variable proteins. PANTHER analysis was used to compare the associated biological function categories of each subset (Figure 5.10). This analysis revealed similar percentages of proteins in each class, with the greatest proportion of proteins associated with metabolism in all subsets, indicating a selective, rather than wholesale alteration, in the hepatocyte metabolic profile.

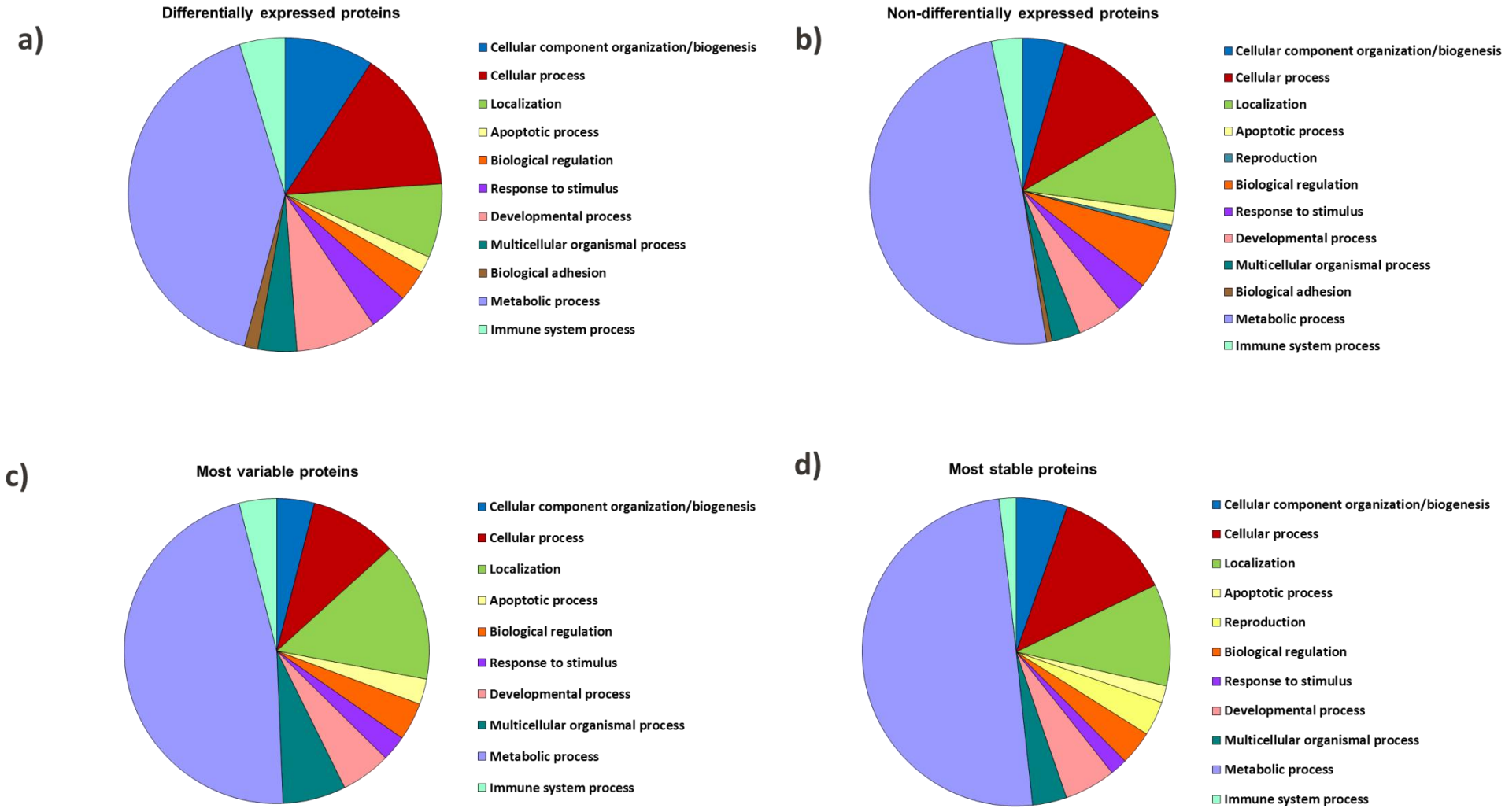

Figure 5.10: PANTHER analysis of biological functions

a) DEPs at 168 hours; **b)** Non-DEPs at 168 hours; **c)** most variable proteins; **d)** most stable proteins. Proteins divided by function and represented as a pie chart.

Figure 5.11 shows the known phase I, II and III drug metabolising enzymes (Guo et al., 2011) which were detected by proteomic analysis. The heatmap highlights the loss of metabolic competence with the majority of Phase I enzymes following a relatively linear pattern of down-regulation towards 168 hours. Phase II/III enzymes appear to show greater stability with some phase III proteins, including multidrug resistance protein 1 (MDR1) and major vault protein (MVP), demonstrating an up-regulation during culture.

Figure 5.12a demonstrates the dedifferentiation pattern of the cytochrome P450s detected by iTRAQ over the 168 hour period. The general trend relative to freshly isolated PHHs is downward, however, with the exception of CYP1A2, CYP2A6 and CYP27A1, all the detected CYP proteins maintained or increased in expression at 24 hours in relation to the freshly isolated cells, showing that at 24 hours the metabolic potential of PHH is mostly maintained. Some CYPs displayed greater stability, such as 2C18 and 4F11, whilst 2B6 and 2C9 demonstrated downward trends, but showed greater variation between the donors.

Western blotting for CYP proteins 2D6, 2E1, 1A2 and the cytoskeletal protein β-actin were consistent with the iTRAQ results, further demonstrating a downward trend with noted variation in the individual dedifferentiation profiles (Figure 5.12b). Furthermore, analysis of CYP450 activity using probe substrates for CYP3A and 2D6 show a loss of functional capacity that is in line with the loss of protein recorded by iTRAQ and western immunoblotting (Figure 5.12c).

In contrast to the CYPs, the protein expression of the transporters identified as being important for drug influx and efflux in the liver (Zamek-Gliszczynski et al., 2012) is relatively stable throughout the 168 hour culture. Only 2 of the 9 detected transporters are significantly down-regulated at 168 hours ($P<0.05$; Figure 5.13), interestingly these are both influx transporters (OATP1B1 and OATP1B3). The general trend of the other detected drug influx transporters is also downwards, as are the trends for efflux transporters MRP6 and

BSEP. Conversely, the remaining efflux transporters (MDR1, MRP2 and MRP3) show a maintenance or upward trend in expression during culture.

Comparison of the trend in the CYP and transporter proteins with previously published hepatocyte monolayer gene expression data (Richert et al., 2006) allows further investigation of the loss of metabolic competence (Table 5.7). All CYPs with a reported gene expression >30% at 72 hours maintained protein expression >60% at 168 hours. Conversely, at 72 hours, the mRNA of CYP1A2, 2A6, 2B6, 2C8, 2E1, 3A4, 4A11, 4F2, 4F3 and 27A1 is reported to drop to below 10% of freshly isolated PHH (Richert et al., 2006). When the protein expression of these CYPs is compared, the majority, with the exception of CYP4F2 and 4F3, show significant down-regulation at 168 hours, suggesting that the loss of CYPs can be mainly associated with reduced transcription. This association is shown in Figure 5.14, demonstrating that whilst all CYPs protein expression at 168 hours is not significantly correlated with mRNA expression at 72 hours (Figure 5.14a); there is a significant correlation between mRNA at 72 hours and protein at 168 hours for the significantly down-regulated CYPs (Figure 5.14b). This rule was found to be less true of the transporters investigated in this study, with BSEP, OAT2 and OCT1 all having mRNA <10% at 72 hours; however, despite a downward trend, they are not significantly down-regulated at 168 hours.

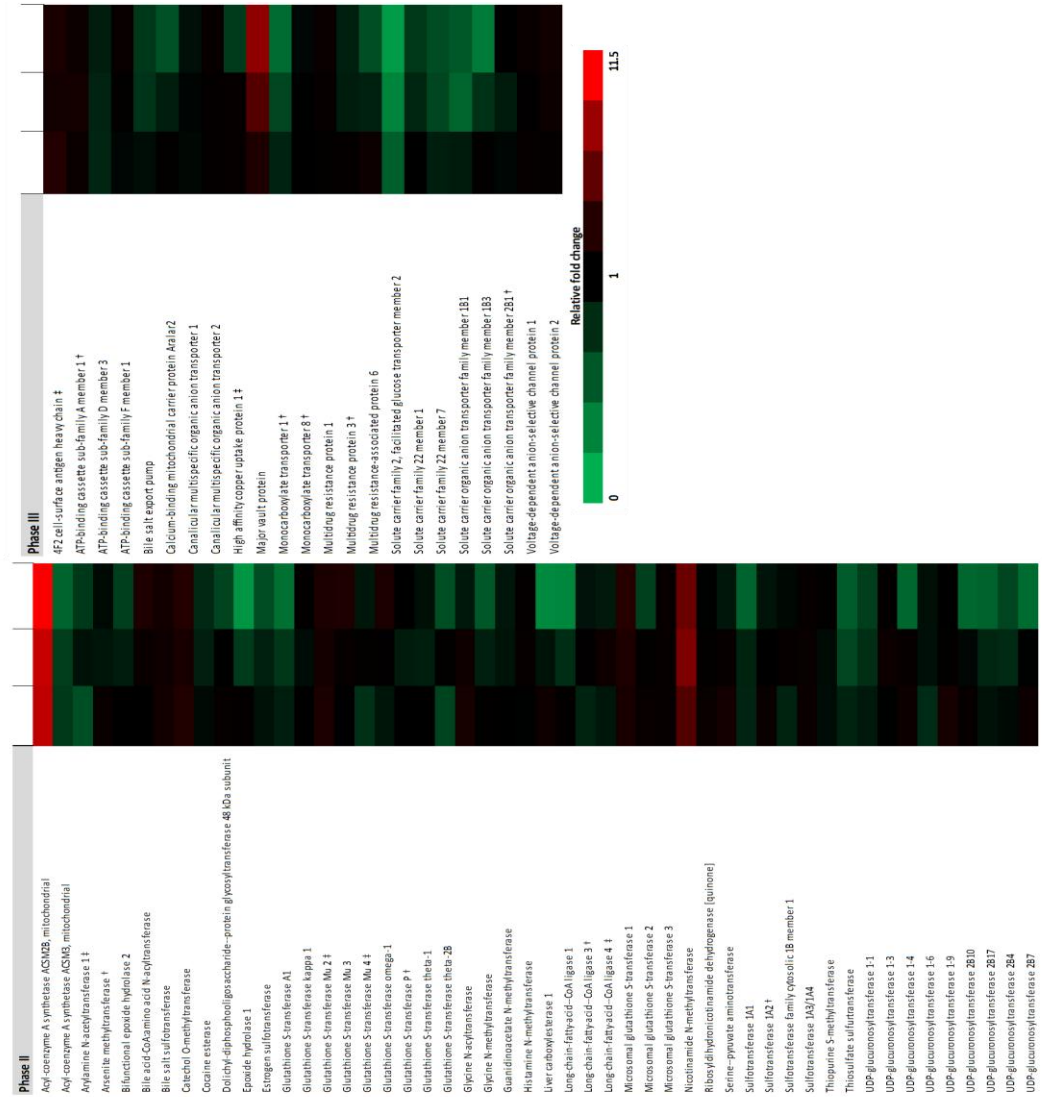

Figure 5.11: Loss of hepatic metabolic phenotype.

ADME Phase I, II and III enzyme heatmap. Red: up-regulated, green: down-regulated. Intensity of colour: relative fold change. Data derived from n≥3 donors unless stated (†) n=2 or (‡) n=1.

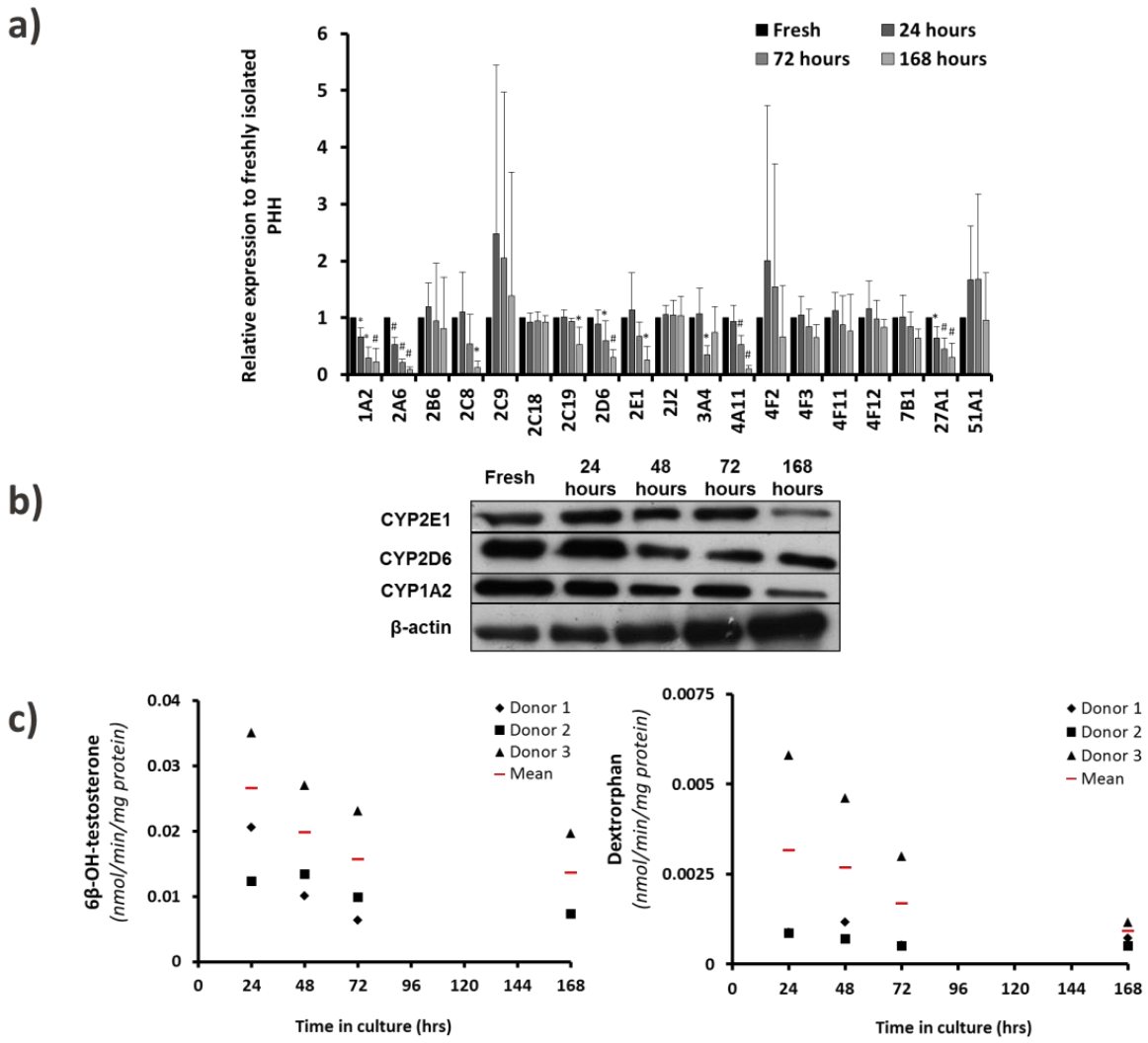

Figure 5.12: Loss of CYP proteins and metabolism during dedifferentiation of PHH.

a) CYP450s over 168 hours (n=5); error bars: SD; One-way ANOVA: (*) $p<0.05$, (#) $p<0.01$); **b)** Western blots for CYP450s and β-actin **c)** Metabolic function of CYP3A (testosterone) and CYP2D6 (dextromethorphan) and detection of respective metabolites (6β-OH-testosterone and dextrorphan) detected by LC-MS-MS (n=3 donors; error bars: SD). One-way ANOVA: (*) $p<0.05$.

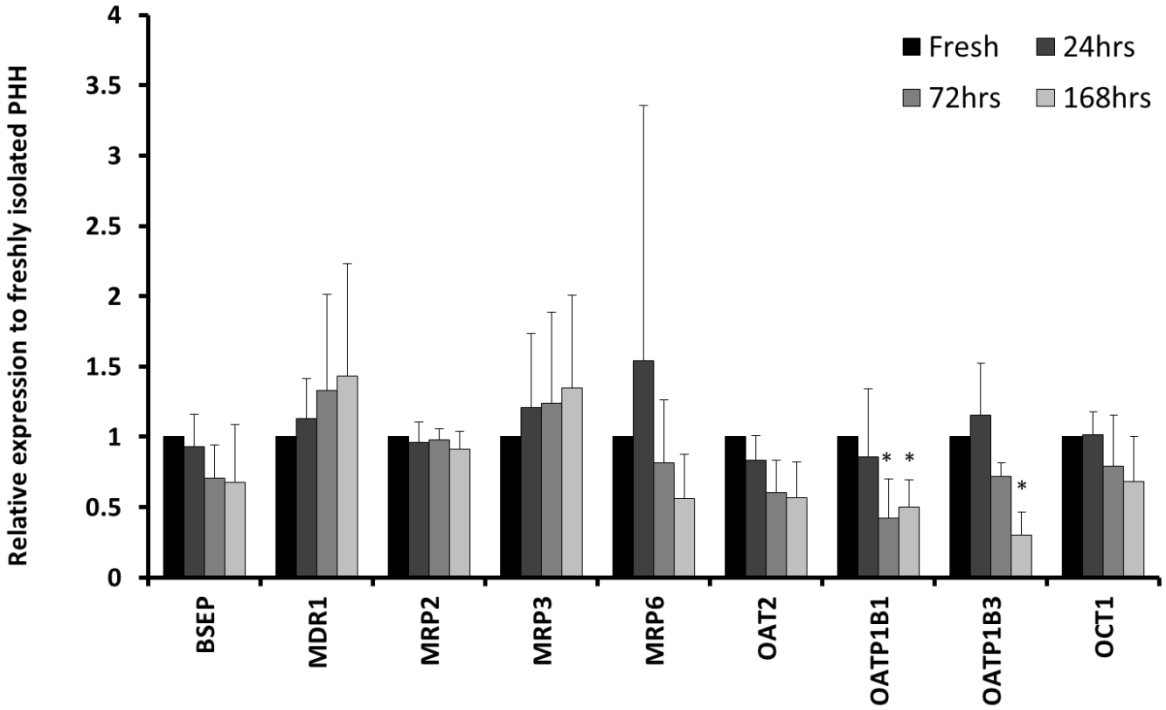

Figure 5.13: ADME transporters protein expression during dedifferentiation.

Error bars SD,* significant p<0.05 by one-way ANOVA

Abbreviations: BSEP: bile salt export pump; MDR: multiple drug resistance protein; MRP: multidrug resistance-related protein; OAT: organic anion transporting polypeptide; OATP: organic anion transporter; OCT: organic cation transporter

	Protein expression % of freshly isolated cells			Protein degradation		mRNA expression % of freshly isolated cells
CYP450	**Protein expression** 24hrs	**Protein expression** 72hrs	**Protein expression** 168hrs	**Average half-life by 72 hour trend (hrs)**	**Average half-life by 168 hour trend (hrs)**	**mRNA expression at 72hrs** (Richert *et al.*, 2006)
1A2	66.94	28.88	22.08	48.54	89.29	7.17
2A6	52.68	21.68	9.06	42.37	76.92	4.78
2B6	119.38	95.1	81.22	2500	555.56	3.21
2C8	110.8	54.44	12.72	96.15	96.15	1.38
2C9	247.56	205.00	138.32	-	-	33.30
2C18	92.43	94.90	92.52	500	1000	277.60
2C19	101.96	93.85	52.72	714.28	200	17.89
2D6	89.22	60.22	30.86	92.59	116.28	11.92
2E1	113.94	67.64	26.44	142.85	119.05	2.99
2J2	106.37	105.35	103.23	2500	-	30.80
3A4	106.78	34.48	74.38	63.29	192.31	8.58
4A11	93.52	52.46	9.96	80.65	90.91	1.88
4F2	201.00	154.69	66.05	-	-	7.72
4F3	104.98	84.23	64.95	277.78	250	4.67
4F11	112.84	88.4	76.76	555.56	384.62	79.38
4F12	116.3	97.54	83.08	-	625	17.00
7B1	101.55	84.60	63.93	263.18	238.10	77.32
27A1	64.01	44.69	29.98	59.52	102.04	6.18
51A1	167.27	168.21	96.22	-	-	100

Transporter	**Protein expression** 24hrs	**Protein expression** 72hrs	**Protein expression** 168hrs	**Average half-life by 72 hour trend (hrs)**	**Average half-life by 168 hour trend (hrs)**	**mRNA expression at 72hrs** (Richert *et al.*, 2006)
BSEP	93.12	70.73	67.66	128.21	217.39	6.03

MDR1	113.23	132.66	143.25	-	-	305.33
MRP2	95.98	97.78	90.95	1250	1000	182.66
MRP3	121.02	123.91	134.63	-	-	162.10
MRP6	154.21	81.57	56.16	12500	227.27	40.78
OAT2	83.33	60.57	57.04	89.29	161.29	5.75
OATP1B1	85.57	42.50	50.26	64.1	131.58	12.27
OATP1B3	115.59	71.76	30.38	172.41	128,21	6.10
OCT1	101.26	79.37	68.09	200	250	6.23

Table 5.7: Comparison of proteomic CYP and drug transporter expression profile during dedifferentiation with previously reported gene expression and protein degradation rates.

Protein half-life calculated using linear regression at 72 and 168 hours of culture. Gene expression data is derived from previously published literature using similar monolayer culture conditions (Richert et al., 2006).

Abbreviations: BSEP: bile salt export pump; MDR: multiple drug resistance protein; MRP: multidrug resistance-related protein; OAT: organic anion transporting polypeptide; OATP: organic anion transporter; OCT: organic cation transporter

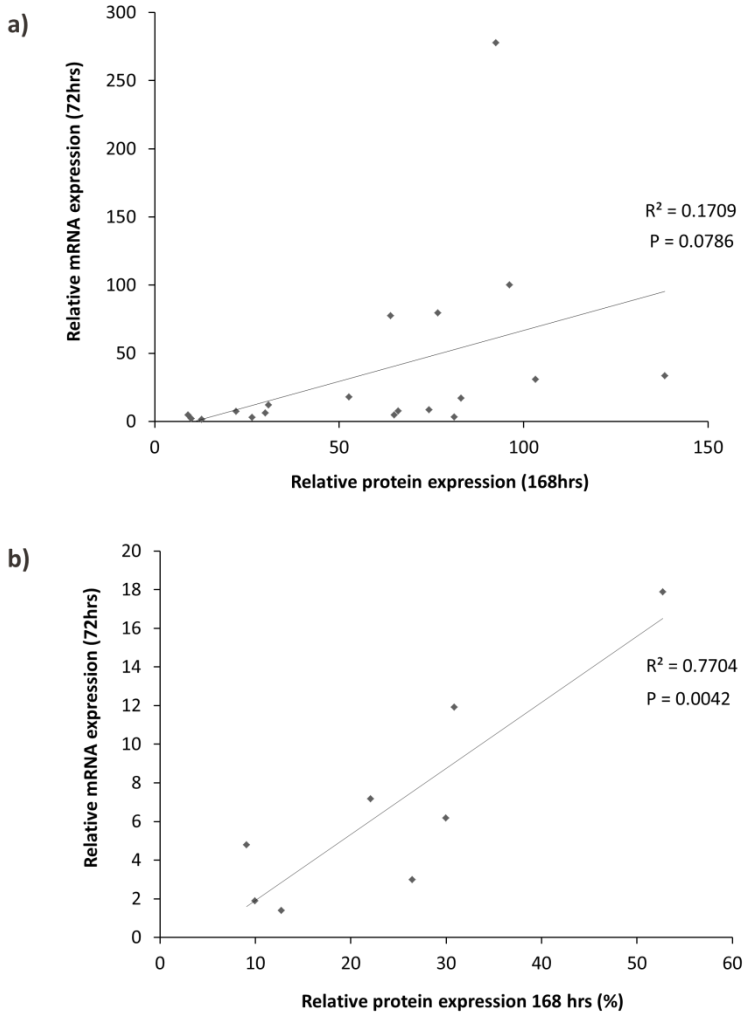

Figure 5.14: Correlation between protein expression at 168 hours and mRNA expression at 72 hours

a) all CYPs and **b)** CYPs which are significantly down-regulated at 168 hours. Gene expression data is derived from previously published literature using similar monolayer culture conditions (Richert et al., 2006). $P<0.05$ classed as significant according to linear correlation analysis.

Pathway analysis of ADME proteins reveals the pathways and transcription factors predicted to underlie the loss of specific metabolic functions

Targeted analysis of the transcription factors which are associated with the ADME DEPs revealed the specific regulators which are significantly perturbed and may cause the loss of ADME proteins during dedifferentiation (Table 5.8). In-keeping with published literature (Fraczek et al., 2013), HNF1α, C/EBP and HNF1β were amongst the most significantly associated regulators with the loss of metabolic competence. Interestingly, FECH (Ferrochelatase), a key enzyme in the production of heme, found to be significantly down-regulated at 168 hours (Table 5.S2), is highly associated with the differentially expressed ADME proteins. SMARCB1 is also significantly associated with the ADME proteomic profile at 168 hours.

Investigation into the predicted transcription factor binding sites of differentially expressed and non-differentially expressed CYPs revealed the factors that may underlie the selectivity found in the loss of xenobiotic CYPs (Table 5.9). This analysis predicted binding sites for HSF2 to be highly enriched in the CYPs which were not differentially expressed; whereas, ZEB1, FOXO1 and NF-Y binding sites are almost exclusively predicted to be located upstream of the differentially expressed CYPs.

Upstream Regulator	p-value of overlap
HNF1A	0.000873
FECH	0.00813
C/EBP	0.0111
SMARCB1	0.0111
STAT1	0.0111
STAT6	0.0123
FOXA1	0.0123
TNF	0.0382
Ins1	0.0411
HNF1B	0.0411

Table 5.8: Upstream regulator pathway analysis of the ADME DEPs.

Most significantly associated upstream regulators of ADME DEPs ($p<0.05$) as associated by IPA ingenuity software.

Abbreviations: FOXA2: Forkhead Box A2; HNF4α: Hepatic nuclear factor 4 alpha: Ins1: Insulin 1; TNF: Tumor necrosis factor; STAT: signal transducer and activator of transcription; SMARC: SWI/SNF related, matrix associated, actin dependent regulator of chromatin; C/EBP: CCAAT/enhancer binding protein; FECH: Ferrochelatase

Greater expression in maintained CYP promoters	Greater expression in down-regulated CYP promoters
HSF2	Nuclear factor Y
MITF	ZEB1
Androgen receptor	FOXO1
COUP-TF2	TBK-1
ATF6	myogenin / NF-1
Brachyury	
FXR/RXR-alpha	
NK3 Homeobox 1	
Otx2	
TATA Box Binding Protein	
TBX5	

Table 5.9: Predicted transcription factor binding using Mapper^2 software.

The transcription factors with enriched predicted binding in the upstream regions of either the differentially expressed or non-differentially expressed Cytochrome P450s. The transcription factors were included if enrichment was ≥4 CYPs from either group and are ordered according to the amount of enrichment. Analysis of LETFs promoter regions shows the transcription factors with predicted binding in the greatest number of LETFs. Transcriptions factors are ordered according to the number LETFs with predicted binding sites.

Abbreviations: FOX: forkhead Box; HSF: heat shock factor; MITF: microphthalmia-associated transcription factor; COUP-TF: chicken ovalbumin upstream promoter-transcription factor; ATF: activating transcription factor; RXR: retinoid X receptor; FXR: farnesoid X receptor; Otx2: orthodenticle homeobox 2; TBX: T-box transcription factor; ZEB1: zinc finger e-box binding homeobox 1; TANK-binding kinase 1; NF-1: neurofibromatosis type 1

Pyrosequencing reveals the changes to epigenome of the cell during dedifferentiation are highly specific

To investigate the process of xenobiotic dedifferentiation further, we then assessed some of the key genes associated with drug metabolism, namely CYPs and LETFs. *In silico* predictive tools (http://cpgislands.usc.edu/) were used to identify CpG islands found within the promoter regions of each gene. Interestingly, of the CYPs investigated, only CYP2E1 had a predicted CpG island close to the promoter region of the gene, whereas, CYP1A2, CYP2A6, CYP2B6, CYP2D6, CYP3A4 and CYP3A7 did not. Conversely, many of the LETFs had highly enriched regions of CpG sites and numerous predicted CpG islands close to or within the promoter region of the gene. These included: HNF6, C/EBP family and the FOXA family. We also found that both HNF1α and HNF4α had regions of enriched CpG sites which fell short of the arbitrary cut off values used by the prediction tool; however, due to their known importance during dedifferentiation, we also included these genes in our analysis. Therefore, our selected gene set consisted of: CYP2E1, HNF1α, HNF4α, HNF6, C/EBPα, FOXA2 and Line1 (a repeated genomic sequence which indicates global methylation status of the tissue; Line1: Long interspersed nuclear elements retrotransposable element 1).

Samples collected from tissue, directly after isolation and after 24 and 168 hours of culture were subjected to pyrosequencing. Despite the presence of CpG islands, the genes HNF6, C/EBPα and FOXA2 showed no methylation at the tissue or culture timepoints examined. Furthermore, despite multiple attempts, including re-designing of the primers, the sequencing primers for CYP2E1 and HNF1α failed to anneal to the PCR product and therefore the methylation status of the gene could not be determined.

Interestingly, Line1 showed very consistent methylation of ~70% throughout the isolation and culture periods, suggesting little change in global methylation status during this period (Figure 5.15a). HNF4α showed a consistent pattern of methylation during the

dedifferentiation process. The tissue methylation status of HNF4α was consistently ~50%, however, this changed dramatically upon isolation, falling to ~25%. These levels then increased to ~35% and decreased back to ~25% during the culture period, although these changes at these timepoints demonstrated greater variation between donors (Figure 5.15b).

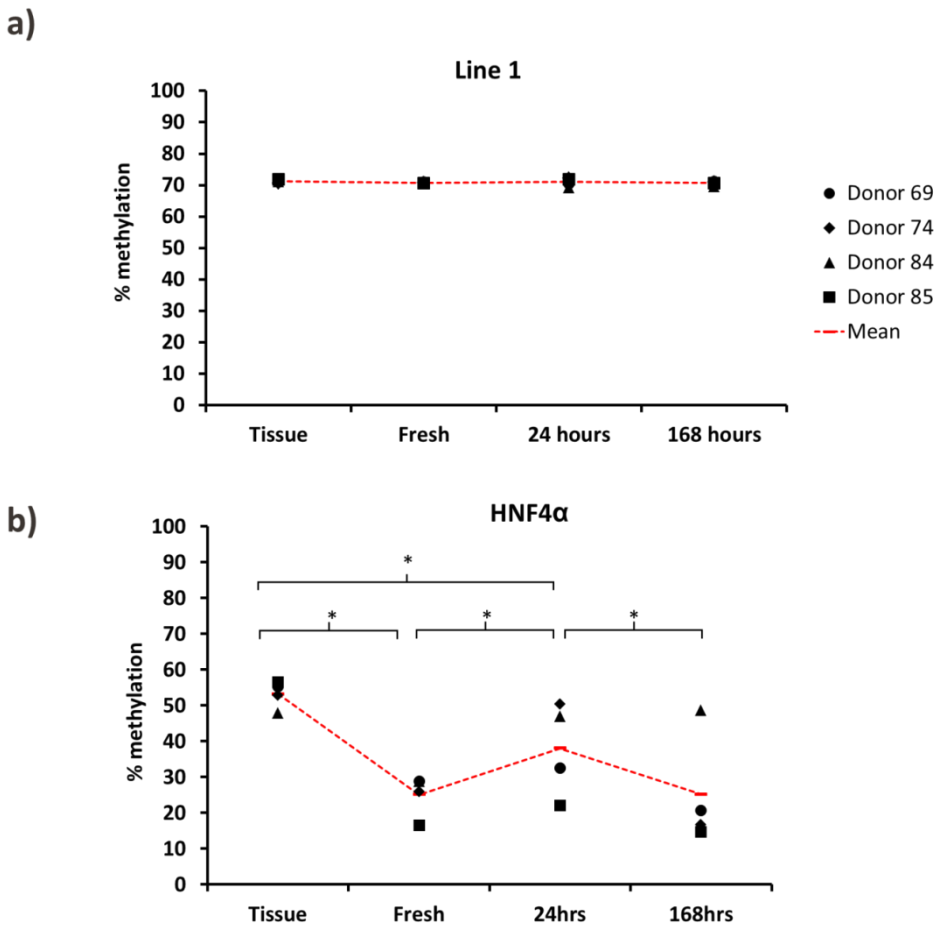

Figure 5.15: Methylation status of PHH during dedifferentiation by pyrosequencing.

a) Line1 and **b)** HNF4α methylation of CpG sites during isolation and culture as determined by pyrosequencing. (*) p>0.05 one-way ANOVA; n=4 donors with 5 CpG sites at each timepoint).

Abbreviations: HNF4α: Hepatic nuclear factor 4 alpha: Line1: Long Interspersed Nuclear Elements Retrotransposable Element 1

5.3. Discussion

In this chapter we have demonstrated the first use of global proteomics as a tool for investigating primary human hepatocyte dedifferentiation, identifying new targets and generating new hypotheses for future examination in simple and complex culture models.

Throughout the analysis, differentially-expressed proteins and associated pathways were found at every time point, suggesting that these mechanisms are well-conserved across donors. The number of significantly differentially expressed proteins increased at each timepoint, which, together with the clustering analysis, suggests an increasing deviation from the freshly-isolated donor phenotype. Grouping of these data showed that dedifferentiation is not solely a change in expression of whole protein classes, but that it is a complex, differentially-controlled and active process, in which selected pathways and functions from many classes are up- or down-regulated.

Cytochrome P450s have been strongly associated with a loss of expression during culture (Rodriguez-Antona et al., 2002), and this is further demonstrated here by the top three most down-regulated proteins at 168 hours: CYP2A6, CYP2C8 and CYP4A11. However, this study allows for these changes to be put into the context of the global cell proteome, revealing the strikingly selective nature of dedifferentiation. Even within single P450 families, selectivity can be seen. For example, whilst CYP2A6 and CYP2C8 are the most down-regulated proteins, CYP2C18 and CYP2J2 remain unaltered by culture conditions. Of further interest, CYP2A6 has been reported to be the largest discriminant between foetal and adult hepatocytes (Rowe et al., 2013); here we show CYP2A6 to be the largest discriminator between freshly isolated and 168 hour cultured hepatocytes.

Understanding how this specificity works is a key question in determining new strategies for hepatocyte culture and for stem cell differentiation protocols. By comparing predicted

transcription factor binding, we have been able to generate a list of enriched transcription factors associated with either differentially expressed or non-differentially expressed CYPs. Future investigations to elucidate the roles of these factors (e.g. HSF2, SP1 and ZEB1) may lead to a greater understanding of the selective loss/maintenance of metabolic competence during dedifferentiation.

Comparisons between differentially-expressed and non-differentially expressed drug metabolizing proteins revealed no single factor which could mediate all the ADME-associated proteomic changes. The results corroborate previous reports showing the importance of HNF1α alongside HNF1β, C/EBP and FOXA1 in dedifferentiation (Padgham et al., 1993). The association of the enzyme ferrochelatase is also of interest. Ferrochelatase catalyses the final step of the heme production pathway and thus its loss of expression would likely reduce the intracellular heme concentration. CYPs are dependent on heme for function and its loss during culture has been reported in mouse hepatocytes (Singh and Veltri, 1991). HNF1α has been shown to regulate ferrochelatase expression (Muppala et al., 2000) and may provide an additional indirect mechanism by which HNF1α can alter ADME protein expression.

Despite being a well-accepted major determinant of hepatic function (Odom et al., 2004), the lack of association of HNF4α with differentially expressed ADME proteins is consistent with HNF4α over-expression studies in rat hepatocytes, which failed to re-establish xenobiotic metabolic function (Naiki et al., 2005). However, our epigenetic analysis revealed changes to the promoter region of HNF4α, suggesting reduced methylation between tissue and cultured cells, which usually indicates increased transcription. Further investigation revealed that this promoter region investigated was actually related to the foetal-associated HNF4α isoforms and may indicate a mechanism by which the isolated PHH is driven towards an immature and less xenobiotic metabolically active phenotype

(Mizuguchi et al., 1998; Drewes et al., 1996). This may, in part, explain the similarity between the hepatic markers detectable in stem cell-derived HLCs and those maintained during PHH dedifferentiation (Rowe et al., 2013; Baxter et al., 2015).

One potential cause of the change in the hepatocyte ADME and proteome-wide phenotype is through alterations in the accessibility of DNA to transcriptional machinery. Our results strongly predict a down-regulation of SMARCB1, a member of the BAF complex which is thought to remodel chromatin structure (Wilson and Roberts, 2011). SMARCB1 been shown to be essential for hepatocyte differentiation (Gresh et al., 2005) and recent work has also linked another member of the BAF complex, SMARCA4, to the enhancement of the ESC-derived HLC phenotype (Mobus et al., 2015). Alterations in chromatin accessibility and transcription factor binding is one of the key first steps in the reprogramming of somatic cells to induced pluripotent stem cells (Papp and Plath, 2013) and similar fundamental mechanisms may play a role in the acquisition of the dedifferentiated phenotype. Efforts to intervene epigenetically using histone deacetylase and DNA methyltransferase inhibitors have been successful in maintaining expression of hepatic functions, although the exact mechanisms are unclear (Fraczek et al., 2013; Fraczek et al., 2012). Taken together, these results highlight the importance of epigenetic regulation in the dedifferentiation process; however, the consequences of these changes and the mechanisms which underlie them remain unclear and require further investigation.

Energy production is another fundamental cellular process affected by dedifferentiation that is highlighted by this study. The proteomic and functional data suggest a dramatic remodelling of the bio-energetic proteome during monolayer culture. These changes lead to a reduction in many mitochondrial-associated proteins, particularly those involved in lipid and fatty acid metabolism. Previous work has implicated AMPK signalling and mitochondrial fusion as part of the adaptation and repolarization of hepatocytes in

sandwich culture following isolation (Fu et al., 2013). Here we have additionally shown both AMPK and mitochondrial fusion pathways to be associated with the bio-energetic adaption to a monolayer culture system. Furthermore, given the remarkable stability of oxidative phosphorylation following plating, during a period of substantial phenotypic change, it appears that these essential processes are preferentially maintained, potentially at the expense of non-survival-essential proteins/functions. One possible driving factor of these findings is the MEK/ERK pathway, which is highlighted by this and other studies (Zellmer et al., 2010) as a factor in dedifferentiation and has previously been shown to reduce rotenone toxicity in neuronal cells (Jiang et al., 2006) and alter both mitochondrial function (Ripple et al., 2013) and lipid/fatty acid metabolism (Yousefi et al., 2012).

Our analysis revealed that the early stages of dedifferentiation are predominantly donor-dependent with the inter-individual variation that exists in the starting donor phenotype being maintained throughout the first 72 hours of culture. Hepatocytes are known to vary between donors (due to both genotypic and environmental factors) (Bhogal et al., 2011) and in function depending on their location/zone in the lobule porto-central axis (Allen et al., 2005); both of these factors also appear to influence the dedifferentiation profile during culture. Similarity to the isolated donor phenotype dissipates with time in culture in all cases, and a convergence towards a reproducible dedifferentiated phenotype was observed. Taken together, these data suggest that the strictly-defined culture system promotes a specific protein expression profile and, as a consequence of the variable PHH phenotype at isolation, the proteome changes required to achieve this dedifferentiated phenotype are also variable. This information has profound implications for the use of hepatocytes for early drug discovery and prediction of DILI; the majority of toxicological endpoints are assessed within 72 hours of isolation, thus the variable dedifferentiation of hepatocytes demonstrated in this study is likely to have an impact on attempts to achieve consistent biological assessment of multiple chemical variables (e.g. libraries of new drugs).

Many of the earliest changes in protein expression during dedifferentiation are related to cell survival and the maintenance of homeostatic functions. The up-regulation of stress-induced survival pathways may be considered as a double-edged sword, on the one hand preventing apoptosis/necrosis and allowing cells to survive during culture, whilst on the other, playing an important role in the loss of the hepatic phenotype. Negative regulation of the hepatic phenotype has been reported to be true for the MEK/ERK and NFκB pathways (Elaut et al., 2006; Fraczek et al., 2013), and are predicted to be up-regulated by this study. Additionally, the most significantly predicted up-regulated factor at 168 hours was heat shock factor 2 (HSF2). Overexpression studies have shown HSF2 to inhibit erythroid differentiation, but to our knowledge, HSF2 has not previously been linked to the hepatic differentiation status (Leppä et al., 1997). Such results emphasise the apparent trade-off between cell survival and a mature hepatic phenotype in traditional *in vitro* systems. Therefore, reducing cellular stress at all stages of culture, particularly during isolation, may be the most successful method of maintaining *both* cell viability and the hepatic phenotype.

Whilst some of the results yielded in this study may be specific to monolayer culture, the use of a rudimentary culture system has allowed the identification of a wide array of known and novel mechanisms through which dedifferentiation influences hepatic phenotype. We believe this approach enables a holistic understanding of the hepatocyte dedifferentiation process, and the knowledge gained in this study has the potential to enhance complex culture systems towards an improved physiological phenotype.

Chapter 6

The role of Nrf2 in the differentiation and dedifferentiation of human hepatocytes

6.1 Introduction

Current culture systems for primary human hepatocyte (PHH) and hepatocyte-like cells (HLCs) are unable to fully support the hepatic phenotype. In order to improve *in vitro* hepatic models, various different strategies have been attempted. These have included our attempts presented in chapters 4 and 5, small compound screens, spheroid cultures and the use of multiple cell types in co-culture systems (Li et al., 2014; Trask et al., 2014; Shan et al., 2013; Tostoes et al., 2012; Gieseck III et al., 2014), which have resulted in improved, but not freshly isolated PHH-comparable, phenotypes. It is therefore clear that more work is needed to further understand the roadblocks which result in an inability to maintain or acquire the hepatic phenotype *in vitro*.

One potential area for investigation is the role of nuclear factor erythroid 2-related factor 2 (Nrf2). Nrf2 is a transcription factor and key exponent of the cellular response to oxidative stress (Bryan et al., 2013). Under basal conditions, Nrf2 is bound by the cysteine rich Kelch-Like ECH-Associated Protein 1 (Keap1), which targets Nrf2 for ubiquitination and subsequent degradation (Itoh et al., 2003). During oxidative stress, Keap1 is altered and can no longer bind to Nrf2, allowing translocation to the nucleus and binding to the antioxidant response element (ARE) located in the promoter regions of the genes controlled by Nrf2 (Bryan et al., 2013).

The Nrf2 transcription factor's role in responding to oxidative stress is well described; however, it has also been shown to have a direct role in the differentiation of certain cell types. For example, the fate determination of haematopoietic cells has been shown to be dependent on the Nrf2/Keap1 complex (Murakami et al., 2014). Nrf2 has also been implicated in the differentiation of cell types such as osteoclasts and adipocytes (Chartoumpekis et al., 2011; Kanzaki et al., 2013).

With regard to the liver, the Notch-Nrf2 axis has been shown to be important in murine liver development, more specifically in driving a cholangiogenic lineage specification following Notch stimulation (Wakabayashi et al., 2013). Furthermore, Nrf2 may also influence the maintenance of the hepatic phenotype. Overexpression of Nrf2 in a mouse model reported P15 as a novel target of Nrf2 (Kohler et al., 2013). P15 has been previously been shown to prevent hepatocyte proliferation and potentially promote the quiescent mature hepatocyte phenotype *in vivo* (Awad et al., 2000).

Reactive oxygen species (ROS), a key activator of Nrf2, has also been reported to play a role during differentiation towards mesoendodermal lineages (Ji et al., 2010) and also in HLC differentiation from mesenchymal stem cells (Khajeniazi et al., 2013). However, understanding how essential the maintenance of ROS at specific intra-cellular levels to HLC differentiation has yet to be achieved. For example, CYP2E1, a protein which is often lacking in HLC cultures, is known to be down-regulated in the presence of oxidative stress (Morel et al., 2000). It is thought that ROS may also act as a signalling intermediate; thus, a mechanism which can control that, i.e. the Nrf2 antioxidant response pathway, may provide an interesting point for perturbation as an indirect mediator of differentiation maturity.

Nrf2 may also interact with important nuclear receptors associated with hepatic function, such as peroxisome proliferator-activated receptor alpha (PPARα). Studies have shown an Nrf2-dependent altered lipid metabolism and a decrease in fatty acid mobilisation in adipose tissue mediated through PPARα signalling cascades, perhaps suggesting a degree of upstream regulation (Xu et al., 2013a).

Within this chapter, we report the use of clustered regularly interspaced short palindromic repeats (CRISPR)/Cas9-based manipulation of Nrf2. CRISPR/Cas9 is a relatively new technology and has been the subject of much excitement due to its ease of use and wide-

ranging capacity, allowing for vast libraries of potential guide RNAs (gRNAs) to be developed (Zhou et al., 2014). The system is based on a bacterial protection mechanism against foreign nucleic acids, where the foreign nucleic acid sequence is recognised through previous exposure and 'cut' by the Cas9 nuclease, yielding the DNA sequence inactive (Wiedenheft et al., 2012). Using this biological process, gRNAs can be designed to target specific parts of the genome, aligning the Cas9 nuclease with the sequence of interest, and subsequently inducing a double stranded break (DSB) (Sander and Joung, 2014). The efficiency of DSBs is thought to be relatively high, ranging from 1-50% depending on the delivery method, cell type used and other experimental variables (Sander and Joung, 2014). The DSB is then repaired by non-homologous end-joining (NHEJ), which is highly error prone and results in the insertion of variable length indels, causing frame-shift mutations and consequently loss of gene function. More advanced systems involve the exogenous introduction of donor sequences for homology directed repair (HDR). Using complementary flanking sequences to target the position of the DSB, HDR can introduce point mutations or genes of choice for selection or knock-in purposes (Sander and Joung, 2014).

Taken together, such work supports Nrf2 as a potentially key determinant of hepatic development and maturity. We therefore hypothesised that Nrf2 may influence the hepatic phenotype and that mechanistically evaluating the relationship using systems such as CRISPR/Cas9 may yield important information regarding the role of Nrf2 during hepatocyte differentiation and dedifferentiation.

Hypothesis: Nrf2 regulates the hepatocyte phenotype during differentiation and dedifferentiation

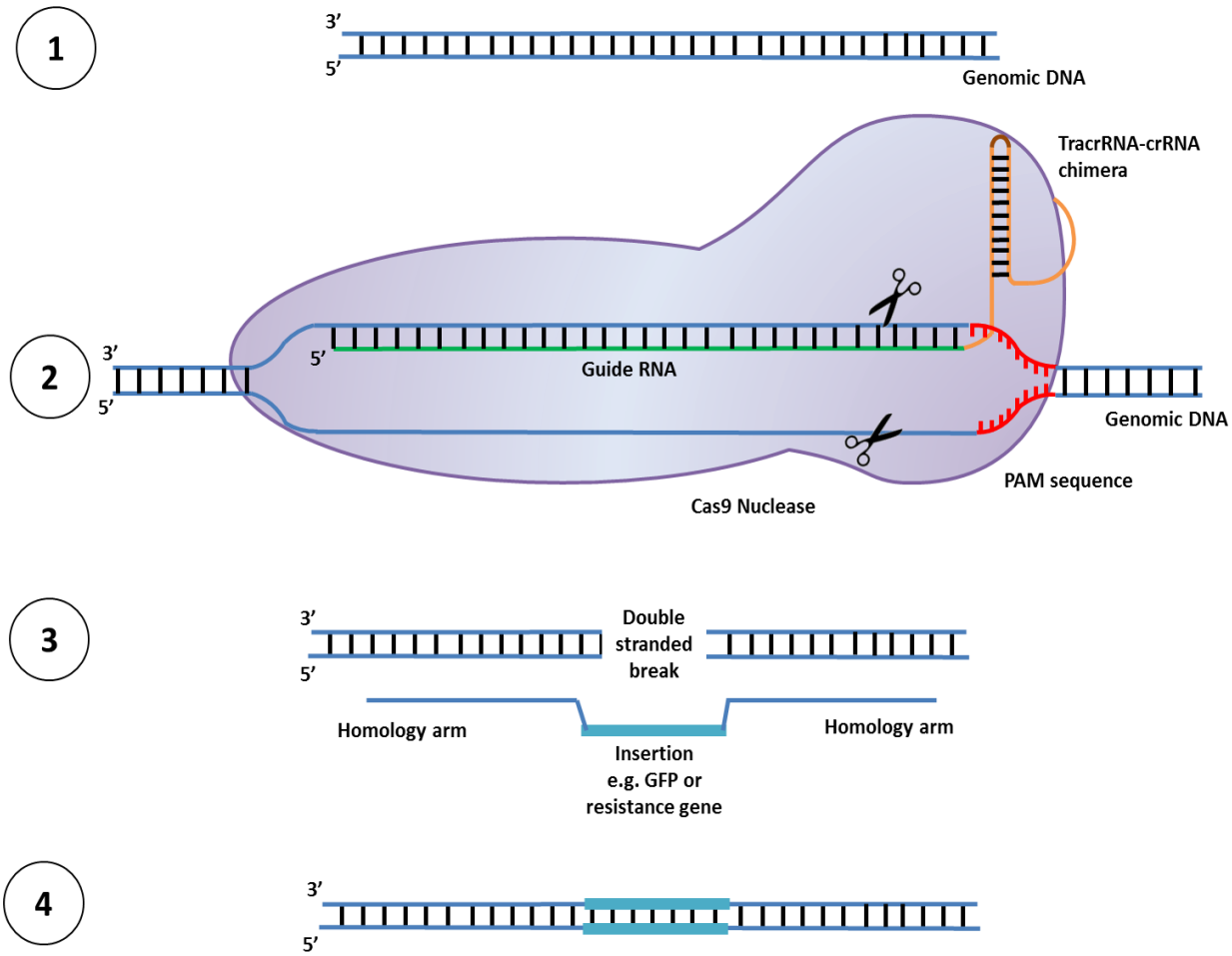

Figure 6.1: Schematic diagram of CRISPR/Cas9 mechanism.

1. The section of genomic DNA is chosen for manipulation and the CRISPR constructs are designed to target this section of DNA. 2. CRISPR/Cas9 constructs target the genomic DNA using guide RNA inserted in the CRISPR backbone (TracrRNA-crRNA). Cas9 nuclease then cuts upstream of a PAM sequence. 3. The cuts result in a double stranded break, which can be repaired by NHEJ or HDR (see text for NHEJ). Homology arms targeting either side of the DSB allow for the insertion of the gene or indel of interest by HDR. 4. Repaired DNA with the inserted gene of interest.

Abbreviations: DSB: Double-stranded break; NHEJ; Non-homologous end-joining; HDR: Homology directed repair; PAM: Protospacer adjacent motif; GFP: Green fluorescent protein

6.2 Results

To investigate if Nrf2 can affect the maintenance and acquisition of the hepatic phenotype, we first established how Nrf2-related proteins changed in expression during the loss of phenotype seen during PHH dedifferentiation.

Using the data generated in chapter 5, the up-/down-regulation of differentially expressed proteins was compared with the previously described Nrf2 relationship, based on published knock-out mice studies (Kitteringham et al., 2010; Walsh et al., 2014) and the ingenuity knowledgebase (table 6.1). The altering expression profile of the differentially expressed proteins suggests, in the main, that Nrf2 is down-regulated during culture.

As Nrf2 was not detected in the proteomic experiment, to test this hypothesis we then investigated the protein expression of Nrf2 during the culture period. Interestingly, given the down-regulation of many related proteins, Nrf2 showed remarkable stability during culture, increasing slightly in some of the donors (figure 6.2a and b). At each timepoint, Nrf2 was found to be inducible following a 2 hour exposure with bardoxolone methyl (CDDO-me), with the degree of induction increasing between 24 and 72/168 hours (figure 6.2b).

Analysis of downstream proteins ectonucleoside triphosphate diphosphohydrolase 5 (ENTPD5) and heme oxygenase (HO-1) further corroborated the findings in table 1, demonstrating down-regulation during culture (figure 6.3). However, NAD(P)H Dehydrogenase, Quinone 1 (NQO1) demonstrated an up-regulation, which was more in-keeping with the pattern seen with Nrf2 protein expression (figure 6.3). Furthermore, in non-dosed conditions, Keap1 protein expression mirrored Nrf2 expression at all timepoints (n=2), as demonstrated by the significant correlation between the two proteins during

culture (figure 6.2c). Interestingly, of the Nrf2-related proteins, only HO-1 appeared to show increased expression when following induction with CDDO-me.

Continuous exposure to CDDO-me through supplementation in the culture media was able to produce an increase in Nrf2 expression over the culture period, without loss of efficacy (figure 6.4). Of note, as with the 2 hour induction, the cells appear to become more inducible during the culture period, increasing in their degree of Nrf2 induction.

Accession no.	Association	Positive/negative Nrf2 regulation	Protein name	Up-/down-regulated at 168 hours	Predicted Nrf2 activation state	P-value
	IPA/KO study	+/-		+/-	+/-	
P04179	IPA	+	Superoxide dismutase [Mn], mitochondrial	+	+	9.95E-08
P11509	IPA	+	Cytochrome P450 2A6	-	-	1.77E-07
Q16836	KO	-	Hydroxyacyl-coenzyme A dehydrogenase, mitochondrial	-	+	9.02E-06
P07099	KO/IPA	+	Epoxide hydrolase 1	-	-	2.46E-05
Q14764	KO	+	Major vault protein	+	+	6.60E-05
Q13451	IPA	+	Peptidyl-prolyl cis-trans isomerase FKBP5	+	+	0.00017
O95831	KO	+	Apoptosis-inducing factor 1, mitochondrial	-	-	0.00018
P04040	IPA/KO	+	Catalase	-	-	0.00019
P63104	KO	+	14-3-3 protein zeta/delta	+	+	0.00026
P14625	IPA	Unknown	Endoplasmin	-	N/A	0.00044
Q00796	KO	+	Sorbitol dehydrogenase	-	-	0.00050
P02679	KO	+	Fibrinogen gamma chain	+	+	0.00128
P21980	KO	-	Protein-glutamine gamma-glutamyltransferase 2	+	-	0.00198
P05177	IPA/KO	+	Cytochrome P450 1A2	-	-	0.00203
P31948	IPA	+	Stress-induced-phosphoprotein 1	+	+	0.00209
P55072	IPA	+	Transitional endoplasmic reticulum ATPase	+	+	0.00212
O00264	KO	+	Membrane-associated progesterone receptor component 1	-	-	0.00237
P43490	KO	+	Nicotinamide phosphoribosyltransferase	+	+	0.00262
P07900	IPA	Unknown	Heat shock protein HSP 90-alpha	+	N/A	0.00307
Q02318	KO	+	Sterol 26-hydroxylase, mitochondrial	-	-	0.00308
Q96I99	KO	+	Succinyl-CoA ligase [GDP-forming] subunit beta, mitochondrial	-	-	0.00333
O14832	KO	+	Phytanoyl-CoA dioxygenase, peroxisomal	-	-	0.00383
P18669	KO	-	Phosphoglycerate mutase 1	+	-	0.00423
P00338	KO	-	L-lactate dehydrogenase A chain	+	-	0.00423
Q9HAV7	KO/IPA	-	GrpE protein homolog 1, mitochondrial	-	+	0.00510
P23141	KO	+	Liver carboxylesterase 1	-	-	0.00532
P06753	KO	-	Tropomyosin alpha-3 chain	+	-	0.00576
P23528	KO	+	Cofilin-1	+	+	0.00577
P30040	IPA	+	Endoplasmic reticulum resident protein 29	-	-	0.00634
O75356	KO/IPA	+	Ectonucleoside triphosphate diphosphohydrolase 5	-	-	0.00690
P09210	IPA	+	Glutathione S-transferase A2	-	-	0.00713
Q9BPW8	KO	+	Protein NipSnap homolog 1	-	-	0.00901
P62826	KO	-	GTP-binding nuclear protein Ran	+	-	0.01000
P14314	KO	+	Glucosidase 2 subunit beta	-	-	0.01011
P48643	KO/IPA	-	T-complex protein 1 subunit epsilon	+	-	0.01242
Q14749	KO	-	Glycine N-methyltransferase	-	+	0.01256
P22760	KO	-	Arylacetamide deacetylase	-	+	0.01369
Q06278	IPA	+	Aldehyde oxidase	-	-	0.01439
P15104	KO	+	Glutamine synthetase	-	-	0.01597
Q96CM8	KO/IPA	+	Acyl-CoA synthetase family member 2, mitochondrial	-	-	0.01626
P11310	KO	-	Medium-chain specific acyl-CoA dehydrogenase, mitochondrial	-	+	0.01648
P80404	KO	+	4-aminobutyrate aminotransferase, mitochondrial	-	-	0.01669
Q15185	KO	-	Prostaglandin E synthase 3	+	-	0.01702
P23284	KO/IPA	+	Peptidyl-prolyl cis-trans isomerase B	-	-	0.01709
Q02252	KO	+	Methylmalonate-semialdehyde dehydrogenase [acylating], mitochondrial	-	-	0.02075
P08263	IPA	+	Glutathione S-transferase A1	-	-	0.02209
O75795	KO	+	UDP-glucuronosyltransferase 2B17	-	-	0.02395
P06737	KO	+	Glycogen phosphorylase, liver form	-	-	0.02462
P05091	KO	+	Aldehyde dehydrogenase, mitochondrial	-	-	0.02824
P36957	KO	-	Dihydrolipoyllysine-residue succinyltransferase component of 2-oxoglutarate dehydrogenase complex, mitochondrial	-	+	0.03211
P22102	KO	+	Trifunctional purine biosynthetic protein adenosine-3	+	+	0.03493

Table 6.1: Nrf2 related differentially expressed proteins during PHH dedifferentiation

Proteins cross-referenced from chapter 5 differentially expressed proteins at 168 hours against Nrf2 knockout studies and IPA knowledgebase for known Nrf2 interactions (Walsh et al., 2014; Kitteringham et al., 2010). The predicted activation state of Nrf2 was then ascertained given the expression of the protein during dedifferentiation.

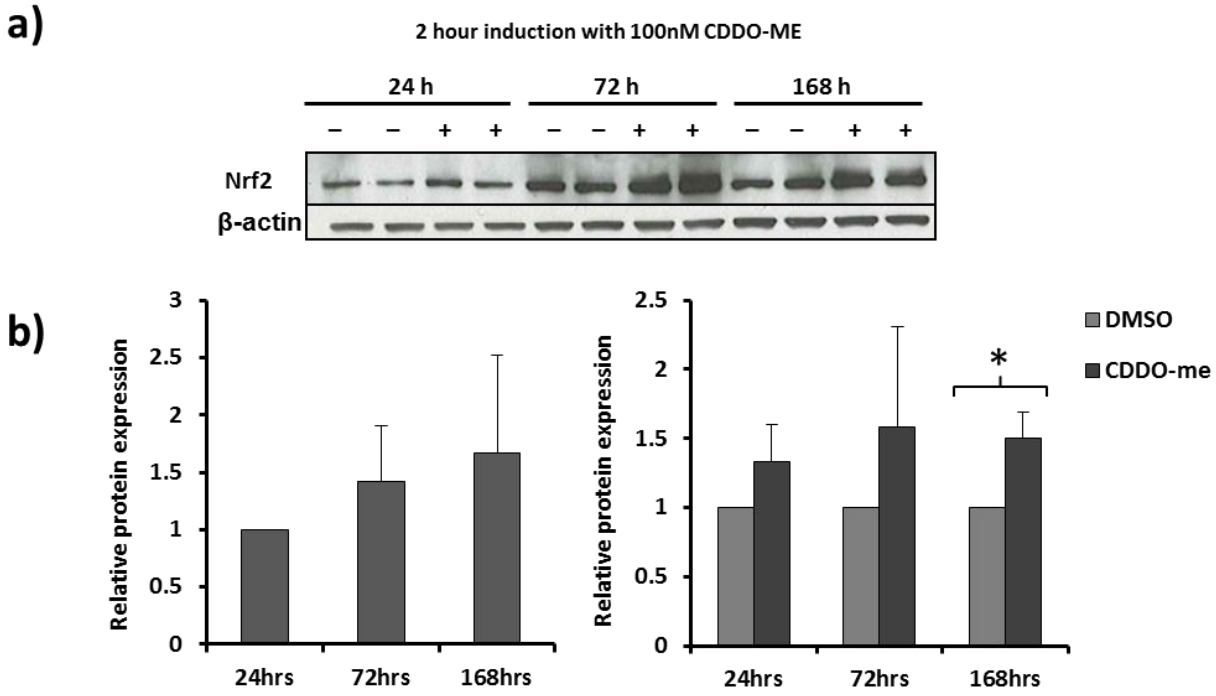

Figure 6.2: PHH Nrf2 expression and inducibility increases during culture

a) Western blot of Nrf2 expression in PHH during 168 hour culture (+) with and (-) without a 2 hour induction with 100nM CDDO-me (-) or 0.5% (v/v) DMSO as a vehicle control. **b)** Densitometry of Nrf2 during culture relative to expression at 24 hours and Nrf2 induction relative to the control samples at each timepoint normalised to β-actin; n=3 donors. (*) denotes $p<0.05$ by paired T-test.

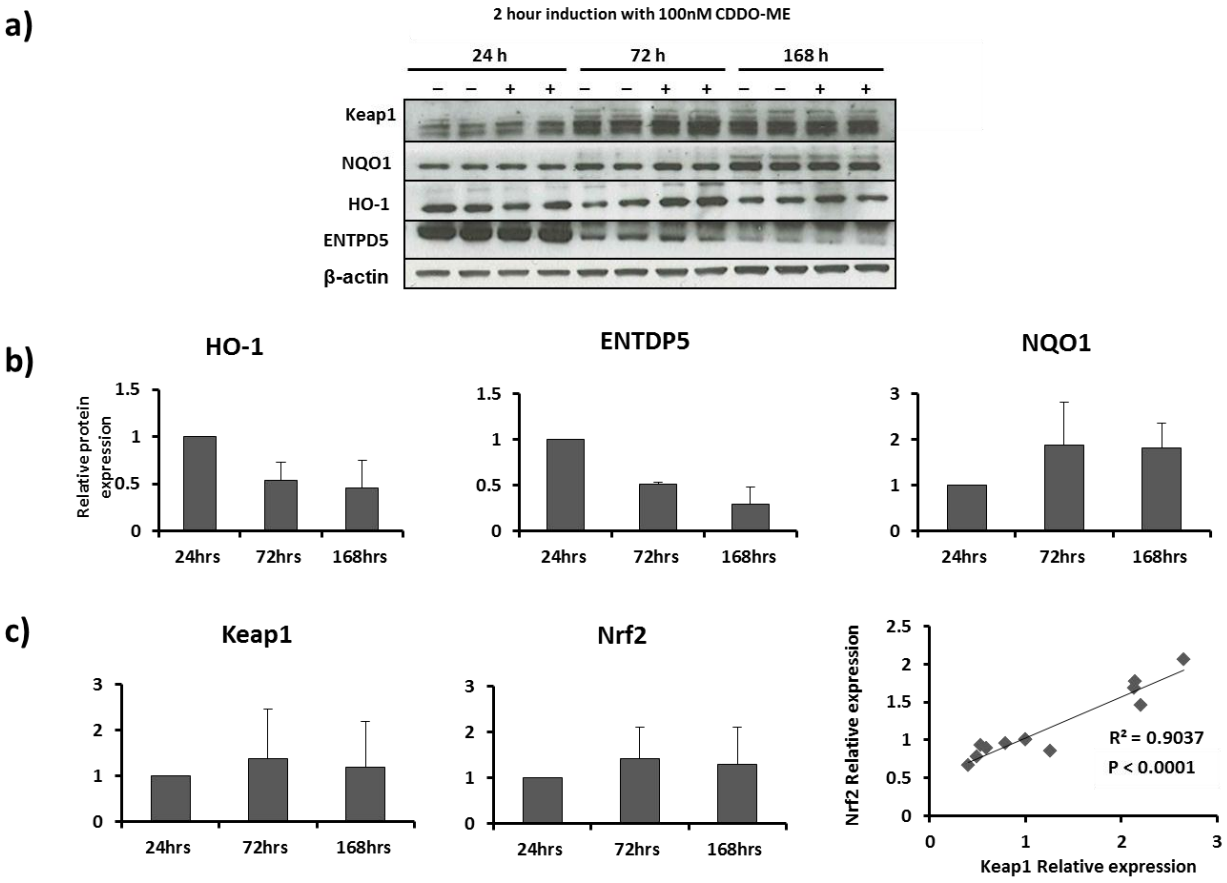

Figure 6.3: PHH Nrf2 up-/downstream proteins show differential expression and inducibility patterns during culture

a) Western blots of Nrf2 up-/downstream protein expression in PHH during 168 hour culture (+) with and (-) without a 2 hour induction with 100nM CDDO-me (-) and 0.5% (v/v) DMSO as a vehicle control. **b)** Protein expression of down-stream targets of Nrf2 during culture, shown relative to the expression at 24 hours; n=2. **c)** Relationship between Nrf2 and key regulator Keap1 and the correlation between these two proteins during culture (n=2 donors). Significance calculated using linear correlation.

Abbreviations: Nrf2: nuclear factor (erythroid-derived 2)-like 2, Keap1: Kelch-Like ECH-Associated Protein 1; NQO1: NAD(P)H Dehydrogenase, Quinone 1; HO-1: Heme oxygenase; ENTPD5: Ectonucleoside Triphosphate Diphosphohydrolase 5.

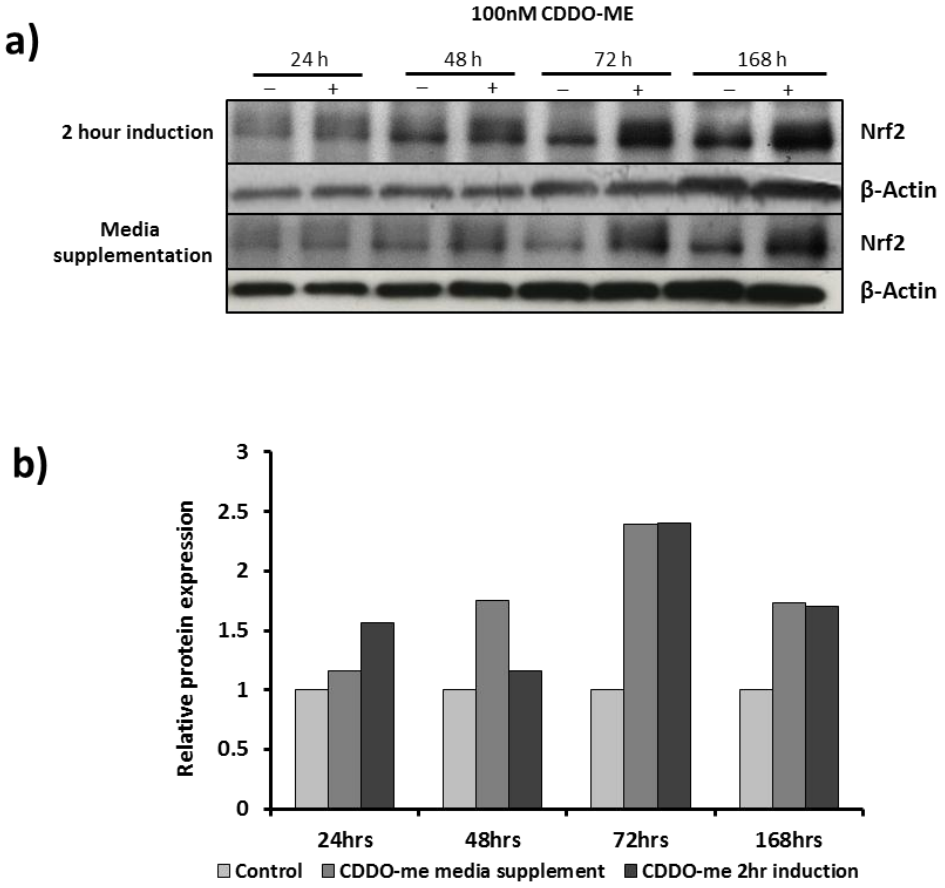

Figure 6.4: Comparison of CDDO-me induction and media supplementation during culture

a) Nrf2 western blots of PHH subjected to acute or chronic exposure through media supplementation of CDDO-me during culture; (-) 0.5% (v/v) DMSO control in induction and normal culture in supplementation, (+) 100nM CDDO-me. **b)** Densitometry comparison of induction and supplementation relative to their respective controls normalised to β-actin; n=1 donor.

Abbreviations: Nrf2: nuclear factor (erythroid-derived 2)-like 2

Phenotypic comparison of PHH cultured in the presence of CDDO-me

We next established if the increase in Nrf2 was functionally important using the Nrf2 downstream protein, NQO1. NQO1 followed a similar pattern to Nrf2, demonstrating increasing expression during the culture period in response to CDDO-me (Figure 6.5). The results suggest a cumulative effect over the culture period, with the 168 hour CDDO-me supplemented PHH demonstrating significantly greater NQO1 expression than both the non-dosed 168 hour time-matched control and the dosed cultures at the earlier timepoints. This was despite Nrf2 showing little difference in induction between 72 and 168 hours (figure 6.2).

We then investigated the effect of Nrf2 induction on specific aspects of cell phenotype which are not directly related to Nrf2 induction. CYP3A4 is a key metabolic enzyme which is perturbed during dedifferentiation (chapter 5) and, to the best of our knowledge, has no known relationship to Nrf2 expression. Across 3 donors we found that CYP3A4 was negatively regulated by the supplementation with CDDO-me; however, this degree of down-regulation varied between donors and was only found to be significantly differentially expressed at 48 hours ($p<0.05$; figure 6.5).

Albumin secretion is a well-established marker of hepatic phenotype and is often used to screen newly established culture conditions. Our results suggested that, across 4 donors, albumin secretion was not altered by Nrf2 induction over the period of culture (Figure 6.5d).

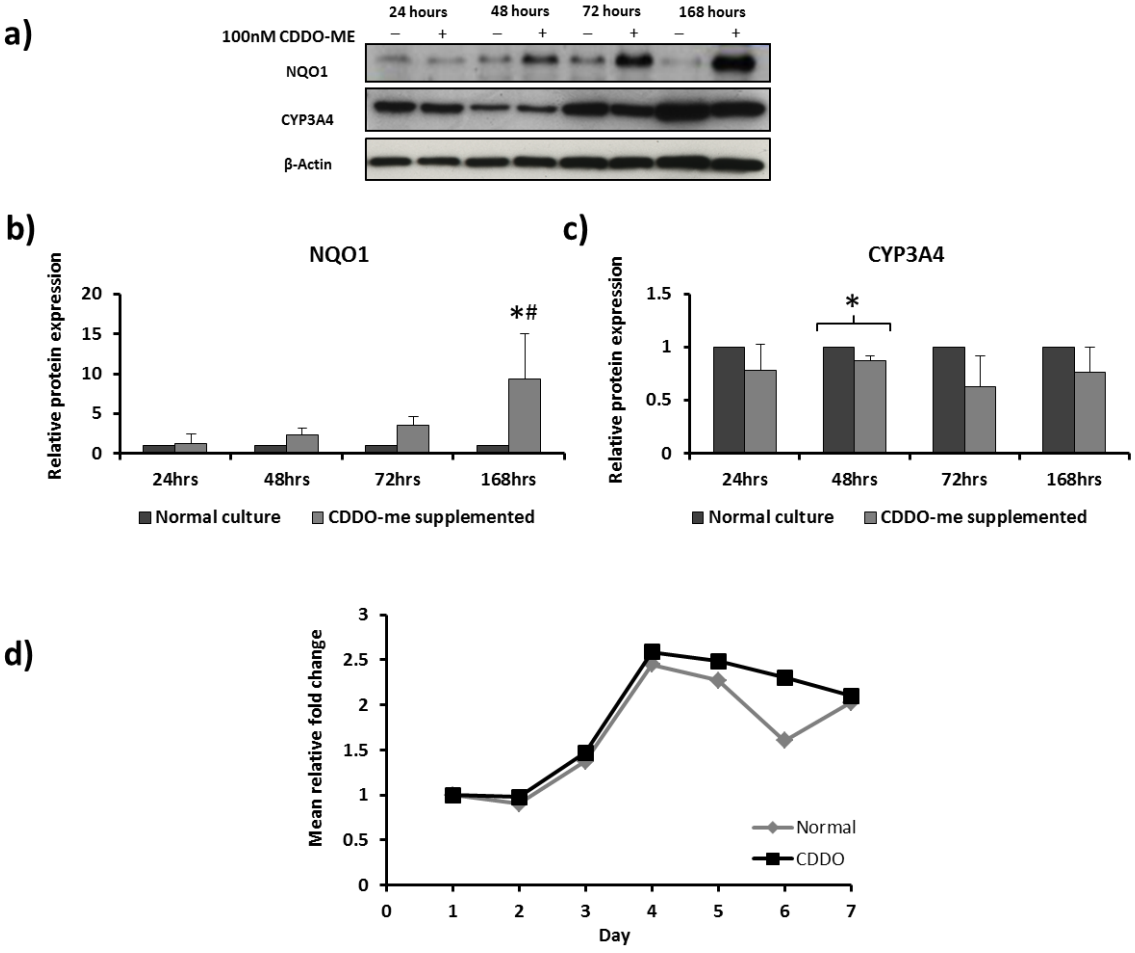

Figure 6.5: Effect of CDDO-me media supplementation on the hepatic phenotype

a) Western blots of NQO1, CYP3A4 and β-actin during culture with and without CDDO-me supplementation. Combined densitometry of **b)** NQO1 and **c)** CYP3A4 during culture with and without supplementation of CDDO-me; n=3 donors. (*) denotes $p<0.05$ by paired T-test vs time-matched control; (#) denotes $p<0.05$ by one-way ANOVA compared to other CDDO-me treated timepoints. **d)** Comparison of normal and CDDO-me supplemented culture albumin secretion detected by ELISA and shown as a relative fold change to the values at 24 hours; n=4 donors.

Abbreviations: Nrf2: nuclear factor (erythroid-derived 2)-like 2; NQO1: NAD(P)H Dehydrogenase, Quinone 1.

Nrf2 during hepatocyte-like cell differentiation

As Nrf2 has known roles in cell differentiation and appears to have a negative impact on the hepatic phenotype, we investigated the role of Nrf2 during pluripotent stem cell differentiation towards hepatocyte-like cells. We first compared the protein levels of Nrf2 in both embryonic (ESC) and induced pluripotent stem cells (iPSCs) with their corresponding HLCs. We found that in all cases the level of Nrf2 protein expression increased from stem cell to HLC to levels which were greater than in freshly isolated PHH (Figure 6.6a-d).

We also investigated the gene expression of Nrf2 to understand how the levels of Nrf2 may be changing during the differentiation period. Our results suggested an initial decrease in Nrf2 gene expression compared to iPSCs at the definitive endoderm stage; however, this preceded a slight increase at the hepatic endoderm stage, followed by a larger 3-fold increase in Nrf2 gene expression at the HLC stage of differentiation (Figure 6.6e).

The functional consequence of the increase in Nrf2 expression was then assessed. NQO1 expression was found to be increase during HLC differentiation in a similar pattern to Nrf2 protein expression, with slight increases in NQO1 protein expression occurring from iPSC to hepatic endoderm stages, followed by a much larger increase between the hepatic endoderm and hepatocyte-like cell stages (figure 6.7).

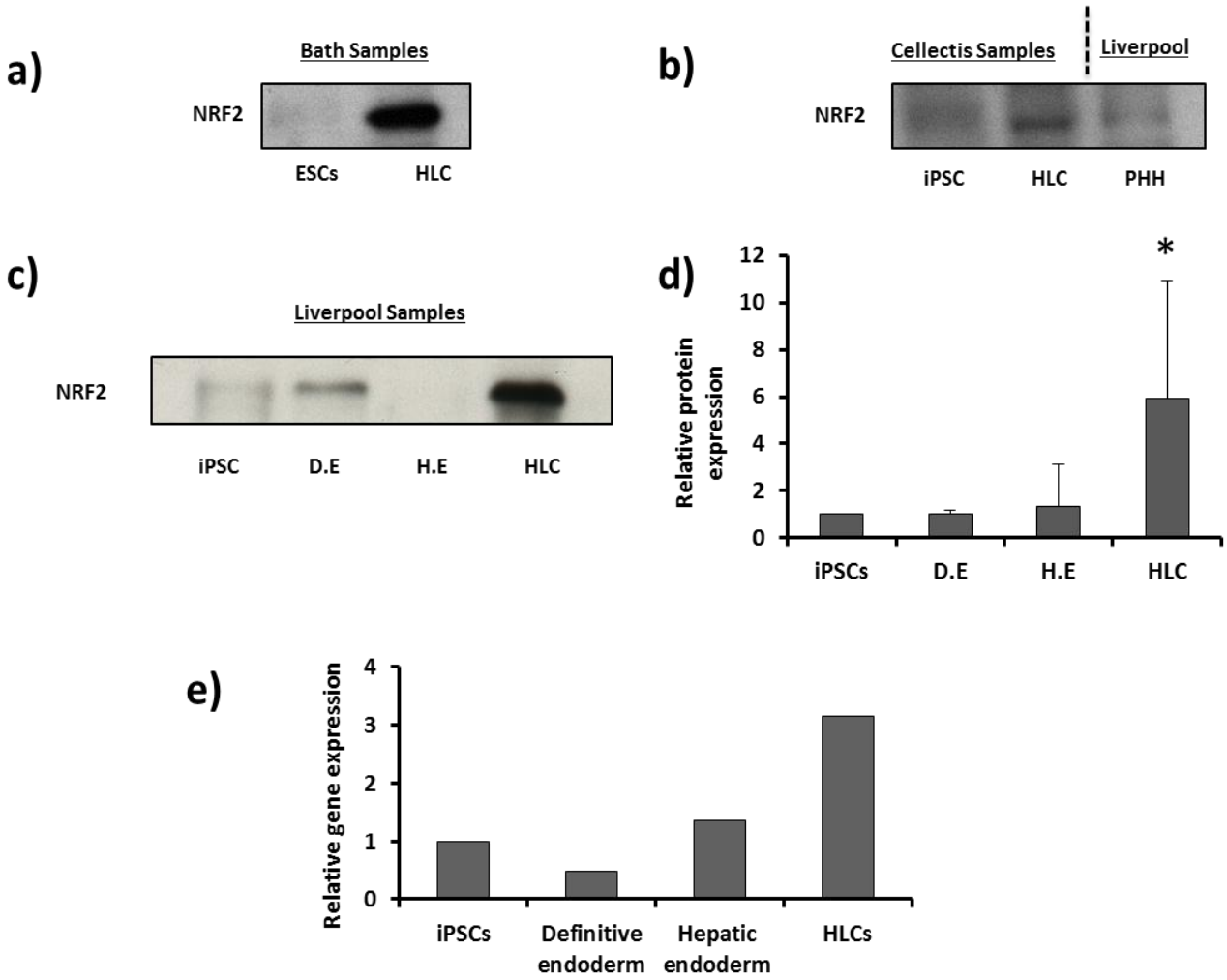

Figure 6.6: Nrf2 protein and gene expression increases during HLC differentiation

a-c) Nrf2 western blots of **a)** Bath ESCs and HLCs **b)** Cellectis iPSCs and HLCs **c)** Liverpool iPSCs, definitive endoderm, hepatic endoderm and HLCs. **d)** Combined densitometry of the protein expression of Nrf2 during differentiation; n=5 iPSC lines; n=5 iPSC lines. (*) denotes $p<0.05$ by one-way ANOVA. **e)** qRT-PCR analysis of Nrf2 during HLC differentiation. $2^{-\Delta\Delta CT}$ displayed as relative fold change to iPSCs normalised to GAPDH; n=2 wells of a single differentiation experiment.

Abbreviations: Nrf2: nuclear factor (erythroid-derived 2)-like 2

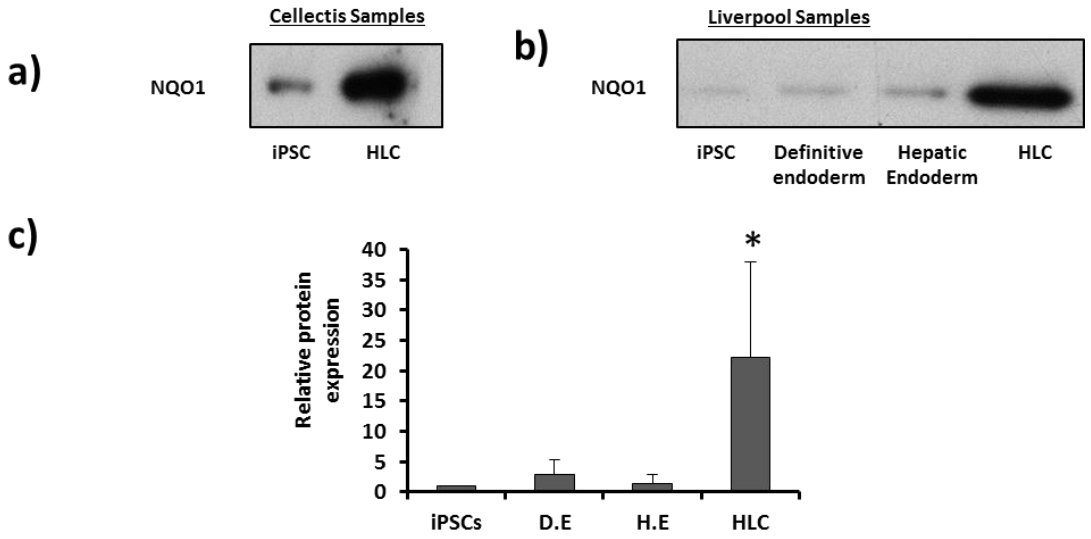

Figure 6.7: NQO1 protein expression increases during HLC differentiation

a) and **b)** NQO1 western blots of **a)** Cellectis iPSCs and HLCs **b)** Liverpool iPSC, definitive endoderm, hepatic endoderm and HLCs. **c)** Combined densitometry of NQO1 during HLC differentiation; n=3 iPSC lines. (*) denotes $p<0.05$ by one-way ANOVA

Abbreviations: NQO1: NAD(P)H Dehydrogenase, Quinone 1;

Manipulating Nrf2 during HLC differentiation with siRNA

As our results with primary hepatocytes suggest that Nrf2 negatively regulates key aspects of hepatic phenotype, and that current HLC differentiation protocols do not achieve a mature hepatic phenotype, we hypothesised that knock-down of Nrf2 during the final stage of differentiation may positively impact the phenotypic maturity of HLCs.

Therefore, we attempted to alter Nrf2 expression using siRNA-based knockdown during the final stage of differentiation. We first investigated how effective the knockdown method was using hepatic endoderm-stage cells and various transfection methods. Our results suggested that knockdown was achievable with all techniques, with a reverse transfection method demonstrating the greatest knockdown in protein expression (Figure 6.8a and b).

As the final period of differentiation is 12 days and the reverse transfection techniques requires re-plating of the cells, we decided to use a protocol which incorporated multiple

forward transfections of siRNA during the culture period (Figure 6.8c). We compared the effects of 2x and 3x transfections of Nrf2 siRNA during the final stage of differentiation; however, when the Nrf2 protein expression was investigated, no knockdown was evident (Figure 6.8d and e).

Furthermore, the gene expression data showed little difference compared to vehicle and non-transfected control differentiations (Figure 6.8f). It was therefore decided that siRNA-based knockdown during differentiation was not an effective method of investigating the role of Nrf2, due to a lack of maintainable efficacy during the differentiation protocol.

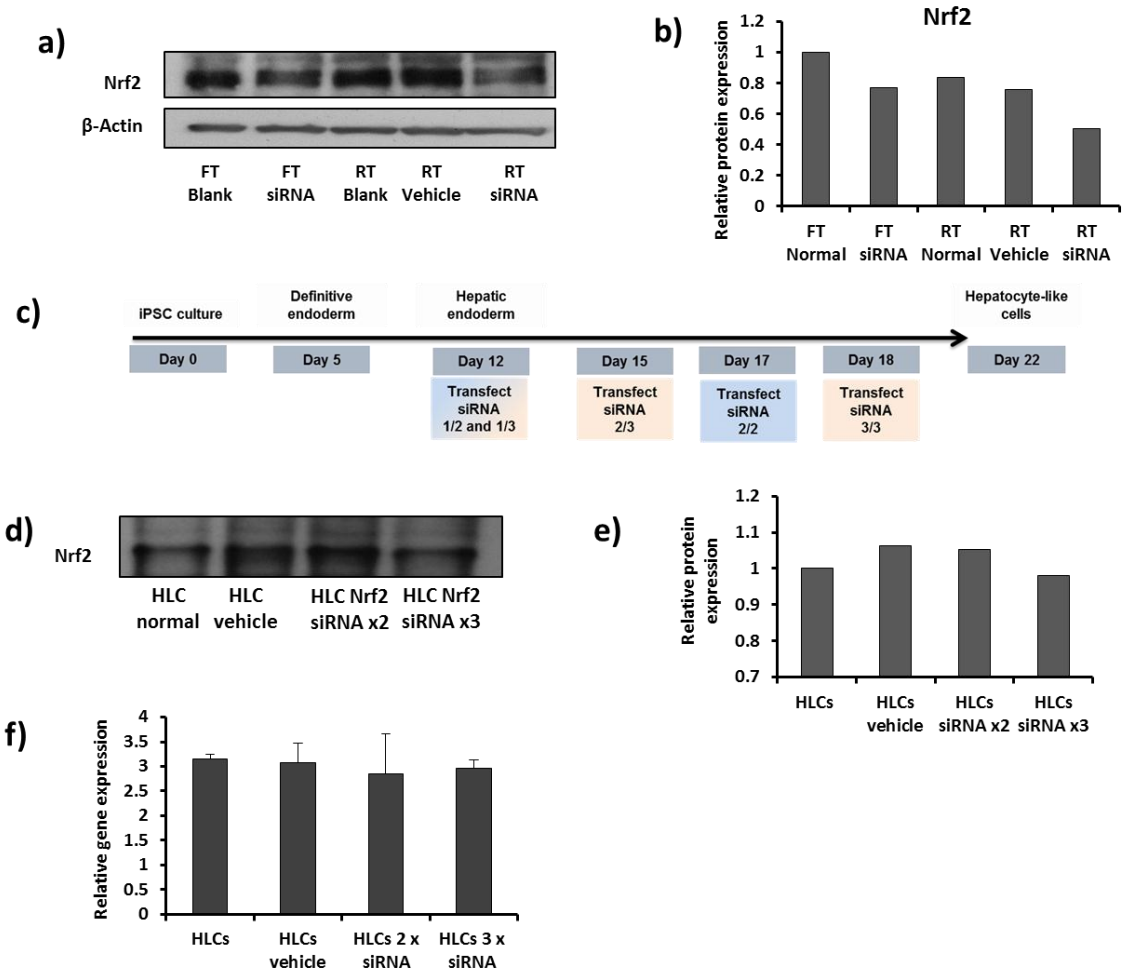

Figure 6.8: Manipulation of Nrf2 with siRNA during HLC differentiation.

a) Western blot and **b)** densitometry of Nrf2 protein expression normalised to β-actin following FT: forward transfection and RT: reverse transfection of siRNA targeted to Nrf2 against non-transfected and vehicle controls; n=1. **c)** Schematic diagram of the protocol used for multiple Nrf2 siRNA transfections during HLC differentiation. **d)** Western blot and **e)** densitometry of Nrf2 at the final stage of differentiation following multiple (2x or 3x) transfections of Nrf2 siRNA with controls; n=1 differentiation experiment; β-actin western blot failed and therefore equal protein loading was confirmed by ponceau red stain (data not shown) **f)** qRT-PCR of Nrf2 at the final stage of differentiation following multiple (2x or 3x) transfections of Nrf2 siRNA with no transfected and vehicle controls. $2^{-\Delta\Delta}$CT displayed as relative fold change to iPSCs normalised to GAPDH; n=2 wells of a single differentiation experiment. Error bars: SEM.

Abbreviations: Nrf2: nuclear factor (erythroid-derived 2)-like 2

CRISPR/Cas9 knockdown of Nrf2 in A549s

To take the investigation forward, we therefore decided to attempt a CRISPR/Cas9-based method of manipulating the iPSCs to knockdown Nrf2. To achieve this, we used a commercially available kit from Santa Cruz. As this was a new system, not previously used in the laboratory, we first attempted the technique using the lung carcinoma cell line A549. A549s have a mutated Keap1 gene which prevents binding to Nrf2 and targeting for degradation; consequently, these cells have very high basal Nrf2 protein expression (Singh et al., 2006).

We established the concentrations of the selection gene, puromycin, to use in the selection of the knockout cells. In-keeping with previous literature (Zhu et al., 2007), A549s were found to be susceptible to 1.5μg/ml puromycin (data not shown). We then optimised the transfection using a non-coding CRISPR/Cas9 control plasmid with green fluorescent protein (GFP) tag. Using fluorescence microscopy, it was found that a good transfection efficiency was achievable using the manufacturer suggested conditions (figure 6.9a).

Using these conditions, we transfected 3 x CRISPR/Cas9 plasmids targeted to different points in the exon regions of the Nrf2 gene and a HDR plasmid containing the puromycin selection gene. Transfections of both conditions were confirmed with fluorescence microscopy (CRISPR/Cas9 plasmid: GFP; HDR plasmid: RFP (red); figure 6.9b and c). The transfected cells were then selected by puromycin and individual colonies picked and expanded. We were also able to generate puromycin-resistant cells at much lower efficiency in the HDR-only control well, most likely through random integration of the HDR plasmid into the cell genome; these cells were used as an additional control in subsequent assays.

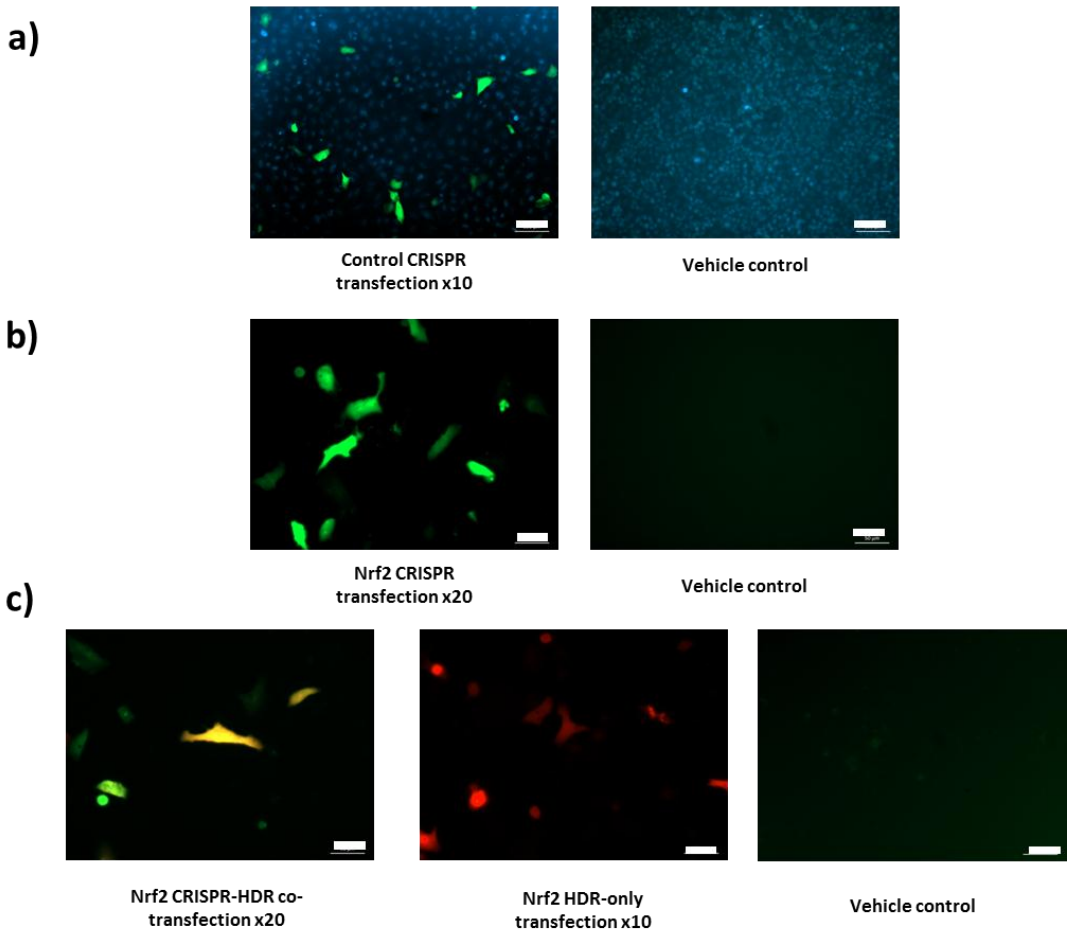

Figure 6.9: Transfection of A549 with CRISPR and HDR plasmids

a) Optimisation of control CRISPR plasmid transfection using fluorescence microscopy. Magnification x100, scale bar: 100µm. **b)** Transfection of A549s with NRF2 CRISPR/Cas9 plasmids (GFP) alone using fluorescence microscopy. Magnification x200, scale bar: 50µm **c)** Combined transfection of Nrf2 CRISPR-Cas9 (GFP) and HDR plasmids (RFP) confirmed by fluorescence microscopy. Magnification x200, scale bar: 50µm.

Analysis of A549s transfected with CRISPR/Cas9 plasmids.

Analysis of the selected A549 selected clones showed mixed results (Figure 6.10). For example, KO4 and KO7 demonstrated an increase in expression of Nrf2 compared to wild-type A549s; whereas KO1 showed a reduction, although no clone showed complete knockout at the protein level. All knockout lines showed lower Nrf2 protein expression than the HDR-only control, which was included as a better representative control of the selection culture conditions.

To test if this change in Nrf2 expression had functional consequences, we also investigated the protein expression of NQO1 (Figure 6.10). All clones which received the CRISPR/Cas9 plasmid showed reduced in NQO1 expression, the degree of which varied between clones. Therefore, despite Nrf2 protein expression remaining, its functional capacity appears to have been reduced.

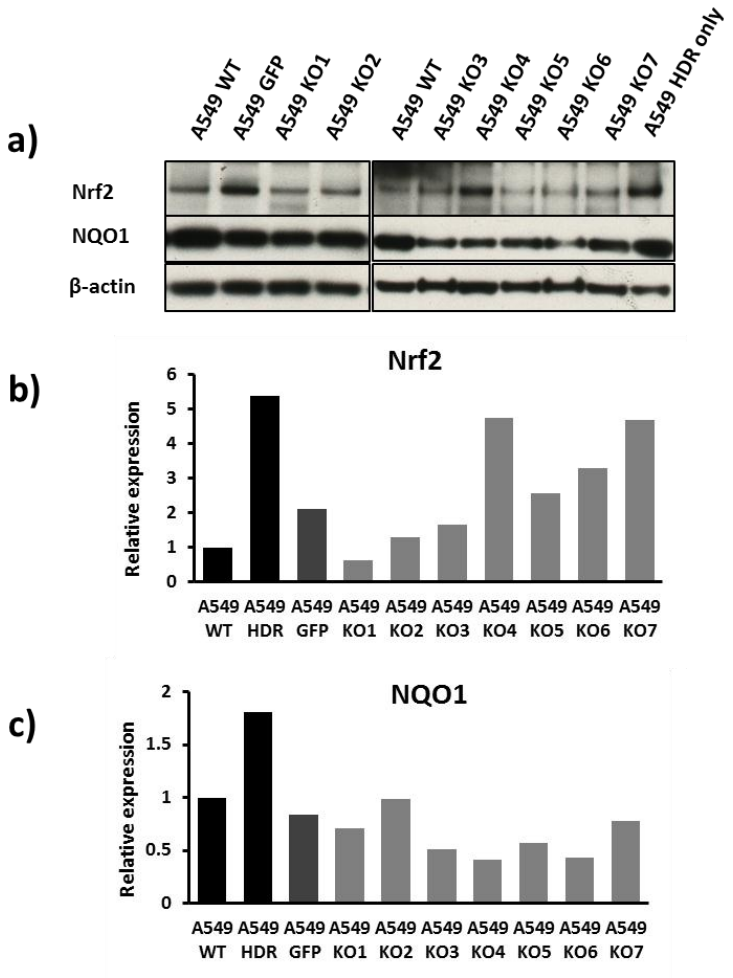

Figure 6.10: Nrf2 and NQO1 protein expression in A549s following CRISPR/Cas9 transfection and isolation

a) Western blots for Nrf2, NQO1 and β-actin in A549 wild type (WT), HDR-only and knock out lines. **b)** and **c)** densitometry for NRF2 and NQO1 western blots. Results normalised to β-actin and shown relative to A549 WT. Each clone: n=1.

Abbreviations: Nrf2: nuclear factor (erythroid-derived 2)-like 2; NQO1: NAD(P)H Dehydrogenase, Quinone 1.

Optimising CRISPR/Cas9 knockdown in iPSCs

The transfection of pluripotent stem cells is known to be difficult (Villa-Diaz et al., 2010). Therefore, further optimisation of the transfection technique was required before CRSIPR/Cas9 could be attempted.

Several conditions were investigated based on a recent paper which describes methods for enhancing plasmid transfection of ESCs (Villa-Diaz et al., 2010). These conditions were: forward transfection, reverse transfection, modified reverse transfection (transfection complexes plated with Matrigel) and 1% DMSO. Our results demonstrated no GFP+ve cells in the various conditions analysed (Figure 6.11a).

We therefore attempted a different transfection reagent, Lipofectamine 3000. We found that this technique allowed for the transfection of the control plasmid, albeit at low efficiency (Figure 6.11b). No difference in efficiency was found across the various conditions, although reverse transfection was noted to cause greater toxicity. Therefore, forward transfection using Lipofectamine 3000 was taken forward for transfection of the Nrf2 CRISPR/Cas9 plasmids.

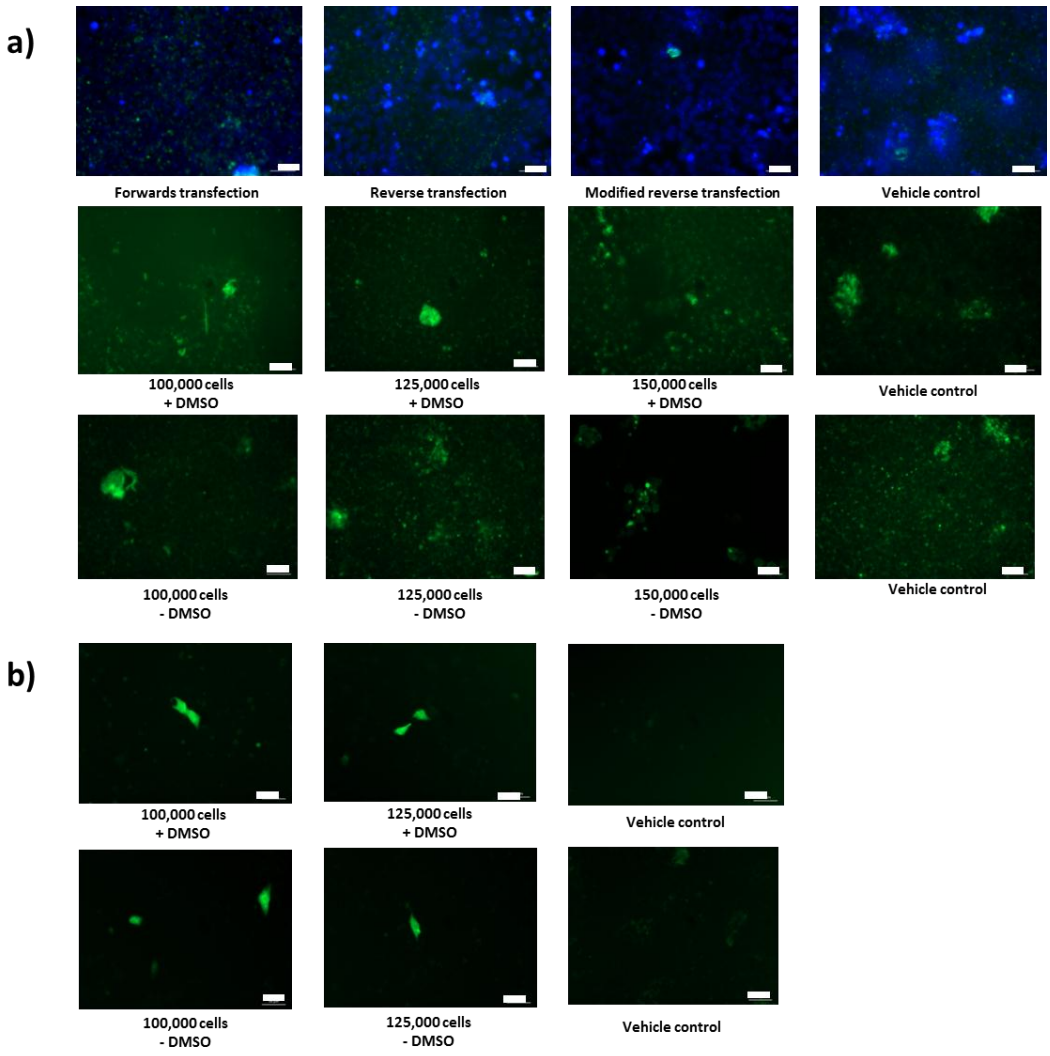

Figure 6.11: Transfection of iPSCs with non-coding CRISPR plasmid using different transfection reagents.

a) UltraCruz and **b)** Lipofectamine 3000. Various transfection techniques, cell density and with or without 1% DMSO investigated by fluorescence microscopy for uptake of GFP containing non-coding CRISPR/Cas9 control plasmid (GFP). Magnification x200, scale bar: 50µm

CRISPR/Cas9 knockdown of Nrf2 in iPSCs

Using the optimised conditions, we then attempted to derive a Nrf2 knockout iPSC line using the CRISPR/Cas9-HDR system. Figure 6.12a demonstrates successful transfection of the CRISPR/Cas9 and HDR plasmids into the iPSCs using fluorescence microscopy. The efficiency was noted to be low, but this was in-keeping with the optimisation results presented in figure 6.11. A small degree of cell death was noted between pre- and post-transduction (figure 6.12b); however, this was not greater than the cell death observed in the vehicle control.

Following puromycin selection (0.5mg/ml), large-scale cell death was noted throughout the cultures with very few cells remaining. After extended culture, one clone was noted at day 18 post-transfection (Figure 6.12c). This was subsequently tracked over 7 days to ascertain its growth and morphological characteristics. Our results showed little-to-no growth of the colony during this period.

Furthermore, live staining analysis of cell surface markers at day 25 of culture revealed no expression of the iPSC marker Tra-1-60. The immunofluorescence images demonstrate a diffuse signal which lacked the defined staining seen in previously stained Liv1W cells. Subsequent attempts to expand this clone further using manual picking resulted in no attachment or propagation.

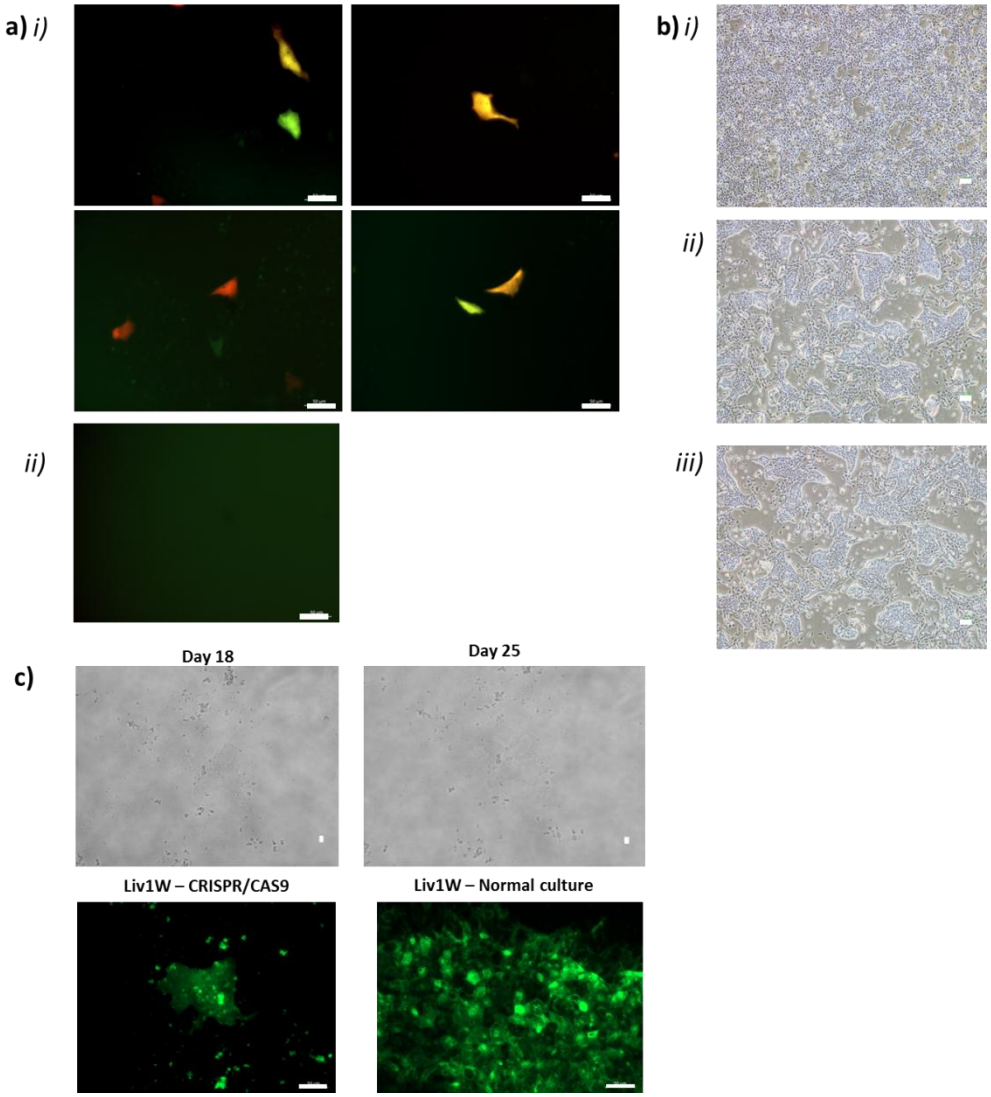

Figure 6.12: Successful transfection of iPSCs with CRISPR/Cas9 and HDR plasmids using optimised conditions did not result in expandable Nrf2 KO clones

a) i) Fluorescence microscopy of CRISPR/Cas9 Nrf2 plasmid (GFP) and HDR plasmid (RFP) in transfected cells. Magnification x200, scale bar: 50µm. **b)** Phase contrast images of i) pre-transfection; ii) 24 hours post-transfection with CRISPR/Cas9 Nrf2 and HDR plasmids; iii) 24 hours post-transfection vehicle control. Magnification x40, scale bar: 100µm. **c)** Morphological and immunofluorescence assessment of CRISPR/Cas9 transfected cells after puromycin selection. IF: Magnification x200, scale bar: 50µm Cells selected with 0.5mg/ml puromycin. Phase contrast images: 200x magnification; scale bar 10µm.

6.3 Discussion

The work presented in this chapter represents an attempt to better understand the role of Nrf2 in hepatocyte differentiation and dedifferentiation.

Our initial hypothesis was based on the hepatocyte dedifferentiation work reported in chapter 5. Of the differentially expressed proteins at 168 hours, the Nrf2-related proteins suggested that Nrf2 function was inhibited. However, upon investigation of the Nrf2 protein expression, the level was maintained or increased during culture. One known mechanism of Nrf2 regulation is via the protein Keap1 (Itoh et al., 2003). Our results show the protein expression of Keap1 closely mirrors that of Nrf2 during the culture period. This suggests that as Nrf2 increases, so does Keap1 and vice versa in a homeostatic-like response. Moreover, the downstream protein NQO1 continues to rise during culture, suggestive of a cumulative effect of Nrf2 activation. Furthermore, despite little apparent change in the ratio between Nrf2 and Keap1 protein expression levels, some Nrf2-related proteins reduce in expression, whilst others increase, a suggesting a degree of Nrf2 dysregulation during PHH culture. Investigating the nuclear versus cytoplasmic Nrf2 protein expression levels may further elucidate the mechanisms of action contributing to the Nrf2-related protein expression profile described in table 6.1.

One potential factor which could generate a selective Nrf2-related protein profile and is known to be both active during dedifferentiation and interact with Nrf2, is NFκB. The cross-talk between these two factors has been reported in numerous papers (Buelna-Chontal and Zazueta, 2013), which describe how both factors can inhibit the other through various mechanisms. One of these potential mechanisms is through the NFκB-mediated p65-dependent recruitment of HDAC3 to the binding area of Nrf2 (antioxidant response element: ARE), causing hypoacetylation of the ARE in the promoter region and inhibiting Nrf2-dependent expression (Liu et al., 2008a). This would allow for a selective loss of Nrf2-

related proteins which have Nrf2 and NFκB binding sites in close proximity. Further work elucidating these mechanisms may explain the up- and down-regulation of Nrf2-related proteins despite no clear change in Nrf2 protein content.

The reduction of CYP3A4 protein expression following Nrf2 induction with CDDO-me was an intriguing result as, to the best of our knowledge, this interaction has not been previously reported in hepatocytes. It is perhaps unsurprising given the free radicals which are produced by the cytochromes P450 even in the absence of substrate (Zangar et al., 2004). Therefore, as Nrf2 is the master-regulator of the response to oxidative stress, a mechanism to reduce CYP3A4 protein and consequently free radical production is logical. Another potential cause of the loss of CYP3A4 is through Nrf2's relationship with the proteasome (Chapple et al., 2012), as it has previously been shown that proteasome inhibition causes the suppression of CYP3A4 protein expression (Zangar et al., 2003). Further work is required to confirm that this a Nrf2-mediated mechanism, including siRNA targeting Nrf2 and Keap1 to modulate protein expression, with a reduced possibility for the off-target effects associated with pharmacological modulation. One known off-target effect of CDDO-me is as an inhibitor of NFκB (Shishodia et al., 2006); however, NFκB is thought to reduce CYP3A4 expression (Zangar et al., 2008), therefore its inhibition is unlikely to be the cause of reduced CYP3A4 protein expression.

Nrf2's role in hepatic differentiation is of emerging importance. Recent work has pointed towards Nrf2 being a downstream effector of Notch signalling (Wakabayashi et al., 2013), skewing the bipotent decision between hepatocyte and cholangiocyte lineages towards the latter. Therefore, if true, Nrf2 expression in hepatocytes is likely to have a detrimental effect in terms of mature phenotype. Our results suggest that a similar mechanism may be inhibiting the generation of HLCs which are restricted to the hepatic lineage during the final maturation phase (Baxter et al., 2010). Our analysis was conducted across four different

starting pluripotent lines (one ESC and three iPSCs) and three different differentiation protocols from three different laboratories, suggesting that the phenomenon is highly conserved across cell types and protocols. In general, the greatest Nrf2 expression was seen in the HLCs generated from the University of Bath and the lowest in those supplied from Cellectis. The inverse was true in terms of cell morphology and homogeneity, further suggesting that Nrf2 negatively regulates HLC purity and phenotype.

As part of our studies, we attempted to establish whether the observed correlation was a functional relationship; however, we were unable to develop an efficacious method for manipulating Nrf2 expression in iPSCs or during HLC differentiation. This difficulty is likely to be multi-faceted.

For example, across the A549 knockout lines generated, no complete loss of Nrf2 was detected; however, the loss NQO1 expression across all lines suggested that Nrf2 function was disrupted. This may be due to numerous causes. The CRISPR/Cas9 system used was purchased from Santa Cruz and contained three CRISPR plasmids which cut the gene in three separate exon locations and three homology-dependent repair plasmids which inserts the puromycin selection gene into the cut areas. However, due to difficulties in producing the HDR plasmids, only one of the three HDR plasmids were received from Santa Cruz and could therefore be used. This reduced the chances of success in creating a complete knockout clone. When HDR is not used as a repair option, the cell uses a NHEJ repair mechanism which is prone to error and therefore often results in a mutated gene and loss of expression (Maruyama et al., 2015). However, it may also result in a mutated protein which is still produced but has reduced efficacy or is non-functional (Sander and Joung, 2014).

Another potential cause of incomplete Nrf2 knockout in all lines is the known importance of Nrf2 to cancer cell lines proliferation and survival (Lister et al., 2011). Thus, all clones

with complete knockout may have entered apoptosis or been out-grown, resulting in only those clones which had incomplete knockout being both puromycin-resistant and capable of expansion in culture. The lack of complete knockdown may also be caused by heterogeneous population of cells which may be addressed through single cell cloning to derive a homogenous population (Longo et al., 2013). We did not follow this path for two reasons: firstly, the knockdown of Nrf2 often causes a dramatic reduction in cell growth properties and it is therefore likely to be difficult to derive a single cell clone; secondly, the A549 cell line was not to be used to address our hypothesis.

We therefore continued our investigation using the CRISPR/Cas9 in our established iPSC lines. Following the development of a technique allowing for transfection of iPSCs, we attempted to derive an Nrf2 knockout iPSC line. However, we were unable to generate any clones using the puromycin selection technique. This may be due to the combined effect of low transfection efficiency and the single HDR plasmid meaning that no cell received the correct combination of CRISPR/Cas9 and HDR.

Nrf2 has recently been shown to have an important role in maintaining pluripotency in embryonic stem cells (Jang et al., 2014). Therefore, knockdown of Nrf2 may have negative consequences in terms of pluripotent capacity. As pluripotent stem cells are thought to be highly sensitive to cell stress and a disruption of the Nrf2 pathway may lead to apoptosis through enhanced levels of oxidative stress, changes in cell cycle and/or changes to the pluripotent regulatory network (Gonzales et al., 2015; Liu et al., 2013). However, it must be noted the Nrf2 knock out mouse model is non-lethal (Kitteringham et al., 2010). The combined effect of these factors with the low efficiency of transfection makes the generation of Nrf2 knockout iPSCs a particularly difficult prospect. Further work may look into the use of different delivery mechanisms, such as using nucleofection rather than cationic liposome-based methods (Byrne et al., 2015; Chatterjee et al., 2011) or even viral

constructs to enhance delivery efficiency. It has previously been shown that adenovirus delivery of FOXA2 and HNF1α during HLC differentiation can enhance the hepatic phenotype (Takayama et al., 2012); therefore, a similar mechanism of delivering Nrf2 siRNA may prove to be a more successful delivery method. Alternatively, the pharmacological inhibitor brusatol may be used (Olayanju et al., 2015).

Taken together, this chapter has demonstrated novel unreported roles for Nrf2 in both hepatocyte differentiation and dedifferentiation *in vitro*. The importance of Nrf2 to maintaining and acquiring the hepatic phenotype remains to be determined and concerted efforts are being made within our laboratory to ensure a method of mechanistically assessing the role of Nrf2, particularly during HLC differentiation, is achieved.

Chapter 7

General discussion

7.1 Introduction

The research presented in this thesis represents our attempts to better understand and enhance *in vitro* models of hepatotoxicity. The need for this work stems from the inability of current culture systems to adequately support the mature hepatic phenotype, preventing effective screening and triaging of potentially dangerous compounds in drug development pipelines (Godoy et al., 2013). Furthermore, due to a lack of clinical relevance, post-toxicity mechanistic studies investigating how and why DILI occurred are also often not achievable with current hepatotoxicity models. As a consequence, DILI remains a huge burden on healthcare systems around the world and has large financial costs for pharmaceutical companies.

Our work has utilised a combination of innovative techniques and novel insights which should serve to enhance the understanding of hepatic models. We have established a range of reprogramming and differentiation protocols and used these to investigate the potential for utilising the inherent epigenetic memory which is found in iPSCs to improve the differentiation of hepatocyte-like cells (HLCs). We also used a step-back approach to investigate primary human hepatocytes (PHH) dedifferentiation from a proteomic perspective, attempting to understand which factors are driving the dramatic loss of phenotype during culture. This is particularly pertinent as current culture systems cannot maintain a fully mature hepatic phenotype; therefore, attempts to derive stem cell-based hepatic models are likely to fail given the inability of the culture system to support the desired phenotype. A noticeable trend in the PHH dedifferentiation proteomic dataset was the loss of Nrf2-related proteins during culture. Nrf2 is a transcription factor with well-described roles in the response to oxidative stress; however, a growing body of work also suggests roles for Nrf2 during development (Wakabayashi et al., 2013). We aimed to

investigate this in relation to PHH and HLCs through pharmacological and genetic manipulation techniques.

This chapter aims to summarise the work presented hitherto and put the results presented into the context of the field of hepatotoxicity whilst also discussing how the research could be taken forward to further enhance the development of more clinically representative models of hepatotoxicity.

7.2 Implications and future perspectives

7.2.1 Assessing the importance of the starting somatic cell for iPSC generation

Chapters 3 and 4 represent our attempts to develop and optimise reprogramming techniques for different cell types for the subsequent generation of HLCs. Across three donors we found only slight, non-significant, advantages to starting with PHH over human dermal fibroblasts (HDFs). The lack of significant differences between starting cell types points towards the importance of other factors being of similar or greater influence in determining the quality of hepatic differentiation.

The methods developed in chapter 4 and used in chapter 5 to differentiate our iPSCs to HLCs were based on numerous published protocols; however, it should be acknowledged that the protocol used is not as complex as some more recently reported techniques. One such example is a protocol developed by Aspund *et al.,* describing a method which greatly reduces the inter-clone variation in HLC differentiation capacity (Asplund et al., 2015). The use of such a protocol may allow for reduced impact of other factors which influence HLC differentiation and give a clearer understanding of the influence of starting cell type. Furthermore, the use of a 3D culture system, such as spheroid-based models (Takayama et al., 2013; Subramanian et al., 2014), which enhances hepatic phenotype may generate HLCs of greater maturity and further accentuate the small differences seen between the starting cell types in the monolayer system used in this study.

To allow for a full understanding of the differentiation capacity of the iPSCs generated, we attempted to assess the cells at all stages of culture and use a wide-range of assays that go above and beyond previously reported investigations into epigenetic memory and HLCs. Despite this, a fuller understanding of the differences, if any, between the cells may be achieved by incorporating more experimental approaches. These include global

assessments of cell phenotype, e.g. iTRAQ proteomics. An omic-based approach would allow an unbiased investigation of phenotype, rather than the panel-based approach presented in this thesis. Establishing the protein expression and inducibility of CYPs would also be of interest to understanding the pharmacological profile of the cells in basal and induced states. Furthermore, the use of toxicity assays with known hepatotoxins may further allow for functional differences to be ascertained. However, comparison of toxicological phenotypes is perhaps premature given the clear lack of mature pharmacological phenotype in the HLCs generated, making any results using the relatively blunt endpoint of toxicity difficult to interpret.

Notwithstanding the potential of using an improved differentiation protocol or any further differences found in future assessments, any improvement in phenotype must be weighed against the restricted phenotypic range of, and the specialised techniques and infrastructure required to isolate, PHH. Furthermore, the cell-type specific advantage reported previously in hepatocytes and other cell types has been shown to be transient (Lee et al., 2012; Takayama et al., 2014). The epigenetic studies performed in chapter 4 demonstrate this convergence of PHH-derived clones towards HDF-derived clones methylation status as passage number increases. Therefore, taken together, the data presented in these chapters does not provide enough evidence to warrant the use of PHH over HDFs as a starting cell type due the inherent disadvantages of using PHH over HDFs.

Of these disadvantages, phenotypic restriction is perhaps the most pertinent for the use of PHH-derived iPSCs for use in modelling DILI. The comparative ease at which HDFs of peripheral mononuclear blood cells (PBMCs) can be accessed and isolated means that donors of interest can be specifically chosen based on the study requirements (Agu et al., 2015; Aasen and Belmonte, 2010). This opens up the possibility for disease-specific modelling of genetic conditions, which has been shown to be possible in HLCs in the case of

alpha-1-antitrypsin disease (Yusa et al., 2011; Wilson et al., 2015). Moreover, for such conditions, HLCs may also be used for studies of drug efficacy, whilst further studies may wish to look at other genetic traits which will likely influence liver function, such as type I diabetes.

Uniquely, iPSCs also offer the possibility to model idiosyncratic DILI *in vitro* (Krueger et al., 2014). Idiosyncratic DILI is currently beyond the remit of all other non-iPSC *in vitro* models due to the inability to 'choose' the phenotype of the model. Much work is still required to fully realise the potential, but incremental steps are being made in developing such models. For example, recent work by Takayama *et al*., showed that CYP2D6 gene expression in HLCs was dependent on the donor profile (Takayama et al., 2014). CYP2D6 is of particular interest as high frequency polymorphisms within the population result in different rates of metabolism and clearance for drugs using this pathway, such as tamoxifen (Hoskins et al., 2009). This variation was shown in the HLCs with differential toxicity profiles observed in response to tamoxifen (Takayama et al., 2014). Such panel screening methods would be highly informative for drugs which are predicted to interact with proteins with known variation across populations.

Furthermore, despite reports that mitochondrial function is significantly lower than in PHH, (Yu et al., 2012), mitochondrial-based diseases have also been modelled using HLCs (Li et al., 2015). iPSC-derived HLCs generated from patients suffering from Alpers-Huttenlocher syndrome, a disorder caused by mutations in mitochondrial DNA polymerase gamma, showed enhanced susceptibility to valproic acid. This mirrored the hepatotoxicity observed in the clinic. Moreover, the authors were then able to use these cells to establish the cause of the toxicity: the increase occurrence of mitochondrial permeability transition pore opening, and using cyclosporine A, rescue the toxicological phenotype (Li et al., 2015). This study highlights the capacity of iPSC-derived HLCs for generating novel information

regarding existing diseases/disease-specific toxicity susceptibility and developing new strategies to treat these conditions.

Therefore, given the wide-ranging potential of the phenotypic-range associated with iPSCs derived from easily accessible cell types, the reported small and transient phenotypic advantage associated with using of PHH as a starting cell type is not great enough to warrant replacement of HDF and PBMC-derived iPSCs in future studies.

7.2.2 The roadblocks inhibiting the generation of mature hepatocyte-like cells from pluripotent stem cells

The work presented in chapter 4 demonstrated that there was little-to-no enhancement of hepatic phenotype when different starting cell types were used. Therefore, as we have established that current protocols are using the most appropriate starting cell type, it is clear that the development of better differentiation techniques which can produce hepatocyte-like cells with a mature phenotype are required.

Chapter 6 presented our attempts to interrogate the role of Nrf2 during hepatocyte differentiation and dedifferentiation. The results demonstrated a potentially negative relationship between Nrf2 and the hepatic phenotype. This is generally in-keeping with a broader rule that in times of cell stress, the hepatic phenotype, particularly in terms of xenobiotic metabolism, is down-regulated. This is likely to be caused by a combination of the hepatocyte attempting to reduce total cellular stress and focus the cells available resources on cell survival associated functions.

Much work is being focussed on the development of models which better represent the hepatic niche for the final maturation stage of differentiation. However, the initial stages of differentiation remain relatively undeveloped since the first use of Activin A (D'Amour et al., 2005). This is of particular importance given the work by Chen et al., who showed that despite similarities, Nodal- and Activin A-based differentiation to definitive endoderm, both of which are active in normal development, yielded cells with similar but different phenotypes (Chen et al., 2013). The work went on to describe later stage functional differences in endodermal cells ability to form insulin/c-peptide-expressing cells *in vivo*. Of note, it has previously been shown that the Activin A/Nodal signalling pathway can alter chromatin marks of key developmental genes in ESCs (Bertero et al., 2015).

This raises interesting questions in terms of producing HLCs, i.e. how important are the intermediate phenotypes during differentiation? And how do they compare to the *in utero* situation? (Figure 7.1). Most differentiation assays use a panel of markers to confirm the cells are definitive or hepatic endoderm, yet comparing this to the relevant stage of development is particularly difficult. The advent of laser-capture microscopy may allow transcriptomic profile of each developmental stage to be compared with the *in vitro* equivalents. Perhaps more pertinent are the epigenetic changes that occur in the enhancer regions of each gene before expression is turned on. This is true during cellular reprogramming (Papp and Plath, 2013) and similar mechanisms have been shown to influence endodermal differentiation to pancreatic cells (Wang et al., 2015). If the profile of primed genes and enhancer regions differs between *in utero* and *in vitro* conditions, then the inability to produce a fully mature hepatocyte is perhaps unsurprising. Whilst the exact mechanisms have not been delineated, the downstream epigenetic effects have been investigated. Park et al., showed that the promoter regions of CYP1A1, CYP1A2, CYP1B1, CYP2D6, and CYP2E1 were hypermethylated in HLCs but hypomethylated in PHH (Park et al., 2015). This work suggests that the epigenetic profile of the cell has not followed the standard pattern of differentiation, either through a failure to prime these genes for expression at earlier stages of differentiation or an inability to promote a more mature phenotype in current culture conditions.

This hypothesis is given further credence by the recent paper which reported the development of iMPCs (induced multi-potent progenitor cells; somatic cells reprogrammed to an expandable definitive endoderm cell type) (Zhu et al., 2014). As part of this research the authors successfully used a Notch inhibitor to improve differentiation of the iMPCs towards hepatocyte-like cells. However, when Notch inhibition was attempted with iPSC-derived HLCs, no enhancement in phenotype was noted (Zhu et al., 2014). Therefore, the cells which are maintained as endodermal cells have a different inherent response to the

same culture conditions, suggesting different capacity for the cell to react to a developmentally relevant cue. Further work is required to investigate the differences between these cell types at the endodermal stage of differentiation.

The Notch/Wnt axis is well-described in the bi-potent cell-fate decision made during liver development and regeneration (Chapple et al., 2012); however, to the best of our knowledge, manipulating this pathway has not been routinely used to enhance hepatic maturation. The work described in chapter 6 may provide a mechanism to explain the differences between development and *in vitro* differentiation. A proposed down-stream mediator of Notch signalling is Nrf2 (Wakabayashi et al., 2013). The high levels of Nrf2 during the maturation of HLCs from iPSCs suggests either that Notch signalling is highly active in these cells or that cellular stress is high at this late stage of *in vitro* differentiation. As a consequence, Notch/Wnt manipulation may fail to result in an improved phenotype through a failure of upstream pathway manipulation to alter Nrf2 expression levels beyond the required threshold or that the high Nrf2 expression in HLCs is unrelated to the Notch/Wnt axis and is instead due to the cellular stress of *in vitro* differentiation; however, the detrimental downstream effects on phenotype are the same. Manipulation of Nrf2 during differentiation is on-going in our laboratory as we strive to better understand its role in hepatic differentiation.

The use of microbial-derived lithocholic acid and vitamin K2 has recently been shown to enhance the metabolic phenotype of HLCs (Avior et al., 2015). Such work highlights the need to look 'outside of the box' in terms of standard developmental models. For example, during pre- and post-natal development, the immune system is primed against multiple antigens through exposure to environmental or vaccine-derived pathogens (Salzman, 2014; Ygberg and Nilsson, 2012). It may therefore be the case that the metabolic qualities of the liver need to be 'primed' using the relevant substrates; ostensibly, standard maturation

media does not represent the physiological conditions, i.e. the media is both static and does not contain the by-products of ingested material, e.g. substrates such as caffeine or products of the microbiome, such as the aforementioned lithocholic acid (Avior et al., 2015). This hypothesis shares similarities with an idea proposed by Zanger *et al* (Zangar et al., 2004; Zangar et al., 2003), whom suggested a mechanism of selective CYP regulation based on the presence of a substrate for that isoform.

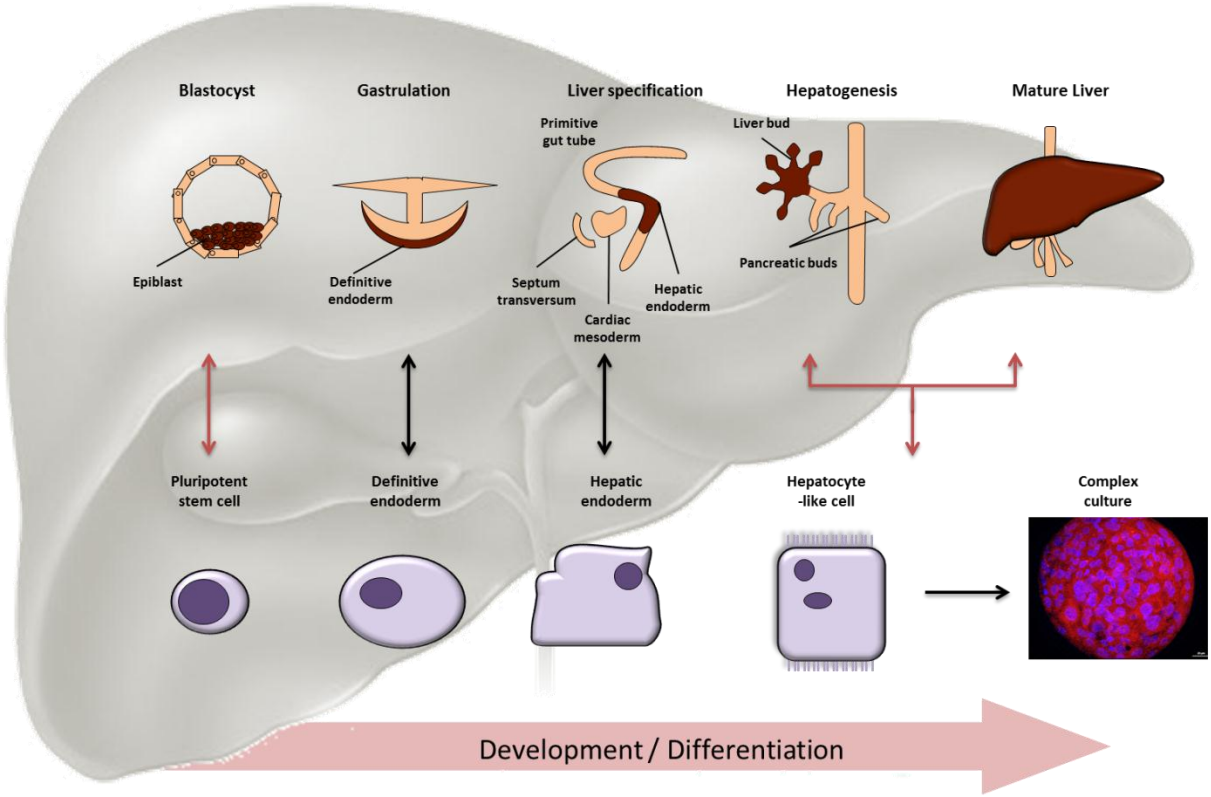

Figure 7.1: Comparison of liver development and *in vitro* differentiation towards the hepatic lineage.

Schematic diagram demonstrating the points of comparison used during the differentiation of HLCs. Orange arrows represent commonly used comparators at the stage of interest; black arrows represent points of comparison which are not currently used and may be used to derive further information. Immunofluorescence image is a PHH spheroid culture stained for albumin (red) and Hoechst 33342 stain (blue). Scale bar 10µm.

7.2.3 Current utilities for hepatocyte-like cells from pluripotent stem cells

As demonstrated by chapters 3 and 4, the lack of a fully mature hepatic phenotype currently precludes the use of HLCs for the investigation of studies which require a high metabolic capacity; however, HLCs should not be viewed as a one-for-all model and have been shown to be fit-for-purpose in numerous research areas which do not require the bio-activation/metabolism of compounds or substrates.

For example, the use of HLCs has been shown to be of benefit when investigating direct apoptosis-driven toxicity, with HLCs demonstrating a more similar apoptotic pathway profile to cryopreserved hepatocytes, than those seen in the Huh7 cell line (Sjogren et al., 2014). The same study also demonstrated the long-term stability of cytochrome P450 metabolism over a 7 day period. As demonstrated in chapter 3, CYP metabolism in PHH drops markedly during culture, restricting analysis to acute exposure. Therefore, the metabolic stability of HLCs, albeit at lower levels than PHH, may allow for the investigation of chronic exposure to compounds.

Other uses include the modelling of cholesterol metabolism. Krueger et al., demonstrated the expression of a range of apolipoproteins required for all aspects of cholesterol metabolism in HLCs, including the active secretion of cholesterol into the culture medium (Krueger et al., 2013). Furthermore, they reported reduced cholesterol secretion in response to statins, demonstrating a model capable of predicting perturbation of an important hepatocyte function when exposed to a given compound.

HLCs have also been reported as being amenable for use modelling hepatitis C (HCV) infection, supporting the full life-cycle of the virus (Carpentier et al., 2014; Schwartz et al., 2012; Roelandt et al., 2012). Consequently, the efficacy of drugs targeting the HCV life cycle could be tested in a HLC-based model system. In addition, the aforementioned study using

iPSCs-derived from patients suffering from Alpers-Huttenlocher syndrome (Li et al., 2015), demonstrates the possibility of using HLCs to model hepatocyte mitochondrial function and response to chemical perturbation.

Taken together, it is clear that whilst HLCs are not yet fit for all purposes, they are capable of modelling many liver-unique functions and associated toxicity, diseases and/or chemical perturbations within a stable, physiologically relevant and genotypically normal hepatic model.

7.2.4 Deriving novel information from the proteomic assessment of primary human hepatocyte differentiation

The results described in chapter 5 demonstrate the dynamic and selective proteomic changes which occur during dedifferentiation. This assessment is the first of its kind to assess human hepatocyte dedifferentiation in a proteomic context; however, despite this, the majority of the results generated were in-keeping with previous studies which have investigated dedifferentiation using rodent cells (Kim et al., 2010b; Rowe et al., 2010; Zellmer et al., 2010). The similarity suggests that the mechanisms of dedifferentiation are conserved across species and the proteomic changes we observed mirror transcriptional changes described in other studies. Consequently, our study confirms the translatability of these findings in both rodent-to-human and mRNA-to-protein contexts.

Unlike previous omic studies, our work did not attempt to compare two or more culture systems (Kim et al., 2010b; Rowe et al., 2010) and instead aimed to directly address the driving mechanisms of dedifferentiation. Through this approach we were able to investigate the transcription factors which may underlie the loss of the xenobiotic hepatic phenotype, producing some potential insights into the sudden loss of cytochrome P450 expression in monolayer culture systems. We found that binding sites for ZEB1, a known

transcriptional repressor which induces epithelial-mesenchymal transition (Liu et al., 2008b), were exclusively located of the CYPs which were down-regulated during culture. Therefore, it is tempting to speculate that the EMT forced upon PHH in monolayer culture, causes an up-regulation of ZEB1 and consequently binding to, and inhibition of, selected CYPs. This provides a hypothetical mechanism by which the enhancements of CYP expression seen in 3D culture systems may work (Tostoes et al., 2012).

Furthermore, FOXO1, which is the main target of insulin signalling (Matsumoto et al., 2006), is another transcription factor which has a predicted binding site in the upstream region of the down-regulated, but not maintained, CYPs. Insulin is used in the culture media to boost glucose uptake and improve plating efficiency, morphology and functionality following isolation and during culture (Mooradian and Mariash, 1987; Klein et al., 2002; Fraczek et al., 2013). However, as insulin was present in the media throughout this study and the CYPs which have FOXO1 predicted binding sites in the gene promoter region were significantly down-regulated, it may be hypothesised that FOXO1 also plays a role in the loss of xenobiotic phenotype. This may be a reflection of the static nature of culture system used, with insulin a constitutive part of the culture media; whereas, the situation in man is much more dynamic. Recently, Siller *et al*., demonstrated the advantage of using pulses of growth factors during HLC differentiation (Siller et al., 2015) and the same technique may better reflect the physiological waves of insulin which are released upon food intake in man.

Of further interest, several factors associated with the maintained CYPs are related to developmental processes (i.e. MITF, COUP-TFII, Brachyury, TBX5, OTx2 and the androgen receptor) or stress responses (i.e. HSF2 and ATF6). Some have hypothesised that the process of dedifferentiation is a reversion to a less mature phenotype (Baxter et al., 2015; Rowe et al., 2013) caused by the cellular stress of isolation and culture, with similar effects

noted following injury prior to regeneration (Kakizaki et al., 2007). This is also in-keeping with our analysis of the foetal HNF4α promoter becoming demethylated following isolation and culture. The presence of binding sites for these transcription factors in the upstream regions of the maintained CYPs may therefore indicate a mechanism by which stress and/or developmental associated factors are able to maintain CYPs that are essential to cell survival and accommodate the loss of other factors, such as HNF1α activity, which non-essential CYPs (i.e. xenobiotic-associated) cannot.

The investigation of proteome represents a global assessment of the functional unit of the cell, i.e. the protein; however, the presence of a protein does automatically indicate that it is functional. For example, phosphorylation and ubiquitination can strongly influence protein function, as can the location of the protein within the cell. Therefore, to fully understand the changes of dedifferentiation, post-translational modifications must also be taken into account. The importance of such modifications is highlighted by figure 7.2. This data represents the networks which Ingenuity pathway analysis associated with the dedifferentiation process at 168 hours, with the inference being that the more connected the protein, the more pivotal a role it plays in the process being investigated. Highlighted by black boxes are the proteins Ubiquitin C and Sumo2. These proteins are central to the network and therefore are likely to have an important role in the process of dedifferentiation.

SUMOylation of HNF4α has been reported by Zhou et al., during hepatic differentiation and was shown to alter protein stability in an ubiquitin-dependent manner (Zhou et al., 2012). Thus, changes in the post-translational modification of proteins are likely to be another key determinant driving the loss of hepatic phenotype during culture and utilising post-translational proteomics may yield greater information regarding the process (Mann and Jensen, 2003).

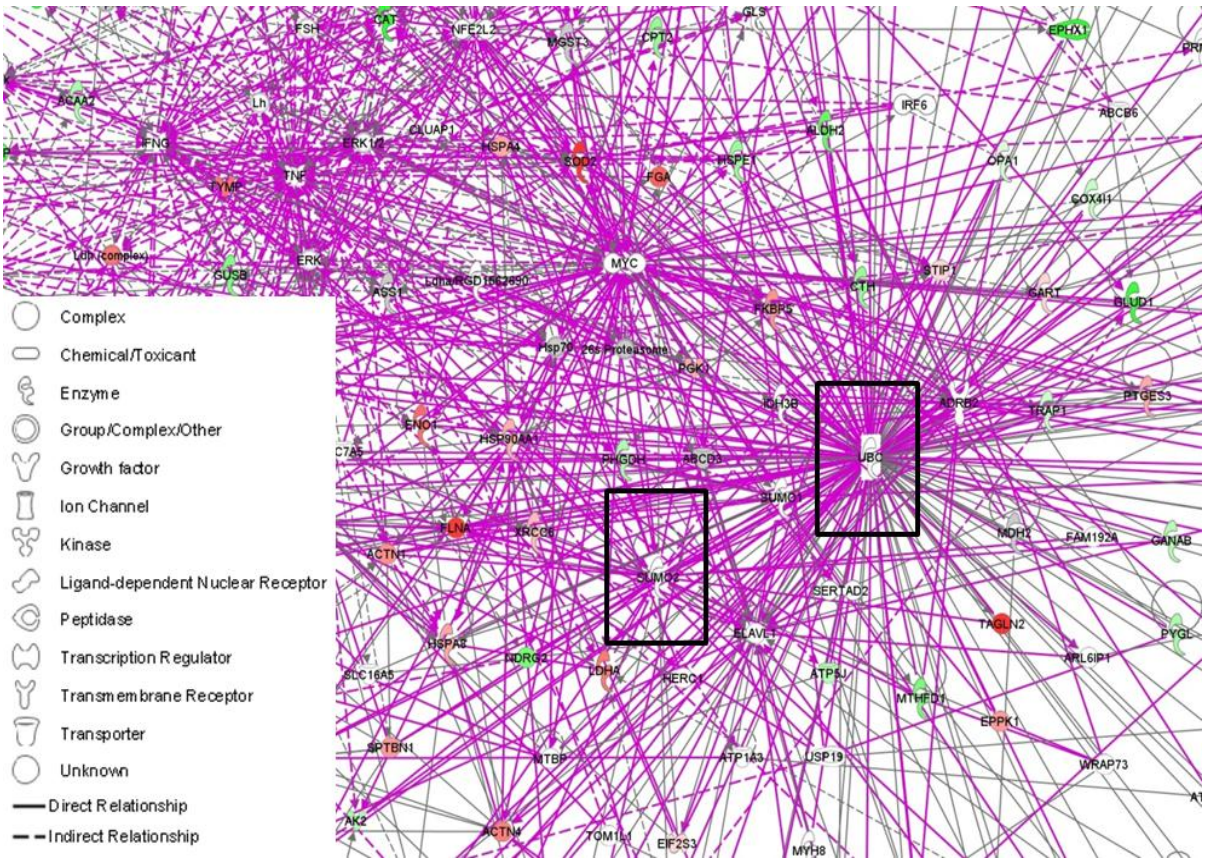

Figure 7.2: Combining interconnected networks associated with dedifferentiation at 168 hours of culture highlight potential roles for Ubiquitin C and Sumo2.

IPA Ingenuity generated networks from the differentially expressed proteins combined using the merge network function. Proteins in green: down-regulated. Proteins in red: Up-regulated. Grey proteins: non-differentially expressed proteins. White proteins: non-detected proteins inserted to make network. Purple lines: Inter-network relationships. Grey lines: Individual network relationships.

There is little doubt that complex co- and 3D-culture systems offer enhanced phenotypic maintenance; however, by using a simple culture system in a step-back approach, we have been able to identify novel factors which may be targeted by changes in culture techniques or through the use of small molecules. Expanding the scope of this study and building upon the hypotheses generated will yield greater information regarding the importance of these factors in the maintenance of PHH.

PHH dedifferentiation is a complex and multi-faceted process (summarised in figure 7.3). At the earliest timepoints, stress-associated factors dominated the up-regulated pathways and proteins. These pathways likely drive the loss of phenotype but are also imperative for ensuring cell survival and inhibition often leads to loss of viability (Fremin et al., 2012); therefore, addressing the source of the stress is an important consideration. Perhaps the greatest cause of this stress is the collagenase-based digestion and ischemia-reperfusion injury which the cells are subjected to during isolation (Elaut et al., 2006). As a consequence, the cells are compromised prior to being placed into the various culture systems. Given the resources which are being directed towards the incremental development of complex hepatic culture models, replacing or developing the relatively crude collagenase digestion technique offers an area which has the potential for giant leaps in the maintenance of the hepatic phenotype *in vitro*.

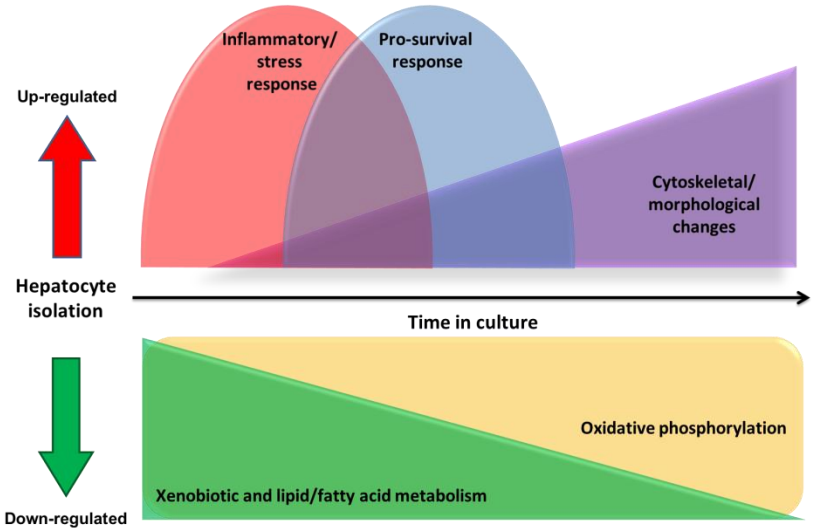

Figure 7.3: Dynamic waves of hepatocyte dedifferentiation. Schematic diagram of the time-dependent changes of specific protein groups during dedifferentiation.

7.3. Final comments

To conclude, the hypotheses investigated in this thesis will be commented on individually.

Hypothesis 1:

The use of primary human hepatocyte-derived iPSCs to generate hepatocyte-like cells yields an improved maturity in hepatocyte-like cell phenotype when compared to HDF-derived iPSCs from the same donor.

Comment: HLCs differentiated from PHH-derived iPSCs of 3 donors showed little to no significant difference in the expression of genes at all stages of culture or differentiation compared to HDF-derived iPSCs. This was also true of methylation and functional analysis studies. Therefore, we found this hypothesis to be false. Future investigations may wish to confirm these findings in more advanced models or using omic technologies.

Hypothesis 2:

Mechanistic evaluation of the primary human hepatocyte proteome during monolayer will yield novel information and hypotheses regarding the dedifferentiation process.

Comment: Global proteomic analysis of PHH during culture provided novel understanding of the driving mechanisms of dedifferentiation process. These findings should provide the basis of further investigations into the effect that these factors have in both simple and complex culture systems.

Hypothesis 3:

Nrf2 regulates hepatocyte phenotype during differentiation and dedifferentiation

Comment: Investigation into the role of Nrf2 in hepatocyte dedifferentiation demonstrated a potentially negative relationship between Nrf2 induction and key metabolic protein

CYP3A4. The levels of Nrf2 were also found to increase during the differentiation of pluripotent stem cells to HLCs. Future work is now required to manipulate the levels of Nrf2 during HLC differentiation to mechanistically evaluate its role in the process.

8.1 Bibliography

Aasen T and Belmonte JCI. (2010) Isolation and cultivation of human keratinocytes from skin or plucked hair for the generation of induced pluripotent stem cells. *Nat. Protocols* 5: 371-382.

Abu-Absi SF, Hansen LK and Hu W-S. (2004) Three-dimensional co-culture of hepatocytes and stellate cells. *Cytotechnology* 45: 125-140.

Agarwal S, Holton KL and Lanza R. (2008) Efficient differentiation of functional hepatocytes from human embryonic stem cells. *Stem Cells* 26: 1117-1127.

Agu Chukwuma A, Soares Filipa AC, Alderton A, et al. (2015) Successful Generation of Human Induced Pluripotent Stem Cell Lines from Blood Samples Held at Room Temperature for up to 48 hr. *Stem Cell Reports*.

Aitken AE, Richardson TA and Morgan ET. (2006) Regulation of drug-metabolizing enzymes and transporters in inflammation. *Annu Rev Pharmacol Toxicol* 46: 123-149.

Akiyama TE and Gonzalez FJ. (2003) Regulation of P450 genes by liver-enriched transcription factors and nuclear receptors. *Biochim Biophys Acta* 1619: 223-234.

Alexandre E, Viollon-Abadie C, David P, et al. (2002) Cryopreservation of adult human hepatocytes obtained from resected liver biopsies. *Cryobiology* 44: 103-113.

Allen JW and Bhatia SN. (2003) Formation of steady-state oxygen gradients in vitro: application to liver zonation. *Biotechnol Bioeng* 82: 253-262.

Allen JW, Khetani SR and Bhatia SN. (2005) In vitro zonation and toxicity in a hepatocyte bioreactor. *Toxicol Sci* 84: 110-119.

Ambrosino G, Basso SM, Varotto S, et al. (2005) Isolated hepatocytes versus hepatocyte spheroids: in vitro culture of rat hepatocytes. *Cell Transplant* 14: 397-401.

Anokye-Danso F, Trivedi CM, Juhr D, et al. (2011) Highly efficient miRNA-mediated reprogramming of mouse and human somatic cells to pluripotency. *Cell Stem Cell* 8: 376-388.

Asplund A, Pradip A, van Giezen M, et al. (2015) One Standardized Differentiation Procedure Robustly Generates Homogenous Hepatocyte Cultures Displaying Metabolic Diversity from a Large Panel of Human Pluripotent Stem Cells. *Stem Cell Reviews and Reports*: 1-15.

Avior Y, Levy G, Zimerman M, et al. (2015) Microbial-derived lithocholic acid and vitamin K2 drive the metabolic maturation of pluripotent stem cells-derived and fetal hepatocytes. *Hepatology* 62: 265-278.

Awad MM, Sanders JA and Gruppuso PA. (2000) A potential role for p15(Ink4b) and p57(Kip2) in liver development. *FEBS Lett* 483: 160-164.

Bar-Nur O, Russ HA, Efrat S, et al. (2011) Epigenetic memory and preferential lineage-specific differentiation in induced pluripotent stem cells derived from human pancreatic islet beta cells. *Cell Stem Cell* 9: 17-23.

Basma H, Soto-Gutierrez A, Yannam GR, et al. (2009) Differentiation and transplantation of human embryonic stem cell-derived hepatocytes. *Gastroenterology* 136: 990-999.

Bataller R and Brenner DA. (2005) Liver fibrosis. *J Clin Invest* 115: 209-218.

Baxter M, Withey S, Harrison S, et al. (2015) Phenotypic and functional analyses show stem cell-derived hepatocyte-like cells better mimic fetal rather than adult hepatocytes. *J Hepatol* 62: 581-589.

Baxter MA, Rowe C, Alder J, et al. (2010) Generating hepatic cell lineages from pluripotent stem cells for drug toxicity screening. *Stem Cell Res* 5: 4-22.

Bertero A, Madrigal P, Galli A, et al. (2015) Activin/Nodal signaling and NANOG orchestrate human embryonic stem cell fate decisions by controlling the H3K4me3 chromatin mark. *Genes & Development* 29: 702-717.

Betel D, Wilson M, Gabow A, et al. (2008) The microRNA.org resource: targets and expression. *Nucleic Acids Res* 36: 149-153.

Bhatia SN, Yarmush ML and Toner M. (1997) Controlling cell interactions by micropatterning in co-cultures: hepatocytes and 3T3 fibroblasts. *J Biomed Mater Res* 34: 189-199.

Bhogal RH, Hodson J, Bartlett DC, et al. (2011) Isolation of Primary Human Hepatocytes from Normal and Diseased Liver Tissue: A One Hundred Liver Experience. *PLoS ONE* 6: e18222.

Bilzer M, Roggel F and Gerbes AL. (2006) Role of Kupffer cells in host defense and liver disease. *Liver Int* 26: 1175-1186.

Bolleyn J, Fraczek J, Vinken M, et al. (2011) Effect of Trichostatin A on miRNA expression in cultures of primary rat hepatocytes. *Toxicol In Vitro* 25: 1173-1182.

Bondy SC and Naderi S. (1994) Contribution of hepatic cytochrome P450 systems to the generation of reactive oxygen species. *Biochemical Pharmacology* 48: 155-159.

Bone HK, Nelson AS, Goldring CE, et al. (2011) A novel chemically directed route for the generation of definitive endoderm from human embryonic stem cells based on inhibition of GSK-3. *J Cell Sci* 124: 1992-2000.

Brolen G, Sivertsson L, Bjorquist P, et al. (2010) Hepatocyte-like cells derived from human embryonic stem cells specifically via definitive endoderm and a progenitor stage. *J Biotechnol* 145: 284-294.

Brophy CM, Luebke-Wheeler JL, Amiot BP, et al. (2009) Rat hepatocyte spheroids formed by rocked technique maintain differentiated hepatocyte gene expression and function. *Hepatology (Baltimore, Md.)* 49: 578-586.

Bryan HK, Olayanju A, Goldring CE, et al. (2013) The Nrf2 cell defence pathway: Keap1-dependent and -independent mechanisms of regulation. *Biochemical Pharmacology* 85: 705-717.

Buelna-Chontal M and Zazueta C. (2013) Redox activation of Nrf2 & NF-κB: A double end sword? *Cellular Signalling* 25: 2548-2557.

Buganim Y, Faddah DA, Cheng AW, et al. (2012) Single-cell gene expression analyses of cellular reprogramming reveal a stochastic early and hierarchic late phase. *Cell* 150: 1209-1222.

Buganim Y, Faddah DA and Jaenisch R. (2013) Mechanisms and models of somatic cell reprogramming. *Nat Rev Genet* 14: 427-439.

Byrne SM, Ortiz L, Mali P, et al. (2015) Multi-kilobase homozygous targeted gene replacement in human induced pluripotent stem cells. *Nucleic Acids Res* 43: e21.

Cai J, Zhao Y, Liu Y, et al. (2007) Directed differentiation of human embryonic stem cells into functional hepatic cells. *Hepatology* 45: 1229-1239.

Campion SN, Johnson R, Aleksunes LM, et al. (2008) Hepatic Mrp4 induction following acetaminophen exposure is dependent on Kupffer cell function. *Am J Physiol Gastrointest Liver Physiol* 295: G294-304.

Carpentier A, Tesfaye A, Chu V, et al. (2014) Engrafted human stem cell-derived hepatocytes establish an infectious HCV murine model. *J Clin Invest* 124: 4953-4964.

Castell JV, Jover R, Martinez-Jimenez CP, et al. (2006) Hepatocyte cell lines: their use, scope and limitations in drug metabolism studies. *Expert Opin Drug Metab Toxicol* 2: 183-212.

Castilho-Fernandes A, de Almeida DC, Fontes AM, et al. (2011) Human hepatic stellate cell line (LX-2) exhibits characteristics of bone marrow-derived mesenchymal stem cells. *Exp Mol Pathol* 91: 664-672.

Cayo MA, Cai J, DeLaForest A, et al. (2012) 'JD' iPS cell–derived hepatocytes faithfully recapitulate the pathophysiology of familial hypercholesterolemia. *Hepatology* 56: 2163-2171.

Chang C-Y, Chen S-M, Lu H-E, et al. (2015) N-butylidenephthalide Attenuates Alzheimer's Disease-Like Cytopathy in Down Syndrome Induced Pluripotent Stem Cell-Derived Neurons. *Scientific Reports* 5: 8744.

Chapple SJ, Siow RC and Mann GE. (2012) Crosstalk between Nrf2 and the proteasome: therapeutic potential of Nrf2 inducers in vascular disease and aging. *Int J Biochem Cell Biol* 44: 1315-1320.

Chartoumpekis DV, Ziros PG, Sykiotis GP, et al. (2011) Nrf2 activation diminishes during adipocyte differentiation of ST2 cells. *Int J Mol Med* 28: 823-828.

Chatterjee P, Cheung Y and Liew C. (2011) Transfecting and Nucleofecting Human Induced Pluripotent Stem Cells. *Journal of Visualized Experiments : JoVE*: 3110.

Chen AE, Borowiak M, Sherwood RI, et al. (2013) Functional evaluation of ES cell-derived endodermal populations reveals differences between Nodal and Activin A-guided differentiation. *Development* 140: 675-686.

Chen G, Gulbranson DR, Hou Z, et al. (2011) Chemically defined conditions for human iPS cell derivation and culture. *Nature methods* 8: 424-429.

Chen YF, Tseng CY, Wang HW, et al. (2012) Rapid generation of mature hepatocyte-like cells from human induced pluripotent stem cells by an efficient three-step protocol. *Hepatology* 55: 1193-1203.

Chien Y, Chang YL, Li HY, et al. (2015) Synergistic effects of carboxymethyl-hexanoyl chitosan, cationic polyurethane-short branch PEI in miR122 gene delivery: accelerated differentiation of iPSCs into mature hepatocyte-like cells and improved stem cell therapy in a hepatic failure model. *Acta Biomater* 13: 228-244.

Chin MH, Mason MJ, Xie W, et al. (2009) Induced pluripotent stem cells and embryonic stem cells are distinguished by gene expression signatures. *Cell Stem Cell* 5: 111-123.

Choi SM, Kim Y, Shim JS, et al. (2013) Efficient drug screening and gene correction for treating liver disease using patient-specific stem cells. *Hepatology* 57: 2458-2468.

Chung K-M, Kolling Iv FW, Gajdosik MD, et al. (2014) Single Cell Analysis Reveals the Stochastic Phase of Reprogramming to Pluripotency Is an Ordered Probabilistic Process. *PLoS ONE* 9: e95304.

Collier R. (2009) Drug development cost estimates hard to swallow. *Canadian Medical Association Journal* 180: 279-280.

Czekaj P and Skowronek R. (2012) *Transcription Factors Potentially Involved in Regulation of Cytochrome P450 Gene Expression*.

D'Amour KA, Agulnick AD, Eliazer S, et al. (2005) Efficient differentiation of human embryonic stem cells to definitive endoderm. *Nat Biotechnol* 23: 1534-1541.

Darnell M, Ulvestad M, Ellis E, et al. (2012) In vitro evaluation of major in vivo drug metabolic pathways using primary human hepatocytes and HepaRG cells in suspension and a dynamic three-dimensional bioreactor system. *J Pharmacol Exp Ther* 343: 134-144.

Davies EC, Green CF, Taylor S, et al. (2009) Adverse Drug Reactions in Hospital In-Patients: A Prospective Analysis of 3695 Patient-Episodes. *PLoS ONE* 4: e4439.

DiMasi JA, Hansen RW and Grabowski HG. (2003) The price of innovation: new estimates of drug development costs. *J Health Econ* 22: 151-185.

Ding BS, Nolan DJ, Butler JM, et al. (2010) Inductive angiocrine signals from sinusoidal endothelium are required for liver regeneration. *Nature* 468: 310-315.

Drewes T, Senkel S, Holewa B, et al. (1996) Human hepatocyte nuclear factor 4 isoforms are encoded by distinct and differentially expressed genes. *Molecular and Cellular Biology* 16: 925-931.

Duan Y, Catana A, Meng Y, et al. (2007) Differentiation and enrichment of hepatocyte-like cells from human embryonic stem cells in vitro and in vivo. *Stem Cells* 25: 3058-3068.

Duan Y, Ma X, Zou W, et al. (2010) Differentiation and characterization of metabolically functioning hepatocytes from human embryonic stem cells. *Stem Cells* 28: 674-686.

Ek M, Soderdahl T, Kuppers-Munther B, et al. (2007) Expression of drug metabolizing enzymes in hepatocyte-like cells derived from human embryonic stem cells. *Biochem Pharmacol* 74: 496-503.

Elaut G, Henkens T, Papeleu P, et al. (2006) Molecular mechanisms underlying the dedifferentiation process of isolated hepatocytes and their cultures. *Curr Drug Metab* 7: 629-660.

Evans MJ and Kaufman MH. (1981) Establishment in culture of pluripotential cells from mouse embryos. *Nature* 292: 154-156.

Fox ES, Thomas P and Broitman SA. (1987) Comparative studies of endotoxin uptake by isolated rat Kupffer and peritoneal cells. *Infect Immun* 55: 2962-2966.

Fraczek J, Bolleyn J, Vanhaecke T, et al. (2013) Primary hepatocyte cultures for pharmaco-toxicological studies: at the busy crossroad of various anti-dedifferentiation strategies. *Archives of Toxicology* 87: 577-610.

Fraczek JE, Vinken M, Tourwe D, et al. (2012) Synergetic effects of DNA demethylation and histone deacetylase inhibition in primary rat hepatocytes. *Invest New Drugs* 30: 1715-1724.

Fremin C, Ezan F, Guegan JP, et al. (2012) The complexity of ERK1 and ERK2 MAPKs in multiple hepatocyte fate responses. *J Cell Physiol* 227: 59-69.

Fu D, Mitra K, Sengupta P, et al. (2013) Coordinated elevation of mitochondrial oxidative phosphorylation and autophagy help drive hepatocyte polarization. *Proceedings of the National Academy of Sciences* 110: 7288-7293.

Fujita S, Eguchi A, Okabe J, et al. (2006) Sendai virus-mediated gene delivery into hepatocytes via isolated hepatic perfusion. *Biol Pharm Bull* 29: 1728-1734.

Fusaki N, Ban H, Nishiyama A, et al. (2009) Efficient induction of transgene-free human pluripotent stem cells using a vector based on Sendai virus, an RNA virus that does not integrate into the host genome. *Proc Jpn Acad Ser B Phys Biol Sci* 85: 348-362.

Ghodsizadeh A, Taei A, Totonchi M, et al. (2010) Generation of liver disease-specific induced pluripotent stem cells along with efficient differentiation to functional hepatocyte-like cells. *Stem Cell Rev* 6: 622-632.

Giacomini KM, Huang SM, Tweedie DJ, et al. (2010) Membrane transporters in drug development. *Nat Rev Drug Discov* 9: 215-236.

Gieseck III RL, Hannan NRF, Bort R, et al. (2014) Maturation of Induced Pluripotent Stem Cell Derived Hepatocytes by 3D-Culture. *PLoS ONE* 9: e86372.

Godoy P, Hengstler JG, Ilkavets I, et al. (2009) Extracellular matrix modulates sensitivity of hepatocytes to fibroblastoid dedifferentiation and transforming growth factor beta-induced apoptosis. *Hepatology* 49: 2031-2043.

Godoy P, Hewitt NJ, Albrecht U, et al. (2013) Recent advances in 2D and 3D in vitro systems using primary hepatocytes, alternative hepatocyte sources and non-parenchymal liver cells and their use in investigating mechanisms of hepatotoxicity, cell signaling and ADME. *Archives of Toxicology* 87: 1315-1530.

Goldring CE, Norris A, Kitteringham N, et al. (2015) Mechanism-Based Markers of Drug-Induced Liver Injury to Improve the Physiological Relevance and Predictivity of In Vitro Models. *Applied In Vitro Toxicology* 1: 175-186.

Gomez-Lechon MJ, Donato MT, Castell JV, et al. (2003) Human hepatocytes as a tool for studying toxicity and drug metabolism. *Curr Drug Metab* 4: 292-312.

Gonzales Kevin Andrew U, Liang H, Lim Y-S, et al. (2015) Deterministic Restriction on Pluripotent State Dissolution by Cell-Cycle Pathways. *Cell* 162: 564-579.

Gonzalez F, Boue S and Izpisua Belmonte JC. (2011) Methods for making induced pluripotent stem cells: reprogramming a la carte. *Nat Rev Genet* 12: 231-242.

Gresh L, Bourachot B, Reimann A, et al. (2005) The SWI/SNF chromatin-remodeling complex subunit SNF5 is essential for hepatocyte differentiation. *The EMBO Journal* 24: 3313-3324.

Gruenke LD, Konopka K, Cadieu M, et al. (1995) The stoichiometry of the cytochrome P-450-catalyzed metabolism of methoxyflurane and benzphetamine in the presence and absence of cytochrome b5. *J Biol Chem* 270: 24707-24718.

Guengerich FP. (2001) Common and uncommon cytochrome P450 reactions related to metabolism and chemical toxicity. *Chem Res Toxicol* 14: 611-650.

Guengerich FP. (2008) Cytochrome P450 and Chemical Toxicology. *Chem Res Toxicol* 21: 70-83.

Guenther MG, Frampton GM, Soldner F, et al. (2010) Chromatin structure and gene expression programs of human embryonic and induced pluripotent stem cells. *Cell Stem Cell* 7: 249-257.

Guo L, Dial S, Shi L, et al. (2011) Similarities and Differences in the Expression of Drug-Metabolizing Enzymes between Human Hepatic Cell Lines and Primary Human Hepatocytes. *Drug Metabolism and Disposition* 39: 528-538.

Hannan NR, Segeritz CP, Touboul T, et al. (2013) Production of hepatocyte-like cells from human pluripotent stem cells. *Nat Protoc* 8: 430-437.

Hansel MC, Gramignoli R, Blake W, et al. (2014) Increased reprogramming of human fetal hepatocytes compared with adult hepatocytes in feeder-free conditions. *Cell Transplant* 23: 27-38.

Hay DC, Fletcher J, Payne C, et al. (2008a) Highly efficient differentiation of hESCs to functional hepatic endoderm requires ActivinA and Wnt3a signaling. *Proc Natl Acad Sci USA* 105: 12301-12306.

Hay DC, Zhao D, Fletcher J, et al. (2008b) Efficient differentiation of hepatocytes from human embryonic stem cells exhibiting markers recapitulating liver development in vivo. *Stem Cells* 26: 894-902.

Hay DC, Zhao D, Ross A, et al. (2007) Direct differentiation of human embryonic stem cells to hepatocyte-like cells exhibiting functional activities. *Cloning Stem Cells* 9: 51-62.

Heslop JA, Hammond TG, Santeramo I, et al. (2015) Concise review: workshop review: understanding and assessing the risks of stem cell-based therapies. *Stem Cells Transl Med* 4: 389-400.

Hodges RE and Minich DM. (2015) Modulation of Metabolic Detoxification Pathways Using Foods and Food-Derived Components: A Scientific Review with Clinical Application. *Journal of Nutrition and Metabolism* 2015: 23.

Hoedemakers RMJ, Morselt HWM, Scherphof GL, et al. (1995) Heterogeneity in secretory responses of rat liver macrophages of different size. *Liver* 15: 313-319.

Hoehme S, Brulport M, Bauer A, et al. (2010) Prediction and validation of cell alignment along microvessels as order principle to restore tissue architecture in liver regeneration. *Proceedings of the National Academy of Sciences* 107: 10371-10376.

Hofmann AF. (2009) The enterohepatic circulation of bile acids in mammals: form and functions. *Front Biosci (Landmark Ed)* 14: 2584-2598.

Homolya L, Varadi A and Sarkadi B. (2003) Multidrug resistance-associated proteins: Export pumps for conjugates with glutathione, glucuronate or sulfate. *Biofactors* 17: 103-114.

Hoskins JM, Carey LA and McLeod HL. (2009) CYP2D6 and tamoxifen: DNA matters in breast cancer. *Nat Rev Cancer* 9: 576-586.

Hou P, Li Y, Zhang X, et al. (2013) Pluripotent Stem Cells Induced from Mouse Somatic Cells by Small-Molecule Compounds. *Science* 341: 651-654.

Hu S, Wilson KD, Ghosh Z, et al. (2013) MicroRNA-302 increases reprogramming efficiency via repression of NR2F2. *Stem Cells* 31: 259-268.

Ingelman-Sundberg M, Sim SC, Gomez A, et al. (2007) Influence of cytochrome P450 polymorphisms on drug therapies: pharmacogenetic, pharmacoepigenetic and clinical aspects. *Pharmacol Ther* 116: 496-526.

Itoh K, Wakabayashi N, Katoh Y, et al. (2003) Keap1 regulates both cytoplasmic-nuclear shuttling and degradation of Nrf2 in response to electrophiles. *Genes to Cells* 8: 379-391.

Jakoby WB and Ziegler DM. (1990) The enzymes of detoxication. *J Biol Chem* 265: 20715-20718.

Jang J, Wang Y, Kim HS, et al. (2014) Nrf2, a regulator of the proteasome, controls self-renewal and pluripotency in human embryonic stem cells. *Stem Cells* 32: 2616-2625.

Ji AR, Ku SY, Cho MS, et al. (2010) Reactive oxygen species enhance differentiation of human embryonic stem cells into mesendodermal lineage. *Exp Mol Med* 42: 175-186.

Jia B, Chen S, Zhao Z, et al. (2014) Modeling of hemophilia A using patient-specific induced pluripotent stem cells derived from urine cells. *Life Sciences* 108: 22-29.

Jiang Q, Yan Z and Feng J. (2006) Neurotrophic factors stabilize microtubules and protect against rotenone toxicity on dopaminergic neurons. *J Biol Chem* 281: 29391-29400.

Jiang W, Zhang D, Bursac N, et al. (2013) WNT3 Is a Biomarker Capable of Predicting the Definitive Endoderm Differentiation Potential of hESCs. *Stem Cell Reports* 1: 46-52.

Jozefczuk J, Prigione A, Chavez L, et al. (2011) Comparative analysis of human embryonic stem cell and induced pluripotent stem cell-derived hepatocyte-like cells reveals current drawbacks and possible strategies for improved differentiation. *Stem Cells Dev* 20: 1259-1275.

Ju C, Reilly TP, Bourdi M, et al. (2002) Protective role of Kupffer cells in acetaminophen-induced hepatic injury in mice. *Chem Res Toxicol* 15: 1504-1513.

Jungermann K and Kietzmann T. (1996) Zonation of parenchymal and nonparenchymal metabolism in liver. *Annu Rev Nutr* 16: 179-203.

Jungermann K and Kietzmann T. (1997) Role of oxygen in the zonation of carbohydrate metabolism and gene expression in liver. *Kidney Int* 51: 402-412.

Kajiwara M, Aoi T, Okita K, et al. (2012) Donor-dependent variations in hepatic differentiation from human-induced pluripotent stem cells. *Proc Natl Acad Sci USA* 109: 12538-12543.

Kakizaki S, Yamazaki Y, Kosone T, et al. (2007) Gene expression profiles of drug-metabolizing enzymes and transporters with an overexpression of hepatocyte growth factor. *Liver Int* 27: 109-119.

Kanzaki H, Shinohara F, Kajiya M, et al. (2013) The Keap1/Nrf2 protein axis plays a role in osteoclast differentiation by regulating intracellular reactive oxygen species signaling. *J Biol Chem* 288: 23009-23020.

Khajeniazi S, Allameh A, Soleimani M, et al. (2013) Changes in COX-2 and oxidative damage factors during differentiation of human mesenchymal stem cells to hepatocyte-like cells is associated with downregulation of P53 gene. *Biol Chem* 394: 1213-1222.

Kia R. (2014) Novel approaches using human induced pluripotent stem cells and microRNAs in the development of relevant human hepatocyte models for drug induced liver injury. *Department of Molecular and Clinical Pharmacology.* University of Liverpool.

Kia R, Sison RL, Heslop J, et al. (2013) Stem cell-derived hepatocytes as a predictive model for drug-induced liver injury: are we there yet? *Br J Clin Pharmacol* 75: 885-896.

Kietzmann T, Dimova EY, Flugel D, et al. (2006) Oxygen: modulator of physiological and pathophysiological processes in the liver. *Z Gastroenterol* 44: 67-76.

Kim D, Kim CH, Moon JI, et al. (2009) Generation of human induced pluripotent stem cells by direct delivery of reprogramming proteins. *Cell Stem Cell* 4: 472-476.

Kim K, Doi A, Wen B, et al. (2010a) Epigenetic memory in induced pluripotent stem cells. *Nature* 467: 285-290.

Kim Y, Lasher CD, Milford LM, et al. (2010b) A comparative study of genome-wide transcriptional profiles of primary hepatocytes in collagen sandwich and monolayer cultures. *Tissue Eng Part C Methods* 16: 1449-1460.

Kitteringham NR, Abdullah A, Walsh J, et al. (2010) Proteomic analysis of Nrf2 deficient transgenic mice reveals cellular defence and lipid metabolism as primary Nrf2-dependent pathways in the liver. *J Proteomics* 73: 1612-1631.

Klein HH, Ullmann S, Drenckhan M, et al. (2002) Differential modulation of insulin actions by dexamethasone: studies in primary cultures of adult rat hepatocytes. *J Hepatol* 37: 432-440.

Kleinsmith LJ and Pierce GB, Jr. (1964) Multipotentiality of Single Embryonal Carcinoma Cells. *Cancer Res* 24: 1544-1551.

Kmiec Z. (2001) Cooperation of liver cells in health and disease. *Adv Anat Embryol Cell Biol* 161: 1-151.

Koche RP, Smith ZD, Adli M, et al. (2011) Reprogramming Factor Expression Initiates Widespread Targeted Chromatin Remodeling. *Cell Stem Cell* 8: 96-105.

Kohler UA, Kurinna S, Schwitter D, et al. (2013) Activated Nrf2 impairs liver regeneration in mice by activation of genes involved in cell cycle control and apoptosis. *Hepatology* 6: 26964.

Kondo T, Asai M, Tsukita K, et al. (2013) Modeling Alzheimer's Disease with iPSCs Reveals Stress Phenotypes Associated with Intracellular Aβ and Differential Drug Responsiveness. *Cell Stem Cell* 12: 487-496.

Konig J, Nies AT, Cui Y, et al. (1999) Conjugate export pumps of the multidrug resistance protein (MRP) family: localization, substrate specificity, and MRP2-mediated drug resistance. *Biochim Biophys Acta* 1461: 377-394.

Kordes C, Sawitza I, Gotze S, et al. (2013) Hepatic stellate cells support hematopoiesis and are liver-resident mesenchymal stem cells. *Cell Physiol Biochem* 31: 290-304.

Kordes C, Sawitza I, Götze S, et al. (2012) Stellate Cells from Rat Pancreas Are Stem Cells and Can Contribute to Liver Regeneration. *PLoS ONE* 7: e51878.

Kordes C, Sawitza I and Haussinger D. (2009) Hepatic and pancreatic stellate cells in focus. *Biol Chem* 390: 1003-1012.

Krueger W, Boelsterli UA and Rasmussen TP. (2014) Stem Cell Strategies to Evaluate Idiosyncratic Drug-induced Liver Injury. *Journal of Clinical and Translational Hepatology* 2: 143-152.

Krueger WH, Tanasijevic B, Barber V, et al. (2013) Cholesterol-Secreting and Statin-Responsive Hepatocytes from Human ES and iPS Cells to Model Hepatic Involvement in Cardiovascular Health. *PLoS ONE* 8: e67296.

Kuang Z, Huang Z, Li Y, et al. (2015) Overexpression of CYP3A5 attenuates inducibility and activity of CYP3A4 in HepG2 cells. *Mol Med Rep* 11: 2868-2874.

Kusunoki Y, Ikarashi N, Hayakawa Y, et al. (2014) Hepatic early inflammation induces downregulation of hepatic cytochrome P450 expression and metabolic activity in the dextran sulfate sodium-induced murine colitis. *Eur J Pharm Sci* 54: 17-27.

Kuthan H and Ullrich V. (1982) Oxidase and oxygenase function of the microsomal cytochrome P450 monooxygenase system. *Eur J Biochem* 126: 583-588.

Lakehal F, Dansette PM, Becquemont L, et al. (2001) Indirect cytotoxicity of flucloxacillin toward human biliary epithelium via metabolite formation in hepatocytes. *Chem Res Toxicol* 14: 694-701.

Larson AM, Polson J, Fontana RJ, et al. (2005) Acetaminophen-induced acute liver failure: results of a United States multicenter, prospective study. *Hepatology* 42: 1364-1372.

Lasher CD, Rajagopalan P and Murali TM. (2011) Discovering networks of perturbed biological processes in hepatocyte cultures. *PLoS ONE* 6: 0015247.

Lavon N, Yanuka O and Benvenisty N. (2004) Differentiation and isolation of hepatic-like cells from human embryonic stem cells. *Differentiation* 72: 230-238.

Lazarou J, Pomeranz BH and Corey PN. (1998) Incidence of adverse drug reactions in hospitalized patients: a meta-analysis of prospective studies. *Jama* 279: 1200-1205.

LeCluyse E, Alexandre E, Hamilton G, et al. (2005) Isolation and Culture of Primary Human Hepatocytes. In: Helgason C and Miller C (eds) *Basic Cell Culture Protocols.* Humana Press, 207-229.

Lee SB, Seo D, Choi D, et al. (2012) Contribution of hepatic lineage stage-specific donor memory to the differential potential of induced mouse pluripotent stem cells (iPSC). *Stem Cells* 30: 997-1007.

Leppä S, Pirkkala L, Saarento H, et al. (1997) Overexpression of HSF2-β Inhibits Hemin-induced Heat Shock Gene Expression and Erythroid Differentiation in K562 Cells. *Journal of Biological Chemistry* 272: 15293-15298.

Li CY, Stevens KR, Schwartz RE, et al. (2014) Micropatterned cell-cell interactions enable functional encapsulation of primary hepatocytes in hydrogel microtissues. *Tissue Eng Part A* 20: 2200-2212.

Li S, Guo J, Ying Z, et al. (2015) Valproic acid-induced hepatotoxicity in alpers syndrome is associated with mitochondrial permeability transition pore opening-dependent apoptotic sensitivity in an induced pluripotent stem cell model. *Hepatology* 61: 1730-1739.

Liao B, Bao X, Liu L, et al. (2011) MicroRNA cluster 302-367 enhances somatic cell reprogramming by accelerating a mesenchymal-to-epithelial transition. *J Biol Chem* 286: 17359-17364.

Lister A, Nedjadi T, Kitteringham NR, et al. (2011) Nrf2 is overexpressed in pancreatic cancer: implications for cell proliferation and therapy. *Mol Cancer* 10: 37.

Lister R, Pelizzola M, Kida YS, et al. (2014) Corrigendum: Hotspots of aberrant epigenomic reprogramming in human induced pluripotent stem cells. *Nature* 514: 126-126.

Liu GH, Qu J and Shen X. (2008a) NF-κB/p65 antagonizes Nrf2-ARE pathway by depriving CBP from Nrf2 and facilitating recruitment of HDAC3 to MafK. *Biochimica et Biophysica Acta - Molecular Cell Research* 1783: 713-727.

Liu H, Kim Y, Sharkis S, et al. (2011) In vivo liver regeneration potential of human induced pluripotent stem cells from diverse origins. *Sci Transl Med* 3: 82ra39.

Liu H, Ye Z, Kim Y, et al. (2010a) Generation of endoderm-derived human induced pluripotent stem cells from primary hepatocytes. *Hepatology* 51: 1810-1819.

Liu Julia C, Guan X, Ryan Jeremy A, et al. (2013) High Mitochondrial Priming Sensitizes hESCs to DNA-Damage-Induced Apoptosis. *Cell Stem Cell* 13: 483-491.

Liu Y, El-Naggar S, Darling DS, et al. (2008b) ZEB1 Links Epithelial-Mesenchymal Transition and Cellular Senescence. *Development* 135: 579-588.

Liu YP, Vink MA, Westerink J-T, et al. (2010b) Titers of lentiviral vectors encoding shRNAs and miRNAs are reduced by different mechanisms that require distinct repair strategies. *RNA* 16: 1328-1339.

Livak KJ and Schmittgen TD. (2001) Analysis of relative gene expression data using real-time quantitative PCR and the 2(-Delta Delta C(T)) Method. *Methods* 25: 402-408.

Longo PA, Kavran JM, Kim MS, et al. (2013) Generating mammalian stable cell lines by electroporation. *Methods Enzymol* 529: 209-226.

Lu HF, Chua KN, Zhang PC, et al. (2005) Three-dimensional co-culture of rat hepatocyte spheroids and NIH/3T3 fibroblasts enhances hepatocyte functional maintenance. *Acta Biomater* 1: 399-410.

Lüningschrör P, Hauser S, Kaltschmidt B, et al. (2013) MicroRNAs in pluripotency, reprogramming and cell fate induction. *Biochimica et Biophysica Acta (BBA) - Molecular Cell Research* 1833: 1894-1903.

Mallon BS, Hamilton RS, Kozhich OA, et al. (2014) Comparison of the molecular profiles of human embryonic and induced pluripotent stem cells of isogenic origin. *Stem cell research* 12: 376-386.

Mann M and Jensen ON. (2003) Proteomic analysis of post-translational modifications. *Nat Biotechnol* 21: 255-261.

Marinescu VD, Kohane IS and Riva A. (2005) The MAPPER database: a multi-genome catalog of putative transcription factor binding sites. *Nucleic Acids Res* 33: 91-97.

Marion MJ, Hantz O and Durantel D. (2010) The HepaRG cell line: biological properties and relevance as a tool for cell biology, drug metabolism, and virology studies. *Methods Mol Biol* 640: 261-272.

Martin-Armas M, Simon-Santamaria J, Pettersen I, et al. (2006) Toll-like receptor 9 (TLR9) is present in murine liver sinusoidal endothelial cells (LSECs) and mediates the effect of CpG-oligonucleotides. *J Hepatol* 44: 939-946.

Martin GR. (1981) Isolation of a pluripotent cell line from early mouse embryos cultured in medium conditioned by teratocarcinoma stem cells. *Proceedings of the National Academy of Sciences* 78: 7634-7638.

Martin GR and Evans MJ. (1974) Morphology and Growth of a Pluripotent Teratocarcinoma Cell Line and Its Derivatives in Tissue Culture. *Cell* 2: 163-172.

Martin GR and Evans MJ. (1975) Differentiation of clonal lines of teratocarcinoma cells: formation of embryoid bodies in vitro. *Proceedings of the National Academy of Sciences* 72: 1441-1445.

Maruyama T, Dougan SK, Truttmann MC, et al. (2015) Increasing the efficiency of precise genome editing with CRISPR-Cas9 by inhibition of nonhomologous end joining. *Nat Biotech* 33: 538-542.

Matsumoto M, Han S, Kitamura T, et al. (2006) Dual role of transcription factor FoxO1 in controlling hepatic insulin sensitivity and lipid metabolism. *The Journal of Clinical Investigation* 116: 2464-2472.

McCuskey RS, Bethea NW, Wong J, et al. (2005) Ethanol binging exacerbates sinusoidal endothelial and parenchymal injury elicited by acetaminophen. *J Hepatol* 42: 371-377.

Meier PJ. (1988) Transport polarity of hepatocytes. *Semin Liver Dis* 8: 293-307.

Meier PJ and Stieger B. (2002) Bile salt transporters. *Annu Rev Physiol* 64: 635-661.

Meier Y, Cavallaro M, Roos M, et al. (2005) Incidence of drug-induced liver injury in medical inpatients. *Eur J Clin Pharmacol* 61: 135-143.

Mi H, Muruganujan A, Casagrande JT, et al. (2013) Large-scale gene function analysis with the PANTHER classification system. *Nat. Protocols* 8: 1551-1566.

Miyoshi N, Ishii H, Nagano H, et al. (2011) Reprogramming of mouse and human cells to pluripotency using mature microRNAs. *Cell Stem Cell* 8: 633-638.

Mizuguchi T, Mitaka T, Hirata K, et al. (1998) Alteration of expression of liver-enriched transcription factors in the transition between growth and differentiation of primary cultured rat hepatocytes. *J Cell Physiol* 174: 273-284.

Mobus S, Yang D, Yuan Q, et al. (2015) MicroRNA-199a-5p inhibition enhances the liver repopulation ability of human embryonic stem cell-derived hepatic cells. *J Hepatol* 62: 101-110.

Mooradian AD and Mariash CN. (1987) Effects of insulin and glucose on cultured rat hepatocyte gene expression. *Diabetes* 36: 938-943.

Moore RN and Moghe PV. (2009) Expedited growth factor-mediated specification of human embryonic stem cells toward the hepatic lineage. *Stem Cell Res* 3: 51-62.

Morel Y, de Waziers I and Barouki R. (2000) A repressive cross-regulation between catalytic and promoter activities of the CYP1A1 and CYP2E1 genes: role of H(2)O(2). *Mol Pharmacol* 57: 1158-1164.

Morishima Y, Peng HM, Lin HL, et al. (2005) Regulation of cytochrome P450 2E1 by heat shock protein 90-dependent stabilization and CHIP-dependent proteasomal degradation. *Biochemistry* 44: 16333-16340.

Moriya N, Kataoka H, Fujino H, et al. (2014) Different expression patterns of hepatic cytochrome P450 s during anaphylactic or lipopolysaccharide-induced inflammation. *Pharmazie* 69: 142-147.

Muppala V, Lin C-S and Lee Y-H. (2000) The Role of HNF-1α in Controlling Hepatic Catalase Activity. *Molecular Pharmacology* 57: 93-100.

Murakami S, Shimizu R, Romeo PH, et al. (2014) Keap1-Nrf2 system regulates cell fate determination of hematopoietic stem cells. *Genes Cells* 19: 239-253.

Murphy SV and Atala A. (2014) 3D bioprinting of tissues and organs. *Nat Biotech* 32: 773-785.

Naiki T, Nagaki M, Asano T, et al. (2005) Adenovirus-mediated hepatocyte nuclear factor-4alpha overexpression maintains liver phenotype in cultured rat hepatocytes. *Biochem Biophys Res Commun* 335: 496-500.

Nakagawa M, Koyanagi M, Tanabe K, et al. (2008) Generation of induced pluripotent stem cells without Myc from mouse and human fibroblasts. *Nat Biotechnol* 26: 101-106.

Nallani SC, Strong JM and Huang SM. (2008) Use of Hepatocytes for Characterizing a Candidate Drug's Metabolism and Drug Interaction Potential. *Hepatotoxicity.* John Wiley & Sons, Ltd, 69-87.

Neubauer K, Wilfling T, Ritzel A, et al. (2000) Platelet-endothelial cell adhesion molecule-1 gene expression in liver sinusoidal endothelial cells during liver injury and repair. *J Hepatol* 32: 921-932.

Nguyen TV, Ukairo O, Khetani SR, et al. (2015) Establishment of a hepatocyte-kupffer cell coculture model for assessment of proinflammatory cytokine effects on metabolizing enzymes and drug transporters. *Drug Metab Dispos* 43: 774-785.

Nibourg GA, Huisman MT, van der Hoeven TV, et al. (2010) Stable overexpression of pregnane X receptor in HepG2 cells increases its potential for bioartificial liver application. *Liver Transpl* 16: 1075-1085.

No DY, Lee S-A, Choi YY, et al. (2012) Functional 3D Human Primary Hepatocyte Spheroids Made by Co-Culturing Hepatocytes from Partial Hepatectomy Specimens and Human Adipose-Derived Stem Cells. *PLoS ONE* 7: e50723.

O'Hara SP, Tabibian JH, Splinter PL, et al. (2013) The dynamic biliary epithelia: Molecules, pathways, and disease. *J Hepatol* 58: 575-582.

Odom DT, Zizlsperger N, Gordon DB, et al. (2004) Control of Pancreas and Liver Gene Expression by HNF Transcription Factors. *Science* 303: 1378-1381.

Olayanju A, Copple IM, Bryan HK, et al. (2015) Brusatol provokes a rapid and transient inhibition of Nrf2 signaling and sensitizes mammalian cells to chemical toxicity-implications for therapeutic targeting of Nrf2. *Free Radic Biol Med* 78: 202-212.

Ostapowicz G, Fontana RJ, Schiodt FV, et al. (2002) Results of a prospective study of acute liver failure at 17 tertiary care centers in the United States. *Ann Intern Med* 137: 947-954.

Padda MS, Sanchez M, Akhtar AJ, et al. (2011) Drug induced Cholestasis. *Hepatology (Baltimore, Md.)* 53: 1377-1387.

Padgham CR, Boyle CC, Wang XJ, et al. (1993) Alteration of transcription factor mRNAs during the isolation and culture of rat hepatocytes suggests the activation of a proliferative mode underlies their de-differentiation. *Biochem Biophys Res Commun* 197: 599-605.

Pan YZ, Gao W and Yu AM. (2009) MicroRNAs regulate CYP3A4 expression via direct and indirect targeting. *Drug Metabolism and Disposition* 37: 2112-2117.

Papp B and Plath K. (2013) Epigenetics of Reprogramming to Induced Pluripotency. *Cell* 152: 1324-1343.

Park BK, Boobis A, Clarke S, et al. (2011) Managing the challenge of chemically reactive metabolites in drug development. *Nat Rev Drug Discov* 10: 292-306.

Park H-J, Choi Y-J, Kim JW, et al. (2015) Differences in the Epigenetic Regulation of Cytochrome P450 Genes between Human Embryonic Stem Cell-Derived Hepatocytes and Primary Hepatocytes. *PLoS ONE* 10: e0132992.

Penaloza CG, Estevez B, Han DM, et al. (2014) Sex-dependent regulation of cytochrome P450 family members Cyp1a1, Cyp2e1, and Cyp7b1 by methylation of DNA. *Faseb j* 28: 966-977.

Pirmohamed M, Breckenridge AM, Kitteringham NR, et al. (1998) Adverse drug reactions. *BMJ* 316: 1295-1298.

Pirmohamed M, James S, Meakin S, et al. (2004) Adverse drug reactions as cause of admission to hospital: prospective analysis of 18 820 patients. *BMJ* 329: 15-19.

Polo Jose M, Anderssen E, Walsh Ryan M, et al. (2012) A Molecular Roadmap of Reprogramming Somatic Cells into iPS Cells. *Cell* 151: 1617-1632.

Polo JM, Liu S, Figueroa ME, et al. (2010) Cell type of origin influences the molecular and functional properties of mouse induced pluripotent stem cells. *Nat Biotechnol* 28: 848-855.

Prakash C and Vaz ADN. (2008) Drug Metabolism: Significance and Challenges. *Nuclear Receptors in Drug Metabolism.* John Wiley & Sons, Inc., 1-41.

Preziosi P. (2004) Science, pharmacoeconomics and ethics in drug R&D: a sustainable future scenario? *Nat Rev Drug Discov* 3: 521-526.

Puligilla C, Dabdoub A, Brenowitz SD, et al. (2010) Sox2 Induces Neuronal Formation in the Developing Mammalian Cochlea. *The Journal of Neuroscience* 30: 714-722.

Rahl PB, Lin CY, Seila AC, et al. (2010) c-Myc regulates transcriptional pause release. *Cell* 141: 432-445.

Ramasamy TS, Yu JS, Selden C, et al. (2013) Application of three-dimensional culture conditions to human embryonic stem cell-derived definitive endoderm cells enhances hepatocyte differentiation and functionality. *Tissue Eng Part A* 19: 360-367.

Rambhatla L, Chiu CP, Kundu P, et al. (2003) Generation of hepatocyte-like cells from human embryonic stem cells. *Cell Transplant* 12: 1-11.

Rashid ST, Corbineau S, Hannan N, et al. (2010) Modeling inherited metabolic disorders of the liver using human induced pluripotent stem cells. *J Clin Invest* 120: 3127-3136.

Reeves HL and Friedman SL. (2002) Activation of hepatic stellate cells: a key issue in liver fibrosis. *Front Biosci* 7: 808-826.

Richert L, Liguori MJ, Abadie C, et al. (2006) Gene expression in human hepatocytes in suspension after isolation is similar to the liver of origin, is not affected by

hepatocyte cold storage and cryopreservation, but is strongly changed after hepatocyte plating. *Drug Metab Dispos* 34: 870-879.

Ripple MO, Kim N and Springett R. (2013) Acute Mitochondrial Inhibition by Mitogen-activated Protein Kinase/Extracellular Signal-regulated Kinase Kinase (MEK) 1/2 Inhibitors Regulates Proliferation. *Journal of Biological Chemistry* 288: 2933-2940.

Roberts RA, Ganey PE, Ju C, et al. (2007) Role of the Kupffer cell in mediating hepatic toxicity and carcinogenesis. *Toxicol Sci* 96: 2-15.

Rodriguez-Antona C, Donato MT, Boobis A, et al. (2002) Cytochrome P450 expression in human hepatocytes and hepatoma cell lines: molecular mechanisms that determine lower expression in cultured cells. *Xenobiotica* 32: 505-520.

Roelandt P, Obeid S, Paeshuyse J, et al. (2012) Human pluripotent stem cell-derived hepatocytes support complete replication of hepatitis C virus. *J Hepatol* 57: 246-251.

Rouhani F, Kumasaka N, de Brito MC, et al. (2014) Genetic Background Drives Transcriptional Variation in Human Induced Pluripotent Stem Cells. *PLoS Genet* 10: e1004432.

Rowe C, Gerrard DT, Jenkins R, et al. (2013) Proteome-wide analyses of human hepatocytes during differentiation and dedifferentiation. *Hepatology* 58: 799-809.

Rowe C, Goldring CE, Kitteringham NR, et al. (2010) Network analysis of primary hepatocyte dedifferentiation using a shotgun proteomics approach. *J Proteome Res* 9: 2658-2668.

Russo MW, Galanko JA, Shrestha R, et al. (2004) Liver transplantation for acute liver failure from drug induced liver injury in the United States. *Liver Transpl* 10: 1018-1023.

Salzman NH. (2014) The role of the microbiome in immune cell development. *Ann Allergy Asthma Immunol* 113: 593-598.

Sancho-Martinez I and Belmonte JCI. (2013) Stem cells: Surf the waves of reprogramming. *Nature* 493: 310-311.

Sander JD and Joung JK. (2014) CRISPR-Cas systems for editing, regulating and targeting genomes. *Nat Biotech* 32: 347-355.

Schmidt R and Plath K. (2012) The roles of the reprogramming factors Oct4, Sox2 and Klf4 in resetting the somatic cell epigenome during induced pluripotent stem cell generation. *Genome Biology* 13: 1-11.

Schneider CA, Rasband WS and Eliceiri KW. (2012) NIH Image to ImageJ: 25 years of image analysis. *Nat Meth* 9: 671-675.

Schwanhausser B, Busse D, Li N, et al. (2011) Global quantification of mammalian gene expression control. *Nature* 473: 337-342.

Schwartz RE, Trehan K, Andrus L, et al. (2012) Modeling hepatitis C virus infection using human induced pluripotent stem cells. *Proceedings of the National Academy of Sciences* 109: 2544-2548.

Sgro C, Clinard F, Ouazir K, et al. (2002) Incidence of drug-induced hepatic injuries: A French population-based study. *Hepatology* 36: 451-455.

Shackel NA, Gorrell MD and McCaughan GW. (2002) Gene array analysis and the liver. *Hepatology* 36: 1313-1325.

Shan J, Schwartz RE, Ross NT, et al. (2013) Identification of small molecules for human hepatocyte expansion and iPS differentiation. *Nature chemical biology* 9: 514-520.

Shiraki N, Umeda K, Sakashita N, et al. (2008) Differentiation of mouse and human embryonic stem cells into hepatic lineages. *Genes Cells* 13: 731-746.

Shishodia S, Sethi G, Konopleva M, et al. (2006) A synthetic triterpenoid, CDDO-Me, inhibits IkappaBalpha kinase and enhances apoptosis induced by TNF and chemotherapeutic agents through down-regulation of expression of nuclear factor

kappaB-regulated gene products in human leukemic cells. *Clin Cancer Res* 12: 1828-1838.

Shruti K, Shrey K and Vibha R. (2011) MicroRNAs: tiny sequences with enormous potential. *Biochem Biophys Res Commun* 407: 445-449.

Si-Tayeb K, Noto FK, Nagaoka M, et al. (2010) Highly Efficient Generation of Human Hepatocyte–like Cells from Induced Pluripotent Stem Cells. *Hepatology (Baltimore, Md.)* 51: 297-305.

Siller R, Greenhough S, Naumovska E, et al. (2015) Small-Molecule-Driven Hepatocyte Differentiation of Human Pluripotent Stem Cells. *Stem Cell Reports* 4: 939-952.

Singh A, Misra V, Thimmulappa RK, et al. (2006) Dysfunctional KEAP1–NRF2 Interaction in Non-Small-Cell Lung Cancer. *PLoS Medicine* 3: e420.

Singh G and Veltri KL. (1991) A mechanism for the loss of cytochrome P-450 in primary mouse hepatocytes. *Mol Cell Biochem* 108: 151-156.

Sison-Young RL, Mitsa D, Jenkins RE, et al. (2015) Comparative Proteomic Characterization of 4 Human Liver-Derived Single Cell Culture Models Reveals Significant Variation in the Capacity for Drug Disposition, Bioactivation, and Detoxication. *Toxicol Sci* 147: 412-424.

Sistonen J, Fuselli S, Palo JU, et al. (2009) Pharmacogenetic variation at CYP2C9, CYP2C19, and CYP2D6 at global and microgeographic scales. *Pharmacogenet Genomics* 19: 170-179.

Sjogren AK, Liljevald M, Glinghammar B, et al. (2014) Critical differences in toxicity mechanisms in induced pluripotent stem cell-derived hepatocytes, hepatic cell lines and primary hepatocytes. *Archives of Toxicology* 88: 1427-1437.

Sleyster EC and Knook DL. (1982) Relation between localization and function of rat liver Kupffer cells. *Lab Invest* 47: 484-490.

Sommer CA, Stadtfeld M, Murphy GJ, et al. (2009) Induced pluripotent stem cell generation using a single lentiviral stem cell cassette. *Stem Cells* 27: 543-549.

Song Z, Cai J, Liu Y, et al. (2009) Efficient generation of hepatocyte-like cells from human induced pluripotent stem cells. *Cell Res* 19: 1233-1242.

Soufi A, Donahue G and Zaret KS. (2012) Facilitators and impediments of the pluripotency reprogramming factors' initial engagement with the genome. *Cell* 151: 994-1004.

Stevens LC. (1958) Studies on transplantable testicular teratomas of strain 129 mice. *J Natl Cancer Inst* 20: 1257-1275.

Su T and Waxman DJ. (2004) Impact of dimethyl sulfoxide on expression of nuclear receptors and drug-inducible cytochromes P450 in primary rat hepatocytes. *Arch Biochem Biophys* 424: 226-234.

Subramanian K, Owens DJ, Raju R, et al. (2014) Spheroid culture for enhanced differentiation of human embryonic stem cells to hepatocyte-like cells. *Stem Cells Dev* 23: 124-131.

Subramanyam D, Lamouille S, Judson RL, et al. (2011) Multiple targets of miR-302 and miR-372 promote reprogramming of human fibroblasts to induced pluripotent stem cells. *Nat Biotech* 29: 443-448.

Sullivan GJ, Hay DC, Park IH, et al. (2010) Generation of functional human hepatic endoderm from human induced pluripotent stem cells. *Hepatology* 51: 329-335.

Synnergren J, Heins N, Brolen G, et al. (2010) Transcriptional profiling of human embryonic stem cells differentiating to definitive and primitive endoderm and further toward the hepatic lineage. *Stem Cells Dev* 19: 961-978.

Szkolnicka D, Farnworth SL, Lucendo-Villarin B, et al. (2013) Accurate Prediction of Drug-Induced Liver Injury Using Stem Cell-Derived Populations. *Stem Cells Translational Medicine* 3: 141-148.

Takagi S, Nakajima M, Kida K, et al. (2010) MicroRNAs regulate human hepatocyte nuclear factor 4α, modulating the expression of metabolic enzymes and cell cycle. *Journal of Biological Chemistry* 285: 4415-4422.

Takagi S, Nakajima M, Mohri T, et al. (2008) Post-transcriptional regulation of human pregnane X receptor by micro-RNA affects the expression of cytochrome P450 3A4. *J Biol Chem* 283: 9674-9680.

Takahashi K, Tanabe K, Ohnuki M, et al. (2007) Induction of Pluripotent Stem Cells from Adult Human Fibroblasts by Defined Factors. *Cell* 131: 861-872.

Takahashi K and Yamanaka S. (2006) Induction of Pluripotent Stem Cells from Mouse Embryonic and Adult Fibroblast Cultures by Defined Factors. *Cell* 126: 663-676.

Takahashi R, Sonoda H, Tabata Y, et al. (2010) Formation of hepatocyte spheroids with structural polarity and functional bile canaliculi using nanopillar sheets. *Tissue Eng Part A* 16: 1983-1995.

Takayama K, Inamura M, Kawabata K, et al. (2012) Generation of metabolically functioning hepatocytes from human pluripotent stem cells by FOXA2 and HNF1alpha transduction. *J Hepatol* 57: 628-636.

Takayama K, Kawabata K, Nagamoto Y, et al. (2013) 3D spheroid culture of hESC/hiPSC-derived hepatocyte-like cells for drug toxicity testing. *Biomaterials* 34: 1781-1789.

Takayama K, Morisaki Y, Kuno S, et al. (2014) Prediction of interindividual differences in hepatic functions and drug sensitivity by using human iPS-derived hepatocytes. *Proceedings of the National Academy of Sciences of the United States of America* 111: 16772-16777.

Takebe T, Sekine K, Enomura M, et al. (2013) Vascularized and functional human liver from an iPSC-derived organ bud transplant. *Nature* 499: 481-484.

Thomas S and Bonchev D. (2010) A survey of current software for network analysis in molecular biology. *Hum Genomics* 4: 353-360.

Thomson JA, Itskovitz-Eldor J, Shapiro SS, et al. (1998) Embryonic Stem Cell Lines Derived from Human Blastocysts. *Science* 282: 1145-1147.

Tostoes RM, Leite SB, Miranda JP, et al. (2011) Perfusion of 3D encapsulated hepatocytes: a synergistic effect enhancing long-term functionality in bioreactors. *Biotechnol Bioeng* 108: 41-49.

Tostoes RM, Leite SB, Serra M, et al. (2012) Human liver cell spheroids in extended perfusion bioreactor culture for repeated-dose drug testing. *Hepatology* 55: 1227-1236.

Touboul T, Hannan NR, Corbineau S, et al. (2010) Generation of functional hepatocytes from human embryonic stem cells under chemically defined conditions that recapitulate liver development. *Hepatology* 51: 1754-1765.

Trask OJ, Jr., Moore A and LeCluyse EL. (2014) A micropatterned hepatocyte coculture model for assessment of liver toxicity using high-content imaging analysis. *Assay Drug Dev Technol* 12: 16-27.

Trokovic R, Weltner J, Noisa P, et al. (2015) Combined negative effect of donor age and time in culture on the reprogramming efficiency into induced pluripotent stem cells. *Stem cell research* 15: 254-262.

Tsuchiya Y, Nakajima M, Takagi S, et al. (2006) MicroRNA regulates the expression of human cytochrome P450 1B1. *Cancer Research* 66: 9090-9098.

Tsutsui H and Nishiguchi S. (2014) Importance of Kupffer cells in the development of acute liver injuries in mice. *Int J Mol Sci* 15: 7711-7730.

Ukairo O, Kanchagar C, Moore A, et al. (2013) Long-Term Stability of Primary Rat Hepatocytes in Micropatterned Cocultures. *Journal of Biochemical and Molecular Toxicology* 27: 204-212.

Ulvestad M, Nordell P, Asplund A, et al. (2013) Drug metabolizing enzyme and transporter protein profiles of hepatocytes derived from human embryonic and induced pluripotent stem cells. *Biochemical Pharmacology* 86: 691-702.

Villa-Diaz LG, Garcia-Perez JL and Krebsbach PH. (2010) Enhanced Transfection Efficiency of Human Embryonic Stem Cells by the Incorporation of DNA Liposomes in Extracellular Matrix. *Stem Cells Dev* 19: 1949-1957.

Wakabayashi N, Skoko JJ, Chartoumpekis DV, et al. (2013) Notch-Nrf2 axis: Regulation of Nrf2 gene expression and cytoprotection by Notch signaling. *Mol Cell Biol* 34: 653-663.

Walsh J, Jenkins RE, Wong M, et al. (2014) Identification and quantification of the basal and inducible Nrf2-dependent proteomes in mouse liver: biochemical, pharmacological and toxicological implications. *J Proteomics* 108: 171-187.

Wang A, Yue F, Li Y, et al. (2015) Epigenetic priming of enhancers predicts developmental competence of hESC-derived endodermal lineage intermediates. *Cell Stem Cell* 16: 386-399.

Warmflash A, Sorre B, Etoc F, et al. (2014) A method to recapitulate early embryonic spatial patterning in human embryonic stem cells. *Nat Meth* 11: 847-854.

Warren L, Manos PD, Ahfeldt T, et al. (2010) Highly efficient reprogramming to pluripotency and directed differentiation of human cells with synthetic modified mRNA. *Cell Stem Cell* 7: 618-630.

Watanabe A, Hashmi A, Gomes DA, et al. (2007) Apoptotic hepatocyte DNA inhibits hepatic stellate cell chemotaxis via toll-like receptor 9. *Hepatology* 46: 1509-1518.

Watkins PB. (2005) Idiosyncratic liver injury: challenges and approaches. *Toxicol Pathol* 33: 1-5.

Weiskirchen R and Tacke F. (2014) Cellular and molecular functions of hepatic stellate cells in inflammatory responses and liver immunology. *Hepatobiliary Surg Nutr* 3: 344-363.

Wester K, Jonsson AK, Spigset O, et al. (2008) Incidence of fatal adverse drug reactions: a population based study. *Br J Clin Pharmacol* 65: 573-579.

Wiedenheft B, Sternberg SH and Doudna JA. (2012) RNA-guided genetic silencing systems in bacteria and archaea. *Nature* 482: 331-338.

Wilke RA, Lin DW, Roden DM, et al. (2007) Identifying genetic risk factors for serious adverse drug reactions: Current progress and challenges. *Nature Reviews Drug Discovery* 6: 904-916.

Williams JA, Ring BJ, Cantrell VE, et al. (2002) Comparative Metabolic Capabilities of CYP3A4, CYP3A5, and CYP3A7. *Drug Metabolism and Disposition* 30: 883-891.

Wilson Andrew A, Ying L, Liesa M, et al. (2015) Emergence of a Stage-Dependent Human Liver Disease Signature with Directed Differentiation of Alpha-1 Antitrypsin-Deficient iPS Cells. *Stem Cell Reports* 4: 873-885.

Wilson BG and Roberts CWM. (2011) SWI/SNF nucleosome remodellers and cancer. *Nat Rev Cancer* 11: 481-492.

Wu TY, Jen MH, Bottle A, et al. (2010) Ten-year trends in hospital admissions for adverse drug reactions in England 1999-2009. *J R Soc Med* 103: 239-250.

Xu C, Li CY and Kong AN. (2005) Induction of phase I, II and III drug metabolism/transport by xenobiotics. *Arch Pharm Res* 28: 249-268.

Xu J, Donepudi AC, Moscovitz JE, et al. (2013a) Keap1-Knockdown Decreases Fasting-Induced Fatty Liver via Altered Lipid Metabolism and Decreased Fatty Acid Mobilization from Adipose Tissue. *PLoS ONE* 8: 0079841.

Xu Y, Wei X, Wang M, et al. (2013b) Proliferation Rate of Somatic Cells Affects Reprogramming Efficiency. *Journal of Biological Chemistry* 288: 9767-9778.

Ygberg S and Nilsson A. (2012) The developing immune system - from foetus to toddler. *Acta Paediatr* 101: 120-127.

Yousefi B, Darabi M, Baradaran B, et al. (2012) Inhibition of MEK/ERK1/2 Signaling Affects the Fatty Acid Composition of HepG2 Human Hepatic Cell Line. *BioImpacts : BI* 2: 145-150.

Yu J, Hu K, Smuga-Otto K, et al. (2009) Human Induced Pluripotent Stem Cells Free of Vector and Transgene Sequences. *Science* 324: 797-801.

Yu J, Vodyanik MA, Smuga-Otto K, et al. (2007) Induced pluripotent stem cell lines derived from human somatic cells. *Science* 318: 1917-1920.

Yu Y, Liu H, Ikeda Y, et al. (2012) Hepatocyte-like cells differentiated from human induced pluripotent stem cells: Relevance to cellular therapies. *Stem cell research* 9: 196-207.

Yusa K, Rashid ST, Strick-Marchand H, et al. (2011) Targeted gene correction of alpha1-antitrypsin deficiency in induced pluripotent stem cells. *Nature* 478: 391-394.

Zamek-Gliszczynski MJ, Hoffmaster KA, Tweedie DJ, et al. (2012) Highlights from the International Transporter Consortium second workshop. *Clin Pharmacol Ther* 92: 553-556.

Zangar RC, Bollinger N, Verma S, et al. (2008) The Nuclear Factor-κB Pathway Regulates Cytochrome P450 3A4 Protein Stability. *Molecular Pharmacology* 73: 1652-1658.

Zangar RC, Davydov DR and Verma S. (2004) Mechanisms that regulate production of reactive oxygen species by cytochrome P450. *Toxicol Appl Pharmacol* 199: 316-331.

Zangar RC, Kocarek TA, Shen S, et al. (2003) Suppression of cytochrome P450 3A protein levels by proteasome inhibitors. *J Pharmacol Exp Ther* 305: 872-879.

Zanger UM and Schwab M. (2013) Cytochrome P450 enzymes in drug metabolism: Regulation of gene expression, enzyme activities, and impact of genetic variation. *Pharmacology & Therapeutics* 138: 103-141.

Zellmer S, Schmidt-Heck W, Godoy P, et al. (2010) Transcription factors ETF, E2F, and SP-1 are involved in cytokine-independent proliferation of murine hepatocytes. *Hepatology* 52: 2127-2136.

Zhang S, Chen S, Li W, et al. (2011) Rescue of ATP7B function in hepatocyte-like cells from Wilson's disease induced pluripotent stem cells using gene therapy or the chaperone drug curcumin. *Hum Mol Genet* 20: 3176-3187.

Zhou W, Hannoun Z, Jaffray E, et al. (2012) SUMOylation of HNF4alpha regulates protein stability and hepatocyte function. *J Cell Sci* 125: 3630-3635.

Zhou Y, Zhu S, Cai C, et al. (2014) High-throughput screening of a CRISPR/Cas9 library for functional genomics in human cells. *Nature* 509: 487-491.

Zhu Q, Krakowski AR, Dunham EE, et al. (2007) Dual role of SnoN in mammalian tumorigenesis. *Mol Cell Biol* 27: 324-339.

Zhu S, Rezvani M, Harbell J, et al. (2014) Mouse liver repopulation with hepatocytes generated from human fibroblasts. *Nature* 508: 93-97.